THE UNIVERSITY OF MICHIGAN

COLLEGE OF ENGINEERING

High Altitude Engineering Laboratory

Department of Aerospace Engineering

Department of Atmospheric and Oceanic Science

Technical Report

# ACOUSTICS OF METEORS—EFFECTS OF THE ATMOSPHERIC TEMPERATURE AND WIND STRUCTURE ON THE SOUNDS PRODUCED BY METEORS

## Part 2. Effects of Atmospheric Refraction and Attenuation Considerations

Douglas O. ReVelle

ORA Project 010816

supported by:

NATIONAL AERONAUTICS AND SPACE ADMINISTRATION

GRANT NO. NGR 23-005-540

WASHINGTON, D.C.

administered through:

OFFICE OF RESEARCH ADMINISTRATION ANN ARBOR

June 1973

TABLE OF CONTENTS

TABLE OF CONTENTS (Part II) (Continued)

## ACKNOWLEDGMENTS

Without the help of a number of persons, this report would not have been possible. These include my advisor, Dr. F. L. Bartman, the Staff of the High Altitude Engineering Laboratory (especially the secretaries and the work study students), Dr. William Donn and his infrasound research group at Lamont-Doherty Geological Observatory and many others too numerous to mention.

The death, earlier this year, of Mr. Vernon H. Goerke of the NOAA Wave Propagation Laboratory in Boulder, Colorado was a great loss to the entire infrasound research community. His enthusiastic support for our meteor infrasound research will be greatly missed.

Once again I must thank my wife, Ann, for her help during the course of this investigation. In addition to her checking the many figures for possible errors, her ever enthusiastic encouragement brightened up many difficult days.

This research was supported by NASA grant NGR-23-005-540.

LIST OF FIGURES

LIST OF TABLES

## LIST OF SYMBOLS

| | |
|---|---|
| a | radius of the source (roughly analogous to $d_m$) |
| A | meteor cross - sectional area |
| A | absorption coefficient as defined by equation (62) |
| b | as defined by equation (17d) |
| B | absorption coefficient as defined by equation (63) |
| C(z) | adiabatic sound speed as a function of altitude |
| $\overline{C}$ | mean adiabatic sound speed between source and observer |
| C'(z) | as defined by equation (52a) |
| "C" | Plooster's adjustable parameter which determines the region in which the transition from strong shock to weak shock behavior occurs. |
| $C_D$ | coefficient of drag |
| $C_d$ | charge diameter of an explosion of spherical symmetry |
| $C_{eff}(z)$ | effective horizontal sound velocity as a function of altitude |
| $C_{eff}(z)\|_{max}$ | maximum value of the effective horizontal sound velocity |
| $C_i$ | adiabatic sound speed in the ith layer |
| $C_{max}(z)$ | maximum value of the adiabatic sound speed |
| $C_p$ | specific heat of the fluid at constant pressure |
| $C_z$ | adiabatic sound speed at the source altitude |
| d' | 10% distortion distance |
| $d_a$ | remaining propagation distance of the disturbance |
| $d_s$ | distance to the "shocked" state |
| $d_m(z)$ | meteor diameter as a function of altitude |
| $\bar{d}_m$ | average meteor diameter below the altitude where the Knudsen number is less than 0.05 |
| $d_{mE}$ | meteor diameter at z' |

| | |
|---|---|
| $D(R)$ | $\Delta p / \Delta p_z$; absorption decay function as defined by equations (92a) and (92b) |
| $E_o$ | finite amount of energy deposited by the cylindrical blast wave line source per unit path length. |
| $E_t$ | total energy deposited by the spherical blast wave "point" source |
| $f$ | frequency components inherent to the disturbance |
| $f_A$ | acoustic cut-off frequency |
| $f_B$ | Brunt-Väisälä frequency |
| $f_m$ | fundamental (dominant) frequency of the disturbance |
| $f(\bar{\omega}, x)$ | as defined by equation (77) |
| $f(x)$ | as defined by equation (12a) |
| $g$ | acceleration due to gravity |
| $H$ | scale height of the isothermal atmosphere |
| $i$ | layer number index |
| $I$ | intensity at a path distance $\Delta s$ from the source |
| $I'$ | as defined by equation (80d) |
| $I_z$ | initial intensity of the linear acoustic disturbance |
| $k(z)$ | characteristic velocity within the entry plane as a function of altitude |
| $k'(z)$ | characteristic velocity outside the entry plane as a function of altitude |
| $k_o$ | as defined by equation (85) |
| $k_1$ | as defined by equation (85) |
| $K$ | thermal conductivity of the fluid |
| $Kn$ | Knudsen number for $p^*$ constant |
| $\overline{Kn}$ | Knudsen number for p* decreasing exponentially |

| | |
|---|---|
| $\ell$ | length of the line source (measured between the altitude at which the Knudsen number becomes 0.05 and z'''') |
| m | meteor mass |
| m | total intensity absorption coefficient |
| M(z) | meteor Mach number as a function of altitude |
| $\overline{M}$ | average meteor Mach number below the altitude where the Knudsen number is less than 0.05 |
| Ma | $V_s/C$ = shock front Mach number |
| $M_i$ | meteor Mach number in the ith layer |
| $M_{pan}$ | panchromatic magnitude (related to the visual magnitude or brightness of the meteor) |
| $M_E$ | meteor Mach number at z' |
| N | classical symmetric wave shape as commonly referred to in sonic boom problems |
| $N_c$ | cumulative weak nonlinear propagation correction term |
| p(z) | ambient hydrostatic pressure |
| p | pressure at the shock front |
| $\Delta p$ | overpressure (or pressure amplitude) of the disturbance at some specified observation point |
| $(\Delta p)_{RMS}$ | root mean square pressure amplitude |
| $p_o$ | hydrostatic atmospheric pressure at the observer (or ambient atmospheric pressure) |
| $p_g$ | hydrostatic pressure at the ground |
| $\Delta p_z$ | overpressure at the source |
| $\Delta p/p_o$ | overpressure ratio |
| p* | modified ballistic entry parameter |
| $\overline{p^*}$ | geometric mean pressure between the observer's altitude and the altitude where the blast wave was generated |

| | |
|---|---|
| $p_s$ | pressure amplitude of the "shocked" disturbance (also written as $\Delta p$) |
| $p_z$ | hydrostatic pressure at the source altitude |
| $r_m(z)$ | meteor radius as a function of altitude |
| $r_{mE}$ | meteor radius at z' |
| R | actual radius of the shock front at a given time (also generally radial distance from the meteor trajectory) |
| $R_o$ | relaxation radius of the cylindrical blast wave |
| $R_{oi}$ | relaxation radius of the cylindrical blast wave in the ith layer |
| $R_g$ | ground reflection coefficient |
| $R_s$ | spherical blast wave relaxation radius |
| s | path distance coordinate |
| $\Delta s$ | path distance away from an origin point |
| $S_m$ | condensation (as defined by equation (57) ) |
| t | time variable |
| t | time for blast wave to decay out to weak shock conditions |
| t' | total time during the flight of the meteor during which the bow shock wave was generated |
| $t_i$ | time for blast wave to decay out to weak shock conditions for energy deposited within layer i |
| $\overline{t_i}$ | average value of $t_i$ during the meteor entry |
| $t'_i$ | time during the flight of the meteor in layer i during which the bow shock wave was generaged |
| $t'_m$ | value of t' in the mth layer (where Kn(or $\overline{Kn}$) $\leq 0.05$) |
| $t'_N$ | value of t' in the Nth layer (where $\overline{V_i} \rightarrow C$) |
| T | absolute temperature of the gas |
| u(z) | magnitude of the zonal wind as a function of altitude |

| | |
|---|---|
| $v(z)$ | magnitude of the meridional wind as a function of altitude |
| $V(z)$ | meteor velocity as a function of altitude |
| $V_E$ | meteor entry velocity, i.e., $V(z')$ |
| $\overline{V_i}$ | average velocity of the meteor in the ith layer |
| $V_s$ | shock front velocity |
| $W(z)$ | magnitude of the horizontal wind as a function of altitude |
| $x$ | $R/R_o$ scaled distance from the trajectory |
| $x_i$ | value of $x$ in the ith layer |
| $z$ | altitude, increasing upward from $z = 0$ at the surface of the earth, for the isothermal atmospheric model |
| $z'$ | altitude at which the meteor deceleration is first zero |
| $z''''$ | altitude at which the meteor deceleration is again zero |
| $z_o$ | observer's altitude |
| $\Delta z_i$ | layer thickness used in the instantaneous energy release calculations (as defined by equation (22)) |
| $z_I$ | altitude of a tropospheric temperature inversion |
| $z_{ni}$ | altitude, increasing upward from $z = 0$ at the surface of the earth, for the nonisothermal climatological model |
| $z_z$ | source altitude |
| $\alpha$ | Mach angle of the meteor shock cone |
| $\bar{\alpha}$ | total amplitude absorption coefficient |
| $\alpha_D$ | diffusion absorption coefficient |
| $\alpha_K$ | thermal conductivity absorption coefficient |
| $\alpha_{mol}$ | molecular relaxation absorption coefficient |
| $\alpha_{rad}$ | radiation absorption coefficient |
| $\alpha_\mu$ | viscosity absorption coefficient |

| | |
|---|---|
| $\beta$ | absolute value of $(\sigma - \alpha)$ |
| $\gamma$ | ratio of the specific heat of air at constant pressure to that at constant volume |
| $\delta$ | as defined by equation (60) |
| "$\delta$" | efficiency with which cylindrical line source strong shock waves are generated as compared with the results of the asymptotic strong shock solution due to Lin (1954) |
| $\bar{\epsilon}$ | zenith angle of the ray |
| $\sigma$ | entry elevation angle of the meteor |
| $\sigma'$ | elevation angle of the acoustic ray |
| $\lambda$ | mean free path of the neutral gas |
| $\Lambda$ | wavelength components inherent to the disturbance (or wavelength associated with the fundamental frequency of the disturbance) |
| $\Lambda_x$ | East-West horizontal component wavelength of the disturbance |
| $\Lambda_y$ | North-South horizontal component wavelength of the disturbance |
| $\Lambda_z$ | vertical component wavelength of the disturbance |
| $\mu$ | ordinary (shear) viscosity coefficient |
| $\mu'$ | as defined by equation (60) |
| $\xi$ | bulk (volume viscosity coefficient) |
| $\rho$ | perturbation density as defined by equation (57) |
| $\Delta\rho$ | $\rho - \rho_o$ |
| $\rho_o$ | atmospheric density at the observer (or ambient atmospheric density) |
| $\rho_o C$ | characteristic acoustic impedance of the medium |
| $\rho_g$ | atmospheric density at the ground |

LIST OF SYMBOLS (concluded)

| | |
|---|---|
| $\rho_m$ | meteor density |
| $\rho_{mE}$ | meteor density at z' |
| $\rho_z$ | air density at source altitude |
| $\sigma$ | ablation parameter |
| $\tau$ | period of the oscillation |
| $\tau'$ | value of $\tau$ at x' as defined by equation (93a) |
| $\tau_m$ | the period associated with the fundamental (or dominant) frequency of the disturbance |
| $\tau_{mo}$ | wave period as defined at x=10 |
| $\tau_s$ | scaled arrival time |
| $\phi$ | aximuth angle of the meteor heading |
| $\Delta\phi$ | the absolute value of ($\phi$ - $\phi'$) |
| $\phi'$ | azimuth angle of a given ray outside the entry plane as measured $180^o$ from the heading of the ray |
| $\Psi(z)$ | azimuthal direction the horizontal winds are coming from as a function of altitude measured as increasing clockwise from North as viewed from above |
| $\omega$ | angular frequency of the oscillation |
| $\omega_A$ | angular acoustic cut-off frequency |
| $\omega_B$ | angular Brunt-Väisälä frequency |
| $\bar{\omega}$ | assumed wave shape induced by the source |

# FOREWARD

This section constitutes Part 2 of the meteor acoustics report. It deals with both the temperature and wind refraction as well as the attenuation of the meteor produced sounds. The theory as developed in Part 1 is applied where possible to study the effects of a nonuniform but horizontally stratified medium on the propagation and decay of these pressure waves. The primary subjects of Part 3 of this report will be as follows.

Part 3.

Probability of Occurrence of Sound Producing Meteors as well as the Probability of Recording such Signals at the Ground.

Theoretical Analysis of Existing Infrasonic Signals from Meteors.

Summary of the above Research and Suggestions for Future Research.

# IV. EFFECTS OF REFRACTION ON METEOR SOUND PROPAGATION

## A. CYLINDRICAL BLAST WAVE LINE SOURCE MODEL

In order to study the effects of the temperature and wind fields on the propagation of meteor sounds, a model is needed of the process by which the bow shock wave generated by the hypersonic entry into the atmosphere decays to a weak disturbance. Following Lin (1954), Sakurai (1965), Few (1968), Jones, et. al., (1968), Plooster (1968), and Tsikulin (1970), a cylindrical blast wave model of the nonlinear disturbance initiated from an "explosive" line source was considered.

The theoretical problem involved when considering blast waves is that of solving the nonsteady flow of the full nonlinear hydrodynamic equations (where the gravity term can be neglected compared to the tremendous pressure gradients set up during the strong shock expansion of the disturbance) while satisfying a continually shifting boundary condition at the shock front. These equations were first solved assuming ideal gas behavior (Taylor, 1950;Lin, 1954). More recently, solutions allowing for real gas effects have also been obtained (Plooster, 1968; Tsikulin, 1970). Solutions to these equations are sought using the principle of similarity, a concept common to many areas of fluid dynamics. This type of analysis is essentially a transformation of the partial differential equations to a newset of independent variables for which approximate solutions are then possible. This transformation reduces the system to ordinary differential equations which are then solvable by series methods. The application of the similarity concept to hypersonic flow and blast wave propagation is

well established, at least to a first order approximation (Hayes, 1947; Guiraud, et. al., 1965; Tsikulin, 1970).

There are three main features of the solutions to these equations which are of interest to this problem. First, there is the decay of the overpressure ratio ( $\frac{\Delta p}{p_o}$ ) with distance from the trajectory. Secondly, there is the decay of the shock front Mach number versus distance from the trajectory. Finally, the changing blast wave structure (including both the leading shock front and the region behind it) as a function of distance from the trajectory is to be considered. The latter item however is of less significance for this study than the former items. This is because in the case of meteor sounds there is almost no data to test the blast wave predictions against at close range. In addition, the effects of generalized ablation on the structure of the classical blast wave are also unknown as is discussed below. There are additional complications however. Meteor sounds at the earth's surface are relatively rare; precisely how rare is yet to be determined. For this reason infrasonic recordings are to be desired since long distance propagation without great attenuation may be possible and events from different azimuths may be recorded. At large path distances from the source the overall wave structure is more dependent on the atmospheric variations encountered than upon the line source characteristics (DuMond, et. al., 1946, Tsikulin, 1970). In order to make use of continuous infrasonic recordings, knowledge of the meteor event is necessary ( at least at the present time). For our purposes, the Prairie Network (a sixteen station automatic photographic fireball detection system operated by the Smithsonian Institution in the prairies of the U. S. ) will provide this information for the

infrasonic recordings the author hopes to make. See also VI (Part 3) for more details on this.

It seems that the recording of audible sounds from meteors is improbable. In addition, its is very difficult to relate the predictions of classical blast wave theory to the reported audible sounds from meteors. Ablation of meteors during flight produces material which may also generate individual shock waves. The ablation process then diffentiates the bow shock wave (or ballistic wave) from an explosion wave in that ablation occurs as a result of energy transport back from the atmosphere to the meteor reducing its masss to surface area and thereby reducing energy available for the shock wave at progressively lower altitudes (Bronshten, 1964). Furthermore, the sounds from certain meteors which seem to explode, i.e., bolides, are probably not the result of a chemical type point explosion, but rather of the collective action (possibly over a long path distance) of the individual hypersonic fragments generated during fragmentation. See Section VIII (Part 3) for further discussion on all of the possibilities involved. Obviously the single body models discussed in Section III cannot reproduce this gross fragmentation (or total break up) and the resulting multiple shock wave generation problem. In addition various meteors have been observed to fragment apparently as violently as bolides and yet continue along their trajectory (as one main mass with many smaller attending fragments or just as many small fragments whose total mass is comparable to the original single body mass) and still produce audible sounds as their flight progresses (Hindley and Miles, 1970). Much work needs to be done to expand workable meteor source models to include all of these important effects.

That these are common effects is readily evidenced by the many multiple audible sonic boom reports which lead to the description in Section I. Laboratory photographs of the ablating flight of hypersonic bodies show this multiple shock effect quite clearly (Chamberlin, 1968). Here the term sonic boom refers specifically to the pressure disturbance (initially considered as linear) induced by a body traveling at a speed exceeding that of sound (at a given altitude). The term sonic bang refers specifically to the fact that the pressure disturbance is so intense that shock waves are present (Hayes, 1971). Thus it is possible to have bangless booms, i.e. pressure disturbances generated by supersonic bodies without the presence of shock waves. As will be seen shortly, beyond a certain distance from the trajectory the amplitude of the original cylindrical blast wave source will become comparable to that of a sonic boom. Hence beyond a certain distance the wave propagation will become approximately linear even though closer to the source the hypersonic meteor velocity induced disturbances which propagated in a very nonlinear fashion. See Section V for more details on this subject.

The other problem related to the structure of the blast wave and the audible sound phenomena is that meteors of widely varying kinetic energies can produce audible sounds at the ground. As will be seen shortly the velocity of the meteor is a very important factor in determining the structure of the blast wave as a function of distance from the trajectory. Every audible output is likely to be different at different distances from the source and an intercomparison between recorded events would not be easily understood unless at least the velocities of the meteors were known. For all of the above reasons only the first two items mentioned earlier will be considered in this study (with the

exception of the wave shape attenuation considerations in Section V). Their improtance is ultimately in predicting for the effective meteor model the region where the methods of geometrical acoustics can be applied so that ray theory can be used to study the effects of atmospheric refraction on meteor sounds.

It is assumed then that the blast wave explosion analogy can be applied to the hypersonic flow problem for all meteors which reach altitudes such that the Knudsen number is small with V>>C (if the energy release can be considered as instantaneous or if V = constant; see equations (24) and (24a)). While these conditions of flight are maintained the effects of ablation (with regard to the many small shocks generated primarily within the main bow shock) are assumed not to alter significantly the present theoretical predictions. In the case of gross fragmentation or extreme deceleration however this last assumption cannot be considered realistic (i.e. ablation waves must then be considered, Bronshten, 1964). This is the so-called "thermal explosion" effect (Stanyukovich, et. al., 1961). Its applicability has been suggested previously for bodies undergoing considerable deceleration in the atmosphere. Thus still another "explosion" analogy may apply to the meteor sound problem under certain conditions of flight. See Section V and Section VIII (Part 3).

Following Jones et. al. (1968) the first two items can be calculated in two distinct regions. In the strong shock blast wave region (where $p/p_o > 10$) the equation relating $p/p_o$ to distance from the trajectory is as follows:

$$p/p_o = \frac{\gamma}{2(\gamma + 1)} \left( \frac{1}{x^2} \right) \qquad (11)$$

where

$p_o$ = ambient uniform atmospheric pressure which is assumed very small compared to p (This is commonly called the counterpressure)

$p$ = pressure at the shock front

$\gamma$ = ratio of specific heats of air (considered as an ideal diatomic gas such as that $\gamma = 1.40$)

$x$ = $R/R_o$ = scaled distance from the trajectory

$R$ = actual radius of the shock front at a given time

$R_o$ = relaxation radius of the cylindrical blast wave (See equation (15))

Equation (11) is obtained by using the cylindrical blast wave similarity solution of the shock trajectory (due to Lin, 1954) :

$$\tau_s = x^2 \tag{11a}$$

where

$\tau_s = Ct/R_o$ = scaled arrival time of the nonlinear disturbance at a distance R from the trajectory

and the momentum conservation law expressed across the moving shock front (one of three Rankine-Hugoniot relations) which can be approximated for large Ma as:

$$p/p_o = (2\gamma/\gamma + 1)\, Ma^2 \tag{11b}$$

where

$Ma = \dfrac{V_s}{C}$ = shock front mach number

$V_s$ = shock front velocity

$C$ = adiabatic sound speed

Thus by substituting

$$Ma = dx/d\tau_s = \frac{1}{2x} \tag{12}$$

(from equation (11a)) into equation (11b), equation (11) is obtained as is the variation of the shock front Mach number with scaled distance from the trajectory.

These two relations are generally valid as $R \to O$ for $p/p_o \to \infty$ as does Ma. As $R \to \infty$ however $p/p_o \longrightarrow 0$ as does Ma so that in the weak shock limit these relations must be replaced by more realistic expressions. It is to be noted that in equations (11) and (12) that as $R \to 0$ a limit is also reached where the strong shock similarity solution no longer applies.

The similarity solutions to the equations of hydrodynamics are not valid in general for values of $x \lesssim 0.05$ for several reasons. One of these relates to the finite size of the source and to the finite amount of time it takes to deposit the energy to the atmosphere (Sakurai, 1965). In addition, the intense nonlinear nonequilibrium processes taking place in this region (such as multiple ionization and dissociation of the atmospheric and meteoric species; Millman, 1968) void the concept of local thermodynamic equilibrium (Izakov, 1971). These also void the concept of the existence of the classical equation of state of a perfect gas since this by itself implies a near equilibrium state for the gas. Numerical computations of Brode (1955) and Plooster (1968) show that for small x a complex series of shock waves are formed and these oscillate between the origin and the region near $x = 0.1$ moving mass into the main shock front which subsequently propagates outward as the classical blast wave. For values of $x \gtrsim 5 \cdot 10^{-2}$ the size of the meteor (considered as a single body) no longer has a significant effect on the blast wave propagation; i.e., the mechanism of the energy deposition ceases to influence the blast wave propagation after a certain distance from the source has been attained (Groves, 1963; Tsikulin, 1970).

The slower the meteor is traveling the larger this value of x becomes. For example, Tsikulin (1970) using a detonating fuse of finite size and a constant detonation velocity of $\sim 7$ km/sec found $x \simeq 0.1$ to be the smallest value for which the overpressure ratio decay as predicted by the similarity theory compared well with his experimental results. The value $5 \cdot 10^{-2}$ then represents a reasonable lower limit of x for which the similarity theory is applicable. This extimate assumes the meteor to be traveling at a large velocity and is limited in part by the finite size of the meteor itself. It is thus altitude dependent as a function of the

meteor's size and velocity and represents a distance about 10 meteor diameters away from the trajectory. Thus since $x = R/R_o$ and as will be seen in (17), $R_o \sim M \cdot d_m$, $x = R/M \cdot d_m$ so that the smallest x is $10d_m/M \cdot d_m = 10/M$; where M = meteor Mach number. Therefore, the larger M is (within certain limits), the smaller is the value of x for which the results as predicted by equations (11) and (12) will be applicable. As was previously mentioned, for values of x below about 0.05, the extreme nonequilibrium state makes the similarity solution inapplicable however. It should be noted that the estimate of 10 meteor diameters away from the trajectory is also only an approximate value since experimental and theoretical results indicate a range of values of from 3-20 charge diameters away from a chemical explosive source as the region where the strong shock similarity solution is applicable to actual chemical point or line explosions in the atmosphere (Tsikulin, 1970). Fortunately except at small meteor Mach numbers this distance is not very important for the analysis which follows. See equations (24) and (24a). It should be pointed out that the estimates of 3-20 charge diameters is based on our knowledge of spherical and cylindrical explosives and not for actual ablating meteors traveling through the atmosphere. We assume then that this distance estimate is applicable to all meteors which are not undergoing gross fragmentation. Presumably the more violent the frag - mentation process is the farther this limiting distance from the trajectory becomes (within certain limits).

Thus because of several realistic considerations the predictions of the blast wave theory are only of great value in the intermediate shock strength region ( $10 \leq \Delta p/p_o \leq 1$).

As the blast wave propagates outward eventually a region is reached where the strong shock similarity solution no longer applies (where $p \sim p_o$). Following Jones et. al. (1968) a correct limit equation is sought such that as $x \to 0$

$$\frac{2(\gamma + 1)}{\gamma} \left( \frac{\Delta p}{p_o} \right) = f(x) \to x^{-2}$$

and as $x \to \infty$, $f(x) \to x^{-3/4}$ Here f(x) is given by:

$$f(x) = \left[ \left( \frac{3}{8} \right)^{-3/5} \right] \left\{ \left[ 1 + \frac{8}{3}^{8/5} x^2 \right]^{\frac{3}{8}} - 1 \right\}^{-1} \qquad (12\ a)$$

In the above $\frac{\Delta p}{p_o} = \frac{p - p_o}{p_o} = \frac{p}{p_o} - 1$. In accordance with other authors $p/p_o$ is used in the strong shock region whereas $\Delta p/p_o$ is used in the weak shock and linear regions. In the recent work of Plooster (1968), f (x) as just given is modified slightly using constants "C" and "$\delta$". These parameters can be adjusted so that the predictions made using the modified form of (12a) can be readily compared to the several sets of numerical calculations which he made. In Section VIII (Part 3) the effect of these quantities on our present results will be discussed. Here we have assumed that "C" = "$\delta$" = 1.0.

The exponent -3/4 is chosen from both theoretical and experimental evidence regarding the decay of sonic booms from projectiles and aircraft. See also Section V. Under these restrictions equation (11) is replaced by:

$$\frac{\Delta p}{p_o} \cong \frac{2\gamma}{\gamma + 1} \left( \frac{0.4503}{(1 + 4.803\, x^2)^{3/8} - 1} \right) \qquad (13)$$

where $\Delta p = p - p_o$ = maximum shock wave overpressure (amplitude) attained during the positive phase of the disturbance. This decay law has been experimentally verified for $10 \leq \frac{\Delta p}{p_o} \leq 0.04$ (Jones et. al.,

1968: Tsikulin, 1970).

Equation (11b) is now replaced by

$$\frac{\Delta p}{p_o} = \frac{2\gamma}{\gamma + 1} (Ma^2 - 1) \tag{13a}$$

$$\text{therefore } Ma = \left[ \frac{0.4503}{(1 + 4.803x^2)^{3/8} - 1} + 1 \right]^{\frac{1}{2}} \tag{14}$$

which replaces Equation (12).

Equation (13a) comes from the exact Hugoniot relation between $\Delta p/p_o$ and the shock front Mach number, Ma. Note that as $\Delta p/p_o \longrightarrow 0$, i.e., $p/p_o \rightarrow 1$, $Ma \longrightarrow 1$, i.e., the shock front velocity approaches the local adiabatic phase velocity of sound. This is as it should be if the medium is at rest. For $\Delta p/p_o \lesssim 1.0$ ($x \gtrsim 1.0$) the geometrical acoustics ray approach is assumed to be valid and the propagation laws of weak shock waves must then be considered (Jones et. al., 1968). Note that linear sound wave theory is derived under the assumption that $p/p_o \longrightarrow 1$, i.e., $\Delta p/p_o \rightarrow 0$. Sakurai (1965) uses $\Delta p/p_o = 10^{-6}$ as a criterion for linear sound waves. See Section V for a more precise definition of the transition between weak shock and linear acoustic waves.

Beyond $R_o$, i.e., for $x \gtrsim 1.0$, where $\Delta p/p_o = 0.563$ and $Ma = 1.22$, ray acoustics are assumed to be valid but the amplitude of the wave is by no means completely negligible compared to atmospheric pressure. Note that this choice of x is arbitrary within certain limits (Groves, 1964; Tsikulin, 1970). At $10R_o$ the disturbance is still very strong. At distances as great as $100R_o$, $\Delta p/p_o$ is $\sim 10^{-2}$ and very large overpressures (as compared to $\Delta p$ associated with sonic booms from aircraft where typically $\Delta p/p_o \lesssim 10^{-3}$) would still be expected. This assumes that the $x^{-3/4}$ dependence is still valid. When the wave

expansion has proceeded to a distance approaching the length, $\ell$ , of the line source, the further expansion is more nearly that of a spherical wave (Few, 1969). In the exact mathematical formulation of cylindrical blast wave line sources, the line is assumed to be of infinite length (Lin, 1954). The finite length of the line in the case of meteor induced blast waves results in spherical radiation at both ends of the line source (into an upward and downward hemisphere) if the meteor does not "explode" as a bolide before penetrating to z''''. This finite source length is only important then when $R \gtrsim \ell$ . Plooster (1968) has also shown that a finite line source length causes the disturbance produced to deviate slightly from the predictions of the strong shock line source similarity solution. His experimental results indicate a rapid convergence to the similarity solution however. Thus under certain conditions the source can be modeled as a semi-infinite cylindrical charge explosion (Korobeinikov, 1971).

The above discussion assumes the line source to be in the free field; i. e., independent of reflections set up at finite boundaries (i. e., local topographical features). In addition, the diffusing effects of atmospheric turbulence have not as yet been discussed. In Section V and Section VI (Part 3), this effect will be briefly considered again. Equations (13) and (14) are plotted as a function of x in Figures 60 and 61 (for an assumed uniform atmosphere at rest). See also Figure 100a and 100b.

Following Few (1968), the cylindrical blast wave relaxation radius $R_o$ is defined as follows: (for an ideal line source, i. e., of infinite length and assuming the charge diameter is infinitely small):

$$R_o = (E_o/\pi p_o)^{1/2} \qquad (15)$$

where

$E_o$ = finite amount of energy deposited by the source per unit path length and $p_o$ is the ambient hydrostatic atmospheric pressure.

$E_o$ and $R_o$ appear as parameters in the similarity transformation for solving the hydrodynamic equations. $E_o$ involves both the thermal thermal and the kinetic energy carried by the blast wave and is equal to the energy released from the source. Since the assumed hydrodynamic equations do not allow for viscosity and heat conduction as well as for radiation effects, the sum of the thermal and kinetic energy carried by the blast wave (in the strong shock region) must remain constant (Sakurai, 1965).

The inclusion of real gas effects in the cylindrical blast wave problem has recently been accomplished (Plooster, 1968). Plooster has shown that their inclusion reduces slightly $\Delta p/p_o$ as compared with the values predicted assuming ideal gas behavior. Thus this model represents the maximum amplitude case for the strong shock region (within the limitations related to the assumed initial conditions, i.e., "C" = "$\delta$" = 1). For the general inclusion of these near equilibrium radiation losses the reader is referred to the work of Plooster (1971). Further discussion on this subject is limited to Section V and Section VIII (Part 3).

Following Lin (1954) and using the two meteor models developed earlier, $E_o$ can be written as:

$$E_o = \frac{1}{2} \rho_o V^2 C_D A \qquad (16)$$

Thus $E_o$ is readily expressable using the drag force in dynes (or the energy deposited per unit length in erg/cm). Putting this expression in (15) results in the following:

$$R_o = V\left(\frac{C_D A}{2\pi g H}\right)^{1/2} = 0.418\, M \cdot d_m \sim M \cdot d_m \qquad (17)$$

where

$M$ = Meteor Mach Number (i.e., V/C)
$d_m$ = meteor diameter
$\rho_o$ = ambient atmospheric density
$C_D$ = 1.0
$\gamma$ = 1.40

since in this assumed isothermal atmosphere $\rho_o = p_o/gH$ and $C^2 = \gamma gH$.

It should be noted at this point that various authors define $R_o$ differently. A few examples of these definitions are:

Tsikulin (1970), $R_o = \left(\frac{E_o}{p_o}\right)^{1/2}$, Basic Definition (17a)

Tsikulin (1970), $R_o = \left(\frac{2E_o}{p_o}\right)^{1/2}$, Modified Definition (17b)

Sakurai (1965), $R_o = \left(\frac{E_o}{2\pi p_o}\right)^{1/2}$ (17c)

Jones et. al. (1968) $R_o = \left(\frac{4E_o}{\gamma b p_o}\right)^{1/2}$ (17d)

where

$b = 3.94$ for air considered as a diatomic gas (with $\gamma = 1.40$).

The modified definition of Tsikulin was chosen on the basis of his experimental results. The $\sqrt{2}$ factor increase in his modified definition is based on the concept of "TNT equivalence" for supersonic flow. See Section VIII (Part 3) for more details. Thus a range of $R_o$ values are possible using the above definitions. The maximum possible difference in evaluating $R_o$ resulting from these definitions is a factor of 3.53. This uncertainty will enter into the error estimates of the prediction of meteor size and energy release, etc. using the present theory. See Section VII

(Part 3). Following the experimental work of Tsikulin (1970) we have chosen to write the relaxation radius in equation (17) as simply being the product of the meteor Mach number and the meteor diameter.

Thus for Model 1 (Section III), $R_o(z)$ varies as V(z) since the factors inside the square root are assumed constant. $R_o$ versus altitude for the various ranges of the variables chosen earlier is plotted in Figures 62-73 for this model. For Model 2, not only does V(z) change more quickly toward zero than it does for Model 1 (due to ablation), but A now decreases exponentially due to ablation also. As a result $R_o(z)$ as seen in Figures 62-73, becomes far less constant than in the case of Model 1. For both models the extremes at entry, $11.2 \leq V_E \leq 30$km/sec were used. Since few large meteors have ever been observed with $V_E > 30$km/sec, the earlier extreme, 73.2 km/sec. has been discarded.

With this knowledge of $R_o$, Figures 60 and 61 become more meaningful. At x=1, $R=R_o$ and in this vicinity the disturbance can be approximated as a plane weak shock wave. See Section V. Once $R_o$ is known as a function of altitude this decay distance is known as a function of altitude. At about this distance ($x \gtrsim 1.0$) the characteristic velocity of the weak disturbance is defineable and the refractive effects of the temperature and the wind field can then be studied. See Section IV B and C. At $x \gtrsim 1.0$, the original nonsteady flow is approximately steady so that the steady state theory for which the characteristic velocity is derived is then applicable. Beyond about x=1.0 the radius of the blast wave no longer oscillates significantly as it did near smaller x (Brode, 1955) and the assumption of steady flow is then justified (Groves, 1963). Note that the properties of the basic state of the medium must also be assumed steady for this analysis to apply.

It is to be noted that the atmosphere into which the blast wave expands is assumed to be of uniform pressure and at rest. The latter assumption is reasonable since $V_s >> W$ during most of the decay period (where $W$ is the magnitude of the mass average motions in the gas, i. e. winds). The calculations for $R_o$ using the present meteor models indicate that this decay distance for the more energetic (and relatively rare) meteors ($r_{mE} \gtrsim 5$ meters) can approach values up to 1. 0 kilometer and larger. As will be seen in Section V, if $R_o << H$, the effect of the nonuniform medium on the expanding blast wave is not significant (i. e., the shock wave has already become weak before the atmospheric density varies appreciably). See also Section VI (Part 3).

It would appear then that for meteors entering nearly horizontally (i. e., for small $\alpha$) with $R_o << H$, the line orientation is such that the uniform atmosphere assumption is reasonable. This is true then both along $\ell$ and within a distance $R_o$ from the trajectory. At very large $\alpha$ the uniform atmosphere approximation (i. e., along $\ell$) is far less valid. Fortunately as will be seen in Section VI (Part 3) for the meteor size range of interest the maximum probability occurance of meteors is for $\theta$ equal to 35 to $40^o$. Thus for most of the cases of interest the uniform atmosphere assumption (along $\ell$ and out to a distance $R_o$ from the trajectory) appears reasonable. See also Section V D. for the nonuniform atmospheric correction term used between a specified altitude along $\ell$ and lower observation altitudes. When the uniform atmosphere assumption is not reasonable along $\ell$ the primary matter of concern is that p(z), i. e. the ambient hydrostatic pressure, should still remain small compared to the pressure at the shock front during the outward expansion of the pulse. Since meteors are less energetic at lower altitudes (i. e. M decreases ) and the hydrostatic pressure

increases with lower altitudes, for very nonuniform paths the strong shock blast wave region may not form at all (See Groves, 1963). This possibility has not been formally considered in this analysis. See Figures 62-73. See also Section VIII (Part 3).

As will be seen in Section V the blast wave is not significantly altered by changing the ambient density (or pressure) at the altitude and time of the energy release. Groves (1964) and Plooster (1968) have shown that varying the ambient density produces a solution which rapidly converges to the solution using the original ambient values. Thus, as is discussed in Section V, at weak shock amplitude levels the disturbance is not very sensitive to changes in the ambient conditions. Plooster used five different sets of initial conditions for his calculations (i.e., ideal gas, real gas, low density gas, etc.) which produced five different $\Delta p/p_o$ variations with x. See Section VIII (Part 3) for more details on this subject.

In order to consider the refractive effects of the atmosphere on the propagation of meteor sounds one additional concept should be discussed further. In the cylindrical blast wave model a line source of energy, deposited instantaneously, was assumed. In the case of sound generated by lightning discharges the concept of instantaneous energy deposition is quite good. In the general case for meteors, however, this concept needs further clarification.

As was stated earlier, for $z' \geq z \geq z''''$, the meteor trajectory is a straight line. If, however, the entire flight during which the blast wave is generated, is to be considered as an instantaneous energy release, then the following relation must hold (Lin, 1954):

$$\frac{t'}{t} << 1 \qquad (18)$$

where

$t$ = time for the blast wave to decay out to weak shock conditions (i.e., $x \rightarrow 1.0$)

$t'$ = total time during the flight of the meteor during which the bow shock wave was generated

The time t depends on the cylindrical blast wave model and on the criterion chosen for the shock wave to decay to a weak disturbance. This distance from the trajectory has been chosen as $R_o$. Since for Model 1, $R_o$ = f(V) only, t is relatively constant over a portion of the flight. For Model 2, $R_o$ = f(V, A) and t is a rapidly changing function with altitude. For this case an average value of t, can be used to evaluate expression (18). See equations (20) - (23).

The assumed isothermal model atmosphere can be used to evaluate (18) utilizing average quantities as determined over discrete altitude intervals (or layers). Thus the criterion for an instantaneous energy release can now be written as:

$$\frac{\sum_i t_i'}{\overline{t_i}} << 1 \qquad (19)$$

where

$t_i$ = time for the blast wave to decay out to weak shock conditions for energy deposited within layer i.

$\overline{t_i}$ = average value of $t_i$ during the meteor entry

$t_i'$ = time during the flight of the meteor in layer i during which the bow shock wave was generated.

General expressions for t and $t_i$, as a function of x, and t' and $t_i'$ follow. Following Jones et. al. (1968)

$$t = \frac{R_o}{2C}\left[(1 + 4x^2)^{\frac{1}{2}} - 1\right] \qquad (20)$$

for $x \geq 5 \cdot 10^{-2}$ and $R_o << H$

Therefore,
$$t_i = \frac{R_{oi}}{2C}\left[(1+4x_i^2)^{\frac{1}{2}} - 1\right] \qquad (21)$$

or
$$\overline{t_i} = \frac{\overline{R_{oi}}}{2C}\left[(1+4x_i^2)^{\frac{1}{2}} - 1\right] \qquad (21a)$$

Following Groves (1957)
$$t' = \frac{1}{\sin\theta}\sum_{i=m}^{N}\frac{\Delta Z_i}{\overline{V}_i} = t'_m + t'_{m+1} + \ldots + t'_N \qquad (22)$$

where

$i$ = m begins in the layer where Kn (or $\overline{Kn}$) = 0.05

$i$ = N ends in the layer where $\overline{V}_i \rightarrow C$

$\overline{V}_i$ = average velocity of the meteor in the ith layer

$\Delta Z_i$ = layer thickness

$t_i' = \frac{1}{\sin\theta}\left(\frac{\Delta Z_i}{\overline{V}_i}\right)$; and the integral has been replaced by a summation. (23)

The criterion for an instantaneous energy release can then be written as:
$$\frac{1.618 \cdot 10^5}{\sin\theta \cdot \overline{M} \cdot \overline{d}_m}\sum_{i=m}^{N}\left(\frac{1}{M_i}\right) << 1 \qquad (24)$$

where

$\Delta z_i$ = 1 $10^5$ cm

$x$ = 1.0

$\overline{M}$ = average meteor Mach number below the altitude where the Knudsen number is less than 0.05

$\overline{d_m}$ = average meteor diameter below the altitude where the Knudsen number is less than 0.05 (with $\overline{d_m}$ in cm)

and equation (17) has been substituted for $R_{oi}$. See Figures 62-73 and 98a, 98b and 98c. for the results using equation (24)

Equation (24) must be continually tested throughout the meteors flight. In those layers where it is satisfied the concept of an instantaneous energy release is meaningful.

The results of these calculations indicate that for only very large fast meteors is the instantaneous energy release concept justifiable. The question to be answered then is under what conditions can the energy release not be strictly instantaneous and yet the predictions of cylindrical blast wave theory still be applicable. Fortunately Tsikulin (1970) has provided an answer to this question. Tsikulin has shown that it is possible to neglect the fact that the energy release isn't instantaneous under certain conditions of flight. In his analysis he has shown that this problem can be treated as locally one dimensional sufficiently far behind the entering meteor if only two conditions are satisfied. These conditions are:

$$\left.\begin{array}{l} \text{i)}\ V = \text{constant} \\ \text{ii)}\ V >> C \end{array}\right\} \quad \text{with Kn or } \overline{Kn} \leq 0.05 \qquad (24a)$$

The second criterion demands only that $\alpha$, the Mach angle is very small at a distance of many body diameters behind the meteor. At about Mach 15 and greater this angle is already less than four degrees and thus it can be assumed negligibly small. See equation (25) for the definition of $\alpha$. The general oblique shock problem (with a parabolic shape for blunt compact entry bodies traveling at a very large constant velocity with respect to that of sound) can then be reduced to a normal shock problem sufficiently far behind the meteor.

Thus for the regions of flight for which the above criteria are maintained the general equations governing the shock wave propagation can be reduced to those which are solved in the cylindrical blast wave theory. Under these conditions a similarity exists between the

two flows. The regions of applicability of the cylindrical blast wave model using the later criteria as well as the instantaneous energy release criterion are shown in Figures 62-73. It is seen in these figures that in the altitude regions where intense deceleration and ablation are occuring the above criteria can not be met. Thus only for those portions of the trajectory for which $R_o \simeq$ constant and $M \gg 1$ can the analogy between cylindrical blast waves and hypersonic flow be made. This is consistent with the conclusions of Bronshten (1964) regarding ablation and energy transfer from the shock wave back to the meteor. The above conclusions are also consistent with the work of Pan and Sotomayer (1972).

Thus the instantaneous energy release criterion is just a special case of the latter criteria due to Tsikulin. In the instantaneous case V is constant but extremely large. These more general criteria due to Tsikulin allow energy similarity beyond distances on the order of 10 meteor diameters from the trajectory and far enough behind the meteor so that the flow can be considered as locally one dimensional and axi-symmetric. Under these conditions of flight the finite propagation velocity of the pertubation source along $\ell$ can be neglected for the blunt compact entry bodies which have been considered. Thus the cylindrical blast wave analogy to hypersonic flow can be safely extended to much lower altitudes than would be indicated if equation (24) was used strictly as the criterion.

Obviously as $V \rightarrow C$, the sonic boom case must in the limit be realized (again ignoring the total breakup possibilities). This transition region will not be considered at this point. See Section V and Section VIII (Part 3) for additional details.

One further point should be made. In the refraction analysis which follows when $V \neq$ constant (with $V >> C$) the nonsteady problem is then encountered. Rays originating at high altitudes are not related

in time in a steady manner to those originating at lower altitudes. In a full ray tracing analysis where travel times and arrival angles are the goal, the ray tracing must then be carried out in the reference frame of the steady wind field, rather than in that of the meteor trajectory. This is because the Galilean transformation is not valid for the nonsteady problem (Hayes et. al., 1969). Thus in the earlier portions of the meteor entry where $V >> C$ and $V$ = constant this comment is not applicable. In the present analysis which follows a full ray tracing procedure has not been carried out. This will be done for well documented meteor sound observation cases in a later report.

Throughout this analysis the energy conservation principle will be maintained. The above discussions of instantaneous versus steady continuous energy release combined with the attenuation treatment in Section V will assure this to be true.

B. EFFECTS OF THE TEMPERATURE FIELD

In a horizontally stratified steady atmosphere without wind where a slowly varying vertical temperature gradient is allowed, the characteristic velocity, $k(z)$, is constant and remains such throughout the propagation for all plane weak shock front elements originally generated at the same altitude (Groves, 1957). It is to be noted that the characteristic velocity is also often referred to as the Snell's Law constant (Hayes et. al., 1969). Because of the relatively high frequencies which exist near the source a layer thickness of 10 km was chosen for the atmospheric model (i. e. nonisothermal climatological model with linear gradients of temperature allowed within each layer). This value is considerably greater than the wavelengths of the disturbance near the source so that within the context of a W K B slowly varying medium diffraction and reflection effects can be neglected (Craig, 1965). Since in

general the frequency of the pulse decreases as it gets further away from the source, the relatively large layer thickness chosen will satisfy both the frequency at the source as well as at the observer with respect to diffraction and reflection phenomena. See equation (91). See also Section VII (Part 3). The directional variations of the horizontal wind systems as a function of altitude introduce an anisotropic effect which will be considered in Section IV C. For the line source meteor sound problem k(z) can be written as (For downward traveling rays without wind):

$$k(z) = C(z) / |\sin(\theta - \alpha)| \tag{25}$$

where

$\alpha = \sin^{-1}(C(z)/V(z))$ = Mach angle of the meteors shock cone

$\theta$ = horizontal entry angle of the meteor

Expanding the sine term from elementary trigonometry and substituting:

$$\cos\alpha = (V(z)^2 - C(z)^2)^{\frac{1}{2}} / V(z)$$

the following is obtained.

$$k(z) = \frac{C(z)\,V(z)}{|(V^2(z) - C^2(z))^{1/2} \sin\theta - C(z)\cos\theta|} \tag{25a}$$

See Figure 74a and 74b for the geometry of the situation. For $V >> C$ (i.e., $\alpha \rightarrow 0^{\circ}$) (25 a) reduces to

$$k(z) = C(z) / \sin\theta \tag{26}$$

The historical convention for deducing characteristic velocity produces the equation: (with $V >> C$ but without considering winds)

$$k(z) = C(z) / \cos\theta' \tag{26a}$$

In the above, $\theta' = \pi/2 - \theta$, where $\theta'$ is the elevation angle of the acoustic ray. In this analysis $\theta$ has been used throughout for deducing the characteristic velocity.

The characteristic velocity is assumed to be defineable at $R_o$ beyond which the geometrical acoustics approximation is valid. In addition it is also assumed that beyond $R_o$ the disturbance is approximately plane. See also Section V C. In general the larger the meteor and the faster it is traveling, the further $R_o$ is away from the trajectory.

In order to study the effects of the temperature field on the refraction of meteor sounds, Groves' graphical technique (1957) will be utilized. This technique determines whether or not the temperature field will "allow" sounds to follow paths which will reach ground level. The objective then is to determine those conditions under which refractive paths to ground level are possible. In a later report full ray tracing procedures will be used to determine travel times and arrival angles for comparison with well documented meteor sound events.

For a ray starting from a source altitude $z_z$ to reach the ground the following criterion must be satisfied (Groves, 1957):

$$k(z_z) > C_{MAX}(z) \qquad \text{for } 0 \leq z \leq z_z \tag{27}$$

where

$C_{MAX}(z)$ = Maximum value of the adiabatic sound speed between $z_z$ and the ground

For a given meteor the value of $\sigma$ in equation (26) is fixed for $z' \geq z''''$ (i.e., it is the value the meteor had at $z'$). For this reason if $V >> C$, $k(z)$ varies directly as $A \cdot C(z)$ (where A is a constant). It is evident from (26) that $\sigma = 90^o$ (vertical entry) represents the smallest value of $k(z)$ obtainable for any given atmospheric structure. For meteor entry angles approaching $0^o$, $k(z)$ tends toward infinity. The near vertical entry case then represents rays passing through the stratified medium at nearly grazing incidence. It should be noted however that for rays traveling almost horizontally through a given

layer, the criterion expressed in (27) is only approximate. For very small angles to the local horizontal (i.e., approaching $0^{o}$) the ray approach must be abandoned in favor of a full wave treatment, i.e., Snell's law breaks down for purely horizontal rays entering horizontally stratified media (Sachs, 1970). In this case a "critical" ray (which is traveling horizontally)often termed a precursor, lateral or head wave is generated. This wave is not predictable on the basis of ray acoustics alone and arrives earlier than the predicted arrival times obtained using the ray theory. Atmospheric precursors may then be possible. The author is not aware of such observations of this effect however. According to Sachs (1970), this effect is frequently observed in underwater sound propagation studies. In view of later theoretical developments such as the neglect of ray focusing effects in the atmosphere, the precursor wave will not be considered further in this analysis. Also as will be seen in VI (Part 3) the probability of $\theta$ exceeding $65^{o}$ is very small. Thus this case (i.e., $V >> C$ and $\theta = 90^{o}$) is probably not of practical interest for the line source meteor sound propagation problem.

In addition, horizontal inhomogeneities which are neglected here would then have to be included when considering the refraction problem for nearly vertical meteor entry ($\theta \gtrsim 88^{o}$). For more details on ray propagation including the effects of horizontal inhomogeneities in the medium see Warfield (1971). As $\theta$ decreases toward a purely horizontal entry, the value of k(z) in (26) is dominated by the sine term. For very small $\theta$, rays enter the stratified medium nearly vertically (i.e., at right angles to the layers) and essentially unrefracted paths to ground level are then possible. As the meteor slows down such that $V \sim C$, (26) is no longer valid. Equation (25) shows however that k(z)

will tend toward infinity as $\alpha \to \theta$. The altitude region in which this occurs depends primarily on the meteor model chosen.

For the line source model chosen, the effects of refraction on meteor sound propagation will be considered both within and outside of the entry plane. See Figure 75 for the geometry of the situation. It should be noted that for $\theta \equiv 90^{\circ}$ and $\theta \equiv 0^{\circ}$ these two distinctions are not meaningful.

The expressions for the characteristic velocity within and outside of the entry plane can be written as (assuming V >> C):

$$k(z) = C(z) / \sin \theta \tag{28}$$

$$k'(z) = (C(z) / \sin \theta) \left[ \sin^2 \theta + (1 - \frac{2\Delta\phi}{\pi})^2 \cos^2 \theta \right]^{-\frac{1}{2}} \tag{29}$$

where

$k'(z)$ = characteristic velocity outside of the entry plane

$k(z)$ = characteristic velocity within the entry plane

$\Delta\phi = |\phi - \phi'|$

$\phi$ = azimuth angle of the meteor heading (measured as increasing clockwise from North as viewed from above)

$\phi$ = azimuth angle of a given ray outside of the entry plane (as measured $180^{\circ}$ from the heading of the ray)

(Note: when $\Delta\phi = 0^{\circ}$, $k'(z) = k(z)$ and when $\Delta\phi = 90^{\circ}$ ($\frac{\pi}{2}$ radians), $k'(z) = C(z)$)

Thus the assumption V >> C makes equations (28) and (29) independent of the meteor velocity. When considering refraction then the actual meteor models chosen are less crucial to the problem over a relatively large altitude range.

In the discussion which follows there are two types of refractive paths which are to be considered. The first is the direct ray path in the plane of entry. The second is the direct and multipath arrivals outside the entry plane.

Within the entry plane (27) must be satisfied. For $10 < \theta < 90^{o}$, with $V >> C$, the direction of ray travel is such that sounds may initially arrive from the general direction of the meteor heading, but later may arrive traveling toward the general direction of the meteor heading (Wylie, 1932). This simplisitic description is limited by many factors. The meteor must not explode (as a bolide) during the flight. For this case a point source effect would need to be considered. At any one location only a portion of the sound generated along the flight will reach the observer. Local topographic influences must also be considered. In addition refraction aloft (including the effects of winds) will determine the allowed paths to the ground. For small $\theta$, the sine term dominates k(z) and the latter statement does not apply. This refraction aloft must be considered for rays with initially partial downward and upward paths. The description here has considered only the partial downward paths (for $10 < \theta < 90^{o}$). While multipath refractive arrivals are possible within the entry plane, distinguishing them from the direct arrivals would be difficult.

Outside the entry plane the following must be satisfied:

$$k'(z_z) > C_{MAX}(z) \qquad 0 \leq z \leq z_z \qquad (30)$$

For $\Delta\phi \equiv 90^{o}$, $k'(z) = C(z)$ and the ray is again traveling purely horizontally. As before the refraction effects discussed here as $k' \rightarrow C$ are only approximate (for nearly horizontal ray directions). Equation (29) is most likely to satisfy equation (30) for small values of $\Delta\phi$. This implies that direct ray propagation to the ground via refraction is most likely near the entry plane. For small $\Delta\phi$ and $\theta$ the ray directions are nearly vertical and k'(z) is large.

Consider Figure 77. The middle latitude seasonal variation of the sound speed profile shows that for all seasons $C_{MAX}(z) = C_{MAX}(o)$

(for $o \leq z \leq 100$km). See Section IV C. Therefore the only way sounds can reach ground level in the entry plane is if $\theta$ is small enough so that the sine term makes k(z) greater than $C_{MAX}(o)$. Since C(z) varies about ± 10% about some mean value, the $\sin\theta$ dependence becomes important when $\theta \sim 60^{o}$ or less. Outside the entry plane the combination of C(z), $\theta$ and $\Delta\phi$ will determine the possible paths to ground level in the absence of winds (see Figure 75). In the region where $\alpha \rightarrow \theta$, k(z) will approach very large values and refractive propagation to the ground is then possible within the entry plane. When the wind effects are considered in Section IV C these statements will be reconsidered. Small scale temperature profile variations about these seasonal averages will change the time and angle of arrival of these sounds but not the conclusions regarding allowed ray paths to the ground. Tropospheric temperature inversions at an altitude $z_I$ which greatly exceed ground temperature may prevent sounds from reaching ground level, but for all values of k(z) and k'(z) exceeding $C_{MAX}(z_I)$, $0 \leq z_I \leq z$, which may reach a given ground area, refractive paths to ground level are then possible.

## C. COMBINED EFFECT OF THE TEMPERATURE AND THE WIND FIELD

In this section the modifications of Section IV B needed, when considering the effects of steady horizontal wind fields on the propagation of meteor sounds, will be presented. The general case allowing for cross wind propagation effects (i.e., at right angles to a given ray direction) has not been considered in the simple expression for the characteristic velocity as written below. Such effects will not influence the validity of the conclusions reached however. For this more general case, see the theoretical treatment of Groves (1955), Bartman (1967) and Hayes et. al. (1969). See also the work of Diamond (1964).

When steady horizontal winds are considered, equation (25a) becomes:

$$k(z) = \frac{C(z)\ V(z)}{\left|(V^2(z) - C^2(z))^{1/2} \sin\theta - C(z)\cos\theta\right|} + W(z)\cos(\phi - \psi(z)) \tag{31}$$

where

$W(z)$ = magnitude of the horizontal wind as a function of altitude ($\sqrt{u^2 + v^2}$)

$\psi(z)$ = azimuthal direction of the horizontal wind (the direction the winds are coming from measured as increasing clockwise from North as viewed from above) as a function of altitude.

$u(z)$ = magnitude of the zonal wind as a function of altitude

$v(z)$ = magnitude of the meridional wind as a function of altitude

Once again propagation is considered both within and outside of the entry plane. Within the limit of the approximation $V >> C$, equations (28) and (29) now become:

$$k(z) = \frac{C(z)}{\sin\theta} + W(z)\cos\ (\phi - \psi(z)) \tag{32}$$

$$k'(z) = \frac{C(z)}{\sin\theta}\left[\sin^2\theta = (1 - \frac{2\Delta\phi}{\pi})^2\ \cos^2\theta\right]^{\frac{1}{2}} + W(z)\cos(\phi' - \psi(z)) \tag{33}$$

See Figure 76a and 76b for the geometry of the situation.

The criterion for refraction to the ground is now (replacing equation (27) and (30)):

$$k(z)_z > C_{eff}(z)\Big|_{MAX} \qquad \text{for } o \leq z \leq z_z \tag{34}$$

and

$$k'(z_z) > C_{eff}(z)\Big|_{MAX} \qquad \text{for } o \leq z \leq z_z \tag{35}$$

where

$$C_{eff}(z) = C(z) + W(z)\cos(\phi' - \psi'(z)) \tag{36}$$

which is the effective (horizontal) sound velocity as a function of altitude (including the effects of both temperature and wind).

In Figures 80 and 81 effective sound velocities to the East and to the West as a function of altitude and season are shown. These graphs were generated using the information in Figures 77 and 78. In Figure 77 the adiabatic sound speed is plotted as a function of altitude using the nonisothermal climatological model from the U. S. Standard Atmosphere Supplements, 1966 (after Donn and Rind, 1972). In Figure 78 the zonal wind field is plotted as a function of altitude (after Batten, 1961). Figures 80 and 81 were generated using equation (36) after tabulating the information in Figures 77 and 78 in 10km layers. A scalar analysis was then performed on this data to produce Figures 80 and 81. In Figures 78, 80 and 81 only zonal winds have been considered. In middle latitudes for the altitude regions under consideration this is generally a good approximation up to about 80km (Theon et. al., 1972). The meridional winds will certainly influence the direction of propagation to some extent but generally they will have little effect on whether or not (34) and (35) can be satisfied (at least on a climatological mean basis). Within the 10km thick layers chosen, linear gradients of temperature (or sound speed) and horizontal wind are allowed. Note that strictly speaking linear gradients of sound speed and wind do not fulfill the WKB approximation exactly. This is due to the fact the first derivative of such functions is not continuous across the boundary between two consecutive layers. While parabolic gradients will fulfill the approximation of a slowly varying medium exactly they have not been included in the present analysis.

Since layers 10 km thick do not accurately represent small scale vertical atmospheric structure, care was taken in the averaging technique so that the gross vertical atmospheric structure would be

clearly retained. The smaller scale structure referred to above will change the azimuth and elevation angle of the sound arrival but generally it shouldn't influence whether or not refractive paths to the ground exist. The "scale" as used above refers to both the magnitude as well as to the vertical extent of the temperature and wind gradients allowed. Thus a mean value of sound speed and wind was determined at the base of each 10km layer. These values were then connected using straight line segments. This method accounts for the nonsmooth character of Figures 82-97.

We will now consider a purely zonal and a purely meridional meteor entry to illustrate the effect of temperature and wind on meteor sound propagation. With this approximation in mind equations (32) and (33) become (with $10 < \theta < 90^{o}$, $W(z) = u(z)$, and $\Delta\phi = 0$ or $\Delta\phi = 90^{o}$. (See next page)

These equations are valid if $V >> C$ and if $u >> v$ (as a function of altitude). It has been assumed throughout that only rays with initially partial downward paths need to be considered. Attenuation arguments in Section V will be offered to support this statement. For the initially partial downward ray paths the following convention for $\phi$ (and $\phi'$) and $\psi$ have been used. In the entry plane k is in a propagation direction $180^{o}$ from $\phi$. That is for West to East zonal entry the direction of k is Westward and $\phi = 90^{o}$. For East to West entry, k is Eastward and $\phi = 270^{o}$. Outside of the entry plane for meridional entry (North to South or South to North) the direction of $\phi'$ is referenced $180^{o}$ from the actual propagation direction of k. For South to North Entry and propagation from West to East, $\phi' = 270^{o}$ and k is directed Eastward. For propagation from East to West, $\phi' = 90^{o}$. For all the cases $\psi$ is measured as the azimuth from which the wind blows. Note that for the equations which are listed for propagation

| | Zonal Entry | | Meridional Entry | |
|---|---|---|---|---|
| | West to East | East to West | South to North | North to South |
| Westerly Winds $\psi = 270^{o}$ | | | | |
| Prop. to North | $k'(z) = C(z)$ (37) | $k'(z) = C(z)$ (39) | * (41) | $k(z) = \frac{C(z)}{\sin \theta}$ (43) |
| Prop. to East | * | $k(z) = \frac{C(z)}{\sin \theta} + u(z)$ | $k'(z) = C(z) + u(z)$ | $k'(z) = C(z) + u(z)$ |
| Prop. to South | $k'(z) = C(z)$ (38) | $k'(z) = C(z)$ (40) | $k(z) = \frac{C(z)}{\sin \theta}$ (42) | * (44) |
| Prop. to West | $k(z) = \frac{C(z)}{\sin \theta} - u(z)$ | * | $k'(z) = C(z) - u(z)$ | $k'(z) = C(z) - u(z)$ |
| Easterly Winds $\psi = 90^{o}$ | | | | |
| Prop. to North | $k'(z) = C(z)$ (45) | $k'(z) = C(z)$ (47) | * (49) | $k(z) = \frac{C(z)}{\sin \theta}$ (51) |
| Prop. to East | * | $k(z) = \frac{C(z)}{\sin \theta} - u(z)$ | $k'(z) = C(z) - u(z)$ | $k'(z) = C(z) - u(z)$ |
| Prop. to South | $k'(z) = C(z)$ (46) | $k'(z) = C(z)$ (48) | $k(z) = \frac{C(z)}{\sin \theta}$ (50) | * (52) |
| Prop. to West | $k(z) = \frac{C(z)}{\sin \theta} + u(z)$ | * | $k'(z) = C(z) + u(z)$ | $k'(z) = C(z) + u(z)$ |

NOTE: * represents the cases for initially upward heading rays which are not considered here.

out of the entry plane, $\Delta\phi = 90^{o}$. As mentioned earlier, for purely horizontal rays equation (35) is only approximate. These equations have been written only to illustrate the general effect however. Later in this section equation (33) will be used to study the refraction possibilities where $\Delta\phi \neq 90^{o}$.

We will consider Figures 80 and 81. It can be seen that the winds have a profound effect on long distance ducting of sound waves, both as a function of altitude and of season. In summer conditions are favorable for propagation to the west in a sound duct between 40-64 km and the ground (commonly termed the lower sound duct). In winter conditions are favorable for propagation to the east in a duct between 50-85km and the ground. These general remarks refer to ducted sound propagation outside of the entry plane for those rays for which (35) is satisfied. The primary wind systems of interest which produce these seasonally averaged well-defined sound ducts are in the vicinity of the stratopause region. For the stratospheric wind systems, the months of May and October represent transitional periods between the summer and winter regimes. This varies however depending on what altitude region is under consideration. Propagation in the Spring and in the Fall (via multipath sound ducts) is less likely since the stratospheric zonal winds are generally weaker than their summer or wintertime values.

It should be noted that these figures represent the effective sound velocity climatology of this region of the atmosphere. Statistical deviations about these values can be quite large however. (Theon et. al., 1972). The wind and temperature fields in the vicinity of the lower thermosphere can also produce sound ducts with the ground (Craig, 1965). This is commonly termed the upper sound duct (or channel). Very few meteors are large enough for these upper wind and temperature systems

to be significant in terms of refraction during entry. This sound channel may be important however for ducted propagation out of the entry plane if the attenuation of the signal is not too great (Donn and Rind, 1972) See also Section V D.

It appears to be an observational fact that few meteors have ever produced audible sounds at ground level from altitudes above about 50 km (McKinley, 1961). Groves (1957) quotes a value of 60 km for the upper limit, however. While the models developed in III definitely allow for meteor sound sources above this altitude, it would appear that for most of these the fundamental frequency (i.e., the frequency at maximum amplitude) has either shifted significantly below the audible frequency range by the time the pressure signal has reached ground level or the amplitude of the wave is below the audible threshold of the ear. A combination of these may also be possible. For more information on these possibilities see Section V. Also see Figures 82-97 for the refractive path possibilities involved.

In order to deal with equations (32) and (33), several pieces of information regarding the meteor models needs to be summarized. In this analysis the two density extremes of the meteor models developed will be used as upper and lower altitude bounds respectively for the effective model discussed earlier with $0 \leq \sigma \leq 5 \cdot 10^{-12}$ sec$^2$/cm$^2$. Before k(z) and k'(z) can be defined $R_o$ must be reached and this value is a variable depending on both the meteor velocity and on its cross-sectional area. While we are treating only those cases where $R_o << H$ in this analysis we are essentially assuming $z - R_o \cong z$. Therefore k(z) and k'(z) can be defined without considering $R_o$ as long as $R_o << H$. See Section V C. Equation (24a) must also be tested to find out the

altitude regions for which the cylindrical blast wave decay predictions are applicable. In addition the altitude at which the Knudsen number is equal to 0.05 is needed for the effective model discussed above. This information is summarized in Table 4A and 4B.

In the analysis which follows a way was also needed to transfer from the isothermal hydrostatic atmosphere used for the entry dynamics to the climatological nonisothermal atmospheric model. The following values of $z$ and $z_{ni}$ (to the nearest kilometer) were obtained using the deviations in density with altitude between the three atmospheric models shown in Figure 79.

In January:

| $z$ | $z_{ni}$ | Layer Number |
|---|---|---|
| 0 | 0 | 1 |
| 5 | 6 | 1 |
| 10 | 10 | 1 |
| 15 | 15 | 2 |
| 20 | 19 | 2 |
| 25 | 23 | 3 |
| 30 | 27 | 3 |
| 35 | 32 | 4 |
| 40 | 36 | 4 |
| 45 | 40 | 5 |
| 50 | 45 | 5 |
| 55 | 50 | 6 |
| 60 | 55 | 6 |
| 65 | 61 | 7 |
| 70 | 66 | 7 |
| 75 | 71 | 8 |
| 80 | 75 | 8 |
| 85 | 80 | 9 |
| 90 | 85 | 9 |
| 95 | 89 | 10 |
| 100 | 92 | 10 |

In July:

| z | $z_{ni}$ | Layer Number |
|---|---|---|
| 0 | 0 | 1 |
| 5 | 5 | 1 |
| 10 | 11 | 1 |
| 15 | 16 | 2 |
| 20 | 20 | 2 |
| 25 | 24 | 3 |
| 30 | 28 | 3 |
| 35 | 33 | 4 |
| 40 | 37 | 4 |
| 45 | 42 | 5 |
| 50 | 47 | 5 |
| 55 | 53 | 6 |
| 60 | 58 | 6 |
| 65 | 63 | 7 |
| 70 | 69 | 7 |
| 75 | 74 | 8 |
| 80 | 78 | 8 |
| 85 | 82 | 9 |
| 90 | 86 | 9 |
| 95 | 89 | 10 |
| 100 | 92 | 10 |

where

z is in km and refers to the isothermal model listed in Table 5. (throughout this analysis all altitudes are geometric rather than geopotential in nature)

$z_{ni}$ is in km and refers to the nonisothermal climatological model for January and July at $45^{o}$ North latitude from 0-100 km. (U.S. Standard Atmosphere Supplements, 1966).

In the above listings of z versus $z_{ni}$ for January and July, linear interpolations were made where necessary between the layers of ten kilometers in thickness. See Tables 4A and 4B.

Using Figures 80 and 81, propagation in the entry plane was then considered for horizontal entry angles of $70^{\circ}$, $40^{\circ}$ and $10^{\circ}$ for the following cases:

1. Propagation Westward in January
2. Propagation Westward in July

} $\phi = 90^{\circ}$, West to East Entry

3. Propagation Eastward in January
4. Propagation Eastward in July

} $\phi = 270^{\circ}$, East to West Entry

Equations (38), (39), (46) and (47) were used in the calculations. For a graphical representation of the results see Figures 82-85. In the region where $V \longrightarrow C$ these results should be reconsidered in terms of the full expression for k(z), equation (31). Note that had $\phi = 0^{\circ}$ (or $180^{\circ}$) been used in the above calculations for refractive possibilities within the entry plane, wind effects would not have entered into the calculation. This is only because for the atmospheric model presently being utilized, only zonal winds have been considered. See Table 6 for a summary of the calculations.

In Figures 82-85 for $\theta \lesssim 70^{\circ}$, the sind term dominates the wind term (as a function of altitude). In general during entry (i.e. in the immediate proximity of the source), for horizontal entry angles less than about $70^{\circ}$ the refraction effects of the medium are small because of the effect of the sine of the entry angle (within the plane of entry).

Next a consideration of the propagation outside the entry plane will be discussed. For this discussion equation (33) will be utilized as written for meridional entry (South to North) with $\phi = 0^{\circ}$; $\theta = 70^{\circ}$, $40^{\circ}$ and $10^{\circ}$ for the following cases:

With $\phi' = 10^{\circ}$, $40^{\circ}$ and $70^{\circ}$

1. Propagation in January
   a. Ray Heading $10^{\circ}$ West of South (i.e., $190^{\circ}$)
   b. Ray Heading $40^{\circ}$ West of South (i.e., $220^{\circ}$)
   c. Ray Heading $70^{\circ}$ West of South (i.e., $250^{\circ}$)
2. Propagation in July
   a. Ray Heading $10^{\circ}$ West of South
   b. Ray Heading $40^{\circ}$ West of South
   c. Ray Heading $70^{\circ}$ West of South

With $\phi' = 350^{\circ}$, $320^{\circ}$ and $290^{\circ}$

3. Propagation in January
   a. Ray Heading $10^{\circ}$ East of South (i.e., $170^{\circ}$)
   b. Ray Heading $40^{\circ}$ East of South (i.e., $140^{\circ}$)
   c. Ray Heading $70^{\circ}$ East of South (i.e., $110^{\circ}$)

4. Propagation in July
   a. Ray Heading $10^{\circ}$ East of South
   b. Ray Heading $40^{\circ}$ East of South
   c. Ray Heading $70^{\circ}$ East of South

See Figures 86 - 97. For these cases $\Delta\phi = \pi/18$, $\pi/4.5$ and $\pi/2.57$ radians (10, 40 and 70 degrees azimuth from $\phi$) were chosen as illustrative of the general effect. Note as $\Delta\phi$ increases toward $\pi/2$ radians the first term, $C'(z)/\sin\sigma$, approaches C(z) so that the smaller $\Delta\phi$ is, the greater is the probability that (35) will be satisfied. In the above C'(z) is defined as:

$$C'(z) = C(z)\left[\sin^2\sigma + \left(1 - \frac{2\Delta\phi}{\pi}\right)^2 \cos^2\sigma\right]^{\frac{1}{2}} \qquad (52a)$$

For small $\sigma$ the above statement may or may not be true depending primarily on the vertical variations of the horizontal wind field. Note again that as $V \rightarrow C$ these results need to be reconsidered. See Table 7 for a summary of these calculations. In order to better illustrate the general refractive tendency, in both Tables 6 and 7 the original source altitude regions were only chosen for meteors such that $\sigma = 0$ and $\rho_{mE} = 7.7 g/cm^3$, rather than using the entire effective meteor model as shown in Table 4A. and 4B. In addition while many other possible combinations of $\phi$, $\Delta\phi$ and $\sigma$ could have been used, the ones which were finally chosen illustrate most of the possible refractive effects involved. See also Section VII (Part 3) for the refractive analyses which were performed using more realistic atmospheric models in connection with the meteor sound observations.

Once a given ray has been refracted (out of the entry plane) to the ground the possibility of long distance ducting of the signal then exists. If (35) has been satisfied during entry then long distance ducting on a seasonal and directional basis as discussed earlier is applicable. For a further discussion on this possibility see Section V. It has been shown recently by Francis (1972) that in the range of acoustic frequencies of interest, long distance ducting of the ray path should be considered in a spherical earth approximation. If such ray paths were calculated, the plane parallel atmosphere (flat earth) approximation used for the entry dynamics calculations would then have to be suitably modified also. An additional mechanism present during weak shock wave propagation (in addition to wind and temperature gradient refraction) may alter Francis' conclusion since Francis was considering strictly linear sound wave propagation. See Section V.

Note that Figures 82-97 indicate that for $\theta \gtrsim 40^{\circ}$ refractive effects may tend to break up the assumed cylindrical line source geometry. Thus under certain conditions as will be seen in Section V spherical decay laws may be more appropriate than cylindrical decay laws. For $\theta \lesssim 40^{\circ}$ atmospheric refraction is less important and within the limitations imposed in Section V, cylindrical decay should be appropriate out to relatively large scaled distances.

# V. ATTENUATION CONSIDERATIONS

## A. GENERAL INTRODUCTION

Up to this point the attenuation of the pressure pulse produced by the hypersonic passage of a meteor through the atmosphere (in a region where the Knudsen number is small) has not been considered. In order to discuss this attenuation let us briefly review the model we have utilized.

For $V >> C$ and V= constant between z' and z'''', the meteor-atmosphere interaction has been treated using a cylindrical blast wave line source model. For $\sigma = 0$ this model is used to predict the decay of the overpressure ratio into a uniform atmosphere at rest, out to x=1.0 with $R_o = f(V)$ only. Beyond $R_o$ the weak disturbance propagates through an assumed horizontally stratified nonturbulent atmosphere via refractive paths produced by the vertical changes of the temperature and horizontal wind fields. In the case of $\sigma \neq 0$, for a given meteor entry as a function of altitude, $R_o(z)$ decreases more rapidly, i.e. the distance from the trajectory at which the shock wave becomes a weak disturbance is closer to the trajectory for an ablating body than it is for a nonablating body. This fact is reflected in Figures 62-73. Thus for $\sigma = 0$ the cylindrical blast wave model represents a line source explosion of nearly constant blast wave radius. Considering the effective meteor model discussed earlier we are left with a representation of a line source explosion whose "yield" decreases with decreasing altitude. This is bounded at the lower altitudes by a nearly constant blast wave radius. The actual rate at which this output decreases depends on $V_E$, the value of $\sigma$ chosen and also upon the assumed variability of the meteors' cross-sectional area A as a function of altitude (of the main

single body mass). As was discussed in Section IV A, the blast wave analogy for hypersonic flow is not applicable if for $V >> C$, $V \neq$ constant.

As the meteor slows down, the bow shock comes closer to the meteor. Eventually it is attached at the front of the meteor (on a macroscopic scale) and the sonic boom output from an irregularly shaped rapidly decelerating body (or bodies) must be considered. This may occur for a given body size for a meteor Mach number in the altitude region for which equation (24a) can no longer be satisfied. In addition as was mentioned in Section IV A, the thermal "explosion" effect (due to intense ablation as a result of extreme deceleration) may have to be included in any realistic source model in the transition altitude range where neither the cylindrical blast wave analogy or the sonic boom theory can be reasonably applied. Thus, under certain conditions of flight, the intense thermal "explosion" effect may be equated to gross fragmentation or total break up of the body. When such a process occurs "instantaneously" a point source type blast wave solution may then be appropriate. If not, line source "explosion" waves may again be a reasonable approximation to the process under certain restrictions. In this analysis we have restricted the theoretical development primarily to the upper altitude cylindrical blast wave line source model of the meteor-atmosphere interaction.

Thus, in the region of the atmosphere for a given meteor where equation (24a) can no longer be satisfied, the problem of theoretically treating meteor sounds becomes very complex. See Section VIII (Part 3) for a summary of all these considerations.

In the discussion which follows the attenuation will only be considered for the cylindrical blast wave model. This is the line source

type explosion above $z''''$ (with $R_o \simeq$ constant and $M >> 1$).

While effects of turbulent scattering are not quantitatively discussed in what follows it is to be noted that a major effect of atmospheric turbulence is to change a highly directional sound source (such as cylindrically expanding blast waves) to a diffuse source, (a spherical source being an isotropic radiator) especially at great distances from the source (Evans et. al., 1970). Another major effect of turbulent fluctuations in the atmosphere is to give finite thickness to shock fronts (George and Plotkin, 1971). This effect is primarily produced by fluctuations present in the atmospheric boundary layer. Throughout this analysis we will consider shocks as strictly discontinuities however. This is a reasonable approximation even though molecular viscosity and heat conduction act to diffuse the sharpness of the front somewhat (Meyer 1962). Since the finite shock thickness produced as a result of molecular diffusion is much smaller than other characteristic macroscale parameters, the treatment of shocks in a nonturbulent atmosphere as strictly discontinuities is completely justified (Hayes, 1969).

As a result of the action of these turbulent fluctuations higher frequencies in the wave are effectively scattered (the classical N wave shape is rounded at the shock fronts). This phenomenon is roughly analogous to the effective scattering of ultraviolet radiation in the atmosphere (George and Plotkin, 1971). In addition, small and seemingly random pressure spikes are seen on the basic (but rounded) N wave shape (Hilton et. al., 1972). Note that the term turbulence has been used here in a very broad sense. The individual scales of turbulence (i.e., the characteristic eddy sizes of importance) and their overall effect on the propagation of weak nonlinear disturbances in a realistic atmosphere is not well understood and will not be considered further.

These effects are all essentially a process of redistribution of energy. The effect of turbulent scattering along with refractive direct and ducted arrivals makes an absolute determination of the kinetic energy of a meteor using observed overpressures from any one station difficult. In addition diffraction effects associated near shadow zones and the effects of caustics ( as a result of ray focusing) are not considered in this analysis. In the general meteor acoustics problem such focusing effects can occur directly as a result of atmospheric refraction due to the presence of vertical gradients. In addition near and below z'''' "superbooms" (focused sonic booms) can occur as the meteor trajectory rapidly curves toward vertical entry while the meteor is still traveling supersonically. Thus refractive effects may be of great importance in attenuation predictions (especially for long distance multipath ducted propagation) even for the strictly straight, line source problem. For additional comments on these effects the reader is referred to the work of Ribner (1972) and L. W. Parker et. al. (1973). Thus an initially cylindrically spreading wave will become more nearly spherical far from the source because of two realistic considerations. The first is the effect of the finite length of the line source (Few, 1969) and the latter is the diffusing effect of atmospheric turbulence. A full treatment of the latter effect is beyond the scope of this study.

Note also that the acoustics of exploding meteors (i. e., "point" source bolides) are not considered here since the meteor models utilized in Section III do not as of yet allow for such effects. The Pribram Meteorite in Czechoslovakia (1959) is a well documented relatively recent example of such a sound producing event (Ceplecha, 1972). There is a chapter in Astapovichs' book (1958) entitled "Acoustics of Bolides" where he deals more thoroughly with the meteorological aspects of the sounds from exploding meteors (considered as point sources) than is done here.

For the spherical blast wave "point" source problem, $R_s$, the spherical blast wave relaxation radius is defined as: (Few, 1968)

$$R_s = \left( \frac{E_t}{\frac{4\pi}{3} p_o} \right)^{1/3} \tag{53}$$

where

$E_t$ = total energy deposited by the source.

Equation (53) assumes the source is an ideal "point" source, i.e., the "charge" diameter is assumed to have negligible dimensions. In Section VIII (Part 3) the "point"source blast wave problem will be mentioned again.

In his recent work Tsikulin (1970) has shown that both the line and point source problems may have to be considered in the analysis of "exploding" bolides. When the meteor velocity is constant the shape of the wavefront trajectory near the source is parabolic (Lin, 1954) rather than either spherical (for an ideal point source) or cylindrical (for an ideal line source). This effect is seen in bolides which do not "explode" instantaneously, but violently fragment over a few kilometers path distance. One of the major problems in theoretically studying the "point" source problem in the case of meteors is knowing $E_t$. In the final explosion of a bolide (i.e., generally just before dark flight begins) the remaining kinetic energy of the meteor in the altitude region of interest can be assumed equivalent to $E_t$. For multiple explosion bolides the fraction of the meteor's kinetic energy transferred during each energy release is unknown. Solving energy equations under such nonequilibrium conditions is to be sure very difficult. To the authors' knowledge no work has been published on the multiple explosion problem (at various path distances along the meteor's trajectory). For $V >> C$

this introduces a spherically expanding "point" source explosion wave in addition to the cylindrically expanding blast wave which we have considered here. See also Korobeinikov et. al. (1971). In general only the sound effects from the final explosion of a given bolide have been considered since absorption effects are less severe for lower altitude point explosions. A relative comparison of the amount of energy released during either a "line" or "point" source explosion along the meteor trajectory will ultimately determine which wave system will be of primary importance in the attenuation considerations. At present we will only be considering the line source overpressure decay,

The total range of recorded frequencies from all the existing meteor sound observations we have access to, range from audible acoustic waves to gravity waves. The reference here to audible sound is the sonic boom tape recorded by Miss E. M. Brown in Northern Ireland in 1969. See Opik (1970) and Section VII (Part 3) for more details. As will be seen in Section V C and D and Section VIII (Part 3) this rather large range of frequencies results from both the possible variations in the wavefront geometry as well as from the variability of the magnitude of the energy release associated with a given meteor. In addition, the wavefront geometry is dependent upon both the characteristics of the meteor source as well as upon the nature of the atmosphere if the relaxation radius is sufficiently large.

Definitions of the wave frequency regimes of interest follow.

I. Acoustic Wave Frequencies with: (Yih, 1969)

$$\gamma H >> \Lambda \qquad (\Lambda = \Lambda_z \sim \Lambda_x \sim \Lambda_y) \tag{54}$$

where $\Lambda$ = wavelength of the disturbance; $\Lambda_z$ = vertical component wavelength and $\Lambda_x$ and $\Lambda_y$ are East-West and North-South horizontal component wavelengths. Considering $\gamma$ = 1.40 and H = 7.5 km, the

largest wavelength for which equation (54) will be approximately satisfied is 1 km. At C 0.316 km/sec this corresponds to a minimum frequency of 0.316 Hz. The upper limit of this approximation is generally given as $\sim 2.10^4$Hz. Beyond this limit ultrasonic frequencies must be considered (as becomes on the order of a mean free path in length). Thus a more general definition should be written as:

$$\gamma H >> \Lambda > > \lambda \qquad (54a)$$

where

$\lambda$ = mean free path of the neutral gas

II. Acoustic Gravity Wave Frequencies

This region includes frequencies from about 0.316 Hz down to about $2.8 \cdot 10^{-4}$Hz. The commonly used term infrasound (analogous to infrared radiation) thus includes subaudible acoustic frequencies below about 10 Hz (with respect to the human ear) as well as part of the acoustic gravity wave domain as defined above (down to about 100 seconds in period). As defined here infrasound propagation is essentially dispersionless (in an isothermal atmosphere without wind with no dissipation mechanisms acting).

Solutions of the equations governing linear acoustic gravity wave propagation are quadratic in nature. Two branches of wave propagation are then possible. These have been termed the acoustic branch and the internal gravity wave branch. The waves within the acoustic branch which behave like ordinary acoustic waves in the high frequency limit (as defined by (54a)) have a natural cut-off (or resonant) frequency which is given by:

$$\omega_A = \frac{1}{2}\left(\frac{\gamma g}{H}\right)^{\frac{1}{2}} = 2\pi \cdot f_A \qquad (55)$$

where

$f_A$ = acoustic cut-off frequency

$\omega_A$ = angular acoustic cut-off frequency

$g$ = acceleration due to gravity

$H$ = scale height of the assumed isothermal hydrostatic atmosphere

The waves within the acoustic branch have allowed frequencies f such that

$$f > f_A \tag{55a}$$

Using the atmospheric model listed in Table 5, with $\gamma = 1.4$, $\omega_A = 2.12 \cdot 10^{-2}$ rad/sec.

The waves within the gravity wave branch of the acoustic gravity wave domain have a similar cut-off (or resonant) frequency. It is commonly called the Brunt-Väisälä frequency. The waves within the gravity wave branch have allowed frequencies f such that

$$f < f_B \tag{56}$$

where

$f_B = \omega_B / 2\pi$ = Brunt Väisälä frequency

$\omega_B = \left[\frac{(\gamma - 1) g}{\gamma H}\right]^{\frac{1}{2}}$ = angular Brunt-Väisälä frequency

Again for the model in Table 5, with $\gamma = 1.4$, $\omega_B = 1.92 \cdot 10^{-2}$ rad/sec.

For internal waves to propagate (as distinguished from surface waves generated at the boundaries of the medium) equations (55a) and (56) must be satisfied. Thus the theory predicts a spectral gap between $\omega_A$ and $\omega_B$ where internal waves can not propagate. While the surface wave solutions are generally not studied in conventional acoustic gravity wave treatments (Few, 1968), waves within the gravity wave branch are generally referred to as internal gravity waves. Cook (1969) has suggested that since these waves travel slower than the adiabatic sound speed they might easily be termed subsonic oscillations.

Below about $2.8 \cdot 10^{-4}$ Hz (> ~ 1 hour in period) Coriolis effects on a rotating diurnally heated planet must be considered and the atmospheric tide problem is then evident. Since the tidal regime is not of importance to the present study no further discussion on this subject will be made. For further discussion on this general subject, see Craig (1965).

Since predicted periods for the line source meteor sound problem fall in the range from about one to ten seconds, material dispersion (as is predicted for acoustic gravity waves in an isothermal atmosphere without wind) is not significant. Cook (1969) has shown that material dispersive effects are still small at 100 seconds period. See Section V C and D and Section VIII (Part 3). Note that the wave frequency definitions employed here differ somewhat from those of other authors. Acoustic gravity waves have been defined previously for frequencies f satisfying equation (56) even though for $f > f_A$ the general equations governing the wave propagation are the same (Cook, 1969). Thus the present acoustic gravity wave spectrum definition is more consistant in that the acoustic wave (or ordinary sound wave) and the acoustic gravity wave spectrum are logically related.

Obviously these short descriptions are inadequate for a complete understanding of the dynamics of such waves for even relatively simple atmospheric models. They have been presented however for completeness sake only. In Section VIII (Part 3) the more general meteor sound problem will be discussed and the application of these descriptions to this more general problem will become obvious.

The only known meteor event which produced airwaves of periods of several minutes or more (along with the other frequencies

generally inherent to a dispersive atmospheric wave train) was the Great Siberian Meteor of 1908 (Whipple, 1930). Accordingly, for the more probable smaller bodies which deposit much smaller amounts of energy into the atmosphere, dectable gravity waves (as part of a dispersive wave train) are far less likely. Note that from here onward, unless otherwise specified, the term gravity waves refers specifically to internal gravity waves as defined by (56). See also Section V C.

Estimates of the acoustic energy resulting from the mechanical energy deposition process at the meteor, range from about 0.01 - 0.1% of the total energy deposited (Astapovich, 1946; Scorer, 1950). Similar estimates have been made for thunder (lightning discharges producing cylindrical blast waves). Few (1968) obtained a radiated acoustical output of 0.4% of the total energy released. Holmes et. al. (1971) obtained 0.18% for this quantity after making many thunder observations. For low altitude blast waves, estimates for energy loss due to radiation effects are very negligible being on the order of 0.1% or less of the total energy released (unless the shock is very strong, Jones et. al., 1968).

Meteor astronomers commonly deal with a quantity called the luminous efficiency factor. It is defined as that portion of the meteor's kinetic energy which is radiated as visible electromagnetic energy. It has been determined in the past that this efficiency factor increases linearly with the meteor velocity up to certain velocities. Beyond about Mach 30 it levels off and is nearly constant until higher Mach numbers are reached where it then appears to decrease slowly with a further increase in velocity. Over this entire range (determined by wind tunnel experiments or observations of artifical meteors which

are accelerated downward through the atmosphere while being photographed) the luminous efficiency factor increases from 0.1% at the lower Mach numbers to as much as about 1%, (Givens and Page, 1971). Thus at least for the objects tested (iron and steel spheres) the radiation losses are not very significant. It remains to be seen if for other bodies of known composition significant radiation exists in portions of the spectrum other than and including the visible. In the paper by Givens and Page some data on this subject is also presented for actual meteor entry to the atmosphere. From this data which is similar to the simulation data just referred to, the luminous efficiency factor is never greater than about four percent.

Recently, Reed (1972) has suggested that radiation losses for point source explosions at great altitudes ( $\gtrsim$ 50km) may be greater than 10% of the total energy deposition. While radiation losses are not considered further here, this is a topic which should be explored more fully as our understanding of attenuation of blast waves by the atmosphere continues to improve. See Vincenti and Traugott (1971). See also Plooster (1971) and Section VIII (Part 3). The remaining energy deposited via the drag interaction to be accounted for is that used to heat the gas, some 95-99% of the total, depending on the magnitude of the radiation energy losses. Thus it is seen that the conversion of mechanical energy to acoustic energy by the expanding blast wave is not very efficient.

As was noted above, most meteor sound observations which now exist do not have gravity wave frequencies inherent to them. For this reason in what follows attenuation effects will be considered for primarily acoustic frequencies with mention where necessary of the acoustic gravity wave domain.

For waves whose periods exceed about 10-15 seconds, ray theory as envisioned in classical geometrical acoustics is no longer a very useful tool (Cook, 1969). Most of the infrasonic observations of fireballs which now exist are of periods from 3-18 seconds (Goerke, 1971; Wilson, 1972). (we presently have access to only five infrasonic observations however). Therefore at present the ray theory approach seems quite justifiable.

The wave guide mode theory, involving boundary conditions imposed at the "top" of the atmosphere and at the ground can be effectively used to study the spectrum of discrete guided atmospheric oscillation modes (as has been done in the nuclear explosion detection problem) for waves whose period exceeds about 10 seconds. In general, however, for long distance propagation of acoustic gravity waves from a large ( $>$ 1MT) nuclear explosion, cut off periods are usually much greater then 10 seconds while shorter periods are more greatly absorbed. That the mode theory can be a useful tool for this problem is seen in Figure 99. This is a dispersion diagram showing the third and fourth acoustic modes (of the acoustic branch as defined in equation (55a)) of the airwave train recorded in Boulder by Goerke from the Revelstoke Meteorite Event in British Columbia. The analysis is from the work of Lowry and Shoemaker (1967) (private communication with Dr. E. M. Shoemaker; 1972). The theoretical modes shown were predicted for an atmosphere without winds. For the inclusion of steady winds into the theoretical dispersion description the reader is referred to the work of Balachandran (1968). Note that in Figure 99 the amplitude isopleth interval is 1 dyne/cm$^2$. The theoretical dispersion curves shown are based on the 300 km model of the atmosphere used by Pfeffer and Zarichny (1963).

Using Figure 99, Shoemaker has estimated the kinetic energy of the Revelstoke event to be on the order of $10^{19}$ - $10^{20}$ ergs (Carr, 1970). This estimate was made using the dominant period of the waveform, i. e., the period at maximum amplitude. In Section VII (Part 3) an estimate of the kinetic energy of this fireball will be made using a cylindrical blast wave line source model of the phenomena. Thus the conclusions of Tsikulin(1970) and Korobeinikov et. al. (1971) regarding the possible use of both the point and line source blast wave description (or some combination of these) in order to study meteor sound phenomena appear quite reasonable ( at least when considering the most general case with regard to specifying the overall source characteristics). In this regard the terms "detonations" or "detonating" as applied to the sounds produced by meteors may need better delineation in future research on this problem. Previously it has generally only been associated with "point" source type explosions. See VIII (Part 3) for more details.

In what follows then, ray theory will be used wherever possible to trace the acoustic energy from its source to ground level (when refraction effects allow for such ray paths). Attenuation effects will then be considered along these ray trajectories for the cylindrical blast wave line source explosion model.

While Öpik (1959) briefly considered absorption of meteor sounds in his book on meteor physics, it will be seen shortly that his analysis needs considerable modification for the meteor sound problem as invisioned within this paper. To be sure also, the major acoustic frequencies of interest after propagation to the ground from 100km altitude are well below 30 Hz, (Procunier and Sharp, 1971). This was the lowest frequency Öpik considered however. See also Öpik (1970).

We will now consider attenuation of cylindrical blast waves by the atmosphere. In what follows it is assumed that for the frequencies of interest the temperature and wind gradients in the in the atmosphere are the primary refractive mechanisms acting. At gravity wave frequencies gravity gradients can also produce refractive effects (Francis, 1972). In addition, Tolstoy (1965) has suggested density gradients in the atmosphere as acting as a refractive machanism for acoustic wave frequencies. For the nonlinear weak shock problem an additional refractive mechanism occurs which is also not considered here. As the weak shock wave overpressure decays the weak nonlinearity present produces bending of the ray tubes even in an isothermal atmosphere without wind (Tsikulin, 1970; C. Berthet and Y. Rocard (to be published)). Since all the above effects are not considered further here (with the exception of the wind and temperature gradient ray analysis presented in IV B and C), the present theoretical ray description can at best be considered as a first order approximation.

Decay of the overpressure ratio with scaled distance x for cylindrical blast waves expanding into a uniform (constant density) atmosphere at rest was calculated using equation (11) and (13). If we can correct this decay beyond $R_o$ for the attenuation produced by a non-uniform atmospheric path including frequency dependent absorption (for either a weakly nonlinear of linear disturbance as may be appropriate) we will then have a reasonable estimate of the pulse overpressure at any distance and altitude away from the source. See Section V D., equations (92) - (93b) for the final results determined using the above method of reasoning. These results are graphically displayed in Figures 101-115.

## B. ABSORPTION OF "SHOCKED" EXPLOSION WAVES VERSUS THAT OF SMALL AMPLITUDE LINEAR ACOUSTIC WAVES

The general problem of treating the attenuation from an arbitrary cylindrical blast wave line source in a realistic atmosphere is formidable. In fact, the theoretical predictions for point source blast wave attenuation do not always agree well with overpressure observations (Reed, 1972). Well documented measurements of meteor sounds in combination with documented photographic information have the potential for improving this situation however. See Sections VII and VIII (Part 3).

Meteor sounds pose an interesting theoretical problem. Since observation periods in the infrasonic region at great distances from the source range from about 3-54 seconds, aspects of both the acoustic gravity wave dispersion problem, well known in the huge nuclear detonation observations (Balachandran, 1968), as well as the "frozen" fundamental frequency assumption of the smaller yield grenade explosions (Reed, 1972) may at times be applicable. See Section V C. and Section VII (Part 3). In an isothermal hydrostatic atmosphere for acoustic frequencies, material dispersion does not occur (Officer, 1958). If for these frequencies, wind and temperature gradients are allowed, geometrical dispersion can occur (i.e., different frequencies travel with different speeds due to the presence of wind and temperature gradients). For the acoustic gravity wave frequencies, material dispersion occurs even in an isothermal atmosphere without winds. The addition of wind and temperature gradients for a realistic atmosphere contributes the complication of geometrical dispersion effects for this frequency region as well. Fortunately, as will be seen the most probable

occurance of meteor sounds as envisioned within this paper will include primarily acoustic frequencies so that material dispersion effects need not be considered. This greatly simplifies the analysis . As far as the "frozen" fundamental frequency assumption, for strictly linear cylindrical acoustic waves, the fundamental frequency is a function of the observation distance from the source (Remillard, 1960; Meyer, 1962). This is also true of weak cylindrical shock waves (Dumond et. al., 1946). Far from the source spherical wave expansion occurs and the fundamental frequency of the pulse becomes nearly constant. See Section V, C. and D. In Section VII (Part 3), infrasonic meteor sound observations will be analyzed using the theory as primarily developed in Sections IV A and V.

To emphasize the approximate nature of the theoretical discussion regarding attenuation which follows, a brief listing of possible energy losses as given by Evans et. al. (1970) will be summarized. Note that in this analysis attenuation is defined as the total energy removal process, i. e. including the effects of both spreading and absorption of the wave energy.

I. Spreading losses
   - A. Uniform Spreading Losses
   - B. Nonuniform Spreading Losses
     1. Reflection by Finite Boundaries
     2. Refraction by Nonuniform Atmosphere
     3. Scattering by Nonstationary Atmosphere

II Absorption Losses

A. Absorption by Ground and Ground Cover

B. Absorption by the Atmosphere

1. Classical Absorption for Linear Acoustic Waves

a. Viscous Losses
b. Heat Conduction Losses } Stokes-Kirchoff Losses
c. Diffusion Losses
d. Radiation Losses

2. Molecular Relaxation Losses for Linear Acoustic Waves

a. In "Dry" Air
b. In Air with Varying Amounts of Water Vapor

3. Absorption of "Shocked" Explosion Waves (Weak Shock Waves)

4. Absorption of Finite Amplitude Waves (Without Shock Fronts)

II. B. 3 has been added to the above list following the work of Cotten, Donn, and Oppenheim, 1971. In addition, II. B. 4. has been added to the above list for completeness (Blackstock, To Be Published). Finite amplitude (but shockless) wave propagation (and decay) has not been formally considered in this analysis. Note that the weak shock theory as developed in this report (See equation (59)) can only be safely applied in those regions for which $x \geq 1$, i.e. $\Delta p/p_o < 1$ (Morse and Ingard, 1968). Thus, even with the present theory, absorption decay should not be calculated during the initial strong shock phase of the disturbance.

In Figures 101-115, $R_o$ has been specified in the range 10 to 300 meters. During the overpressure calculations (see Section VD., equation ((92) - (93b)) absorption decay was referenced throughout to $x = 1$. In Figures 101-115 however, the decay curves are not shown in each case for distances closer than 5 km from the source (for the family of source height overpressure decay curves).

To treat all of the above losses as a function of wave frequency for a meteor induced line source blast wave is beyond the scope of this report. We will only choose those which are presently best understood and which appear to be most important to this problem.

Up until now we have assumed that at x = 1.0 the strong shock (cylindrical blast wave) has sufficiently decayed that it could be studied using the methods of geometrical acoustics. This conclusion is correct regarding the use of ray paths to follow the propagation of the disturbance (if the medium is assumed to be slowly varying, etc.) With regard to the further decay of the amplitude of the disturbance, however, it will be shown that ordinary, linear, acoustic approximation decay laws are not appropriate until another condition is satisfied. As has been shown by Cotten, Donn, and Oppenheim, (1971), the appropriate decay law under certain conditions is that for "shocked" acoustic waves rather than for linear acoustic waves. The condition for $\Delta p/p_o$ being $<<1$ is necessary but not sufficient to define a linear acoustic wave. As has been shown by the above group, a weak acoustic wave will actually steepen ( i. e., $\Delta p$ increases due to distortion) during part of its propagation downward from the upper atmosphere thus making the displacement gradient at the shock front large so that the wave shape may not be approximately sinusoidal even when $\Delta p/p_o$ is $<< 1$. It is this steepened wave shape which makes the decay over certain regions of the atmospheric path weakly nonlinear. The overriding conclusion is that if the wave was linear at certain altitudes the distortion produced by the cumulative weak nonlinearity effects would cause the wave to form shock fronts under certain conditions. See also Sections V , C and D. Thus , far from the source the processes

of distortion and dispersion will compete with each other to produce the resulting wave shape at any given observation point. As will be seen shortly in this analysis the wave shape is assumed to be known however. The effects of turbulent fluctuations on the resulting wave shape are not quantitatively considered here, but these have been described earlier in a qualitative manner. The conditions for which such "shocked" wave propagation is possible will now be discussed.

It can be shown that a plane sinusoidal acoustic oscillation will distort by 10% in a distance d' given as (Towne, 1967):

$$d' = \frac{\lambda}{20(\gamma + 1)\, S_m} = \frac{C\tau}{34.3(\Delta p/p_o)} \qquad (57)$$

where

$\gamma$ = 1.40

$S_m$ = $\Delta\rho / \rho_o$ , a condensation ( a term from classical acoustics)

$\tau$ = period of the oscillation

$$\frac{\Delta p}{p_o} = S_m \cdot \gamma = \frac{k_1}{x^{1/2}} \left( \frac{p_z}{p_o} \right)^{1/2} \cdot D(R) \qquad (57a)$$

for linear acoustic waves of cylindrical geometry traveling downward into an isothermal atmosphere

$k_1$ = constant (See equation (85))

$p_z$ = hydrostatic pressure at a source altitude $z_z$

$p_o$ = hydrostatic pressure at the observer

For the sonic boom problem( steady state source motion), D(R) = 1, (Cotten, Donn, and Oppenheim, 1971). For the meteor sound problem as envisioned within this paper, D(R) is $\Delta p / \Delta p_z$ as given by

equation (66a) if the energy release is instantaneous. See also equations (92), (92a) and (92b). If the release is not strictly instantaneous an extended source concept expanding outward at the Mach angle can be considered. Once the source ceases to exist free independent wave propagation ( as dependent upon the atmospheric structure) is then approached. Using this extended source concept the present ground overpressure predictions (as developed in Section V D; See Figures 101-115) will increase somewhat (depending primarily on the source altitude considered as well as upon the total flight time of the meteor for which $V >> C$ and V= constant). See also Section VIII (Part 3) for further discussion on this possibility.

Morse and Ingard also calculate a distortion distance for plane sinusoidal acoustic waves. In their analysis however they calculate the distance to the "shocked state" (rather than the 10% distortion distance of Towne as defined in (57)) as:

$$d_s = \frac{C\tau}{5.38 \frac{\Delta p}{p_o}} \qquad (57b)$$

Therefore:

$$d_s = 6.38\ d' \qquad (57c)$$

Throughout this analysis d' is used as the criterion for weak nonlinear versus linear wave propagation as defined in conjunction with equation (58). Equation (57b) gives quantitatively similar results however. Had equation (57b) been used in conjunction with (58) note that the wave could have been termed linear at closer distances to the trajectory than is predicted by using (57) and (58). This would also tend to increase the predicted ground overpressures somewhat, but generally by much less than a factor of two.

With this in mind, an appropriate definition for linear acoustic waves is then:

$$d' > d_a \tag{58}$$

where

$d_a$ = remaining propagation distance of the disturbance (i.e., before it is to be observed).

That is for a wave of a given period, $\Delta p/p_o$ must be small enough for (58) to be satisfied (i.e., the larger $\tau$ is and the smaller $\Delta p/p_o$ is, the larger $d'$ is). To evaluate the value of for a given meteor energy release see Section V C.

Morse and Ingard (1968) have shown that the effects of the nonlinear terms as compared to the viscous terms in the gas dynamical equations are not negligible until $\Delta p$ is small enough for particle displacements as a result of the wave passage to be much less than a mean free path in length. This is consistent with the present analysis. Equations (57) and (58) allow a direct simple test of the effects of the weak nonlinearity on the propagating signal as a function of the distance to be traversed.

To evaluate absorption for plane "shocked" acoustic waves (remote from their source) the following equation applies (Morse and Ingard, 1968):

(59)

$$\frac{dp_s}{ds} = -\left(\frac{\gamma + 1}{\gamma^2 \Lambda}\right)\left(\frac{\rho C^2}{p_o^2}\right) p_s^2 - \left(\frac{3\delta}{2\rho_o C \Lambda^2}\right) p_s$$

where

$$\delta = 4\left[\mu' + K(\gamma - 1)/C_p\right] \tag{60}$$

$p_s$ = pressure amplitude of the "shocked" disturbance

$\mu'$ = $(4/3)\mu + \xi$

$\mu$ = ordinary (shear) viscosity coefficient

$\xi$ = bulk (volume) viscosity coefficient

$p_o$ = average ambient hydrostatic pressure in the fluid

$\rho_o \cong \rho$ = average ambient density in the fluid

K = thermal conductivity of the fluid

$C_p$ = specific heat of the fluid at constant pressure

s = path distance

Equation (59) is in the form:

$$dp_s = -(Ap_s^2 + Bp_s)\, ds \tag{61}$$

where

$$A = (\gamma + 1)/\gamma \Lambda p_o \tag{62}$$

$$B = 3\delta/2\rho_o C\Lambda^2 \tag{63}$$

$$\gamma H >> \Lambda$$

with

$$\rho C^2 \cong \gamma p_o \tag{64}$$

The above approximation (equation (64)) is valid if the density ratio across the shock front does not greatly exceed the ambient density. Theoretically, the strong shock limit of $\rho/\rho_o$ is six for a diatomic

gas i.e., in the limit as $p/p_0 \rightarrow \infty$, $\rho/\rho_0$ approaches a finite limit (Lin, 1954). Far from the source, which is the condition for which (59) has been derived, $\rho/\rho_0 \lesssim 1.5$ (for $x \gtrsim 1$; Plooster, 1968). Equation (64) is then a reasonable approximation (for $x \gtrsim 1$).

The term in $p_s^2$ arises from viscous and heat conduction losses occuring across the entropy jumps at the shock fronts. The term in $p_s$ arises from losses due to these same mechanisms acting in the region between the fronts. In this intermediate region a linear decay of $\Delta p$ (with a constant slope) is assumed between the peak positive overpressure phase and the peak negative underpressure phase of the disturbance. Thus as has been done by many other authors, the wave shape is assumed to be known during the propagation. Note that by assuming the wave shape, distortion and dispersion effects have been indirectly considered. This is because distortion and dispersion compete to produce the resulting wave shape as was noted earlier. Dispersion due to wind and temperature gradients has not been considered however.

The solution to (59) can be written as:

$$\frac{\Delta p}{\Delta p_z}\left[\frac{\Delta p_z + B/A}{\Delta p + B/A}\right] = \exp\left[-B(\Delta s)\right] \quad \text{with} \quad \Delta s \geq 0 \tag{65}$$

where

$\Delta p$ = overpressure at the observer

$\Delta p_z$ = overpressure at the source altitude

For a general nonuniform slant path, the solution to equation (59) can be written:

$$\frac{\Delta p}{\Delta p_z}\left[\frac{\Delta p_z + B/A}{\Delta p + B/A}\right] = \exp\left[-\int B\,ds\right] \tag{65a}$$

After changing to altitude integration, (65a) becomes:

$$\frac{\Delta p}{\Delta p_z}\left[\frac{\Delta p_z + B/A}{\Delta p + B/A}\right] = \exp\left[-\int_{z_o}^{z_z} B\,\frac{dz}{\cos\bar{\epsilon}}\right] \tag{65b}$$

where

$\bar{\epsilon}$ = ray angle measured from the local vertical (zenith angle of the ray)

$z_o$ = observers altitude

$z_z$ = source altitude; $z_z \geq z_o$

Note that in the entry plane $\bar{\epsilon} = \theta$. Outside the entry plane, $\bar{\epsilon}$ ranges from approximately $\theta$ to $90^o$ (corresponding to $\Delta\phi = 90^o$). See Figures 100a and 100b and 116.

Rewriting B in terms of $\bar{\alpha}$ (See equations (66), (68), (72) and (81a)) integrating with f held constant and putting in the values of the constants, (65b) becomes (for an isothermal hydrostatic atmosphere):

$$\frac{\Delta p}{\Delta p_z}\left[\frac{\Delta p_z + B/A}{\Delta p + B/A}\right] = \exp\left[\frac{-4.50\cdot 10^{-8}\, f^2}{\cos\bar{\epsilon}}\left(e^{\frac{z_z}{7.5}} - e^{\frac{z_o}{7.5}}\right)\right] \tag{65c}$$

where

$p = p_o\, e^{-z/H}$

f = fundamental frequency of the disturbance (See equation (78))

$p_o = 1.013 \cdot 10^6$ dynes/cm$^2$

H = 7.5 Km

and for vertical ray paths, $\cos \bar{\epsilon} \rightarrow 1$. (for $\Theta \rightarrow 0^{\circ}$ in the entry plane)

This expression (65c) will be used shortly to evaluate absorption effects along the ray paths in those regions where equation (58) cannot be satisfied. See equations (68) - (72) and (81b).

When equation (58) is satisfied, the absorption decay law is that of plane linear acoustic waves (of sinusoidal shape ) such that (Evans, et. al., 1970).

$$\begin{aligned} I &= I_z e^{-m(\Delta s)} \\ \Delta p &= \Delta p_z e^{-\alpha(\Delta s)} \end{aligned} \tag{66}$$

where

$s$ = path distance from the source ( $\Delta s \geq 0$)

$\bar{\alpha}$ = total amplitude absorption coefficient

$m = 2\bar{\alpha}$ = total intensity absorption coefficient

$I_z$ = initial intensity of the linear acoustic disturbance

$I$ = intensity at path distance $\Delta s$ from the source

$I = (\Delta p^2)_{RMS} / \rho_o C$

$(\Delta p)_{RMS}$ = root mean square pressure amplitude of the disturbance

$\rho_o C$ = characteristic acoustic impedance of the medium

Proceeding as with (65), (66) becomes:

$$\Delta p = \Delta p_z \exp\left[ - \frac{1.48 \cdot 10^{-7} f^2}{\cos \bar{\epsilon}} \left( e^{z_z/7.5} - e^{z_o/7.5} \right) \right] \tag{66a}$$

In general (if the absorption is relatively small):

$$\bar{\alpha} = \alpha_\mu + \alpha_K + \alpha_D + \alpha_{rad} + \alpha_{mol} \tag{67}$$

where

$\alpha_\mu$ = viscosity absorption coefficient

$\alpha_K$ = thermal conductivity absorption coefficient

$\alpha_D$ = diffusion absorption coefficient

$\alpha_{rad}$ = radiation absorption coefficient

$\alpha_{mol}$ = molecular relaxation absorption coefficient

In this analysis the effect of $\alpha_D$, $\alpha_{rad}$, and $\alpha_{mol}$ have been neglected. In general $\alpha_D$ has a very small effect on the results (Evans et. al., 1970). The effects of $\alpha_{rad}$ and $\alpha_{mol}$ may not always be negligible compared to the other absorption coefficients, but their inclusion is beyond the scope of this analysis. For frequencies below about 10Hz the effects of turbulent scattering, which are also basically neglected here ( with regard to possible wave amplitude reduction), are probably more important at times than the effects of $\alpha_{rad}$ and $\alpha_{mol}$. This is dependent on many factors and will not be discussed further. For a thorough discussion on all these effects in a still atmosphere the reader is referred to the excellent treatment by Evans et. al. (1970). Note however that the discussion by Evans et. al. is relevant only to linear acoustic waves of relatively high frequency ( $\gtrsim$ 10 Hz). At present the problem of attenuation of acoustic waves in a realistic atmosphere is not completely understood. This is especially true for the case of weak nonlinear disturbances not attached to a source however.

The functional form of $\overline{\alpha}$ is given as (Morse and Ingard, 1968):

$$\overline{\alpha} = \frac{\omega^2}{2\rho_o C^3}\left[\mu' + K(\gamma - 1)/C_p\right] = \frac{\pi^2}{\rho_o C \Lambda^2}\left(\frac{\delta}{2}\right) \quad (68)$$

where

$\omega = 2\pi f$ = angular frequency of the oscillation

It will be seen in general for most of the frequencies of interest and for the altitude regions where (66a) applies, absorption, being proportional to the frequency squared, will be small. While $\mu$, K and C are all theoretically proportional to $T^{1/2}$, Golitsyn (1961) has reduced (68) to a form independent of variations in C. Here T is the absolute temperature of the gas. Assuming $\mu' = 4/3\ \mu$ he obtained $\bar{\alpha}$ in the form: (with f in Hertz)

$$\bar{\alpha} = 1.03 \cdot 10^{-5} f^2/p \ \text{km}^{-1} \tag{69}$$

with p expressed in millimeters of Hg. (1.333 mb = 1 mm Hg)

This is equivalent to:

$$\bar{\alpha} = 1.37 \cdot 10^{-5} f^2/p \ \text{km}^{-1} \tag{70}$$

with p expressed in mb. ($10^3$ dynes/$\text{cm}^2$ = 1mb)

and

$$\bar{\alpha} = 1.37 \cdot 10^{-2} f^2/p \ \text{km}^{-1} \tag{71}$$

with p expressed in dynes/ $\text{cm}^2$.

While some other authors include both viscosity coefficients in the formulation of $\bar{\alpha}$, in practice, it is difficult to include $\zeta$ for at least two reasons. One of these relates to what its magnitude actually is. Most authors who include the bulk viscosity coefficient assume that both viscosity coefficients are of equal magnitude.(Cotten, Donn and Oppenheim, 1971). This may or may not generally be the case. In any case it is difficult to say what its variation with altitude is and in what region it becomes negligible compared to $\mu$. In addition, according to the development as presented here $\zeta$ is part of the $\alpha_{mol}$

term. While its inclusion has been formally dropped at this point, the use of equation (72) below does make the wave frequency absorption calculation somewhat more realistic. Since reliable measurements in the atmosphere indicate greater frequency absorption than is predicted by using the above expressions, due to some of the effects listed earlier, $\bar{\alpha}$ is usually increased to match the observations so that (Reed, 1972):

$$\bar{\alpha} = 2 \cdot 10^{-5} f^2/p \ \text{km}^{-1} \qquad (72)$$

with p expressed in mb

Since as has been shown certain basically nonlinear processes may enter into the decay of a disturbance from a source of acoustic waves, we will assume that the measurements upon which (72) are based involved only linear acoustic decay effects. Thus equation (72) has been used in developing equations (65c) and(66 a).

## C. ABSORPTION EFFECTS AS A FUNCTION OF THE FUNDAMENTAL WAVE FREQUENCY

In this subsection we will develop an approximate method of evaluating the decay of the explosive cylindrical line source as a function of the fundamental wave frequency along an arbitrary path to the observer.

The large range of velocity, size and the variable value of $R_o$ (z) due to ablation effects makes a general theoretical formulation of this problem as a function of the fundamental wave frequency difficult to develop. Note that typical grenade explosions have values of $R_s$ on the order of a few meters or tens of meters except at very high altitudes (Otterman, 1959). See equation (53). This is also true of thunder where $R_o \simeq$ 2-5 meters (Few, 1968; Jones et. al., 1968).

Meteors are thus a unique natural and variable energy source in that $R_o$ can range from a few meters to a few kilometers according to the models. In terms of ground based measurement it will be seen shortly that the minimum $R_o$ of interest is $\sim$ 10 meters however. Even though it is relatively rare for an observer to see a fireball energetic enough to produce low frequency yet audible sounds, the chances of instrumentally recording such an event at great distances, is not that improbable. See Section VI (Part 3). A knowledge of the event is essential to define the problem more thoroughly at present as current theoretical predictions of classical blast wave attenuation over long distances in a realistic atmosphere are at best very approximate. As a result, for small "point" explosions in the atmosphere, empirical decay laws have been developed to attempt to remedy the situation somewhat (Reed, 1972). In what follows then, two scaling approximations will be employed so that for a given meteor, a test can be made to see which approximation is most appropriate.

Following the work of Groves (1964) and Tsikulin (1970) these two scaling approximations can then be written as:

$$d_m << R_o << H \quad \text{or equivalently:} \quad C_d << R_s << H \qquad (73)$$

$$d_m << R_o \sim H \quad \text{or equivalently:} \quad C_d << R_s \sim H \qquad (74)$$

where

$d_m = 2r_m$ = meteor diameter

$C_d$ = charge diameter of the explosive

Equation (73) is applicable to the majority of relatively small ( $\lesssim$ 2.5 meters radius) fast meteors entering the earth's atmosphere

(subject to the restrictions of applying the cylindrical blast wave theory to the phenomena). Noting that from equation (17), $R_o \sim M \cdot d_m$, equations (73) and (74) can be rewritten as:

$$1 << M << H/d_m \tag{75}$$

$$1 << M \sim H/d_m \tag{76}$$

where

M = meteor Mach number

Note the similarity between equations (73) and (54). See also equation (78) which directly relates $R_o$ to the wavelength of the disturbance. Thus the scale height, H, is readily useable as a practical distance measure of the nonuniformity of a planetary atmosphere. From theoretical meteorology it can formally be expressed as the vertical distance over which the atmospheric density of an isothermal atmosphere decreases by a factor of 1/e from some reference value (Craig, 1965). Thus primarily acoustic fundamental frequencies (satisfying equation (54))are generated for small energy releases (having equivalently small relaxation radii). Internal gravity waves on the other hand, can not be generated in a uniform medium (Tolstoy, 1963). A large relaxation radius (as compared to the scale height) is therefore necessary to ensure that internal gravity waves will be excited near the source. Note also that the equivalent expressions in (73) and (74) do not appear in (75) and (76). The line source problem utilizing a ballistic entry (i.e., with no lift present) produces an expression for the relaxation radius which is independent of the ambient pressure at the source altitude. In the "point" or spherical energy release problem, $R_s$ is dependent on the ambient pressure at the source altitude (See

equation (53)) and such simple expressions can no longer be written. While (74) and (76) are not due directly to the work of Groves or Tsikulin, it is suggested here that these expressions can be used as a necessary condition to test for the presence of a disturbance whose dominant period is in the acoustic gravity wave domain. Since the direction of wave propagation also becomes important in this regime, expression (74), can only be viewed as a necessary condition, but not a sufficient one, for the generation of primarily acoustic gravity waves in the assumed horizontally stratified, isothermal atmosphere.

Equation (74) is applicable to the rare large bodies like the Great Siberian Meteor of 1908. In this analysis only the relatively smaller bodies for which (73) and (75) are applicable will be considered. This is done from the point of view of finding the limiting smallest meteor mass which can be detected at great distances by infrasonic sensors. The detection of the bodies for which (74) and (76) are applicable is relatively easy in comparison (if the event is well reported in the media as is likely for these great events). It should be noted that military microbarograph observations as given by Gault (1970) and Lowry and Shoemaker (1967) indicate this minimum ground detectable threshold to be $m \sim 10^4$ grams ($r_m \sim$ 10-20 cm for a sphere with $3.0 \leq \rho_m \leq 0.3$ g/cm$^3$) with $M_{pan} \sim$ -8 and an entry kinetic energy of $10^{16}$ ergs. Here $M_{pan}$ is the panchromatic magnitude of the meteor. It is directly related to the brightness (or intensity) of the radiation being emitted. See Section VI (Part 3).

These scaling approximations make the problem of dealing with absorption as a function of the fundamental wave frequency much easier to formulate. Considering Mach numbers at entry of about

35 - 100 , equations (73) and (75) are applicable for those meteors with $R_o \leq$ 750 meters (i.e. $R_o \sim$ 0.1H). Since the most probable meteors have $R_o \leq$ 200 meters as calculated from the earlier models, this limiting distance will rarely be exceeded. For the scaling approximation expressed in (74) and (76) where $R_o \sim$ H, i.e. very energetic meteors, the atmospheric medium varies considerably in its constitution over the distance $R_o$ and the acoustic gravity wave dispersion problem as seen in the pressure waves from large nuclear explosions in the atmosphere (equivalently stated in terms of $R_s$) is then evident. For that problem the strong shock blast wave expansion should be calculated over an assumed nonuniform nonisothermal atmospheric path (Sakurai, 1965). Recent numerical calculations by Pierce et. al. (1971) of acoustic gravity waves from large nuclear explosions in the atmosphere use the initial conditions corresponding to the scaling approximation, equation (73) (where $R_s$ is used in place of $R_o$ and the charge diameter is used in place of $d_m$). Reasonable arguments are given however for not using a more realistic source model in their analysis. Thus the previous statement referenced from Sakurai may not be a practical necessity. For the more probable smaller meteors the strong shock wave ($p >> p_o$) has decayed to a weak shock ( $\Delta p << p_o$ with $d_a > d'$) long before the properties of the unperturbed medium have varied considerably

As has been seen, the initial strong shock phase of the disturbance was treated numerically following the work of Lin (1954) and Plooster (1968). The weak shock phase (on eventually to linear acoustic waves) was then considered theoretically using the numerical results as initial conditions for the weak shock propagation. In addition,

the fundamental frequency of the wave at $x = 10$ will be defined shortly following the thunder measurements of Few (1969). It should be noted that the numerical results must first be checked to see whether or not they correctly model the cylindrical blast wave at the ambient conditions at the source altitudes under consideration. Fortunately at the weak shock wave overpressures considered (at $x \geq 1.0$), the numerical solution is not very sensitive to the ambient conditions which were present when the blast wave was initiated (Groves, 1964; Plooster, 1968). See also Section VIII (Part 3). Thus the numerical work of Lin (1954), Plooster (1968) and the experimental measurements of Few (1969) are the correct initial conditions to apply to the meteor cylindrical blast wave line source problem, provided the effects produced by generalized ablation near the source are not too great. As was noted earlier for gross fragmentation this analysis is inappropriate. These initial conditions then, applied in the region where the shock wave is first weak, allow the further decay of the disturbance to be studied theoretically. See also Section V D.

The frozen fundamental frequency assumption (i. e., constant frequency) which is often used to calculate the attenuation of small explosions in the atmosphere (Reed, 1972) is then applicable to meteors for which equation (73) or (75) is satisfied. The frequency can only be considered frozen, however, over relatively short distances.

It has been experimentally observed that the larger the explosive energy release, the lower is the fundamental frequency associated with that explosion (Groves, 1964; Plooster, 1968; Few, 1969; Tsikulin, 1970). In order to relate the fundamental frequency to the energy release theoretically the wave shape near the source must be known.

The meteor sound explosion problem must deal with ablation effects however, and the common N wave shape of the pressure pulse (such as that used for a supersonic projectile) may not adequately describe the meteor induced wave shape near the source (or for all x) for all the possibilities involved. In addition, the front and rear shocks observed for supersonic projectiles are such that for ablating bodies only the front shock is clearly evident (near the source). In the laminar or the turbulent wake behind the body where ablated material has been deposited the rear shock may not be well defined (Chamberlain, 1968). In its place the many shocks produced by the hypersonic fragments are to be found (if ablation occurs as a result of continuous loss of small solid fragments). Thus, the resulting wave shape near the source is difficult to generalize while ablation can occur via many mechanism under many different conditions of flight.

Note that in spherical "point" source explosion waves only one shock initially propagates outward from the source. For the cylindrical problem where ablation effects are not too significant, two shocks propagate outward from the source ( the classical N wave) followed by a wake. Thus spherical waves are more like plane waves than cylindrical waves in their physical properties (Morse and Ingard, 1968).

The fundamental(or characteristic)frequency of the explosion will now be considered in more detail. In the case of cylindrical waves this frequency is a function of the observation distance. Following Few (1969), it is related to the inverse of the relation radius and can be defined as (for $x \geq 1.0$):

$$f_m = \frac{C_z}{f(\bar{\omega}, x)\ R_o}\ ;\quad \text{at } x = 10,\quad f_m = \frac{C_z}{f(\bar{\omega}, 10)\ R_o} \tag{77}$$

where

$f(\bar{\omega}, x)$ = a function whose value depends on the induced wave shape by the explosion at a certain distance from the source. This value is related to the duration of the positive overpressure phase of the expanding blast wave (this relation depends on the wavefront geometry as well as on the assumed shape of the wave). Beyond certain large values of x, $f(\bar{\omega}, x) = f(\bar{\omega})$, i.e., when $R \simeq \ell$ or $x \simeq \ell/R_o$. Here $\bar{\omega}$ refers to the induced wave shape and $C_z$ is the adiabatic sound speed at the source altitude. Note that in the spherical blast wave problem $R_o$ is replaced by $R_s$ in equation (77) (Few, 1969). See also Section VIII (Part 3).

From the experimental measurements of Few (1969) and the numerical work of Plooster (1968) on cylindrically expanding blast waves, $f(\bar{\omega}, 10) \cong 2.81$. Since from the equation (17), $R_o \sim M \cdot d_m$, (77) becomes:

$$f_m = \frac{C_z}{2.81\ M \cdot d_m} \tag{78}$$

or for the general cylindrical blast wave source: (at x = 10)

$$f_m = \frac{C_z}{2.81} \left( \frac{\gamma\ p_o}{E_o} \right)^{\frac{1}{2}} \tag{79}$$

For $d_m$ = 1 cm (which was the smallest diameter for which $V >> C$ and Kn = 0.05 were satisfied for the nonablating meteor model developed in IIIA) and M = 100 ( ~30 km/sec which was the upper velocity

limit due to ablation effects for the second meteor model) the relaxation radius, $R_o$, is 1.0 meter. For $C_z = 3 \cdot 10^2$ m/sec the fundamental frequency at x = 10 is:

$$f_m = \frac{3 \cdot 10^2}{2.81 \cdot 1} = 1.07 \cdot 10^2 = 107 \text{Hz}$$

This high fundamental frequency (short wavelength) will be significantly absorbed over relatively short vertical paths in the atmosphere, whereas for:

$d_m = 5$ meters

$M = 30$

$$\text{At } x = 10, \; f_m = \frac{3 \cdot 10^2}{2.81 \; (1.5 \cdot 10^2)} = 0.712 \text{ Hz}$$

which will propagate relatively great distances before being significantly absorbed. Note that in a general nonisothermal atmosphere these values are dependent upon the altitude of the source. In addition, while weak shock effects are important, $f_m$ will decrease as the wave propagates. This decrease is relatively greater for disturbances associated with smaller values of $R_o$. See Section V D, equation (91).

The fundamental frequency is the frequency at maximum energy (or equivalently stated in terms of the amplitude) at a given distance from the explosion. In his graphical results of the power (energy) spectrum of thunder, Few (1969) has shown both lower and higher frequencies associated with the pressure pulse, but very little energy was associated with frequencies smaller or greater than the fundamental. Presumably in general a significant amount of energy

may be associated with the higher frequencies (depending on ablation effects), which together with the fundamental produce the Fourier representation of a weak shock wave. For the general ablating meteor case the general wave shape is unknown but a leading shock front bounds the beginning of the disturbance. The assumed wave shape of Few (1968) and Plooster (1968) for Thunder will be used for lack of a better understanding of the effect of generalized ablation on the wave shape near the source of meteor induced line source explosion waves. This justifies the use of equation (78). Far from the source the underpressure phase of the wave should "shock" and the resulting wave shape should then correspond roughly to the triangular (sawtoothed) or N wave shape assumed in the derivation of equation (59) (for a plane shocked sound wave). Groves (1964) has shown that for spherical explosion waves, within limits, the difference in the overpressure predictions using either of these two assumed wave shapes discussed above, over equivalent atmospheric paths, were quite small. (i. e., with either one or two shock fronts present in the disturbance). The damping as predicted by equation (59) is appropriate for a continuous sawtoothed plane wave remote from its source. This is not entirely equivalent to the propagation of a N shaped disturbance (or plane wave pulse). While the decay in amplitude of weak shock waves which are not continuously replenished in energy by their source is not well understood, following Cotten, Donn, and Oppenheim (1971) it is assumed that the damping as predicted by equation (59) suitably approximates the damping for an N wave remote from its source (i. e., a disturbance not being continuously resupplied in energy). For the steady state sonic boom problem such replenishment does occur. See also Section VIII (Part 3).

The fundamental frequency, $f_m$, represents therefore the frequency at maximum energy which will propagate the furthest distance in the atmosphere, the higher frequencies being damped by the action of heat conduction and viscosity and the other mechanisms listed earlier (as the weak shock wave decays to a linear acoustic wave).

At this point so that no confusion will result, it should be noted that the fundamental frequency will later be referred to as the dominant frequency, i.e., the frequency at maximum amplitude. See Section VII (Part 3). The usage of the word dominant, instead of fundamental, is to distinguish the term fundamental from the usage it has gained in the acoustic gravity wave dispersion problem. There the term fundamental refers to a single propagation mode of the disturbance (Balachandran and Donn, 1968). As the wave period approaches zero (i.e., the high frequency acoustic limit), the fundamental mode closely resembles the acoustic modes in its behavior. This is reasonable since the group and phase velocity are equal (and in the same direction) in the high frequency limit (for a homogeneous medium). This is not the case, however, if geometrical dispersion is important (frequency dependent phase velocities produced by temperature and wind gradients at acoustic frequencies). Thus estimates of the meteor size, etc., in Section VII (Part 3) will be made using the dominant frequency of the pressure pulse (as defined in equation (78)). In general the total duration of the dispersive wave train will exceed the dominant period of the disturbance. This is especially true at large distances from the source as well as if the acoustic gravity wave realm is encountered. At relatively close range from the meteor the ray theory description allows the path of the dominant frequency of the pulse to be traced

through the atmosphere. For periods greater than about 10 - 15 seconds (generally quite far from the meteor) the ray theory should be abandoned in favor of the dispersion description provided by the acoustic gravity wave theory. As will be seen in Section VD periods greatly exceeding 10 seconds for the meteor line source problem as developed in this analysis should be quite rare. Thus the ray theory of geometrical acoustics appears to be a useful tool in studying meteor induced line source explosion waves. See also Figures 101-115. For the ray tracing methods which have been developed for the acoustic gravity wave realm the reader is referred to the work of Jones (1969).

The frequencies lower than $f_m$ are assumed not to carry a significant amount of wave energy. Since $f_m$ is a function of path distance, while nonlinear effects are important, (see equation (91)), the decay of the overpressure is in general a function of the entire power spectrum near and at relatively great distances from the source. In this analysis, we are assuming that an N wave shaped pulse is adequate over the weak shock wave region of the propagation to give the appropriate absorption for these waves (using equation (65c)).

Thus, the meteor induced waves, beyond a distance $R_o$, propagating into the isothermal nonuniform atmosphere will be considered as weak shock waves until equation (58) can be satisfied . The value of $\tau$ to be used at x = 10 in (58) is therefore $f_m^{-1}$. See equation (91). Note that in the decay predictions $f_m$ has been held constant at its value at x = 10. Thus the frequency absorption calculated using equation (65c) is the maximum possible (if the other mechanisms neglected are small). Beyond the scaled distance where equation (66) applies $f_m$ is nearly constant, so that equation (66)

was integrated exactly for an isothermal atmosphere, i. e., equation (66a). In general the altitude regions where equation (66) is found to be applicable are such that the absorption is very small (at least for disturbances having an associated $R_o$ greater than about 10 meters). Thus the error involved in using the value of $f_m$ at x = 10 in equation (66) rather than the value determined in equation (93a) is generally quite small. See Section V D.

The distinction between weak shock wave decay and linear acoustic wave decay is evident in equation (65c) and (66a). Equation (66a) is applicable strictly to linear acoustic waves as defined by testing equation (58). Equation (65) can be solved in an approximate manner for two limiting extremes. These are:

a) If B is small (i. e., if $B\,\Delta s << 1$ ) and $A >> B$, in a uniform medium, (65) reduces to (Morse and Ingard, 1968):

$$\frac{1}{\Delta p} - \frac{1}{\Delta p_z} = \frac{\gamma + 1}{\gamma}\left(\frac{1}{p_z}\right)\left(\frac{\Delta s}{\Lambda}\right) = A\,(\Delta s) \qquad (80)$$

In this case the amplitude decreases from the value $\Delta p_z$ at some origin point to $\Delta p_z/2$ at a distance $\Delta s$ of $(p_z/\Delta p_z)(\gamma/\gamma+1)$ wavelengths of the disturbance. In this limiting extreme the energy loss is not proportional to $f^2$ as it is in the other cases under consideration. (Here $p_z$ is the ambient hydrostatic pressure in the medium).

For a general nonuniform atmospheric path, equation (80) rewritten as:

$$\frac{1}{\Delta p} - \frac{1}{\Delta p_z} = \int A\, ds \qquad (80a)$$

For an isothermal atmosphere and f (or $\Lambda$) = constant,

(80a) becomes:

$$\frac{1}{\Delta p} - \frac{1}{\Delta p_z} = \frac{\delta + 1}{\delta \cos \bar{\epsilon}} \left(\frac{1}{p_o \Lambda}\right) \int_{z_o}^{z_z} \frac{dz}{e^{-z/H}} \qquad (80b)$$

Integrating and putting in the appropriate constants (80b) becomes:

$$\frac{1}{\Delta p} - \frac{1}{\Delta p_z} = \frac{4.01 \cdot 10^{-5} f}{\cos \bar{\epsilon}} \left[ e^{z_z/7.5} - e^{z_o/7.5} \right] \qquad (80c)$$

where

$p_o = 1.013 \cdot 10^6$ dynes/cm$^2$

C = 0.316 Km/sec = f

$\delta = 1.40$

H = 7.5 km

and $z_z \geq z_o$

Note that if we designate the right hand side of (80c) as I' that $\Delta p$ can then be written as:

$$\Delta p = \frac{\Delta p_z}{I' \Delta p_z + 1} \qquad (80d)$$

Thus for $I' \Delta p_z >> 1$, $\Delta p = \frac{1}{I'}$.

b) If however, $B/A >> p_z$, equation (65) reduces to:

$$\Delta p = \Delta p_z \exp \left[ -B ( \Delta s) \right] \qquad (81)$$

where

$\Delta p$ = overpressure or pressure amplitude of the disturbance at a distance $\Delta s$ from the source, where the amplitude was $\Delta p_z$. (with $\Delta s > 0$)

Note that from (63) and (68), both presently written with $\xi = 0$, the following equation results (Cotten, Donn and Oppenheim, 1971):

$$B = \frac{3\bar{\alpha}}{\pi^2} = 0.304\,\bar{\alpha} \tag{81a}$$

Similarly with (80c), (81) then becomes:

$$\Delta p = \Delta p_z \exp\left[\frac{-4.50 \cdot 10^{-8} f^2}{\cos\bar{\epsilon}}\left(e^{z_z/7.5} - e^{z_o/7.5}\right)\right] \tag{81b}$$

The intermediate case where $B/A \simeq \Delta p$ can also occur however. In order to compute the attenuation of the assumed plane wave for all the possibilities involved, see Section V D. (equations (92), (92a), (92b) and (93)). Note that equation (66) was derived such that $\frac{2\pi}{\Lambda} >> \bar{\alpha}$ so that $1/\bar{\alpha}$ ( the attenuation length) greatly exceeds $\Lambda$ (Lighthill, 1956). In the altitude regions where the linear acoustic theory is applicable (i.e., equation (58) is satisfied after the 10% distortion length is calculated) this restriction will always be satisfied for the present range of parameters being used.

There is still a consideration of the geometry of the expanding wavefronts to be discussed. Near the source (in the near field) the cylindrical geometry, is appropriate for the line source problem. The near field is defined as (Schultz, 1959):

$$\frac{2\pi}{\Lambda}(R - a) << 1 \tag{82}$$

where

$\Lambda$ = wavelength associated with the fundamental frequency of the disturbance. Note that during the nonlinear part of the propagation $\Lambda = f(x^{1/4})$. See equation (91).

R = actual radial distance from the source

a = radius of the source

Since a corresponds roughly to $d_m$, equation (82) becomes:

$$\Lambda >> 2\pi ( R-d_m ) \tag{83}$$

In a similar manner, the far pressure field definition becomes: (assumed valid beyond $R_o$ from the trajectory)

$$R - d_m >> \Lambda / 2\pi \tag{84}$$

In the far pressure field the wavefront is approximately plane. Using (78) (at x = 10), (84) becomes:

$$10 R_o - d_m >> 2.81 R_o / 2\pi$$

Since $R_o >> d_m$ (see equation (73)), the above becomes:

$$10 R_o >> 0.45 R_o$$

or

$$10 >> 0.45$$

While $\Lambda$ has not yet been formally evaluated at x = 1 in this report, Plooster's numerical calculations (1968) indicate that the above inequality at x = 1 would become:

$$1 >> 0.35; \text{ i.e. } f(\varpi, 1) \simeq 2.20$$

The wave frequency absorption equations (65) and (66) developed previously are for plane wavefronts. In the far pressure field the wave front can be assumed planar and then the appropriate decay law can be used to compute the attenuation of the wave pulse as a function of path distance from the source. This is done in Section V D.

The cylindrically expanding wavefront will appear spherical after a distance on the order of the line source length, $\ell$, has been reached. The latter statement assumes that atmospheric turbulence or other atmospheric effects such as refraction are not effective in breaking up the line source before $R = \ell$ is reached. If this is the case then by relating $\ell$ to $d_m$ and therefore to $R_o$, a scaled distance estimate can be made in terms of x as to where the change of cylindrical to spherical geometry occurs. From the effective meteor model this relation can be written as (for an average $d_{mE}$, $\rho_{mE}$ and $\theta$ in the range of extremes considered in Section III (Part 1); See also Figures 62-73 where the constant multiplying $R_o$ has been evaluated beginning at the altitude where Kn or $\overline{Kn}$ first equals 0.05):

$$\ell \sim 3 \cdot 10^3 R_o \text{ at } M_E = 100 \qquad d_{mE} = 10^2 \text{cm} \qquad (84a)$$

$$\ell \sim 9 \cdot 10^3 \cdot R_o \text{ at } M_E = 37 \qquad \rho_{mE} = 3.0 \text{ g/cm}^3 \qquad (84b)$$

$$\theta = 30^o \text{ with } \sigma = 0$$

Note that in Figures 62-73, for large $d_{mE}$, the constant factor multiplying $R_o$ will decrease somewhat. This is caused by the fact that for very large meteors the penetration depth is ultimately limited to values no greater than the finite atmospheric thickness. Is should be noted that in the evaluation of the constant multiplying $R_o$, as used in (84a) and (84b) and as shown in Fig. 62-73, an average value of $R_o$ was first calculated over the altitude range of interest.

Thus cylindrical spreading effects could be expected in general out to values of $x \sim 10^4$. For $R_o = 100$ meters this corresponds to a path distance about 1000 km from the source. Similarly with $R_o = 10$ meters a distance of about 100 km is then appropriate. These probably represent upper limits for each case since the effects of turbulent scattering have been neglected. Beyond $x \sim 10^4$ scaled spherical wave expansion is then appropriate. This will be discussed further in Section V D.

## D. CORRECTION FOR PROPAGATION IN A NONISOTHERMAL NONUNIFORM ATMOSPHERE

The overpressure ratio was calculated in IVA. in the following functional form:

$$\frac{\Delta p}{p_o} = f(x) = \begin{cases} k_o x^{-2} & \text{for } x \longrightarrow 0 \\ k_1 x^{-3/4} & \text{for } x \longrightarrow \infty \end{cases} \tag{85}$$

where

$k_o$ = a constant (See equation (11))

$k_1$ = a constant (See equations (92), (93) and (93b))

$p_o$ = uniform ambient pressure against which the blast wave expands.

In what follows $p_o$ will be replaced by $p_z$ which is the ambient pressure in the source altitude region where the cylindrical blast wave is being generated. Thus for a source with large $\mathcal{O}$, a large source altitude range must be considered, i.e., many different values of $p_z$ must be used. This has been done for the family of curves of different source heights shown in Figures 101-115. For propagation along an arbitrary nonuniform path the following correction factor is applied, (Pierce and Thomas, 1969) from $R_o$ outward assuming $d_m << R_o << H$; i.e., $M >> 1$, See equation (75).

$$\frac{\Delta p}{p_z} = f(x) \left[ \left( \frac{\rho_o}{\rho_z} \right)^{\frac{1}{2}} \left( \frac{C_o}{\bar{C}} \right) \right] N_c \tag{86}$$

where

$N_c$ = nonlinear propagation correction term

$C_o$ = sound speed at the observer

$\rho_z$ = atmospheric density at the source altitude

$\rho_o$ = atmospheric density at the observer; at the ground $\rho_o = \rho_g$

and

$$\overline{C} = \frac{1}{z_z - z_o} \int_{z_o}^{z_z} C(z)\, dz \qquad (87)$$

$$N_c < 1 + z_z/12H$$

where

$z_z$ = source altitude

$z_o$ = observer's altitude

Thus for source altitudes below about 100 km, $N_c < 2.1$; below 50km, $N_c < 1.55$. The inclusion of this term at the present time does not seem justifiable based on the fact that it is a relatively small correction term, i.e., the uncertainty in the density variation is many orders of magnitude greater than $N_c$ over long vertical paths. In addition to the fact that $N_c$ is small, two other points should be noted. The first is that as derived by Pierce and Thomas, $N_c$ assumes an isothermal atmosphere with constant winds. In the present study wind effects are not considered in the damping as developed in equations (65c) and (66a). The second point is that $N_c$ should only be included in the analysis while weak shock effects are important. Thus the approximate values of $N_c$ given above would be reduced still further. In the work of Pierce and Thomas for the steady state sonic boom problem $N_c$ was included over the entire altitude range between the source and observer. Since ground sonic boom measurements are generally made during the weak nonlinear part of the propagation, their inclusion of $N_c$ over the entire path (to compare theoretical predictions with observations) is quite appropiate. Note that $N_c$ is always greater than one since the wave is becoming progressively more linear as it propagates downward

into a medium of increasing density (Pierce et. al., 1969). A further discussion on this subject related to calculations of d' is included later in this section. Setting $N_c = 1.0$ will be seen in Section VII (Part 3) to play a small role in the present error estimates as made for the meteor size predictions using existing meteor sound observations. Thus at this point $N_c$ has been formally set equal to 1.0. See also Tsikulin (1970).

For the lower 100 km of the atmosphere $C_o/\overline{C} \sim 1$ so that (86) becomes: (Kane, 1966):

$$\frac{\Delta p}{p_z} = f(x)\left(\frac{\rho_o}{\rho_z}\right)^{\frac{1}{2}} = f(x)\left(\frac{p_o}{p_z}\right)^{\frac{1}{2}} \tag{88}$$

Therefore

$$\Delta p = f(x)\,(p_o p_z)^{\frac{1}{2}} = f(x)\,\overline{p^*} \tag{89}$$

where

$\overline{p^*} = (p_o p_z)^{\frac{1}{2}}$ which is the geometric mean pressure between the observer's altitude and the altitude where the blast wave was generated.

Equations (85) and (89) can then be written as:

$$\frac{\Delta p}{p_o} = k_o x^{-2} \text{ for } 5\cdot 10^{-2} \lesssim x \lesssim 1.0$$

$$\frac{\Delta p}{\overline{p^*}} = k_1 x^{-3/4} \text{ for } x \gtrsim 1.0 \text{ with } d' < d_a \tag{90}$$

where

$\Delta p = p - p_o$ and at the ground $\overline{p^*} = (p_g p_z)^{\frac{1}{2}}$. Over propagation paths where C varies appreciably, the correction factor expressed in equation (86) is more appropriate than the isothermal atmospheric

path correction expressed in equation (89) (if this variation is or can be presumed known). Note that the nonisothermal nature of the atmospheric medium enters into the decay of a given disturbance both through the term in the brackets in equation (86) as well as through the integrated form of D(R) as given for the isothermal case in equation (92a) for weak shock waves and in equation (92b) for linear acoustic waves. See also equation (92).

The above procedure represents an approximate geometric scaling of the blast wave overpressure decay for a general nonuniform atmospheric path between the observer and the explosion altitude region of interest assuming $d_m << R_o << H$. Note that the $x^{-3/4}$ dependence expressed in (90) is not appropriate after equation (58) has been satisfied. In equations (93) and (93b) expressions are given for the appropriate x dependence after the weak nonlinear propagation effects have become small.

Unless the path taken is known as are the variations in the atmospheric parameters which significantly influence the attenuation along the path, estimates of decay of the disturbance are at best very approximate, i.e., within perhaps an order of magnitude of the overpressure which would be observed. In addition, since the atmospheric parameters are assumed to be in a steady state, only relatively short propagation paths are appropriate. As will be seen in Figures 101-115, present calculations of the decay from the assumed line source do not exceed about 300 km. For nearly vertical propagation (as in the rocket grenade experiments) or for short ducted ray paths ($\lesssim$ 200 km from relatively small ground explosions ), point source blast wave attenuation predictions agree with observations within a factor of about three (Reed, 1972).

Tsikulin (1970) has predicted the amplitude decay from a cylindrical blast wave line source model of an entering meteor using an isothermal model atmosphere (without winds) for meteors such that $d_m << R_o << H$. He assumed the disturbance at $x \geq 1$ to decay as if it was a linear acoustic wave, however. This appears to be quite a common approach (Reed, 1972). As has been shown in this analysis a distinction can now be readily made between weak shock and linear acoustic waves when considering the amplitude decay of a weak disturbance.

The results of Tsikulin generally predict much larger amplitudes than are predicted in this analysis. This is especially true for high source altitudes ( > 50Km). Because he assumed signal linearity beyond $R_o$ for all source heights and wave periods his results are far more optimistic in terms of ground predicted overpressure. As has been seen in this analysis however it is not always correct to assume signal linearity beyond $R_o$. This problem has by no means been solved in its entirety in a realistic manner however, as is evidenced by the recent work of Greene and Whitaker (1968), Varley and Cumberbatch (1969), George and Plotkin (1971), and Kahalas and Murphy (1971).

It is assumed that as the N wave propagates it widens such that (Dummond et. al., 1946):

$$\tau_m = 0.562\, \tau_{mo}\, x^{1/4} \quad \text{for } x \geq 10 \text{ with } d' < d_a \qquad (91)$$

where

$\tau_{mo}$ = value of the fundamental wave period at $x = 10$

$\tau_m = 1/f_m$

Here $\tau_m$ is defined as one period of the wave, i.e., from the beginning of the positive overpressure phase to the end of the negative underpressure phase (to where the pressure disturbance again crosses the

horizontal axis; DuMond et. al, 1946). Note that this is not the same definition as used by Hilton et. al. (1972) and others who work in the sonic boom research area. Apparently atmospheric turbulence effects are partly responsible for the generally complicated variability of the return of the underpressure phase of the wave back to the local predisturbance ambient pressure conditions. Their definition of wave "duration" is from the beginning of the rise of the disturbance from ambient conditions to the time at which the maximum underpressure phase occurs. The difference in evaluating the wave period using these two definitions can at times be substantial depending on the manner in which the underpressure phase returns to the "zero" deviation level. Part of the underpressure phase problem may be due in fact to the cylindrical geometry involved. Morse and Ingard (1968) have shown that an ideal cylindrical source will send out a signal with a sharp beginning but with no ending, i. e., the deviation never returns to the "zero" level (the wavelength indefinitely spreads as the distance increases). Thus either nonuniform atmosphere effects, turbulence effects or both as well as the possibility of spherical wavefront geometry (possibly due to refraction effects or turbulent scattering ) may have some influence on this underpressure phase return problem. We will not consider this problem further in this analysis. In order to use equation (91) however it should be remembered that weak nonlinear effects must be present. See equation (93a) Sample calculations of the wave period using equation (91) compare very favorably with recent observational results obtained at Mach 16 for the reentry of Apollo 15 (Hilton, et. al., 1972). See also the recent theoretical predictions of Pan and Sotomayer (1972) and Section VIII (Part 3). In addition, see Figures 101-115 for predictions of $\tau$ at the ground, i. e., $\tau_g$.

Note that the $x^{1/4}$ dependence was a result obtained for a uniform atmospheric path. While both Meyer (1962) and Remillard (1960) found spreading of $\tau$ proportional to x, respectively for the isothermal atmosphere case (i.e., exponential density decrease with increasing altitude) and for a uniform atmosphere (both for a cylindrical source of linear acoustic waves), we will assume that the $x^{1/4}$ spreading effect is also valid for the general nonuniform atmosphere case. This is also somewhat justifiable while the $x^{-3/4}$ dependence of $\Delta p$ and the $x^{1/4}$ dependence of $\tau$ are mutually consistent (DuMond et. al., 1946). Thus, while we are using the $x^{-3/4}$ dependence for $\Delta p$ with only a $\overline{p^*}$ correction for a nonuniform atmosphere it seems reasonable at this point that while weak nonlinear effects are important that the $x^{1/4}$ spreading of $\tau$ is justifiable (at least to a first order approximation). See also Section VIII (Part 3).

Note that the spreading effect proportional to $x^{1/4}$ is only valid as long as we are dealing with weak shock waves of cylindrical geometry with D(R) = 1. A similar spreading effect is also seen in the spherical blast wave problem, i.e., the finite amplitude propagation effect (Otterman, 1959; Groves, 1964; Kahalas and Murphy, 1971). Linear acoustic waves of spherical geometry do not change their shape as they propagate (in a uniform medium) while all frequencies attenuate at the same rate (Morse and Ingard, 1968). This is entirely as a result of the spherical geometry. Weak shock waves of spherical geometry do spread as they leave the source (as was noted above) because of the weak nonlinearity present. When equation (58) is first satisfied the nonlinear spreading effect associated with weak shock waves of cylindrical geometry, is assumed to cease. Linear acoustic waves of

cylindrical geometry do spread, however, as they leave the source because of geometrical considerations alone, i. e., the wake effect (Morse and Ingard, 1968; Remillard, 1969). At distances from the source comparable to the line source length a transition to spherical wave expansion has been predicted. This transition is inevitable because of both the geometry of the situation as well as upon the diffusing effect of turbulence on the resulting propagation (Few, 1969; Evans et. al., 1970). The scattering problem involved here depends in part on the wavelengths of the disturbance being generated. The smaller the energy release (i. e., for a given large M, the smaller $d_m$ is), the higher is the fundamental frequency (at any given observation distance) and the shorter is the line source length. Thus, the larger $d_m$ is, the larger $R_o$ and $\ell$ become (with certain limits as discussed earlier). These statements have already been put in quantitative form in equation (84a) and (84b). Therefore the smaller the energy release is, the closer to the trajectory the transition from cylindrical to spherical expansion occurs. See Figures 62-73.

For this problem then, we will allow the $x^{1/4}$ nonlinear spreading effect until distances from the source are reached such that $d' > d_a$. From about this distance outward a linear acoustic wave with cylindrical expansion can be assumed with no further spreading effects. It will be seen shortly (See Figures 106 and 111) that the transition from weak shock to linear decay generally occurs earlier, but at about the same path distance at which $R \sim \ell$ (i. e., $x \sim 10^4$). For $\bar{\epsilon} = 0^o$ (vertical downward heading rays) the transition occurs well before $x \sim 10^4$ is reached. As $\bar{\epsilon}$ becomes large i. e., for long slant ray paths, the transition $d' > d_a$ occurs at lower altitudes but still very near where

R approaches $\ell$. The former is only true for disturbances with an associated $R_o \gtrsim 50$ meters however, due to increased absorption over long slant paths from high altitudes, for the higher fundamental frequencies. It should be noted at this point however that in Figures 101-115, the scaled distance $x = 10^4$ has been used throughout for all $R_o$ values considered, i.e., 10-300 meters. Figures 62-73 illustrate that this scaled distance value is a variable depending on M, $d_m$ and $\tau$ (through $R_o$) as well as upon $\theta'$ and $\rho_m$. Thus, when using the present attenuation predictions, in order to relate $R_o$ in altitude to the dynamical meteor models specified in III, at least either M or $d_m$ must first be specified. This is primarily because $R_o$ depends on both M and $d_m$ which by themselves as independent variables greatly influence the altitude region of a meteor induced cylindrical blast wave line source.

Thus, a transition is assumed to occur at the altitude where $d' > d_a$ from weak shock waves of cylindrical geometry to linear acoustic waves of cylindrical geometry. At these great distances from the source further spreading of $\tau$ even for linear sound waves of cylindrical geometry must be very small. At distances $R \gtrsim \ell$, a spherically expanding linear wave picture would then be appropriate. The geometrical argument just presented for linear spherical waves justifies this assumption of no further spreading of $\tau$ for these weak waves. This statement refers only to the dominant frequency of the disturbance and not to the total length of the dispersive wave train that the disturbance is generally imbeded within.

For most observations we hope to make, $\ell$ will probably be $\gtrsim R$ so that the spherical geometry considerations are probably of no great concern. The above statement is based on the detection problem of these relatively small energy releases (as compared with that of megaton nuclear explosions). The pressure signals in general

at distances where $R \sim \ell$ will be seen to be of small enough amplitude so that detection may not always be possible (depending on many uncontrollable factors). See Figures 101-115. If detection is possible for $R \gtrsim \ell$, the pressure signal as recorded by many randomly spaced stations will appear to come from a nearly isotropic source in azimuth (neglecting the refractive and directional effects of the wind and temperature systems). Note that we have implicitly assumed in this discussion that $R_o << H$.

Beginning near the source, in the strong shock region of expansion, the wave energy is assumed to be conserved, except for spreading losses (Sakurai, 1965). Near $x = 1.0$, the weak shock region is approached. As used in equation (90), the exponent -3/4 is the theoretically accepted and minimum observed experimental value that applies to propagation of weak shock waves of cylindrical geometry along a uniform path i.e., homogeneous in density (DuMond et. al., 1946; Whitham, 1952; Tsikulin, 1970). The original experiment was carried out on conical sonic boom waves from supersonic bullets. The decay measurements were conducted in the far pressure field so that the observed decay is that expressed for plane waves (DuMond et. al., 1946). It is assumed that this decay when corrected for a nonuniform isothermal path via $\overline{p^*}$ and absorption as a function of the fundamental frequency via equation (65) and (66) (at appropriate distances from the source using equation (58)) will approximate the actual damping which must occur, i.e., in order that the energy conservation principle be maintained.

Thus, at present, the source is assumed to deposit the energy instantaneously (over the altitude regions shown, i.e., the

solid lines in Figures 62-73, over which V has changed 5% from its value at Kn or $\overline{Kn}$ = 0.05), so that the disturbance will be damped without replenishment as it propagates. See Section VIII (Part 3) for further discussion on the instantaneous versus noninstantaneous energy release considerations, i.e., to the extended source concept alluded to earlier.

Equation (90) can be now written as:

$$\Delta p = \frac{0.525 \cdot \overline{p^*} \cdot D(R) \cdot R_g}{\left\{\left[1 + 4.803 \left(\frac{R}{M(z_z) \cdot d_m(z_z)}\right)^2\right]^{3/8} - 1\right\}} \qquad (92)$$

For $x \gtrsim 1.0$ and with $d' < d_a$

where

R = actual radial path distance from the meteor

D(R) = absorption decay function of the fundamental wave frequency (See equations (92a) and (92b))

$R_g$ = ground reflection coefficient

$M(z_z)$ = meteor Mach number at the assumed source altitude

$d_m(z_z)$ = meteor diameter at the assumed source altitude

$\gamma$ = 1.4

In (92), $\overline{p^*}$ is evaluated between the source and the observer. For vertically downward propagation R = z (depending on the orientation of the meteor trajectory as well as upon the refraction encountered). For slant path propagation, $R = z/\cos\bar{\epsilon}$ where $\bar{\epsilon}$ is the zenith angle of the ray between the source and the observer (with respect to the local vertical). See Figure 100a. and 100b. $\bar{\epsilon}$ can be related to both $\Delta\phi$ and $\theta$, as used in Section IV. This relationship can be written as:

$$\Delta\phi = 90\left[1 - \tan\sigma\cot\bar{\epsilon}\right] \quad \text{in degrees}$$

with $\bar{\epsilon} \geq \sigma$

$\sigma \neq 90^{o}$

$\bar{\epsilon} \neq 0^{o}$

The above expression is graphically displayed in Figure 116. Note that $\bar{\epsilon}$ as defined here is always viewed in a plane perpendicular to the plane containing the ray. Thus in Figures 101-115, the values of $\bar{\epsilon}$ can be used to specify decay for rays generated within the entry plane for either $\sigma = 70^{o}$, $40^{o}$ or $10^{o}$. They can also be used for example for $\sigma = 10^{o}$, for $\bar{\epsilon} = 40^{o}$ and $70^{o}$, outside the plane of entry, as well as for $\sigma = 40^{o}$, $\bar{\epsilon} = 70^{o}$ again for propagation outside the entry plane. The azimuthal direction corresponding to the $\bar{\epsilon}$ values as chosen for propagation outside the entry plane can then be determined using Figure 116.

The appropriate value of D(R) depends in part on $R_o(z)$ for a given meteor, i.e. on $f_m$. Equation (58) must be tested to see if D(R) should be calculated using weak shock wave decay laws or linear acoustic wave decay laws. D(R) depends primarily on how the shape and overpressure ratio of the induced disturbance change with increasing x.

The general form of D(R) to be used when weak shock decay laws are applicable is as follows: (using equation (65c))

$$D(R) = \frac{\Delta p}{\Delta p_z} = \frac{(B/A)\exp\left[\dfrac{-4.50\cdot 10^{-8} f_m^{\,2}}{\cos\bar{\epsilon}}\left(e^{z_z/7.5} - e^{z_o/7.5}\right)\right]}{\left[\Delta p_z\left(1-\exp\left(\dfrac{-4.50\cdot 10^{-8} f_m^{\,2}}{\cos\bar{\epsilon}}\left(e^{z_z/7.5} - e^{z_o/7.5}\right)\right)\right) + B/A\right]} \qquad (92a)$$

where

$\Delta p_z$ = overpressure at the source altitude (as calculated at x = 1.0 via equation (13))

$\Delta p_z = 0.5627\, p_z$

$B/A = 1 \cdot 121 \cdot 10^{-3} f_m$ (with $f_m$ in Hertz)

$C = 0.316$ km/sec (assumed constant)

$\gamma = 1.40$

Several points should now be noted. The first is that the decay of a shocked disturbance depends on the amplitude of the shock front at some chosen origin point. This was not true in the case of strictly linear sinusoidal waves. Secondly, using $x = 1$ to evaluate $\Delta p_z$ is correct if an instantaneous energy release can be assumed. Thus all of the energy is assumed to be deposited during the strong shock region of expansion (Few, 1968), i.e. along the entire line length $\ell$. As has been shown in Section IV A, this is an increasingly poor approximation especially for the less energetic meteors. Using an extended source concept the value of x used in evaluating $\Delta p_z$ can then in general be increased. When using $x = 10$ to evaluate $\Delta p_z$ for example, weak shock damping at high altitudes is 10 times less severe for $R_o = 10$ meters. For $R_o =$ 300 meters, it is 3.5 times less severe. Using this concept it can be shown that the value of x to be used in evaluating $\Delta p_z$ is a function of distance (along $\ell$) away from the meteor. Thus for moderate $\theta$, the higher altitude portions of the disturbance would generally be damped less severely than is now predicted, i.e., larger x values can be used in evaluating $\Delta p_z$ than at lower altitudes closer to the source. For $\theta \gtrsim 40^o$, however, refraction effects may tend to break up the assumed line source geometry. It should also be noted that for a noninstantaneous

energy release, equation (57) predicts that weak shock decay laws will be applicable at greater distances from the source, especially for the high altitude portions of the disturbance. Still, the presently calculated decay is probably the maximum damping which can occur. This is especially true while the energy release has been considered as strictly instantaneous. See Section VIII (Part 3) for further discussion on these possibilities.

When linear acoustic decay laws are applicable D(R) can be written as:

$$D(R) = \frac{\Delta p}{\Delta p_z} = \exp\left[\frac{-1.48\cdot 10^{-7} f_m^{\,2}}{\cos \bar{\epsilon}}\left(e^{z_z/7.5} - e^{z_o/7.5}\right)\right] \qquad (92b)$$

The damping predicted by equation (92a) is generally very selective with respect to the fundamental frequency of the wave. This is also the case for the damping predicted by using equation (92b). At source altitudes above about 95 km for $f_m$ = 10Hz, equation (81b) becomes the approximate form of (92a). Even though (81b) predicts smaller damping than that of linear acoustic waves at the same altitude, it is so severe that the wave quickly becomes linear as is indicated by calculating d'. This is consistent with the discussion by Morse and Ingard on the approximate form of (92a) when $B/A >> \Delta p$. For fundamental frequencies below about 1.0Hz the weak shock damping as predicted by (92a) is much less severe. It is to be recalled however, that equation (61) was derived such that $\gamma H >> \Lambda$.

Thus the formation (or maintenance) of a weak shock wave beyond $R_o$ is caused by both the distortion produced in a nonuniform medium (resulting from the cumulative weak nonlinearity effects) and indirectly to the presence of an explosive source (through $f_m$). The conclusions of this analysis are such that even linear acoustic waves propagating downward from the upper atmosphere would eventually form shock fronts under certain conditions. This is also consistent with the conclusions of Cotten, Donn and Oppenheim (1971). Meyer (1962) found a similar effect due to linear waves propagating upward into a less dense medium. This effect is also described by Craig (1965) and many other authors. While the situation Meyer was considering is similar to the present situation, they are by no means equivalent. In Meyer's case, d' calculations would reveal continually smaller values as the altitude of the disturbance increased. Thus in Meyer's situation the decreasing density in an upward direction caused a continual increase in the nonlinearity of the wave. In the present situation calculations reveal that d' continually becomes larger as further distances from the source are reached. Thus for downward propagating waves from a line source (or similarly with different spreading losses from a point source) the disturbance eventually (after it has become fully distorted) appears progressively more linear. This is true especially for the present, case where an instantaneous energy release was assumed. The advantage of the d' calculation is that the weak nonlinear protion of the propagation can now be readily identified using equation (58) as the testing criterion.

The additional factor in equation (92), $R_g$, due to ground reflection (the echo effect), must be included in the overpressure

prediction, i.e., $R_g = 1.0$, except at the ground. For vertical arrivals over flat "hard" ground $R_g = 2$ (Reed, 1972). In a dense forest (where some microbarograph instruments are located) and for moderate elevation angles of arrival, $1 < R_g < 2$ (Cotten, Donn, and Oppenheim, 1971). Thus $R_g$ is dependent upon both the local topography as well as upon the local vegetation features. In Figures 101-115, $R_g$ was arbitrarily assumed to be 1.5.

The calculations of Tsikulin predict overpressure attenuation decreasing as $x^{-1/2}$. This is correct if the waves are strictly linear cylindrical sound waves (Officer, 1958). He also predicts however no spreading of $\tau$ as the wave leaves the source (for propagation into a medium of exponentially increasing density). Following the conclusions of Morse and Ingard (1968) and Meyer (1962), the spreading effect of $\tau$ for linear waves is a geometrical necessity (for $R < \ell$) due to the presence of wakes in the cylindrical line source case. Therefore, we cannot accept the predictions of Tsikulin with regard to the period of the disturbance remaining constant independent of the observation distance.

Thus for distances such that $d' > d_a$ further overpressure attenuation is then dependent on $x^{-1/2}$. For x values such that $d' > d_a$ but small enough so that $R < \ell$, equation (92) becomes:

$$\Delta p = \frac{0.525 \cdot \overline{p^*} \cdot D(R) \cdot R_g \cdot x^{1/4}}{\left\{\left[1 + 4.803\left(\frac{R}{M(z_z) \cdot d_m(z_z)}\right)^2\right]^{3/8} - 1\right\}} \qquad (93)$$

where

D(R) is given by equation (92b). Again, $R_g = 1.0$, except at the ground. For the above case, equation (91) is replaced by:

$$\tau = \tau' = \text{constant for } x \geq x' \qquad (93a)$$

where

$\tau'$ is the value of $\tau$ from equation (91) at x', where x' is the value of x for which d' first exceeds $d_a$. Note that equation (93) must be reinitialized if equation (92) is first used. See Figures 101-115. For $x \gtrsim 10^2$, equation (93) can be approximated as:

$$p = \frac{0.2917 \cdot p^* \cdot D(R) \cdot R_g}{x^{1/2}} \qquad (93b)$$

For $R \gtrsim \ell$, decay of linear sound waves with scaled spherical geometry is then appropriate and equation (93) would then have to be suitably modified. This decay, for $R > \ell$, will not be considered theoretically in this analysis for the reasons discussed earlier. For more details on this subject see Groves (1964), Tsikulin (1970) and Reed (1972). See also Section VIII (Part 3). The overall effects and variability of turbulent scattering (in addition to the assumption of steady atmospheric parameters) makes such long distance propagation difficult to analyze realistically using the present methodology.

Having seen the absorption predictions as a function of the fundamental frequency of the wave (as well as the attenuation predictions), an additional insight is now possible for interpretation of the meteor models generated in Section III (Part 1). While the absorption decay may be proportional to f or to $f^2$ during the propagation the dynamic possibilities for bow shock generation can now be reconsidered in terms of energy decay considerations (or in terms of measurement or observation of meteor sounds at ground level far from the source; $\ell > R \gg d_m$).

A fundamental frequency of 107Hz (M=100, $d_m$ = 1 cm at x = 10) will propagate vertically only a very short distance in comparison

with the fundamental frequency associated with a $10^4$ gram meteor ($\sim$ 20 cm in radius). See Figures 101-115 for the ground predictions of wave period for the range of $R_o$, $z_z$, and $\bar{\epsilon}$ considered. At M = 100 ($\sim$ 30 km/sec) the relaxation radius will be:

$$R_o = 100 \cdot 4 \cdot 10^{-1} m = 40 \text{ meters}$$

so that

$$f_m = \frac{3 \cdot 10^2}{2.81 \cdot 4 \cdot 10^1} = 2.67 \text{ Hz at } x = 10.9$$

or at M = 30, $f_m$ = 8.90 Hz.

Thus the wave decay case, $R_o \sim H$, where the atmosphere is actually heaved by the blast wave source and where acoustic gravity waves are primarily excited, has not been calculated in this analysis. This is a direct result of the allowed range of meteor parameters (chosen in Section III for the line source problem) so that only acoustic frequencies have been considered (as defined earlier by equation (54)) and the acoustic gravity wave dispersion problem has been basically avoided. The dispersion resulting from absorption of the wave energy (from both weak shock waves and linear sound waves with $\Lambda << \gamma H$) has indirectly been considered however since in order to know the appropriate decay law to use, the wave shape, the overpressure ratio and the period must be known as a function of scaled distance from the trajectory. As was noted earlier in this section the wave shape has been assumed. In order to fully study the dispersion (resulting from both geometrical effects as well as directly due to absorption for acoustic frequencies) the wave shape must be an unknown to be solved for so that the power spectrum of the disturbance will evolve with increasing distance from the source.

Based on the frequencies considered in this analysis the lower sound duct (bounded by the ground at the bottom and the seasonally variable stratospheric wind systems at its upper extent) will be the most probable route for the ray paths since absorption for these frequencies between the ground and the lower thermosphere can at times be severe (Donn and Rind, 1972). For reflection heights near 95km this absorption restriction is less severe than if the temperature and wind fields cause downward return of the rays near 120km. Thus thermospheric long distance ducting may or may not be significant depending primarily on how the temperature and wind structure affect the ray path direction and in so doing its resulting absorption as a function of frequency. Near the source, when direct ray paths to ground level exist, low frequency audible sound (i.e., $f > 10$Hz with $\Delta p$ exceeding the audible threshold of the ear) is then possible for certain meteors which are energetic enough (depending of course on the ablation effects). This applies both within and outside the entry plane for direct ray arrivals assuming the observer is not in or near a shadow zone, i.e. assuming refractive effects allow for ray paths to the observer.

As was stated earlier only rays with initially net downward paths have been considered in this analysis. For shallow entry the nearly vertically upward heading rays will be absorbed greatly due to the rapid increase of mean free path with increasing altitude (by primarily the action of viscosity and heat conduction). For moderate $\theta \sim 45^{\circ}$ perhaps both downward and upward ray paths should be considered. As $\theta \rightarrow 90^{\circ}$, refraction effects make arrival at ground level near the source improbable however and we are only concerned with those rays which can reach ground level. Also as will be seen in

Section VI (Part 3), the maximum occurence of $\sigma$ peaks below $40^{o}$. Therefore in general we are justified in considering only those rays which have initially net downward path directions. In a later report concerned with a full ray tracing analysis of meteor sounds both initial ray directions will be considered. It is to be noted that the k'(z) values (as seen in Figures 86-97) are not symmetric about the entry axis due to the presence of directional wind components as a function of altitude as included in a realistic but horizontally stratified atmospheric model. The refraction therefore is different in general for these two initial ray directions (as is their resulting attenuation with distance).

One additional topic remains to be discussed at this point. This topic relates to observations of meteor sounds for which equations (91) and (92) are applicable. Assuming D(R) = 1, a relation can be derived to estimate the altitude region in which the disturbance was generated. Dividing equation (92) by equation (91) the following approximate expression results:

$$\frac{\Delta p}{\tau} = \frac{0.1847\ \overline{p^{*}}\ C_z}{R} \quad ; \text{For } \ell > R,\ d' < d_a \text{ and } x \gtrsim 10^2 \tag{94}$$

Thus if $\Delta p$, $\tau$ and $R$ are known for a given meteor, if a value of $C_z$ is assumed (i.e., $C_z \sim \overline{C}$ = constant for the assumed isothermal atmosphere) then an estimate of $\overline{p^{*}}$ can be made. While $\overline{p^{*}} = (p_z p_g)^{1/2}$, through the use of the isothermal atmospheric model in Table 5, $z_z$ can be estimated. See Section VII (Part 3) for the possible usefulness of equation (94). Note that R is the actual path distance from the source (which is generally unknown). As a first approximation at relatively great scaled distances from the source

R is equal to the distance from the ground projection of the trajectory to the observer. The aximuth angle as determined at the observer will determine the approximate position along the trajectory which is appropriate when R is estimated ( if cross wind effects are neglected). Thus for (94) to be applied the horizontal range distance from the meteor must exceed the altitude $z_z$ at which the blast wave was generated. In addition the wave must remain a weak cylindrical shock wave all the way between $R_o$ and the observer. Note the similarity between equation (94) and equation (9), p. 113 of DuMond et. al. (1946).

The results of this section will be used in Section VIII (Part 3) in order to determine the source altitude, relaxation radius, size, mass and kinetic energy of the meteors for which documented infrasonic recordings are available. Had these events also been well documented using photographic techniques (such as those of the Prairie Network) more precise decay laws could be determined (on an empirical basis) as well as more precise error limitations on the present meteor parameter predictions.

## BIBLIOGRAPHY (Part 2)


1. Astapovich, I. S., The Power of the Sound Detonations of the Choulak-Kurgan Bolide, Air Technical Intelligence Center, Wright-Patterson AFB, Technical Translation from Byull. Turkin, FAN USSR, No. 2, pp. 77-80, 1946.

2. Astapovich, I. S., Meteoric Phenomena in the Earth's Atmosphere State Publishing House of Physical and Mathematical Literature, Moscow, 640 pp. (in Russian), 1958.

3. Balachandran, N. K., Acoustic-Gravity Wave Propagation in a Temperature and Wind-Stratified Atmosphere, Journal of Atmospheric Sciences, Vol. 25, No. 5, pp. 818-26, September, 1968.

4. Balachandran, N. K., and W. L. Donn, Dispersion of Acoustic Gravity Waves in the Atmosphere, T. M. Georges, Editor, ESSA-ARPA Symposium: Acoustic Gravity Waves in the Atmosphere, Boulder, Colorado, pp. 179-193, 1968.

5. Balachandran, N. K, W. L. Donn and G. Kaschak, On The Propagation Of Infrasound From Rockets: Effects of Winds, J. A. S. A., Volume 50, Number 2 (Part 1), pp. 397-404, 1971.

6. Bartman, F. L., The Rocket-Grenade Experiment for Upper-Air Temperature and Wind, Atmospheric Physics, The University of Michigan Engineering Summer Conferences, Chapter 4, June 5-9, 36 pp., 1967.

7. Bass, H. E., et. al., Atmospheric Absorption of Sound: Analytical expressions, J. A. S. A., Vol. 52, No. 3 (Part 2), pp. 821-25, 1972.

8. Batten, E. S., Wind Systems in the Mesosphere and Lower Thermosphere, J. Meteorology, Vol. 18, pp. 283-91, 1961.

9. Berthet, C., and Y. Rocard, A New Mechanism for the Propagation of Infrasonic Waves at Long Distances in the Atmosphere, J. A. S. A., (To be published).

10. Blackstock, D. T., Finite-Amplitude Infrasonic Waves in the Atmosphere, J. A. S. A., (To be published).

11. Blackstock, D. T., A Comparison Between Weak Shock Theory and Burgers' Equation in Nonlinear Acoustics, Symposium on Aerodynamic Noise, Loughbourough, Leics, England, 21 pp., Available From Technical Information Service as A71-17156, 1970.

12. Blokhintzev, D., Acoustics of an Inhomogeneous Moving Medium I, J. A. S. A., Vol. 18, No. 2, pp. 322-8, 1946

13. Brode, H. L., Numerical Solutions of Spherical Blast Waves, J. Applied Physics, Vol. 26, p. 766, 1955.

14. Brode, H. L., Blast Wave from a Spherical Charge, The Physics of Fluids, Vol. 2, No. 2, pp. 217-29, 1959.

15. Bronshten, V. A., Problems of the Movement of Large Meteoric Bodies in the Atmosphere, NASA TT-F-247, November, 1964.

16. Carr, M. H., Atmospheric Collection of Debris from the Revelstoke and Allende Fireballs, Geochimica et Cosmochimica Acta, Vol. 34, pp. 689-700, 1970.

17. Ceplecha, Z., Private Communication, 1972.

18. Chamberlin, Von Del , Meteorites of Michigan, Bulletin No. 5 of the Geological Survey of Michigan, Lansing, Michigan, 1968.

19. Chimonas G. and W. R. Peltier, The Bow Wave Generated By An Auroral Arc In Supersonic Motion, Planetary and Space Science, Vol. 18, Number 4, pp. 599-612, 1970.

20. Cook, R. K., Atmospheric Sound Propagation, Atmospheric Exploration By Remote Probes, Proc. of the Scientific Meetings of the Panel on Remote Atmos. Probing to the Comm. on Atmos. Science, National Academy of Sciences, and the National Research Council Vol. 2, pp. 633-69, January, 1969.

21. Cospar International Reference Atmosphere 1965, North-Holland Publishing Company, Amsterdam, 1965.

22. Cotten, D. E., W. L. Donn, and A. Oppenheim, On the Generation and Propagation of Shock Waves from Apollo Rockets at Orbital Altitudes, Geophys. J. Roy. Astron. Soc., Vol. 26, pp. 149-59, 1971.

23. Craig, R. A., The Upper Atmosphere-Meteorology and Physics, Academic Press, New York, 1965.

24. Diamond M., Cross Wind Effect on Sound Propagation, J. Applied Meteorology, Vol. 3, No. 2, pp. 208-210, April, 1964.

25. Donn, W. L. and D. Rind, Microbaroms and the Temperature and Wind of the Upper Atmosphere, J. Atmos. Sciences, Vol. 29, pp. 156-172, January, 1972.

26. DuMond, J. W. M. et. al.,A Determination of the Wave Forms and Laws of Propagation and Dissipation of Ballistic Shock Waves, J. A. S. A., Vol. 18, No. 1, pp. 97-118, July, 1946.

27. Evans, L. B. et. al., Absorption of Sound in Air, Wylie Labs, Inc., Huntsville, Alabama, AD 710291, July, 1970.

28. Evans, L. B., et. al., Atmospheric Absorption of Sound: Theoretical Predictions, J. A. S. A., Vol. 51, No. 5 (Part 2), pp. 1565-75, 1972.

29. Few, A.A., Jr. , et. al., A Dominant 200-Hertz Peak in the Acoustic Spectrum of Thunder, J. Geophys. Res., Vol. 72, No. 24, pp. 6149-6154, 1967.

30. Few, A.A., Jr., Thunder, PhD. Thesis, Rice University, November, 1968.

31. Few, A.A., Jr., Power Spectrum of Thunder, J.G.R., Vol. 74, No. 28, pp. 6926-34, 1969.

32. Francis, S.H., Propagation of Internal Acoustic-Gravity Waves Around a Spherical Earth, J. Geophysical Research, Vol. 77, No. 22, pp. 4221-26, 1972.

33. Friedman, M.P. et. al., Effects of Atmosphere and Aircraft Motion on the Location and Intensity of a Sonic Boom, AIAA Journal, Vol. 1, No. 6, pp. 1327-1335, 1963.

34. Gault, D., Saturation and Equilibrium Conditions for Impact Cratering on the Lunar Surface: Criteria and Implications, Radio Science, Vol. 5, No. 2, pp. 273-91, February 1970.

35. George, A.R. and K.J. Plotkin, Propagation of Sonic Booms and Other Weak Nonlinear Waves Through Turbulence, Physics of Fluids, Vol. 14, pp. 548-54, 1971.

36. Georges, T.M., A Program for Calculating Three-Dimensional Acoustic-Gravity Ray Paths in the Atmosphere, NOAA Technical Reprot ERL 212-WPL 16, Boulder, Colorado, 43 pp., August, 1971.

37. Givens, J.J. and W.A. Page, Ablation and Luminosity of Artificial Meteors, J.G.R., Vol. 76, No. 4, pp. 1039-54, 1971.

38. Goerke, V.H., Infrasonic Observations of a Fireball, Sky and Telescope, November, 1966, p. 313.

39. Goerke, V.H., Private Communication, July, 1971.

40. Golitsyn, G.S., On Absorption of Sound in the Atmosphere and Ionosphere, Bull. Acad. Sci., USSR, Izv., Geophys. Ser., No. 6, pp. 618-21, 1961.

41. Grad, H., Equations of Flow in a Rarefied Atmosphere , Rand Corp. Report R-339, 11-1, 1959.

42. Greene, J.S. and W.A. Whitaker, Theoretical Calculations of Traveling Ionospheric Disturbances Generated by Low Altitude Nuclear Explosions, Acoustic Gravity Waves in the Atmosphere, T.M. Georges, Editor, U.S. Government Printing Office, Washington, D.C. , pp. 45-64, 1968.

43. Groves, G. V., Geometrical Theory of Sound Propagation in the Atmosphere, J. Atmos. Terr. Physics, Vol. 7, pp. 113-27, 1955.

44. Groves, G. V., Velocity of a Body Falling Through the Atmosphere and the Propagation of its Shock Wave to Earth, J. Atmos. Terr. Physics, Vol. 10, pp. 73-83, 1957.

45. Groves, G. V., Initial Expansion to Ambient Pressure of Chemical Explosive Releases in the Upper Atmosphere, J. G. R., Vol. 68, No. 10, pp. 3033-47, May 15, 1963.

46. Groves, G. V., Acoustic Pulse Characteristics of Explosive Releases in the Upper Atmosphere, Project Firefly (1962-3), AFCRL Report 364, p. 351, 1964.

47. Groves, G. V., Atmospheric Structure and Its Variations in the Region from 25 to 120 km, AFCRL-71-0410, Environmental Research Papers, No. 368, July 27, 1971.

48. Guiraud, J. P., et. al., Bluntness Effects in Hypersonic Small Disturbance Theory, Basic Developments in Fluid Dynamics, M. Holt, Editor, Vol. 1, pp. 127-247, Academic Press, New York, 1965.

49. Halliday I., The Meteorite Observation and Recovery Project, Bull. Radio and Electrical Engin. Division, National Research Council of Canada, Vol. 20, No. 3, p. 1-4, 1970.

50. Harkrider, D. G., Theoretical and Observed Acoustic - Gravity Waves from Explosive Sources in the Atmosphere, J. G. R., Vol. 69, No. 24, pp. 5295-5321, 1964.

51. Hayes, W. D., On Hypersonic Similitude, Quarterly of Applied Mathematics, Vol. V., No. 1, pp. 105-6, 1947.

52. Hayes, W. D., et. al., Sonic Boom Propagation in a Stratified Atmosphere With Computer Program, NASA CR-1299, April, 1969.

53. Hayes, W. D. and R. F. Probstein, Hypersonic Flow Theory, Vol. 1, 2nd Edition, Academic Press, New York, 1966.

54. Hayes, W. D., Long -Range Acoustic Propagation in the Atmosphere, Institute for Defense Analyses, Arlington, Va., Available from National Technical Information Service as AD 467 017, 39pp., July, 1963.

55. Hayes, W. D., Sonic Boom, Annual Review of Fluid Mechanics, M. VanDyke, W. G. Vincenti and T. V. Wehausen (Editors) Vol. 3, Annual Review, Inc., Palo Alto, CA., pp. 269-90, 1971.

56. Hilton, D. A., et. al., Sonic-Boom Ground-Pressure Measurements from Apollo 15, NASA TN D-6950, 35 pp., September, 1972.

57. Hindley, B. and H. Miles, The Fireball and Meteorite of 1969, April 25, J. Brit. Astro. Assn., Vol. 80, No. 4, pp. 313-22, 1970.

58. Holmes, C. R., M. Brook, P. Krehbiel, and R. McCrory, On the Power Spectrum and Mechanism of Thunder, J. Geophysical Research, Vol. 76, No. 9, pp. 2106-2115, 1971.

59. Izakov, M. N., On Theoretical Models of the Structure and Dynamics of the Earth's Thermosphere, Space Science Reviews, Vol. 12, No. 3, pp. 261-98, 1971.

60. Jones, D. L., et. al., Shock Wave from a Lightning Discharge, J. G. R., Vol. 73, No. 10, pp. 3121-27, May 15, 1968.

61. Jones, W. L., Ray Tracing for Internal Gravity Waves, J. G. R., Vol. 74, No. 8, pp. 2028-33, April 15, 1969.

62. Jones, W. L., Atmospheric Internal Gravity Waves and Tides, Stratospheric Circulation, W. Webb, Editor, Progress in Astronautics and Aeronautics, Vol. 22, pp. 469-82, Academic Press, New York, 1969.

63. Kahalas, S. L., and B. L. Murphy, Second-Order Correction to the Reed-Otterman Theory, Geophysical J. Roy. Astron. Soc., Vol. 26, pp. 379-89, December, 1971.

64. Kane, E. J., Some Effects of the Nonuniform Atmosphere on the Propagation of Sonic Booms, J. A. S. A., Vol. 39, September 26, 1966.

65. Korobeinikov. V. P., Gas Dynamics of Explosions, Annual Review of Fluid Mechanics, M. Van Dyke, W. G. Vincenti and T. V. Wehausen (Editors), Vol. 3, Annual Review, Inc., Palo Alto, CA, pp. 317-346, 1971.

66. Korobeinikov, V. P., P. I. Chushkin and L. V. Shurshalov, Gas Dynamics Of The Flight And Explosion Of Meteorite Bodies In the Earths Atmosphere, UCRL-TRANS-10572, Available from NTIS, Springfield, Virginia, 30 pp., November, 1971.

67. Kushner, S. S., and J. W. Prescott, Propagation of Sound in Air ( Bibliography with Abstracts) The University of Michigan, College of Engineering, June, 1965.

68. Lighthill, M. J., Viscosity Effects in Sound Waves of Finite Amplitude, in Surveys in Mechanics, G. K. Batchelor and H. Bondi (Editors), Cambridge University Press, pp. 251-350, 1956.

69. Lin, S. C., Cylindrical Shock Waves Produced by Instantaneous Energy Release, Journal of Applied Physics, Vol. 25, No. 1, pp. 54-57, January, 1954.

70. Liszka, L. and S. Olsson, On the Generation and Detection of Artifical Atmospheric Waves, J. Atmos. Terr. Physics, Vol, 33, pp. 1933-9, 1971.

71. Lowery, C. J. and E. M. Shoemaker, Airwaves Associated with Large Fireballs and the Frequency Distribution of Energy of Large Meteoroids, Journal of the Meteoritical Soc., Vol. 3, No. 3, pp. 123-4, April, 1967.

72. Manning, J. C., et. al., Wind Velocity Profiles Measured by the Smoke-Trail Method at the Eastern Test Range, 1964, NASA Technical Note D-6746, April, 1972.

73. McKinley, D. W. R., Meteor Science and Engineering, McGraw-Hill Book Co., New York, 1961.

74. Meyer, R. E., On the Far Field of a Body Rising Through the Atmoshpere, J. G. R., Vol. 67, No. 6, pp. 2361-6, June, 1962.

75. Millman, P. M., A Brief Survey of Upper Air Spectra, Physics and Dynamics of Meteors, Editors, Kresak and Millman, D. Reidel Publishing Co., pp. 84-90, 1968,

76. Morse, P. M. and K. U. Ingard, Theoretical Acoustics, McGraw-Hill, 927 pp., 1968.

77. Officer, C. B., Introduction to the Theory of Sound Transmission-Application to the Ocean, McGraw-Hill, New York, 1958.

78. Öpik, E., Physics of Meteor Flight in the Atmosphere, Interscience Publishers, Inc., New York, 1958.

79. Öpik, E., The Sonic Boom of the Boveedy Meteorite, Irish Astron. Journal, Vol. 9, No. 8, pp. 308-310, 1970.

80. Otterman, J., Finite Amplitude Propagation Effect on Shock-Wave Travel Times from Explosions at High Altitudes, J. A. S. A., Vol. 31, No. 4, pp. 470-74, 1959.

81. Pan, Y. S. and W. A. Sotomayer, Sonic Boom of Hypersonic Vehicles, AIAA Journal, Vol. 10, No. 4, pp. 550-1, April, 1972.

82. Pan, Y. S. and M. O. Varner, Studies on Sonic Boom at High Mach Numbers, 5th AIAA Fluid and Plasma Dynamics Conference, Boston, MA, Available from Technical Information Service as A 72-34082, 11 pp., 1972.

83. Parker, L. W., et. al., Godunov Method And Computer Program To Determine The Pressure And Flow Field Associated With A Sonic Boom Focus, NASA-Cr-2127, 109 pp., January, 1973.

84. Pfeffer, R. L. and J. Zarichny, Acoustic - Gravity Wave Propagation In An Atmosphere With Two Sound Channels, Geofisica Pura E. Applicata, Vol. 55, pp. 175-199, 1963.

85. Pierce, A. D. and C. Thomas, Atmospheric Correction Factor for Sonic-Boom Pressure Amplitudes, J. A. S. A., Vol. 46, p. 1366, 1969.

86. Pierce, A. D., J. W. Posey, and E. F. Iliff, Variation of Nuclear Explosion Generated Acoustic - Gravity Wave Forms with Burst Height and With Energy Yield, J. Geophysical Research, Vol. 76, No. 21, pp. 5025-42, 1971.

87. Plooster, M. N., Shock Waves from Line Sources, NCAR-TN-37, 84 pp., National Center for Atmospheric Research, Boulder, Colorado, 1968.

88. Plooster, M. N., Numerical Simulation of Spark Discharges in Air, Physics of Fluids, Vol. 14, No. 10, pp. 2111-23, 1971.

89. Procunier, R. W., Improved Detection of High Altitude Grenades, J. Atmos. Terr. Physics, Vol. 29, pp. 581-7, 1967.

90. Procunier, R. W., and G. W. Sharp, Optimum Frequency for Detection of Acoustic Sources in the Upper Atmosphere, J. Acou. Soc. Amer., Vol. 49, No. 3, (Part 1), pp. 622-26, 1971.

91. Reed, J. W., Attenuation of Blast Waves by the Atmosphere, J. Geophysical Research, Vol. 77, No. 9, pp. 1616-22, 1972.

92. Reed, J. W., Airblast Overpressure Decay at Long Ranges, J. Geophysical Research, Vol. 77, No. 9, pp. 1623-29, 1972.

93. Reed, S. G., Note on Finite Amplitude Propagation Effects on Shock Wave Travel Times from Explosions at High Altitude, J. A. S. A., Vol. 31, p. 1265, 1959.

94. Remillard, W. J., The Acoustics of Thunder, Acoustics Research Lab. Technical Memo. 44, Harvard University, Cambridge, Mass., 1960.

95. Remillard, W. J., Comments of Paper by A. A. Few, A. J. Dessler, Don J. Latham, and M. Brook, "A Dominant 200 Hertz Peak in the Acoustic Spectrum of Thunder, " J. G. R., 74, No. 23, pp. 5555, 1969.

96. Ribner, H. S., Supersonic Turns Without Superbooms, J. A. S. A., Vol. 52, Number 3 (Part 2) pp. 1037-1041, 1972.

97. Sachs, D. A., Precursor Waves From a Continuous Transition Layer in the Sound Speed Profile, Technical Report U-361-222, Cambridge Acoustical Associates, Inc., Cambridge, Massachusetts, 40 pp., AD 713601, August, 1970.

98. Sakurai, A., Blast Wave Theory, Basic Developments in Fluid Dynamics, M. Holt Editor, Vol. 1, pp. 309-375, Academic Press, New York, 1965.

99. Schultz, T. J., Effect of Altitude on Output of Sound Sources, Noise Control, pp. 17-21, May 1959.

100. Scorer, R. S., The Dispersion of a Pressure Pulse in the Atmosphere, Proc. Roy Society A, Vol. 20, pp. 137-157, 1950.

101. Shoemaker, E. M., Private Communication, 1972.

102. Stanyukovich, K. P., The System of Aerial Shock Waves During the Flight and Explosion of Meteors, Meteoritika, Vol. 14, pp. 62-69, 1956.

103. Stanyukovich, K. P. and V. P. Shamilov, Motions of Meteors Through the Earths Atmosphere, Meteoritika, Vol. 20, pp. 54-71, 1961.

104. Stanyukovich, K. P. and V. A. Bronshten, Velocity and Energy of the Tunguska Meteorite, NASA TTF-89, December, 1962.

105. Taylor, G. I., The Formation of a Blast Wave by a Very Intense Explosion I. Theoretical Discussion, Proc. Roy. Soc. London A., Volume 201, p. 159-186, 1950.

106. Theon, J. S., et. al., The Mean Observed Meteorological Structure and Circulation of the Stratosphere and Mesosphere, NASA TR R-375, March, 1972.

107. Tolstoy I., Modes, Rays and Travel Times, J. G. R., Vol. 64, No. 7, pp. 815-821, 1959.

108. Tolstoy I., Effect of Density Stratification on Sound Waves, J. G. R., Vol. 70, No. 24, pp. 6009, 6015, 1965.

109. Tolstoy I., The Theory of Waves in Stratified Fluids Including The Effects of Gravity and Rotation, Reviews of Modern Physics, Vol. 35, Number 1, pp. 207-230, 1963.

110. Towne, D. H., Wave Phenomena, Addison-Wesley, Mass., 1967.

111. Tsikulin, M. A., Shock Waves During the Movement of Large Meteorites in the Atmosphere, Translation Division of the U. S. Naval Intelligence Command, Alexandria, Virginia, available from the National Technical Information Service, Springfield, Virginia as AD 715-537, 1970.

BIBLIOGRAPHY (Part 2) (Concluded)


112. U. S. Standard Atmosphere Supplements, U. S. Government Printing Office, Washington, D. C., 1966.

113. Varley, E., and E. Cumberbatch, Large Amplitude Waves in Stratified Media: Acoustic-Pulses in a Stratified Atmosphere, Center for the Application of Mathematics, Lehigh University, Technical Report No. CAM-110-8, 45 pp., December, 1969.

114. Vincenti, W. G. and S. C. Traugott, The Coupling of Radiative Transfer and Gas Motion, Annual Review of Fluid Mechanics, M. VanDyke, W. G. Vincenti and T. V. Wehausen (Editors), Vol. 3, Annual Review Inc., Ralo Alto, Calif., pp. 89-116, 1971.

115. Warfield, J. T., Acoustic Ray Propagation In Channels With A Horizontal Sound Speed Gradient, Ph. D. Thesis (Applied Mathematics), Rensselaer Polythechnic Institute, 198 pp, 1971.

116. Whipple, F. J. W., The Great Siberian Meteor and the Waves, Seismic and Aerial, which it Produced, Quart. J. Roy. Meteor. Soc., Vol 56, pp. 287-304, 1930.

117. Whitham, G. B., Linearized Flow of a Supersonic Projectile, Comm. Pure and Applied Math, Vol. 5, pp. 301-348, 1952.

118. Whitham, G. B., On the Propagation of Weak Shock Waves, J. Fluid Mechanics, Vol. 1, Part 3, pp. 290-318, 1956.

119. Wilson, C. R., Private Communication, June, 1972.

120. Wylie, C. C., Sounds From Meteors, Popular Astronomy, Vol. 40, No. 5, Whole No. 395, pp. 289-94, May, 1932.

121. Yih, C. S., The Dynamics of Nonhomogeneous Fluids, Macmillan Company, New York, 1965.

122. Yih, C. S., Fluid Mechanics, McGraw-Hill, Inc., New York, 1969.

123. Zeldovich, Y. and Y. Raizer, Physics of Shock Waves and High Temperature Hydrodynamic Phenomena (English Translation by W. Hayes and R. Probstein), Academic Press, New York, 1967.

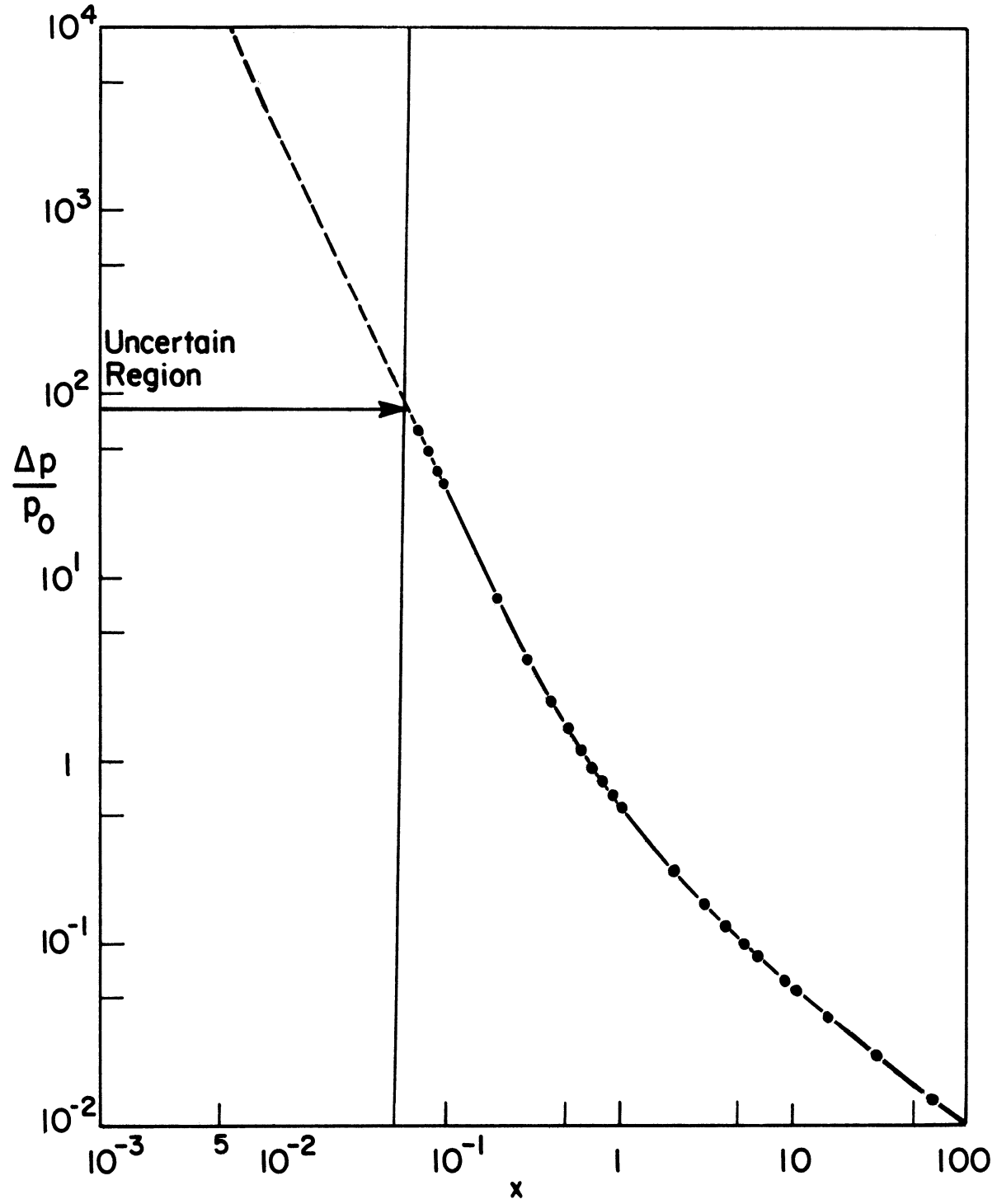


Figure 60. Overpressure ratio as a function of scaled distance from the trajectory.

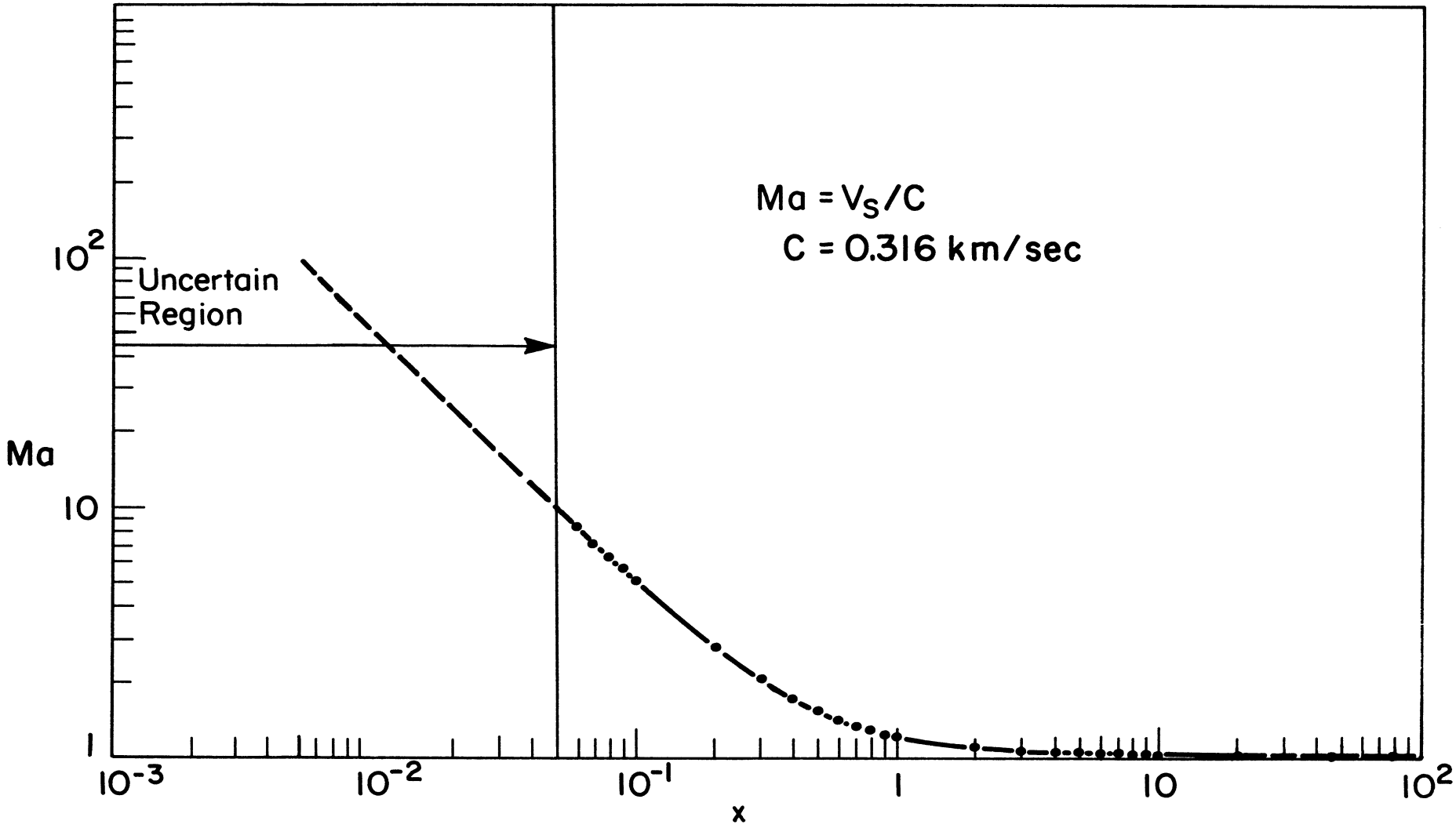


Figure 61. Shock front mach number as a function of scaled distance from the trajectory.

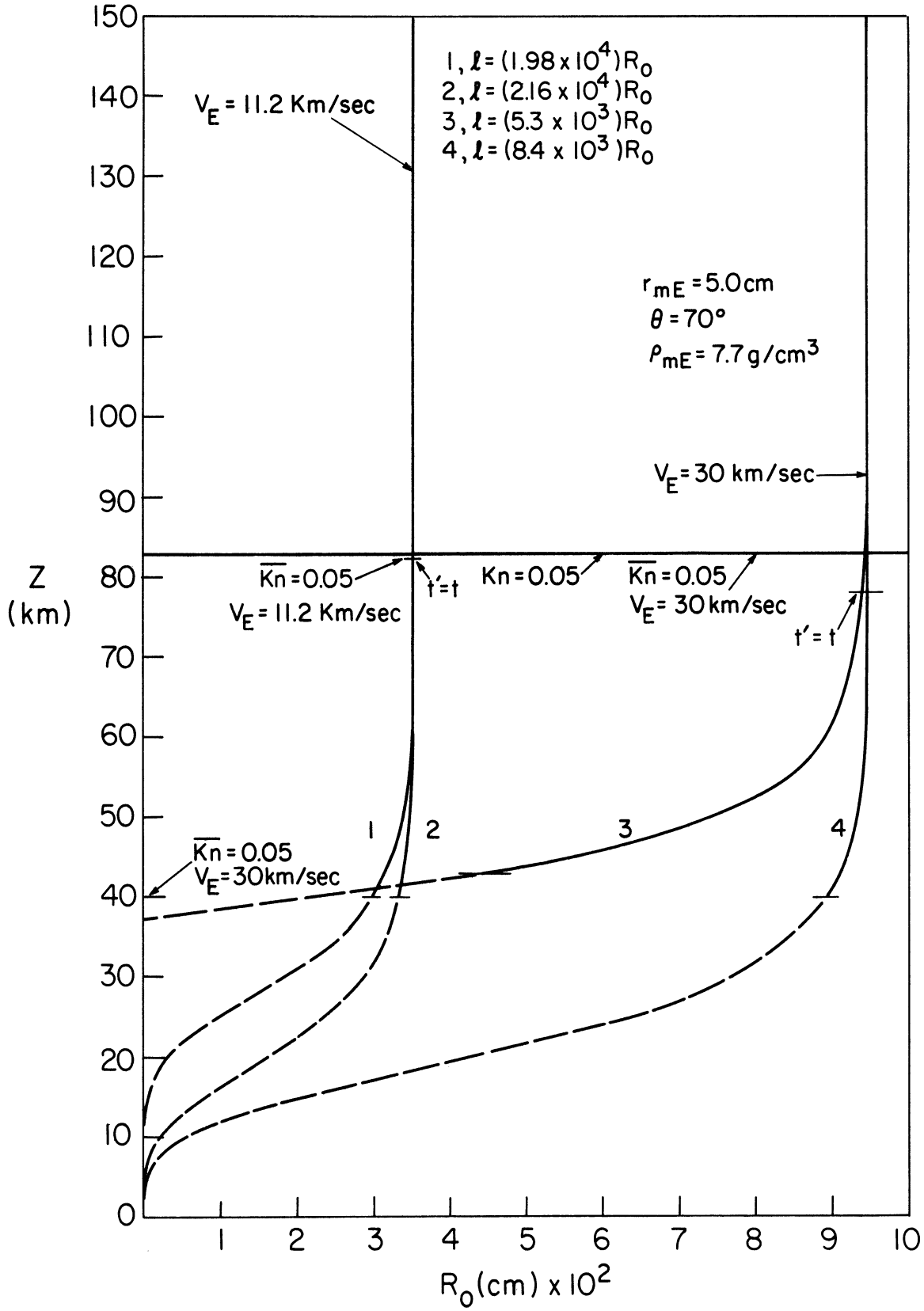


Figure 62. Cylindrical blast wave radius as a function of altitude ( curves 2 and 4, $\sigma=0$; curves 1 and 3, $\sigma=5\cdot10^{-12}$ sec$^2$/cm$^2$; for all curves dashed portion represents altitude region for which cylindrical blast wave theory is not applicable to hypersonic flow ), $\theta=70^{o}$, $d_m=10$ cm, $\rho_m=7.7$ g/cm$^3$.

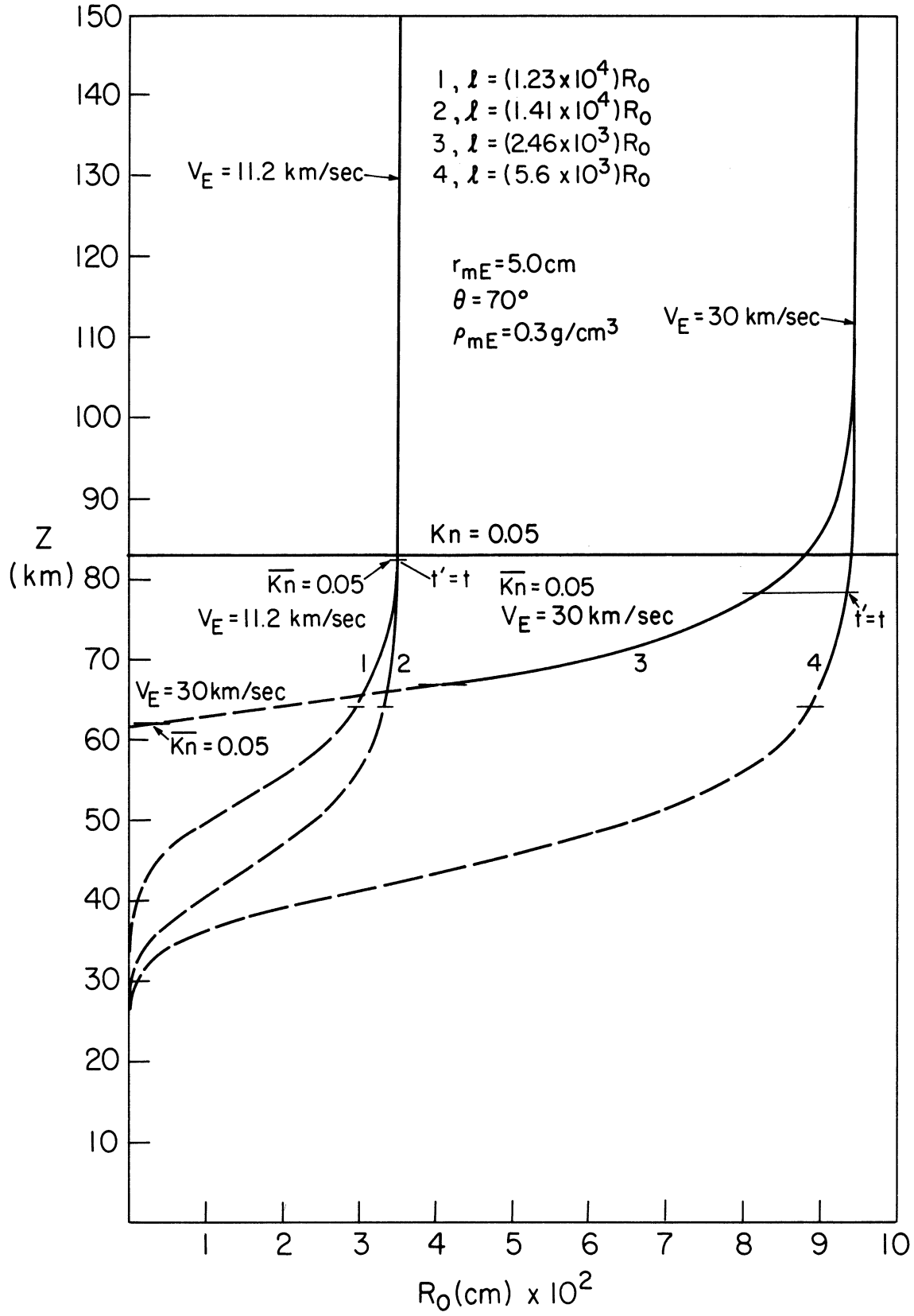


Figure 63. Cylindrical blast wave radius as a function of altitude ( curves 2 and 4, $\sigma=0$; curves 1 and 3, $\sigma=5\cdot10^{-12}$ $sec^2/cm^2$; for all curves dashed portion represents altitude region for which cylindrical blast wave theory is not applicable to hypersonic flow ), $\theta=40^o$, $d_m$= 10 cm, $\rho_m$=7. 7 $g/cm^3$.

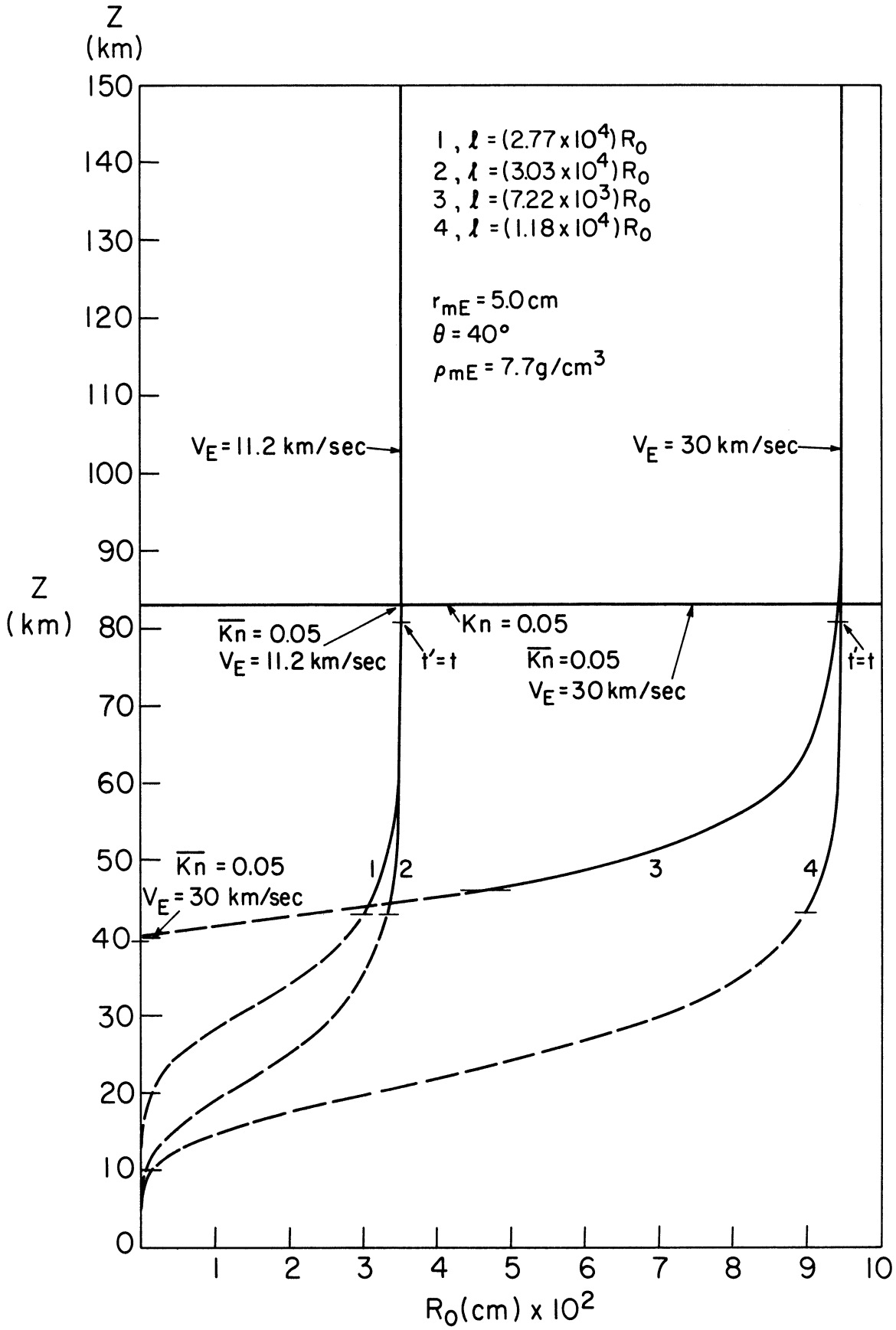


Figure 64. Cylindrical blast wave radius as a function of altitude ( curves 2 and 4, $\sigma=0$; curves 1 and 3, $\sigma=5\cdot10^{-12}$ sec$^2$/cm$^2$; for all curves dashed portion represents altitude region for which cylindrical blast wave theory is not applicable to hypersonic flow ), $\theta=10^o$, $d_m=10$ cm, $\rho_m=7.7$ g/cm$^3$.

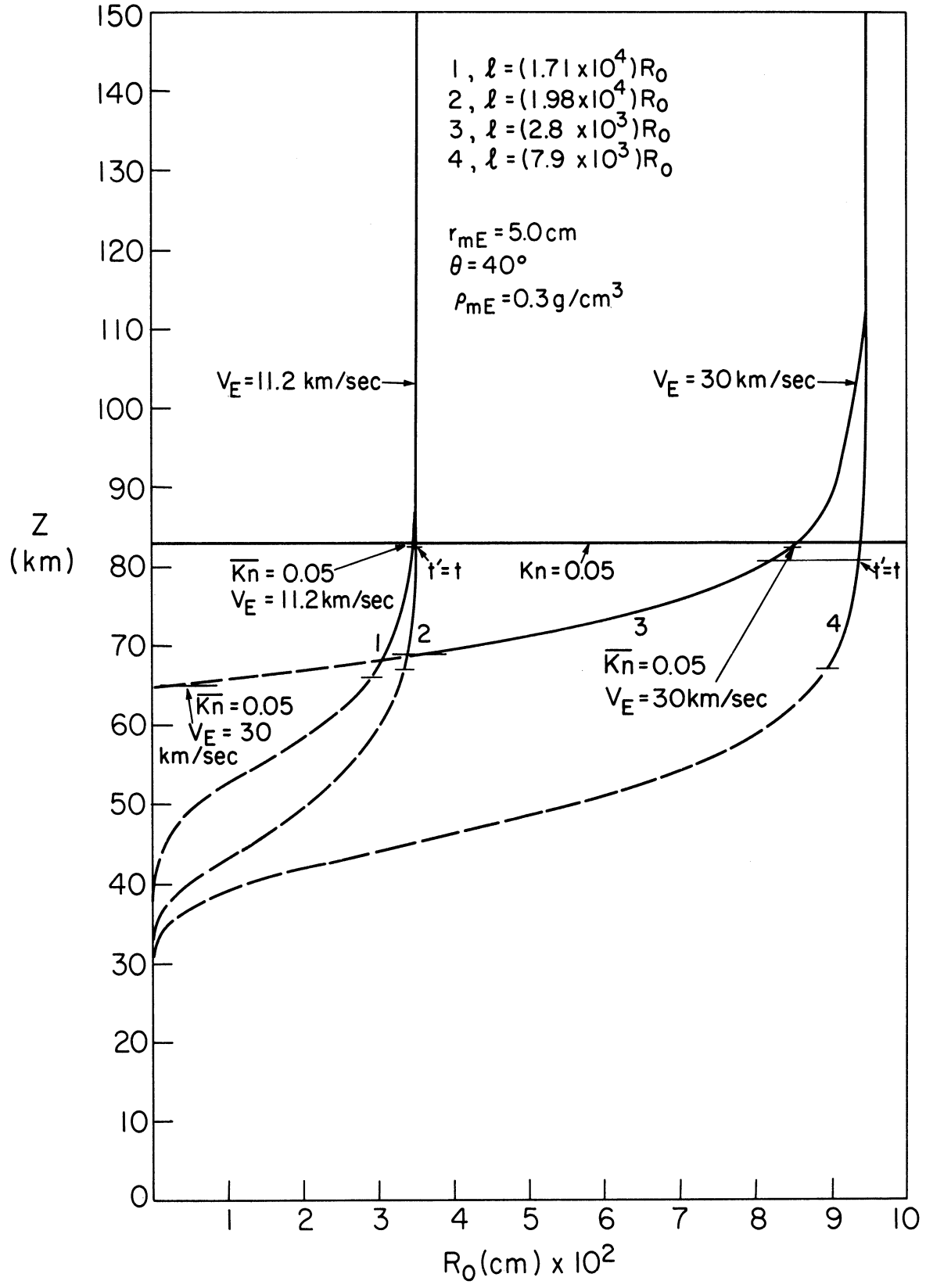


Figure 65. Cylindrical blast wave radius as a function of altitude ( curves 2 and 4, $\sigma=0$; curves 1 and 3, $\sigma=5 \cdot 10^{-12}$ sec$^2$/cm$^2$; for all curves dashed portion represents altitude region for which cylindrical blast wave theory is not applicable to hypersonic flow ), $\theta=70°$, $d_m=10$ cm, $\rho_m=0.3$ g/cm$^3$.

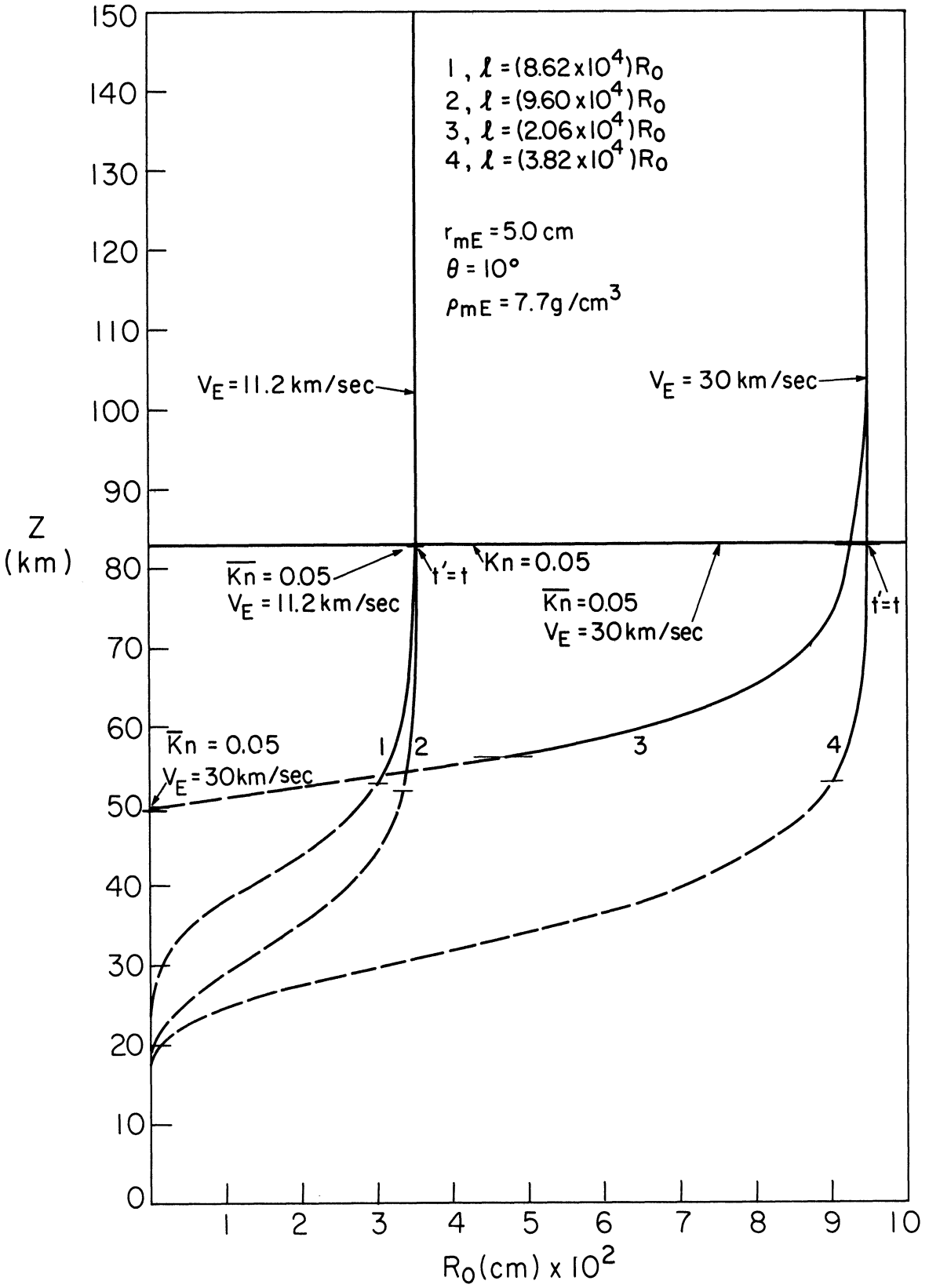


Figure 66. Cylindrical blast wave radius as a function of altitude ( curves 2 and 4, $\sigma=0$; curves 1 and 3, $\sigma=5\cdot10^{-12}$ sec$^2$/cm$^2$; for all curves dashed portion represents altitude region for which cylindrical blast wave theory is not applicable to hypersonic flow ), $\theta=40^o$, $d_m=10$ cm, $\rho_m=0.3$ g/cm$^3$.

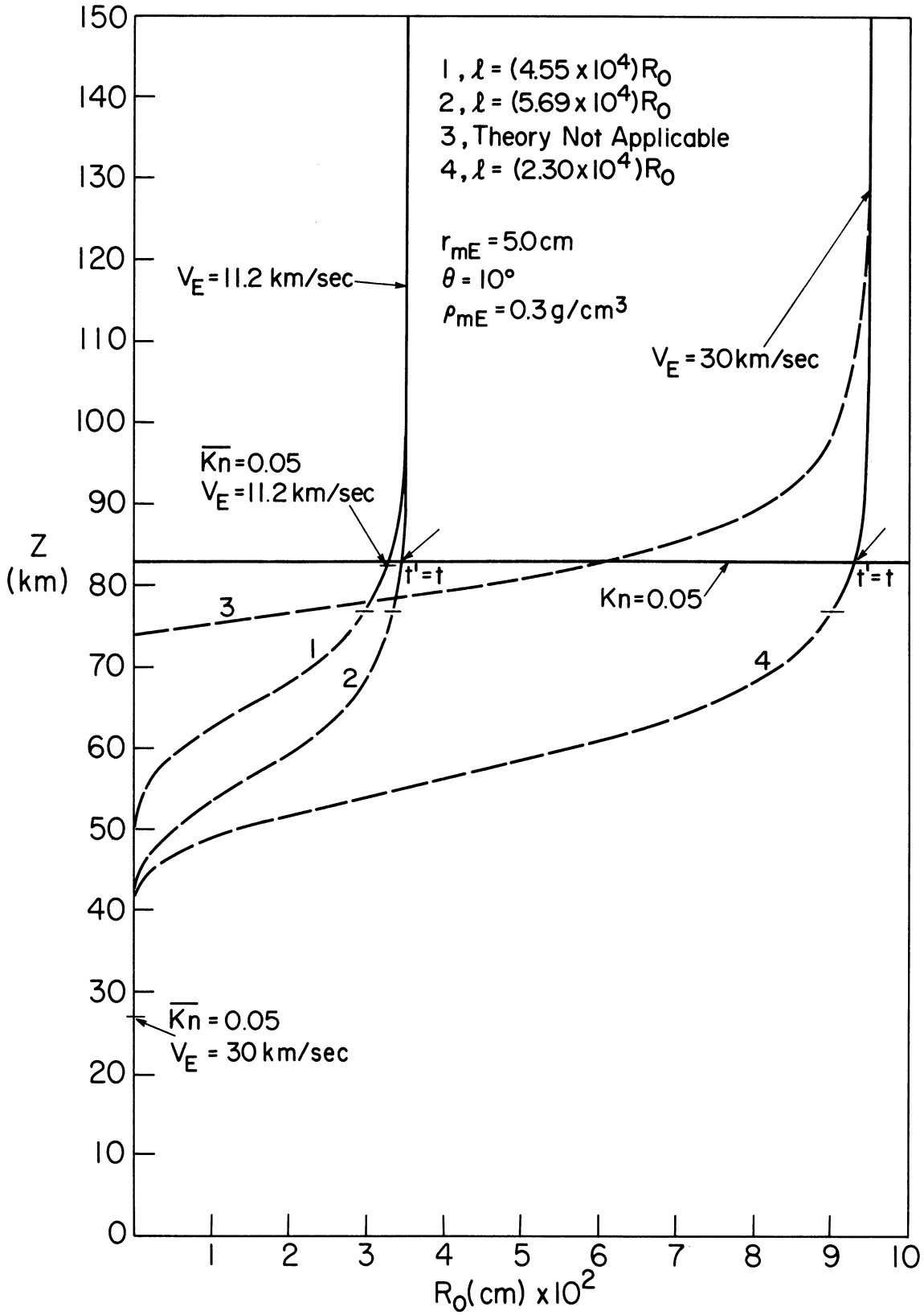


Figure 67. Cylindrical blast wave radius as a function of altitude ( curves 2 and 4, $\sigma=0$; curves 1 and 3, $\sigma=5 \cdot 10^{-12}$ sec$^2$/cm$^2$; for all curves dashed portion represents altitude region for which cylindrical blast wave theory is not applicable to hypersonic flow ), $\theta=10°$, $d_m=10$ cm, $\rho_m=0.3$ g/cm$^3$.

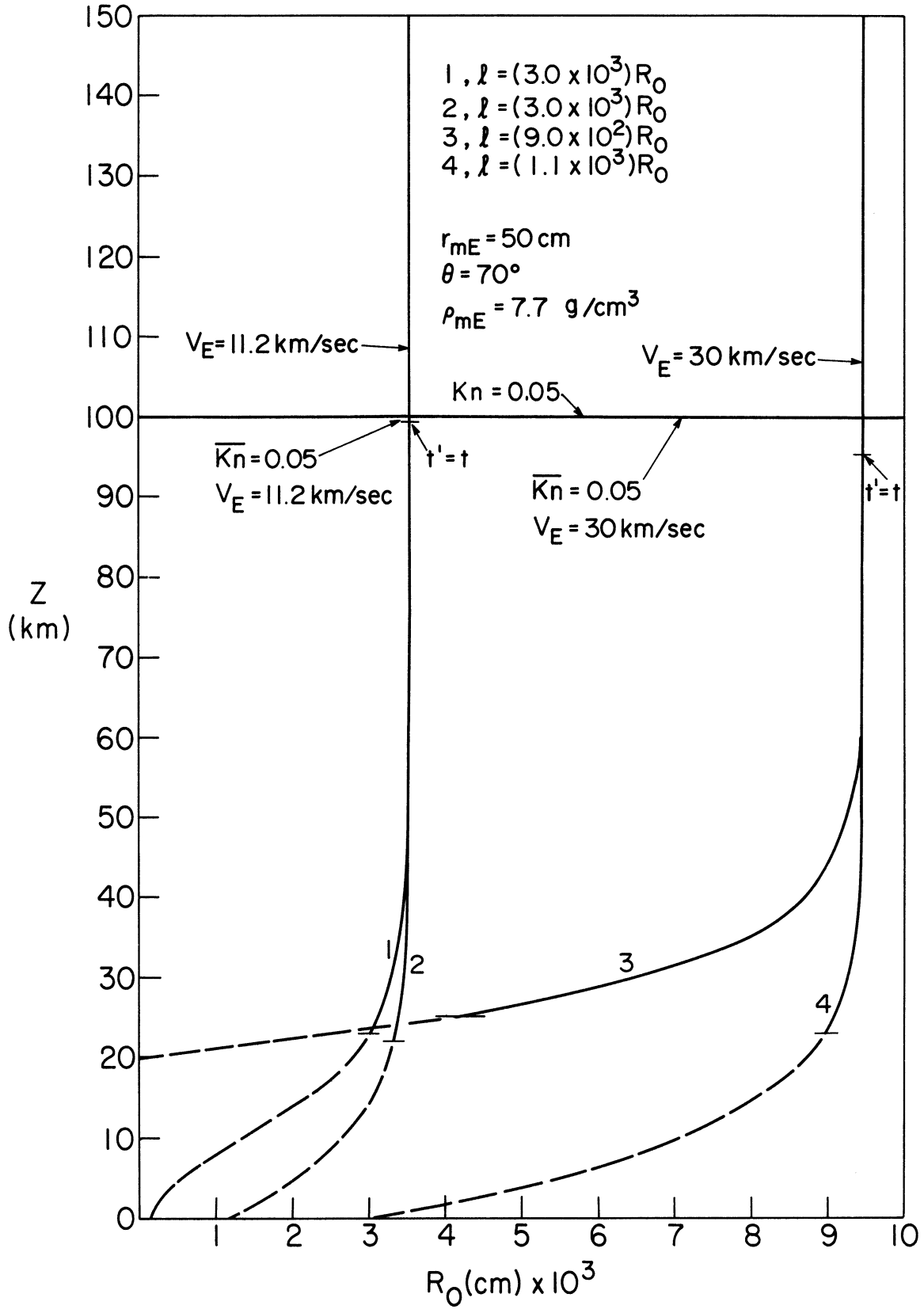


Figure 68. Cylindrical blast wave radius as a function of altitude ( curves 2 and 4, $\sigma=0$; curves 1 and 3, $\sigma=5\cdot10^{-12}$ $sec^2/cm^2$; for all curves dashed portion represents altitude region for which cylindrical blast wave theory is not applicable to hypersonic flow ), $\theta=70^o$, $d_m=$ 100 cm, $\rho_m=7.7$ g/$cm^3$.

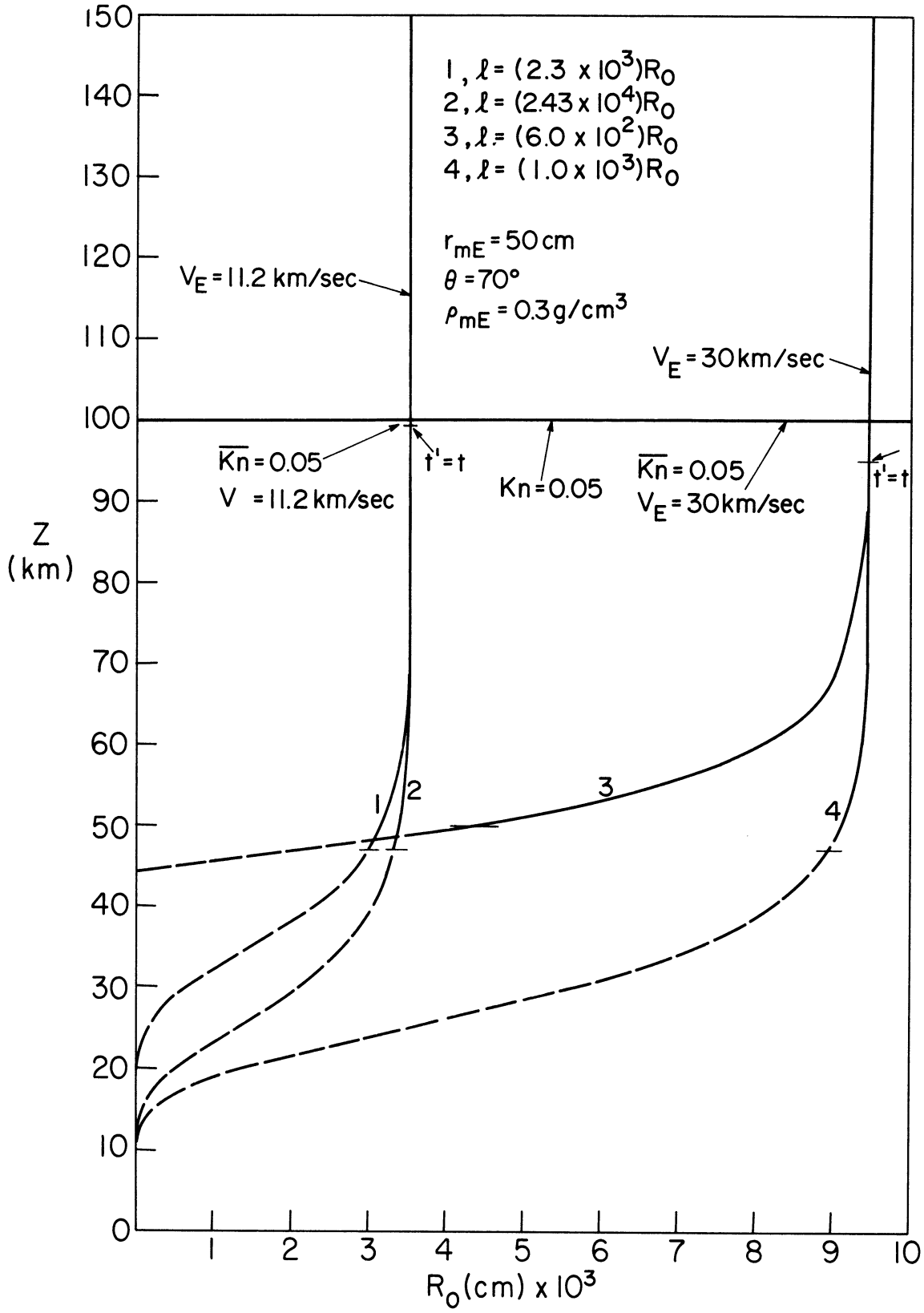


Figure 69. Cylindrical blast wave radius as a function of altitude ( curves 2 and 4, $\sigma=0$; curves 1 and 3, $\sigma=5\cdot10^{-12}$ $sec^2/cm^2$; for all curves dashed portion represents altitude region for which cylindrical blast wave theory is not applicable to hypersonic flow ), $\theta=40^o$, $d_m=100$ cm, $\rho_m=7.7$ g/cm$^3$.

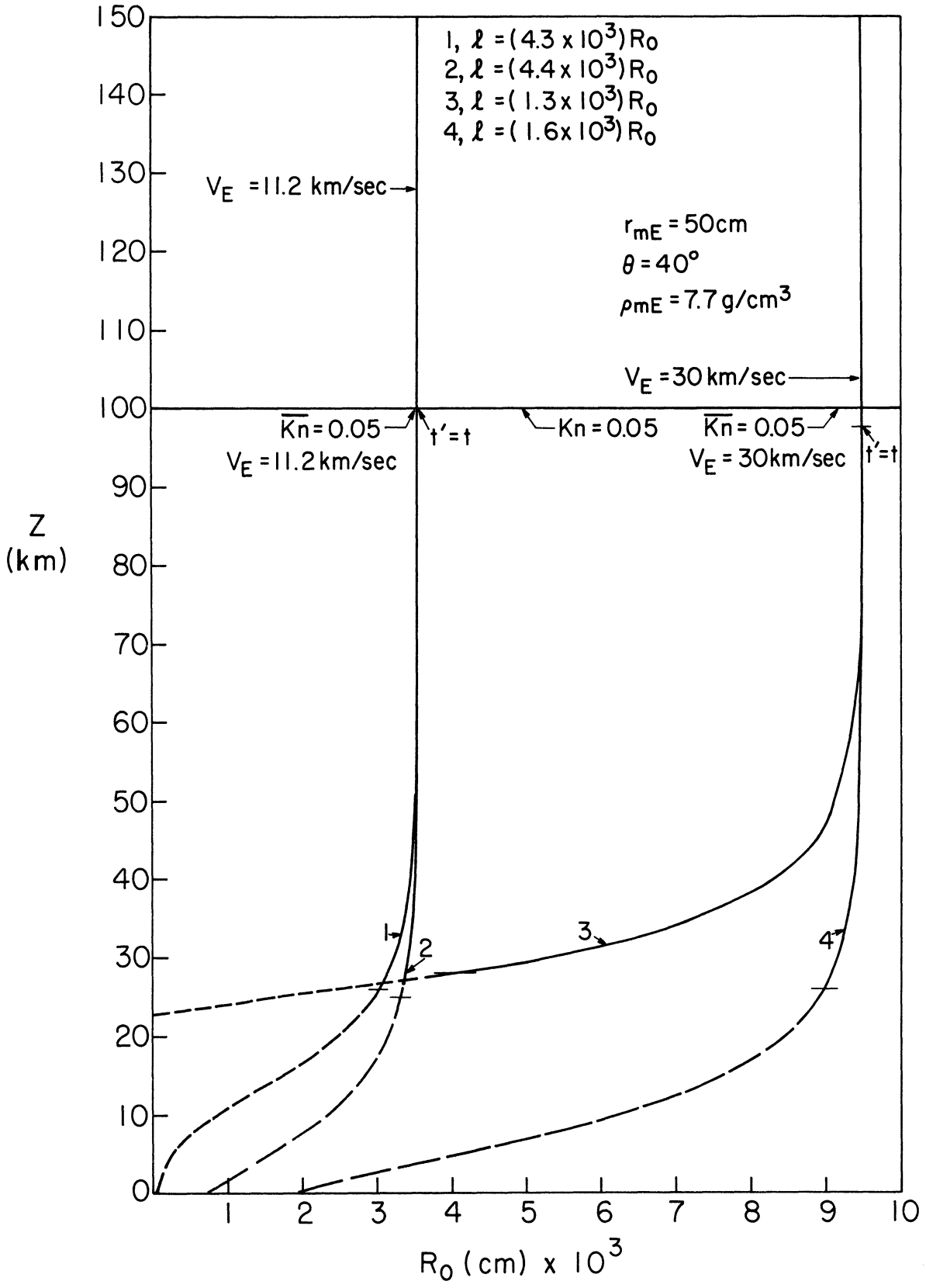


Figure 70. Cylindrical blast wave radius as a function of altitude ( curves 2 and 4, $\sigma=0$; curves 1 and 3, $\sigma=5\cdot10^{-12}$ $sec^2/cm^2$; for all curves dashed portion represents altitude region for which cylindrical blast wave theory is not applicable to hypersonic flow ), $\theta=10^o$, $d_m=100$ cm, $\rho_m=7.7$ $g/cm^3$.

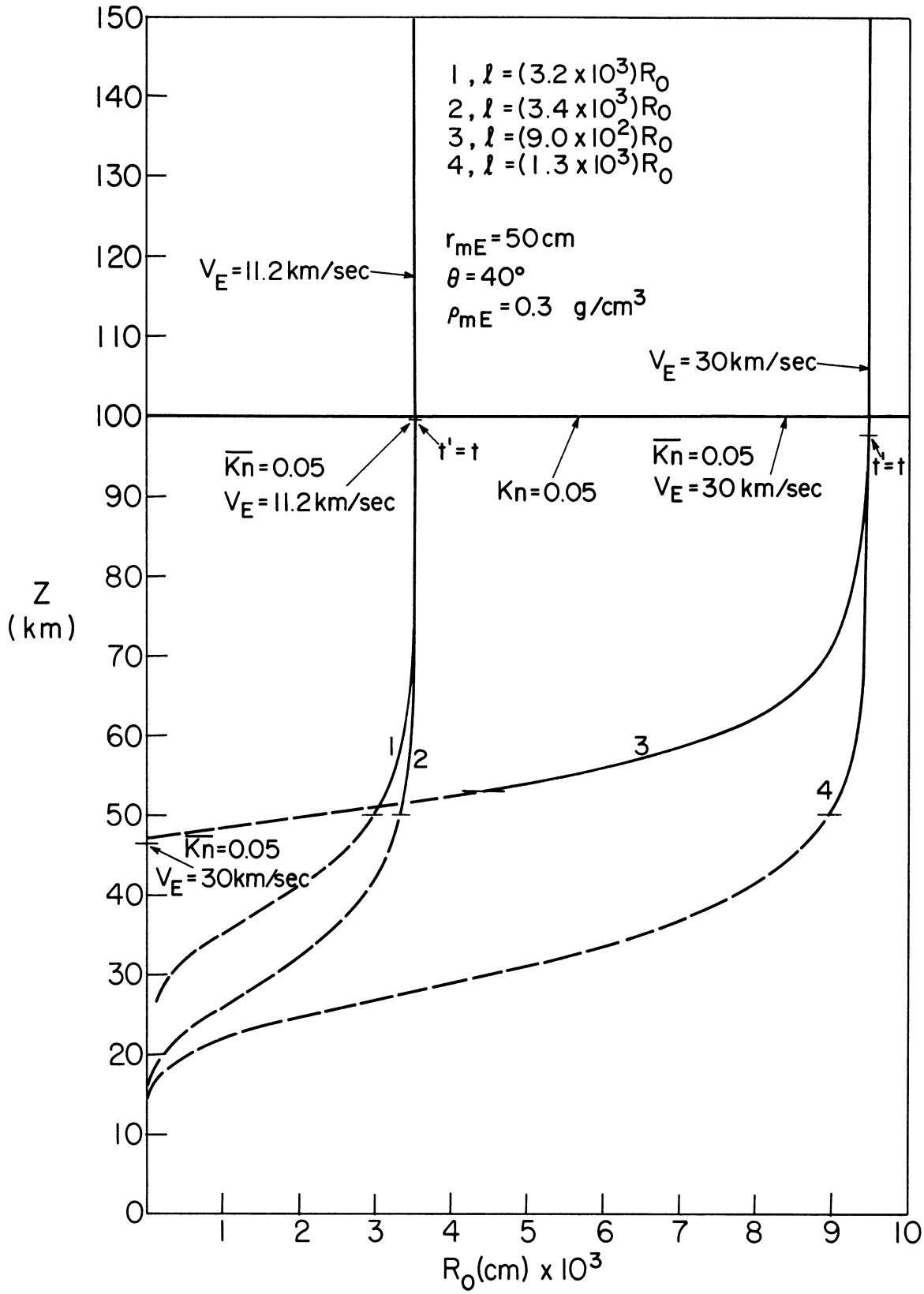


Figure 71. Cylindrical blast wave radius as a function of altitude ( curves 2 and 4, $\sigma=0$; curves 1 and 3, $\sigma=5\cdot10^{-12}$ sec$^2$/cm$^2$; for all curves dashed portion represents altitude region for which cylindrical blast wave theory is not applicable to hypersonic flow ), $\theta=70^{o}$, $d_m=100$ cm, $\rho_m=0.3$ g/cm$^3$.

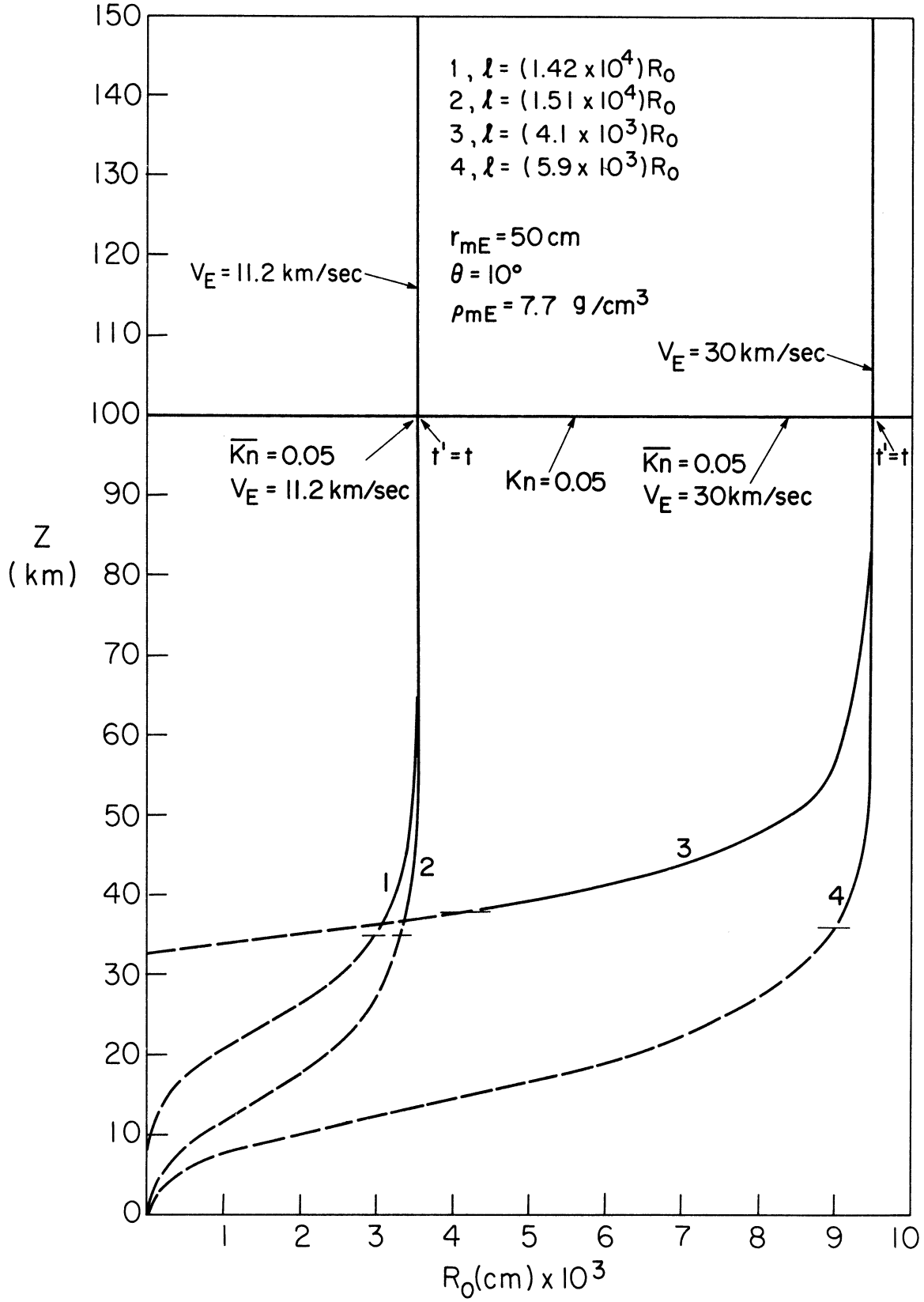


Figure 72. Cylindrical blast wave radius as a function of altitude ( curves 2 and 4, $\sigma=0$; curves 1 and 3, $\sigma=5\cdot10^{-12}$ sec$^2$/cm$^2$; for all curves dashed portion represents altitude region for which cylindrical blast wave theory is not applicable to hypersonic flow ), $\theta=40^{o}$, $d_m=100$ cm, $\rho_m=0.3$ g/cm$^3$.

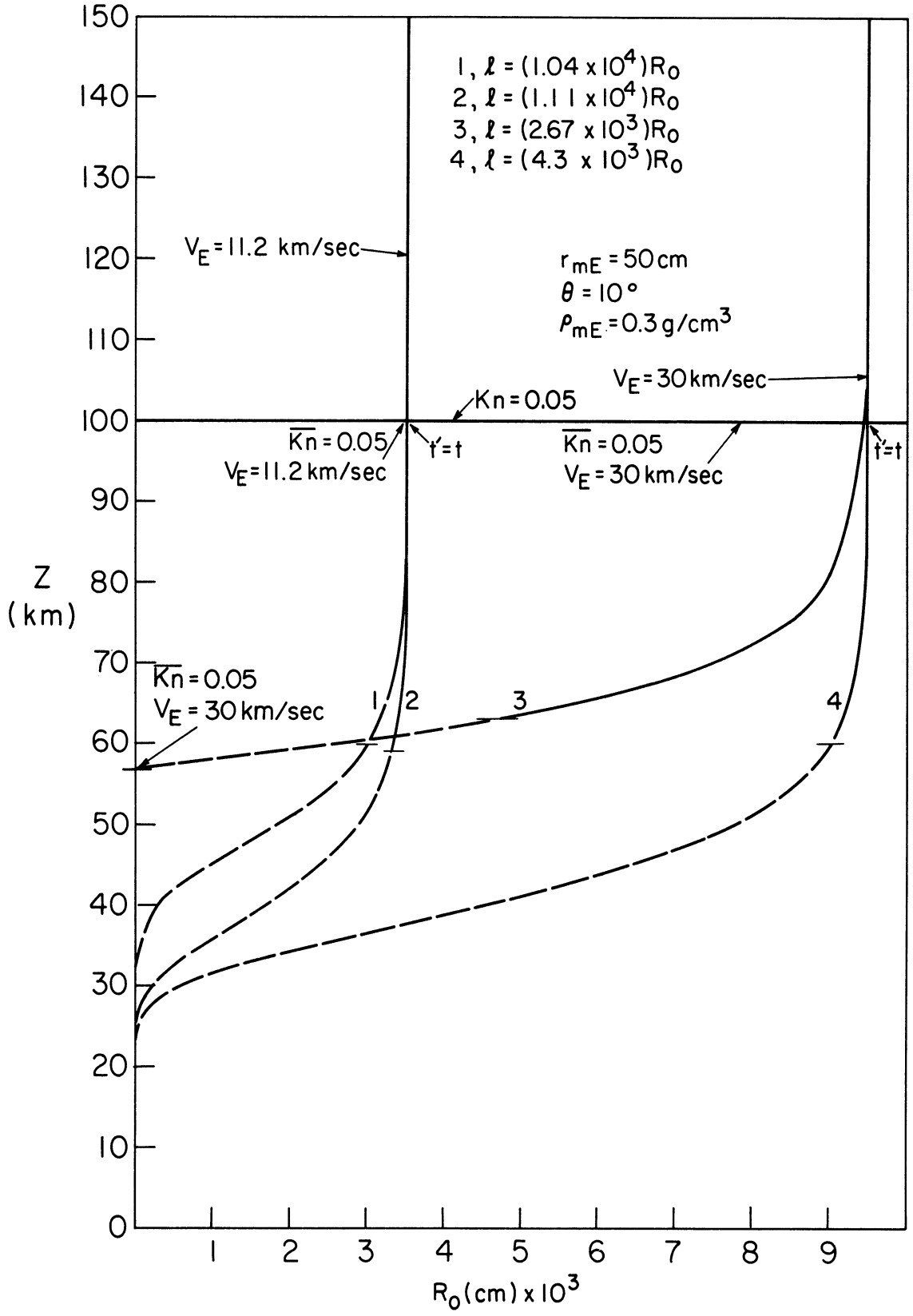


Figure 73. Cylindrical blast wave radius as a function of altitude ( curves 2 and 4, $\sigma=0$; curves 1 and 3, $\sigma=5\cdot 10^{-12}$ $sec^2/cm^2$; for all curves dashed portion represents altitude region for which cylindrical blast wave theory is not applicable to hypersonic flow ), $\theta=10^o$, $d_m=100$ cm, $\rho_m=0.3$ g/cm$^3$.

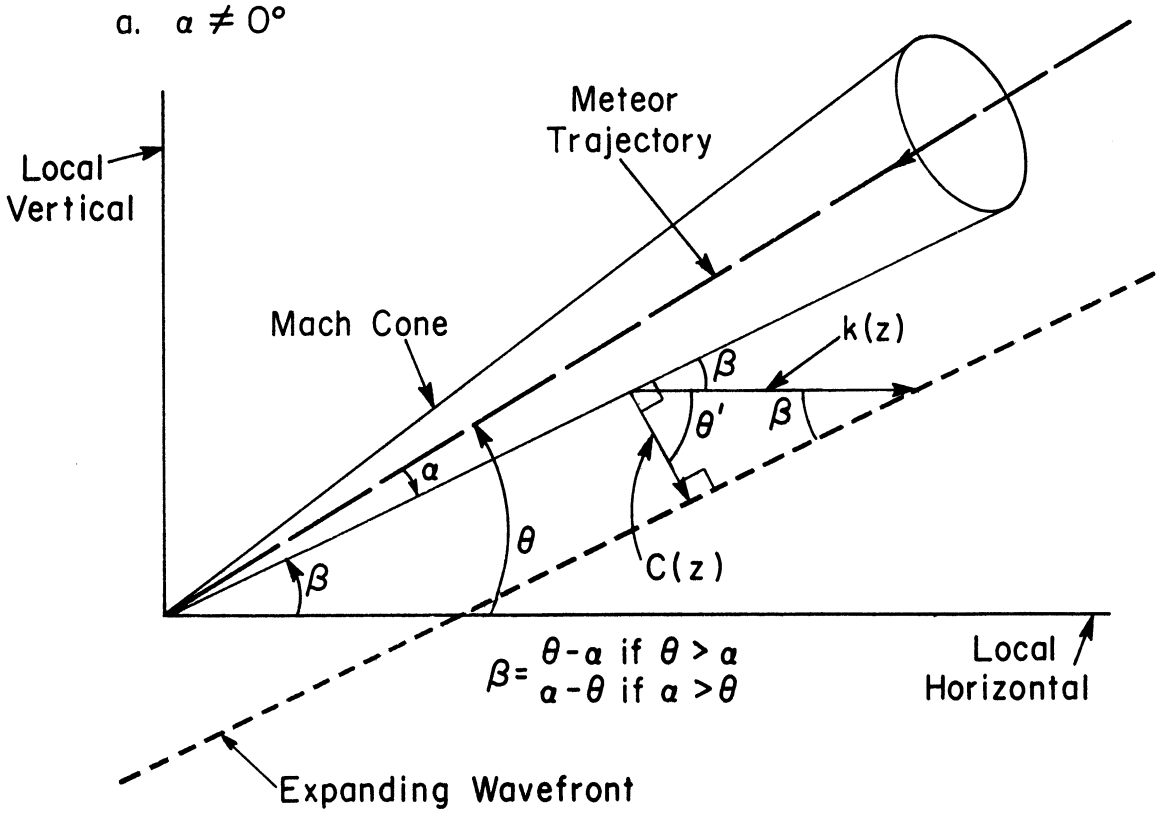


Figure 74a. Characteristic velocity geometry in the entry plane in the absence of wind, $\alpha \neq 0^{o}$.

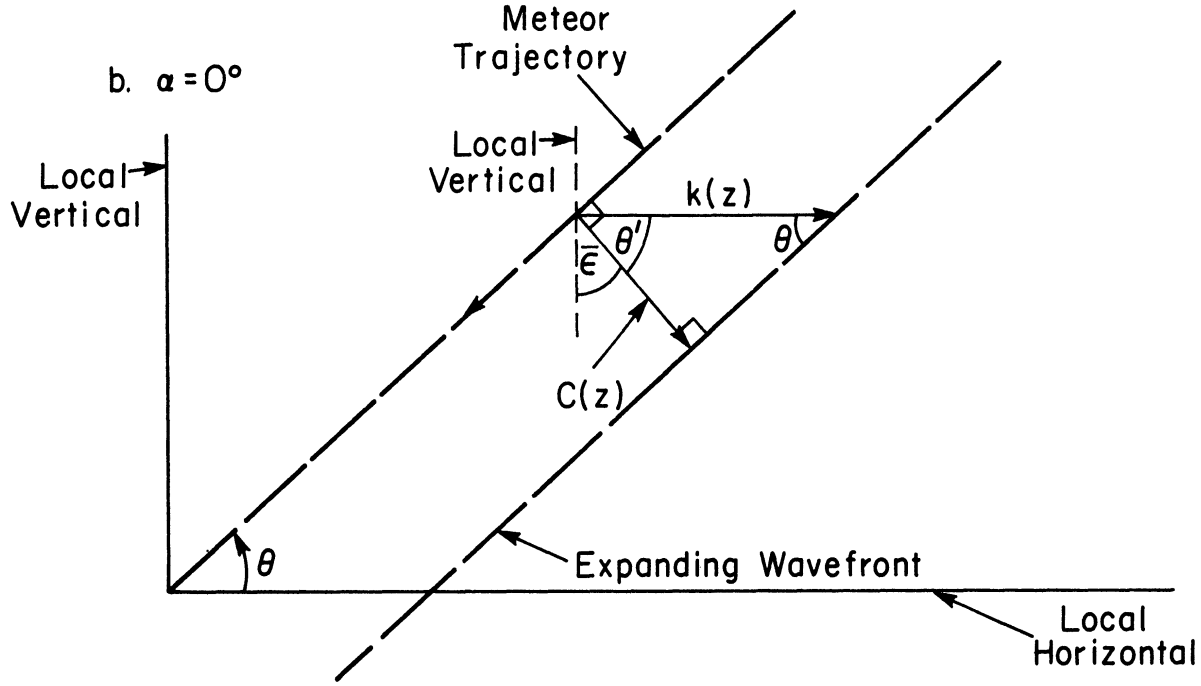


Figure 74b. Characteristic velocity geometry in the entry plane in the absence of wind, $\alpha=0^{o}$.

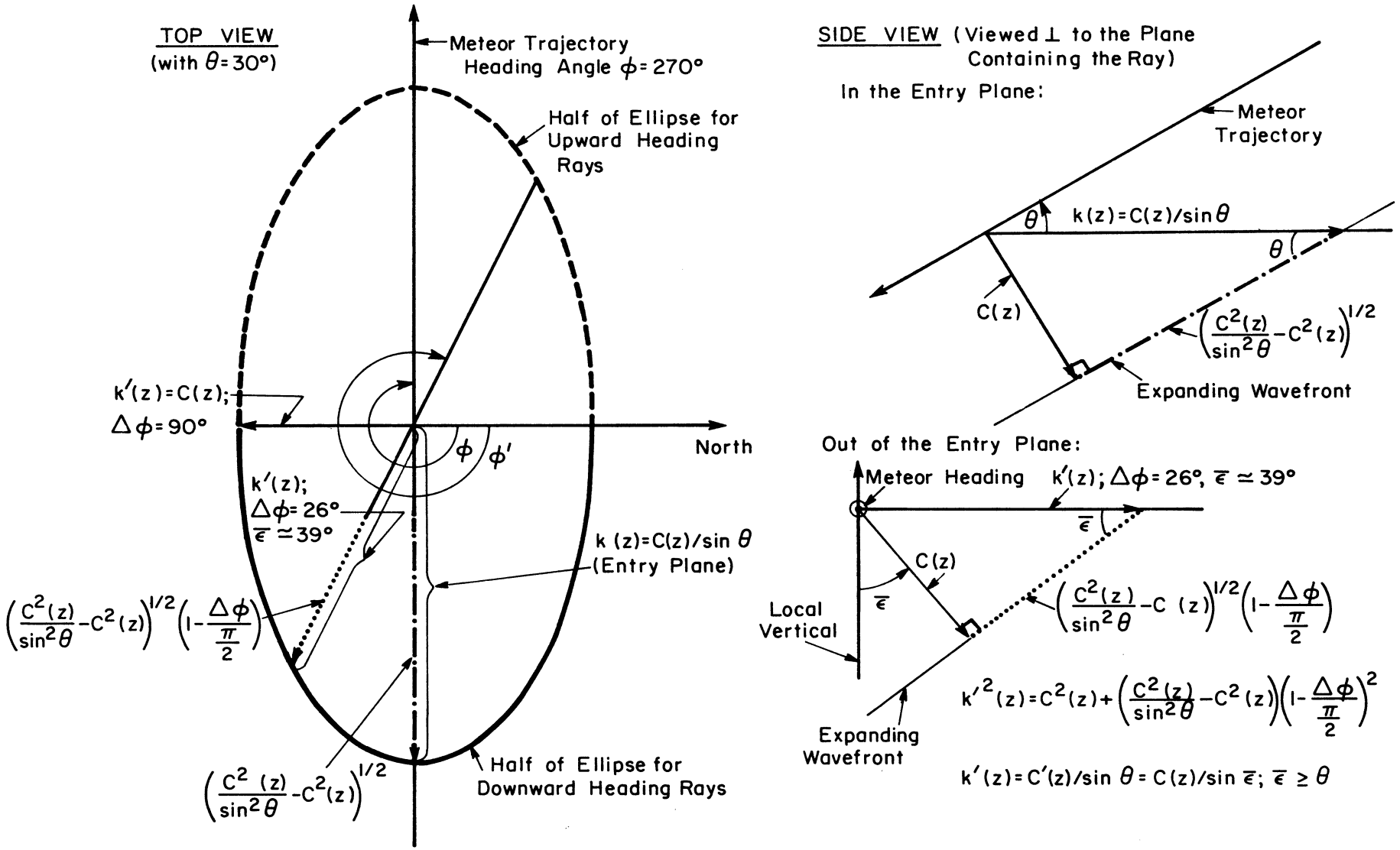


Figure 75. Characteristic velocity geometry out of the entry plane in the absence of wind, $\alpha=0^{o}$.

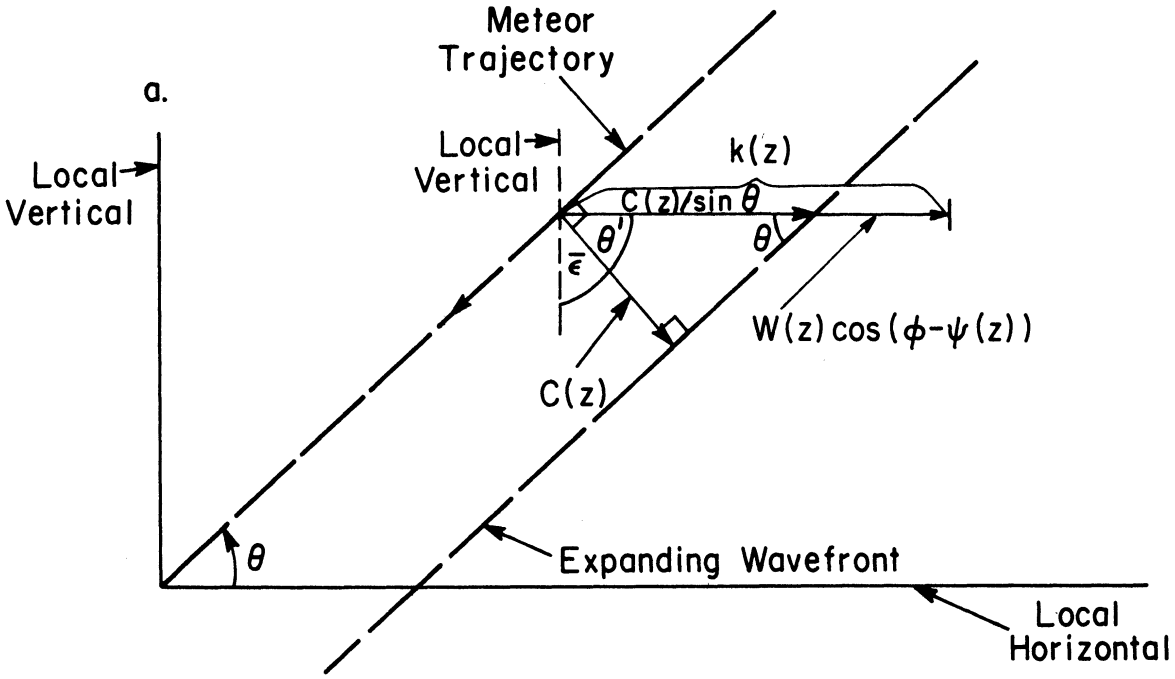


Figure 76a. Characteristic velocity geometry in the entry plane with steady wind, $\alpha=0^{o}$.

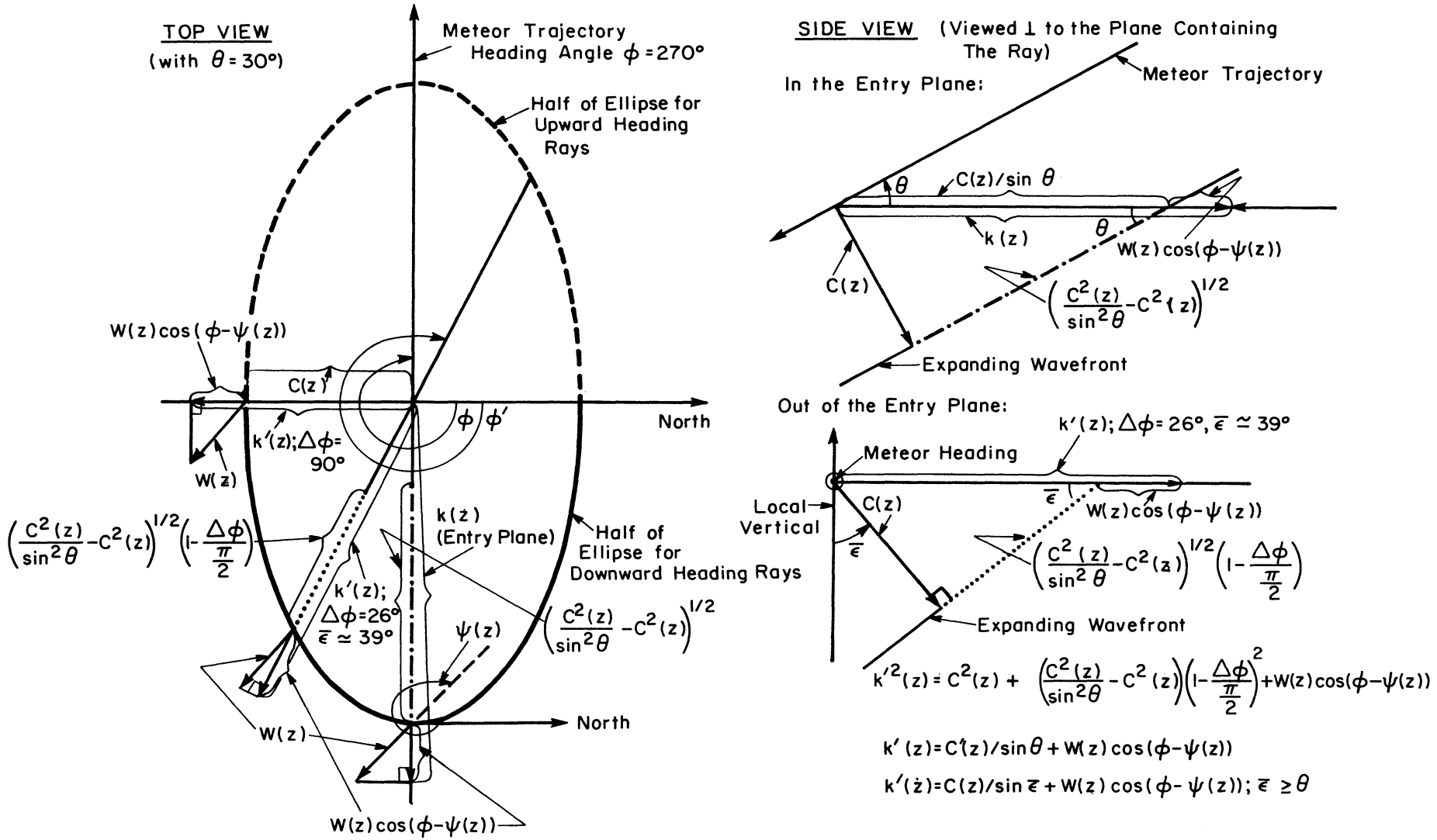


Figure 76b. Characteristic velocity geometry out of the entry plane with steady wind, $\alpha = 0^{o}$.

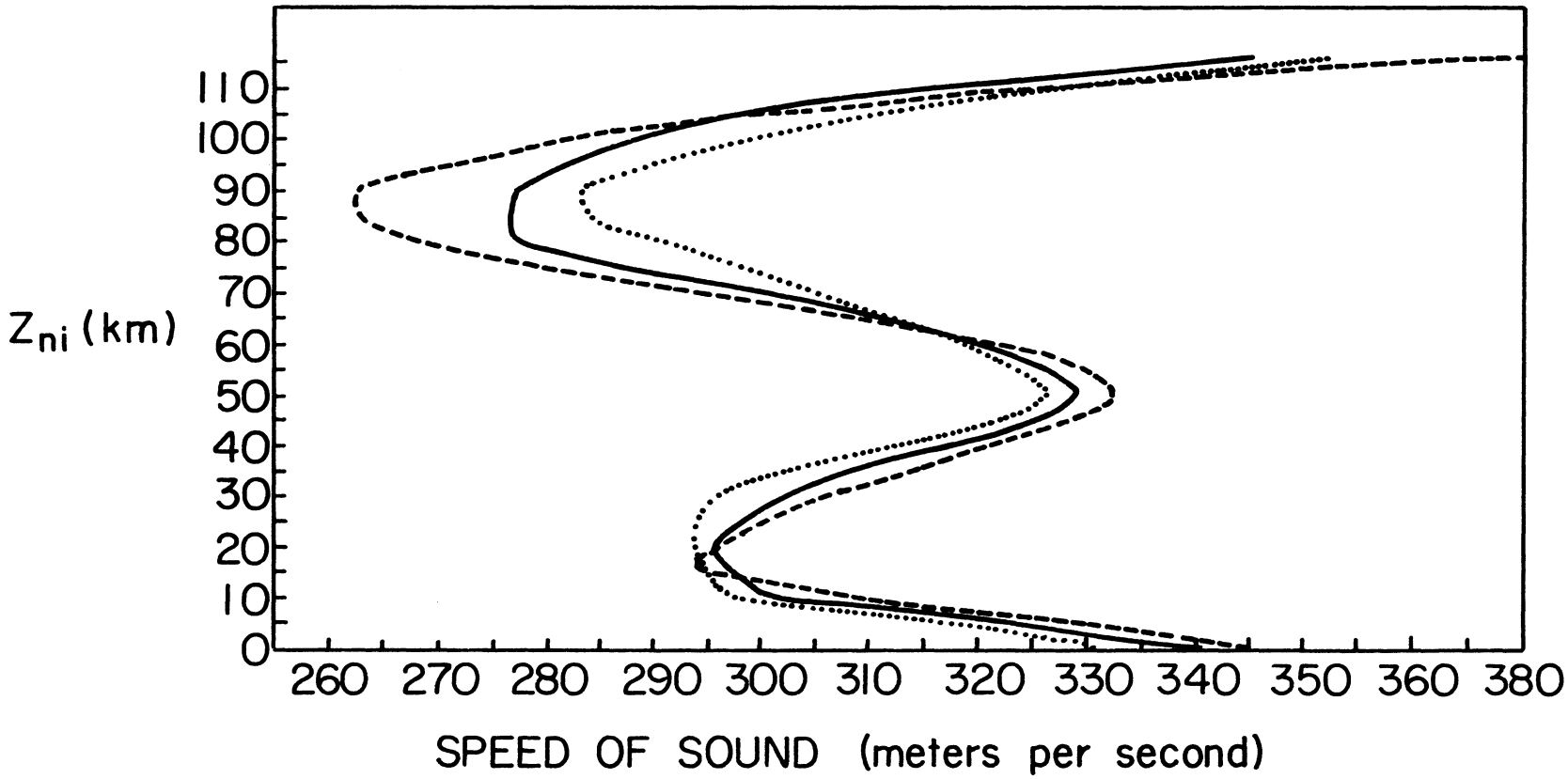


Figure 77. Speed of sound as a function of altitude and season for 45°N latitude, after Donn and Rind, 1972 ( for winter, dotted line; for summer, dashed line; for spring-fall, solid line ).

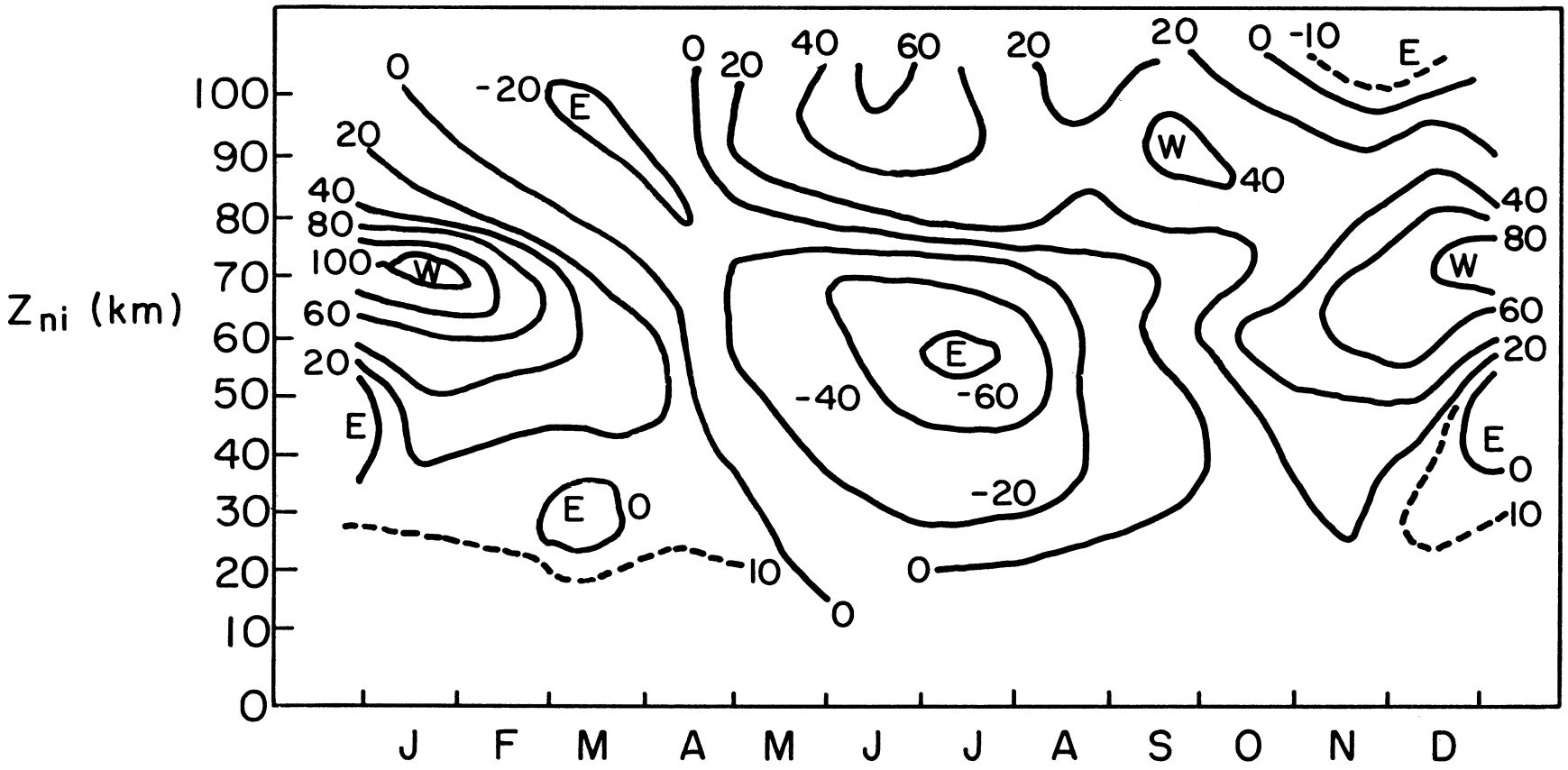


Figure 78. Middle latitude zonal wind field as a function of altitude and time of year, after Batten, 1961 ( speeds in m/sec ).

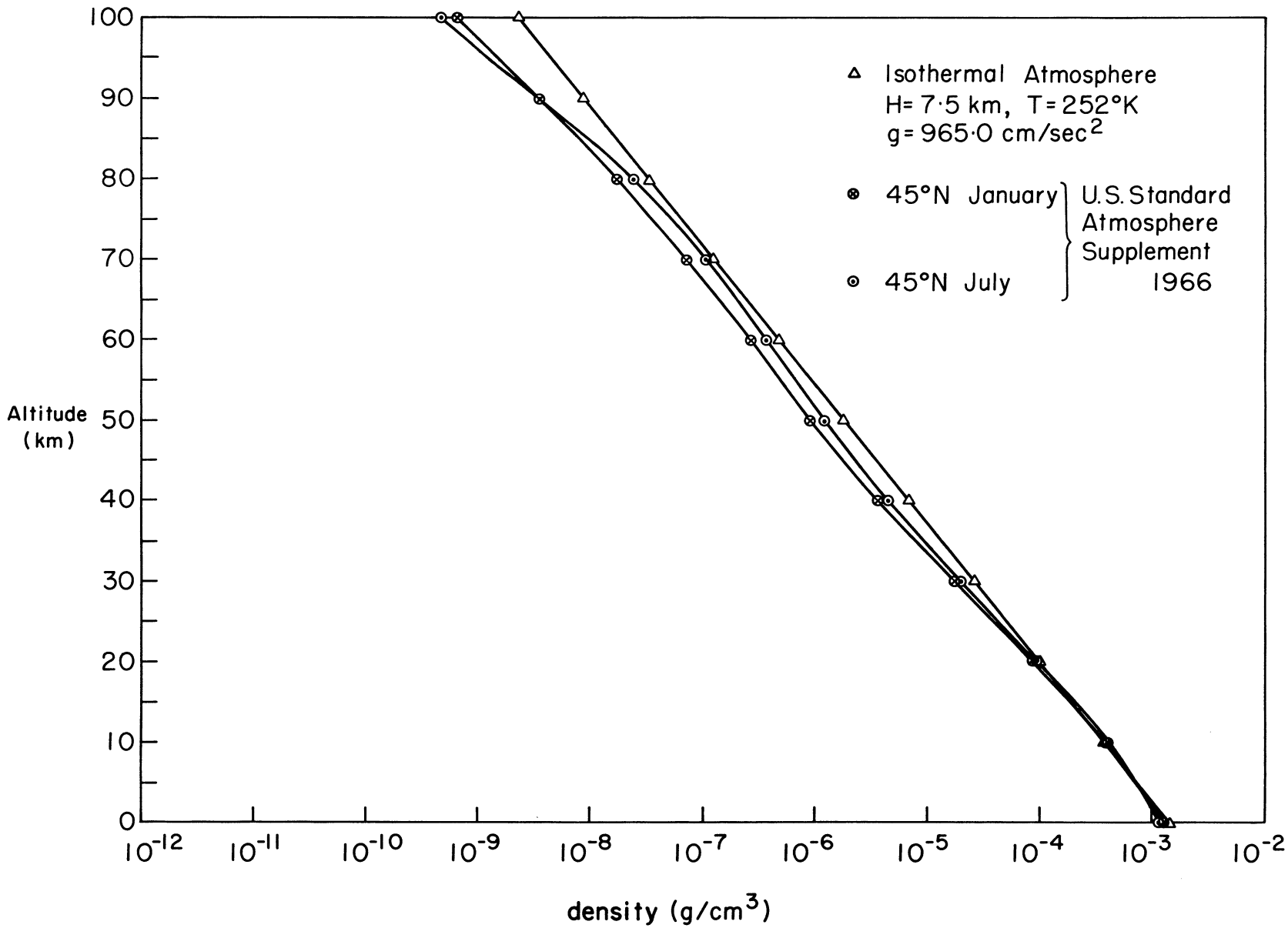


Figure 79. Atmospheric density as a function of altitude.

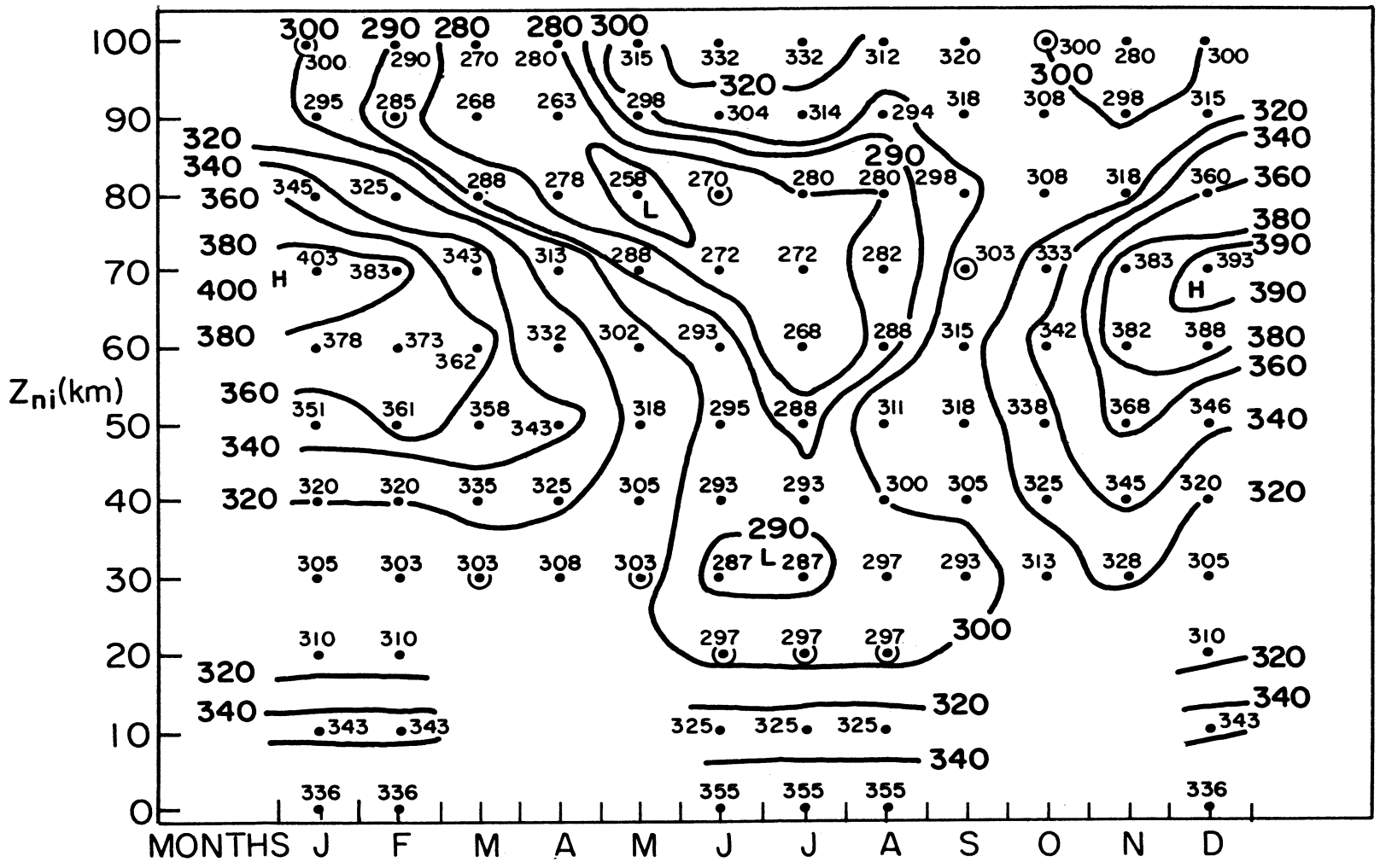


Figure 80. Effective sound velocity as a function of altitude; net propagation direction to the East; circled points indicate mean winds equal to zero ( speeds in m/sec ).

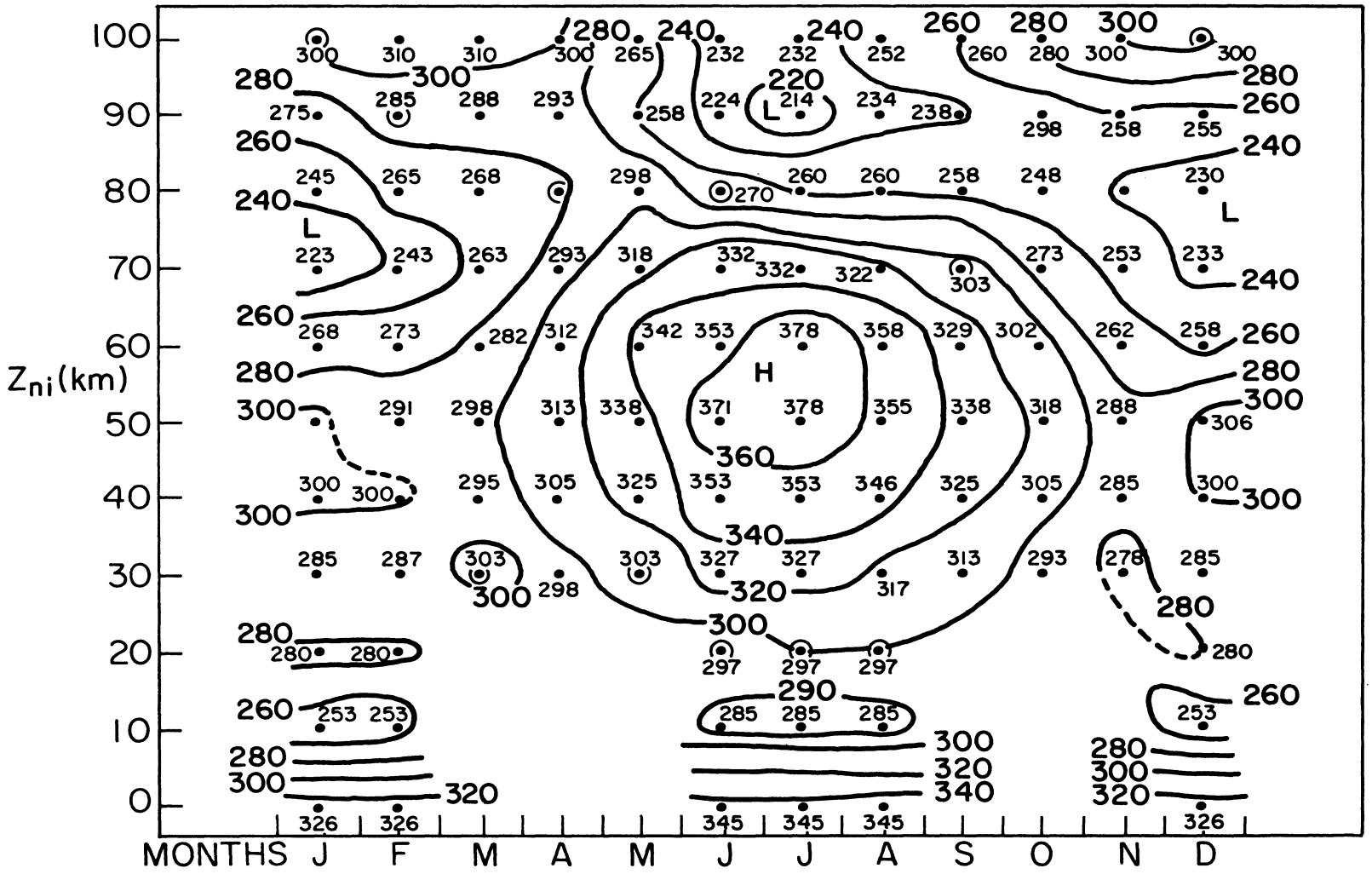


Figure 81. Effective sound velocity as a function of altitude; net propagation direction to the West; circled points indicate mean wind equal to zero ( speeds in m/sec ).

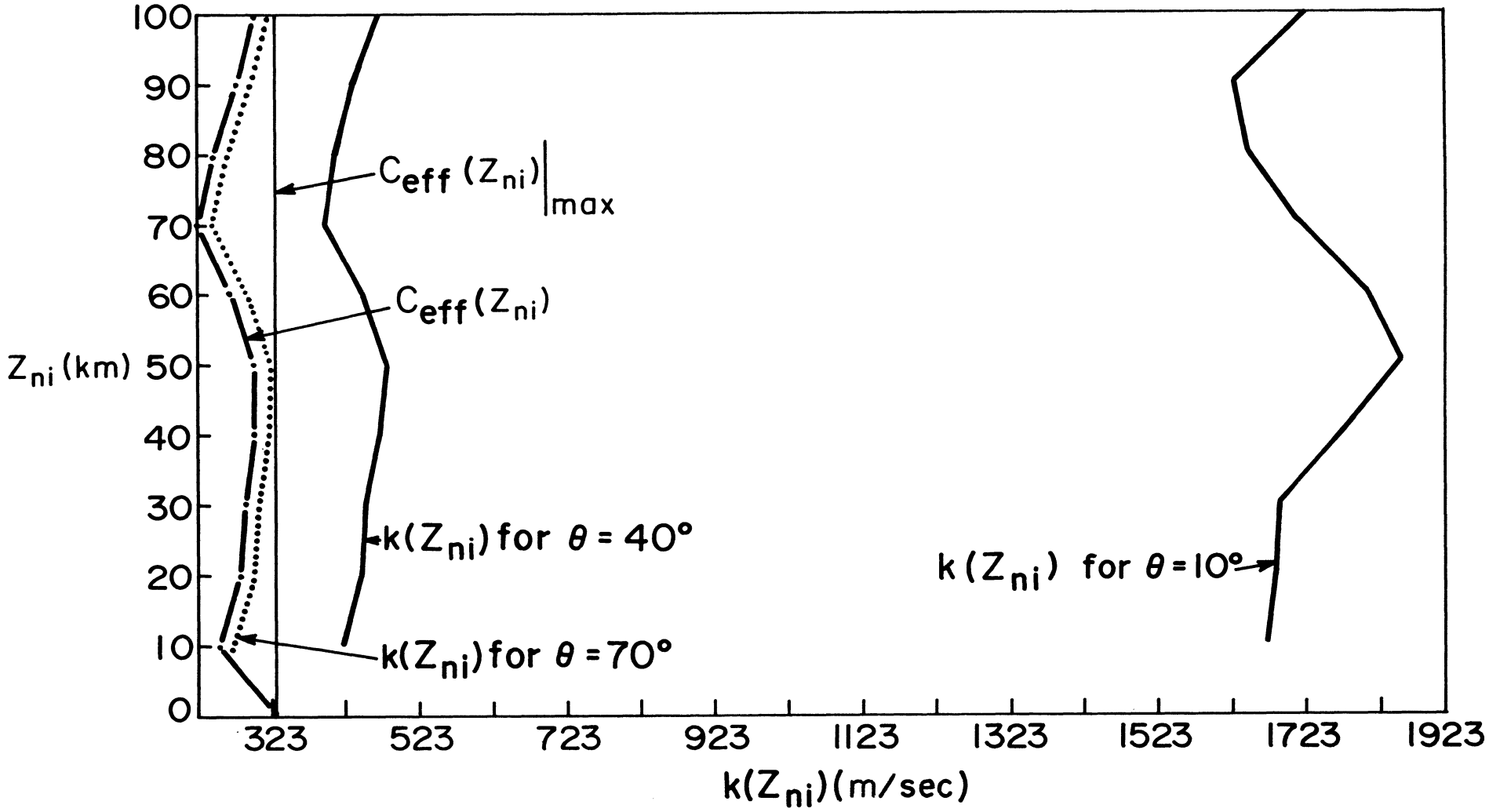


Figure 82. Effective sound velocity and characteristic velocity as a function of altitude in the entry plane, $\phi = 90^{o}$, for propagation West in January, $\theta = 10^{o}$, $40^{o}$ and $70^{o}$. Dotted portions of curves represent situations for which ray paths to the ground are not allowed.

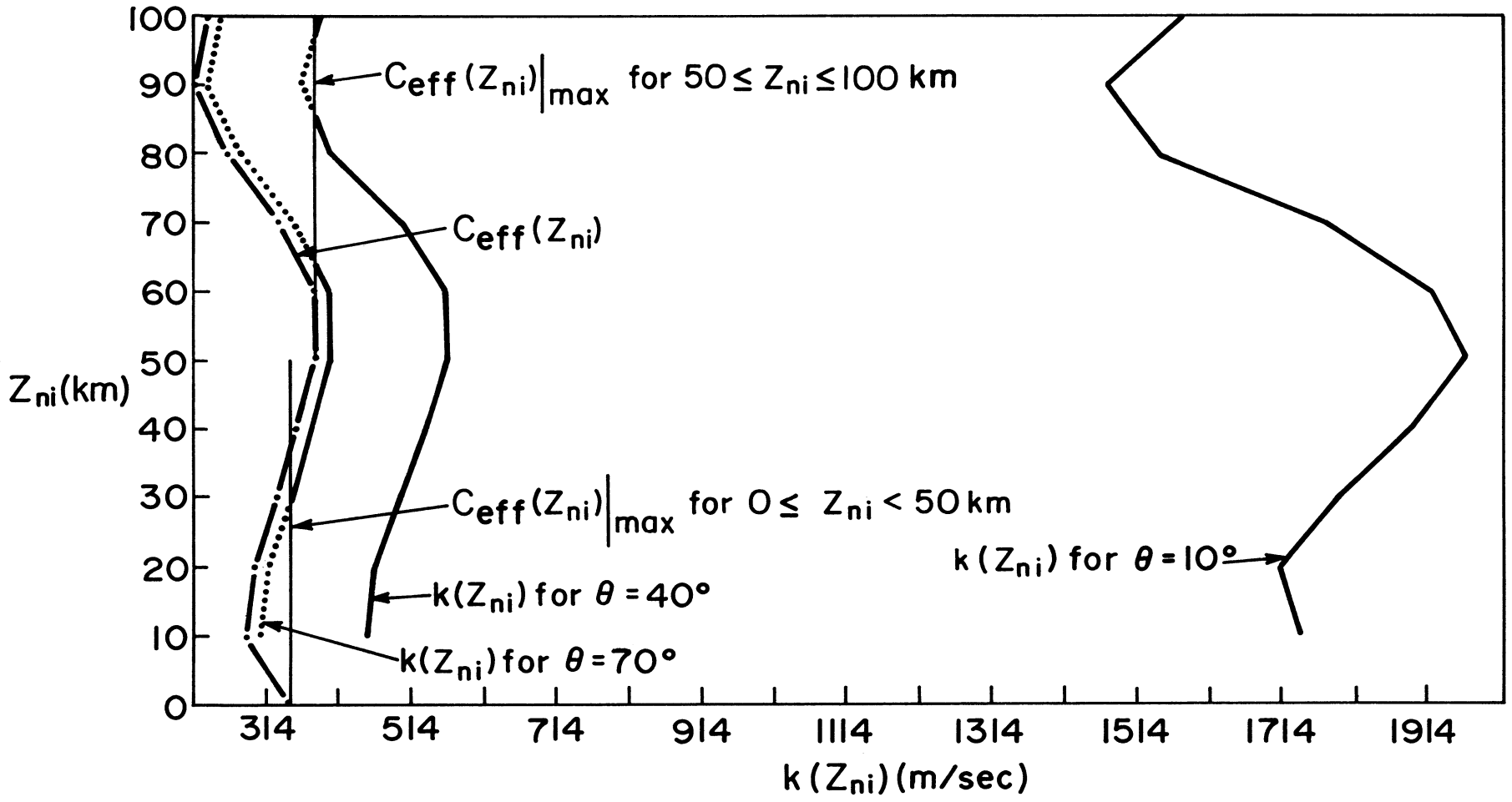


Figure 83. Effective sound velocity and characteristic velocity as a function of altitude in the entry plane, $\phi = 90^{o}$, for propagation West in July, $\theta = 10^{o}$, $40^{o}$ and $70^{o}$. Dotted portions of curves represent situations for which ray paths to the ground are not allowed.

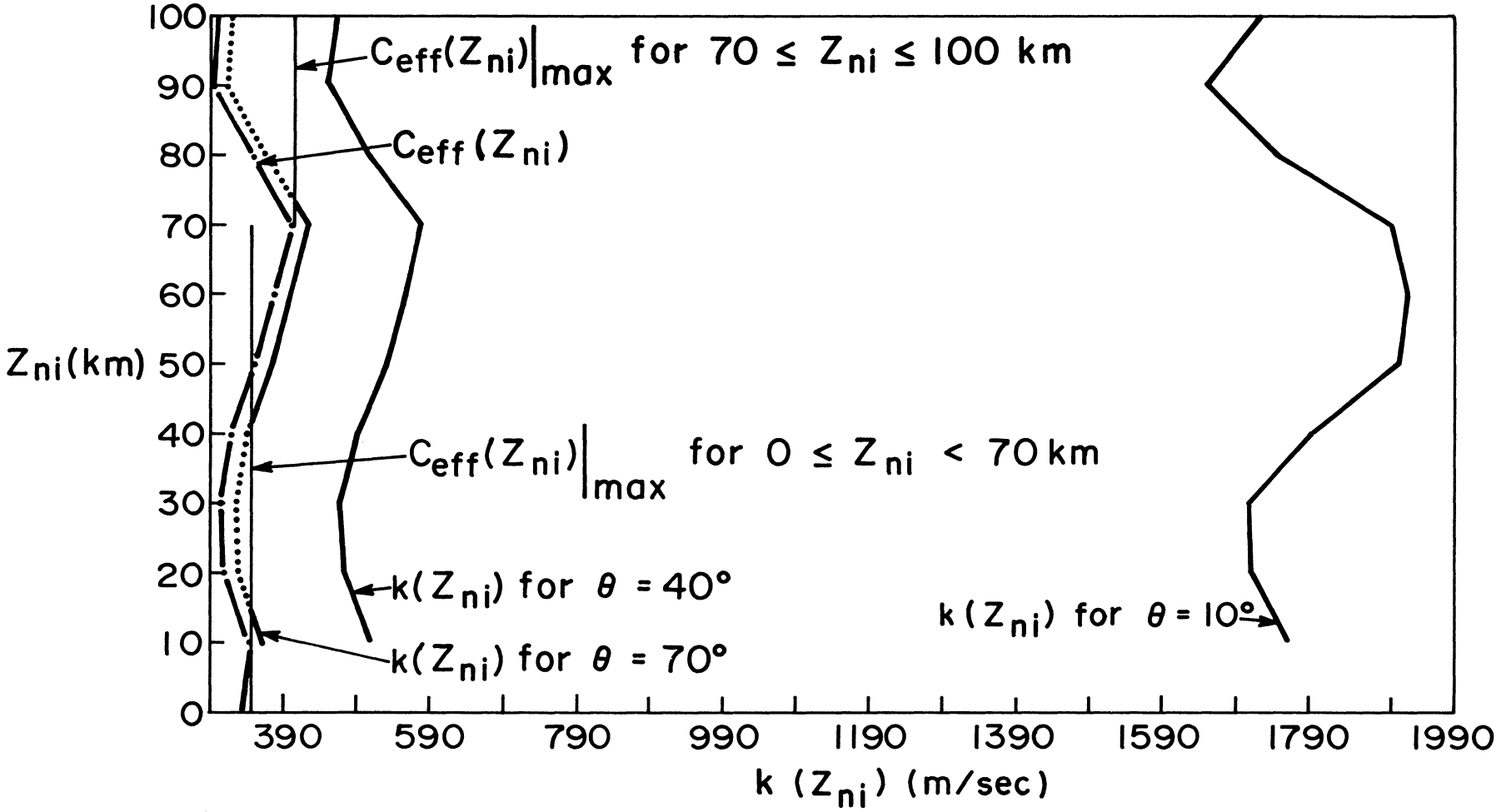


Figure 84. Effective sound velocity and characteristic velocity as a function of altitude in the entry plane, $\phi=270^{o}$, for propagation East in January, $\theta=10^{o}$, $40^{o}$ and $70^{o}$. Dotted portions of curves represent situations for which ray paths to the ground are not allowed.

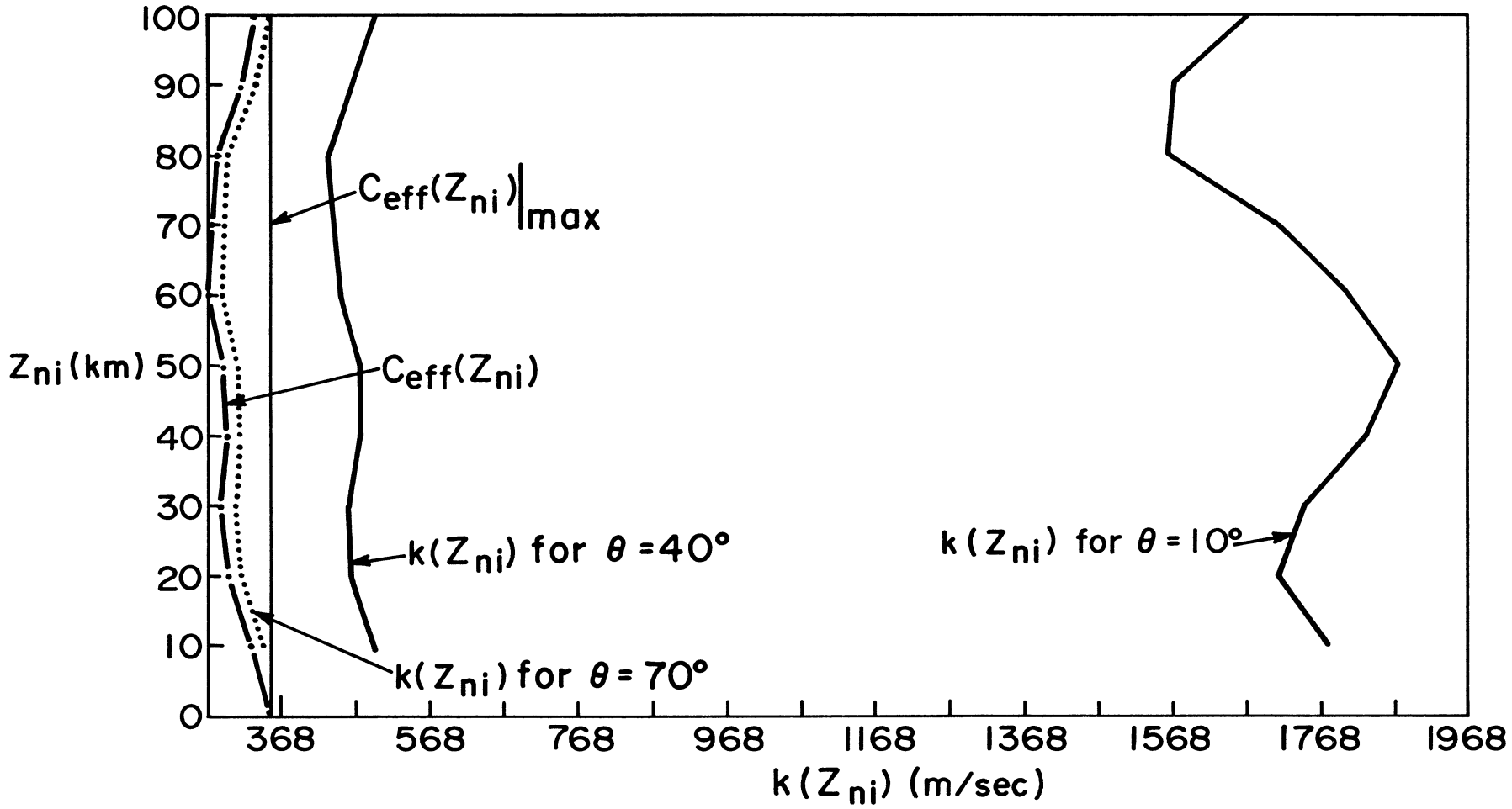


Figure 85. Effective sound velocity and characteristic velocity as a function of altitude in the entry plane, $\phi=270^{o}$, for propagation East in July, $\theta=10^{o}$, $40^{o}$ and $70^{o}$. Dotted portions of curves represent situations for which ray paths to the ground are not allowed.

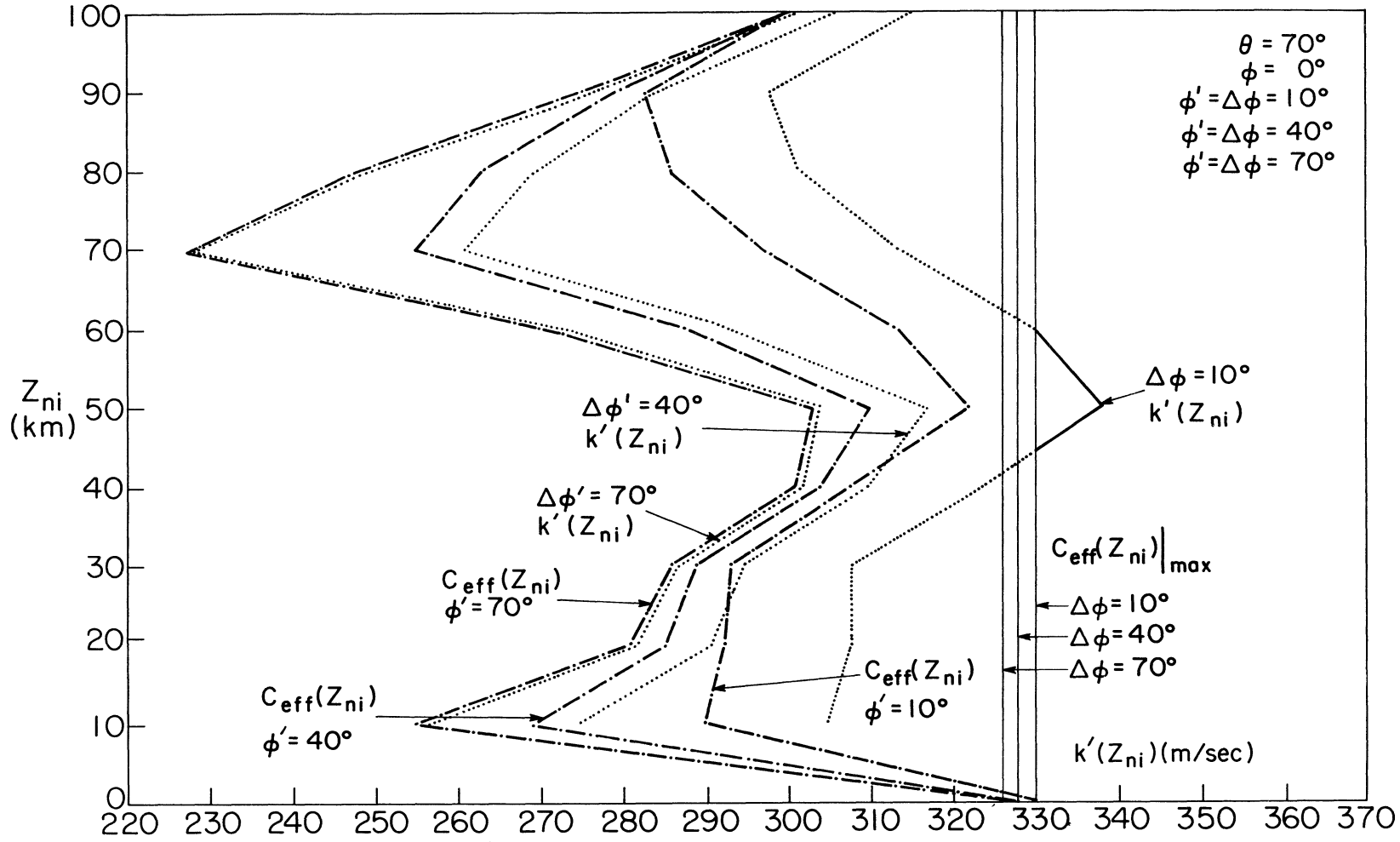


Figure 86. Effective sound velocity and characteristic velocity as a function of altitude out of the entry plane, $\phi=0^{o}$, $\Delta\phi=10^{o}$, $40^{o}$ and $70^{o}$; propagation in January for ray heading West of South, $\theta=70^{o}$. Dotted portions of curves represent situations for which ray paths to the ground are not allowed.

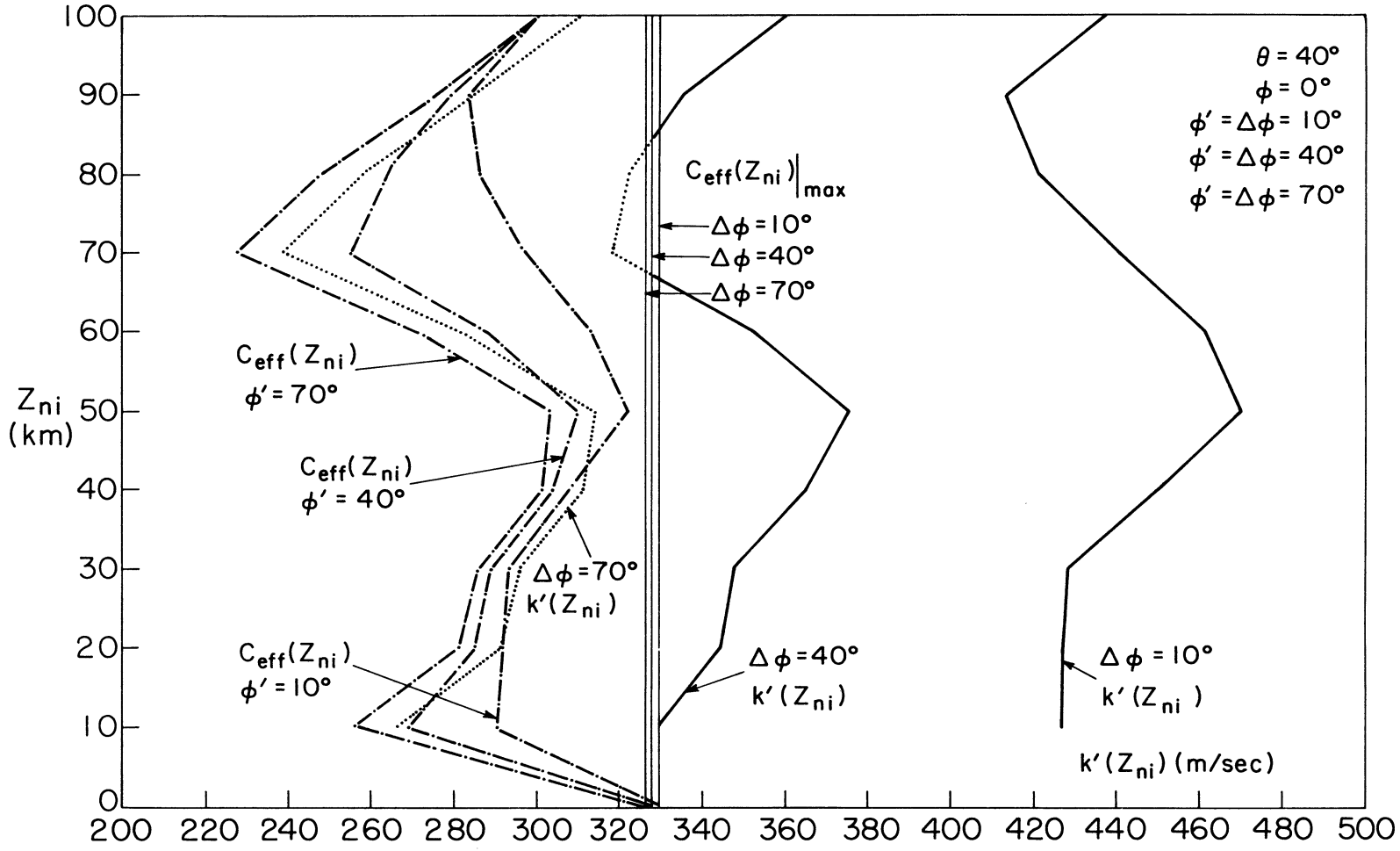


Figure 87. Effective sound velocity and characteristic velocity as a function of altitude out of the entry plane, $\phi=0^{o}$, $\Delta\phi=10^{o}$, $40^{o}$ and $70^{o}$; propagation in January for ray heading West of South, $\theta=40^{o}$. Dotted portions of curves represent situations for which ray paths to the ground are not allowed.

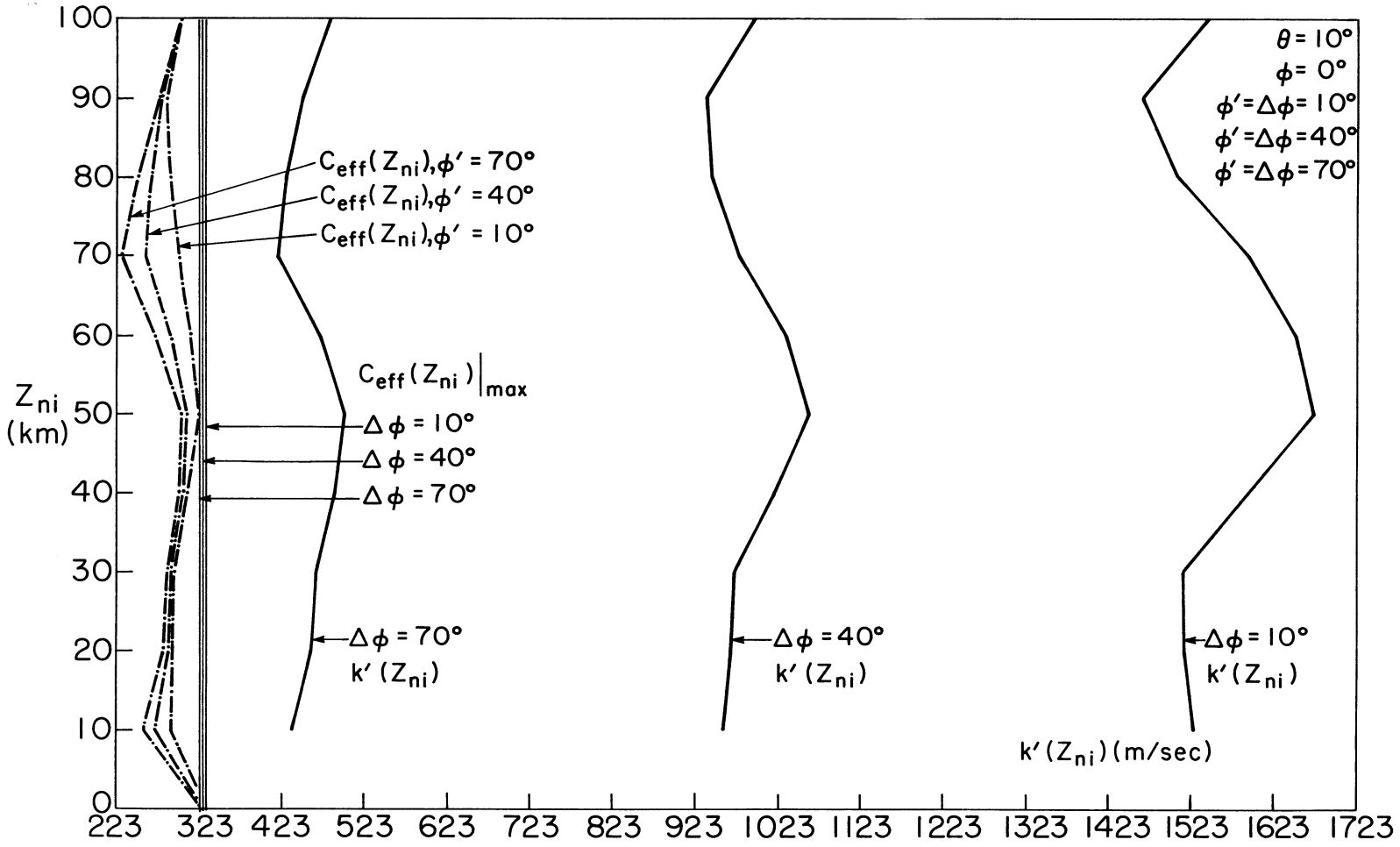


Figure 88. Effective sound velocity and characteristic velocity as a function of altitude out of the entry plane, $\phi=0^{o}$, $\Delta\phi=10^{o}$, $40^{o}$ and $70^{o}$; propagation in January for ray heading West of South, $\theta=10^{o}$. Dotted portions of curves represent situations for which ray paths to the ground are not allowed.

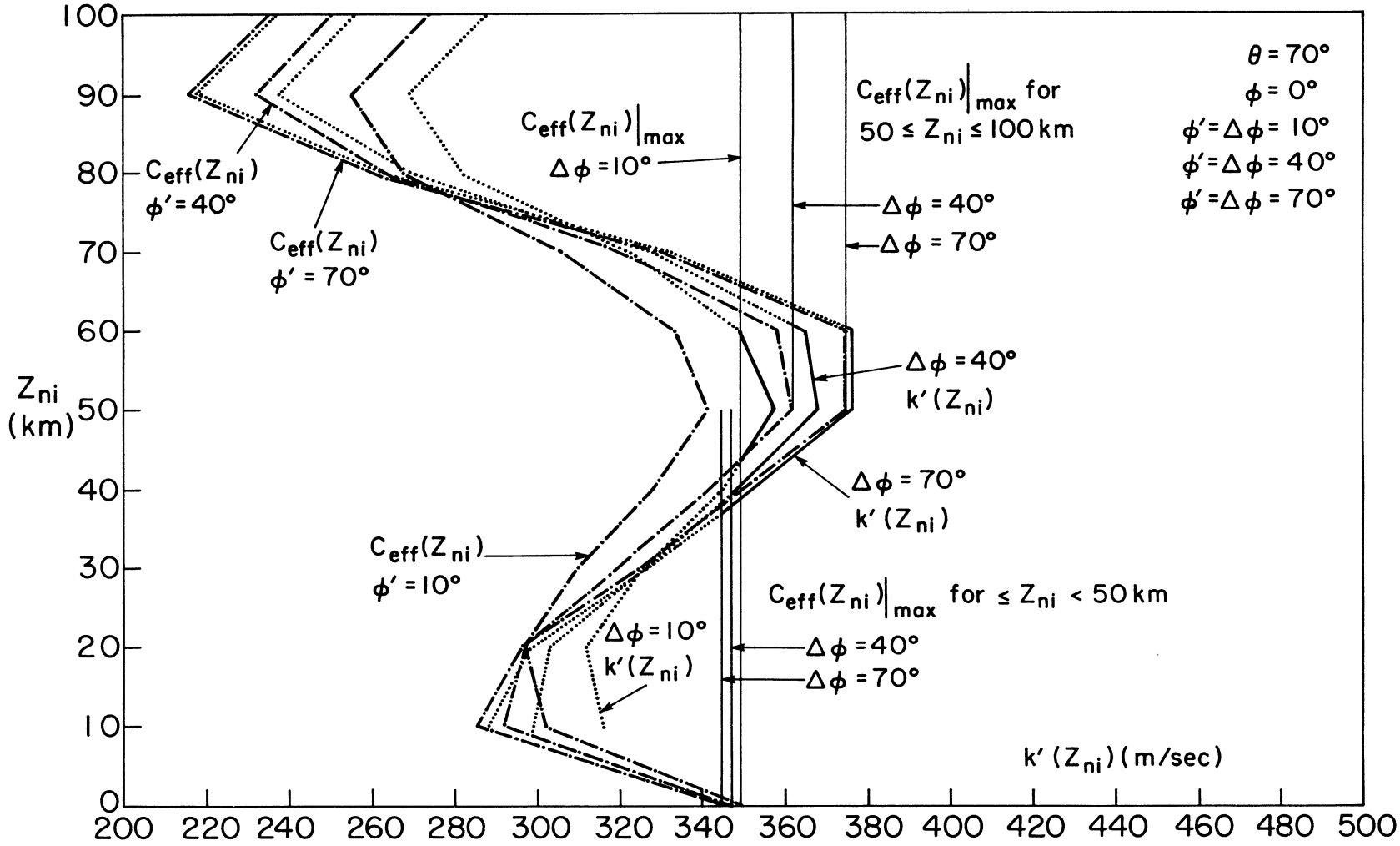


Figure 89. Effective sound velocity and characteristic velocity as a function of altitude out of the entry plane, $\phi=0^{o}$, $\Delta\phi=10^{o}$, $40^{o}$ and $70^{o}$; propagation in July for ray heading West of South, $\theta=70^{o}$. Dotted portions of curves represent situations for which ray paths to the ground are not allowed.

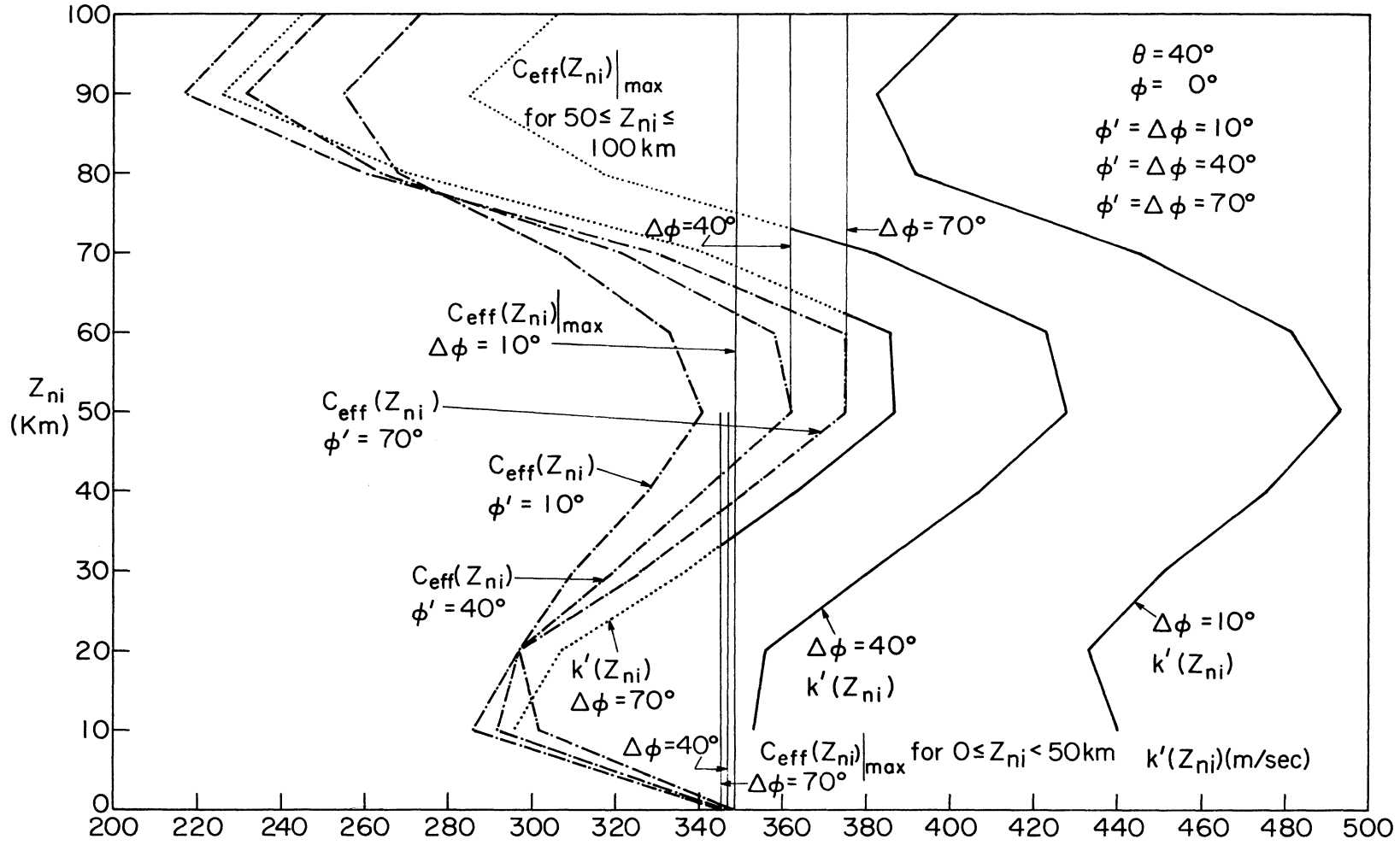


Figure 90. Effective sound velocity and characteristic velocity as a function of altitude out of the entry plane, $\phi=0^{o}$, $\Delta\phi=10^{o}$, $40^{o}$and $70^{o}$; propagation in July for ray heading West of South, $\theta=40^{o}$. Dotted portions of curves represent situations for which ray paths to the ground are not allowed.

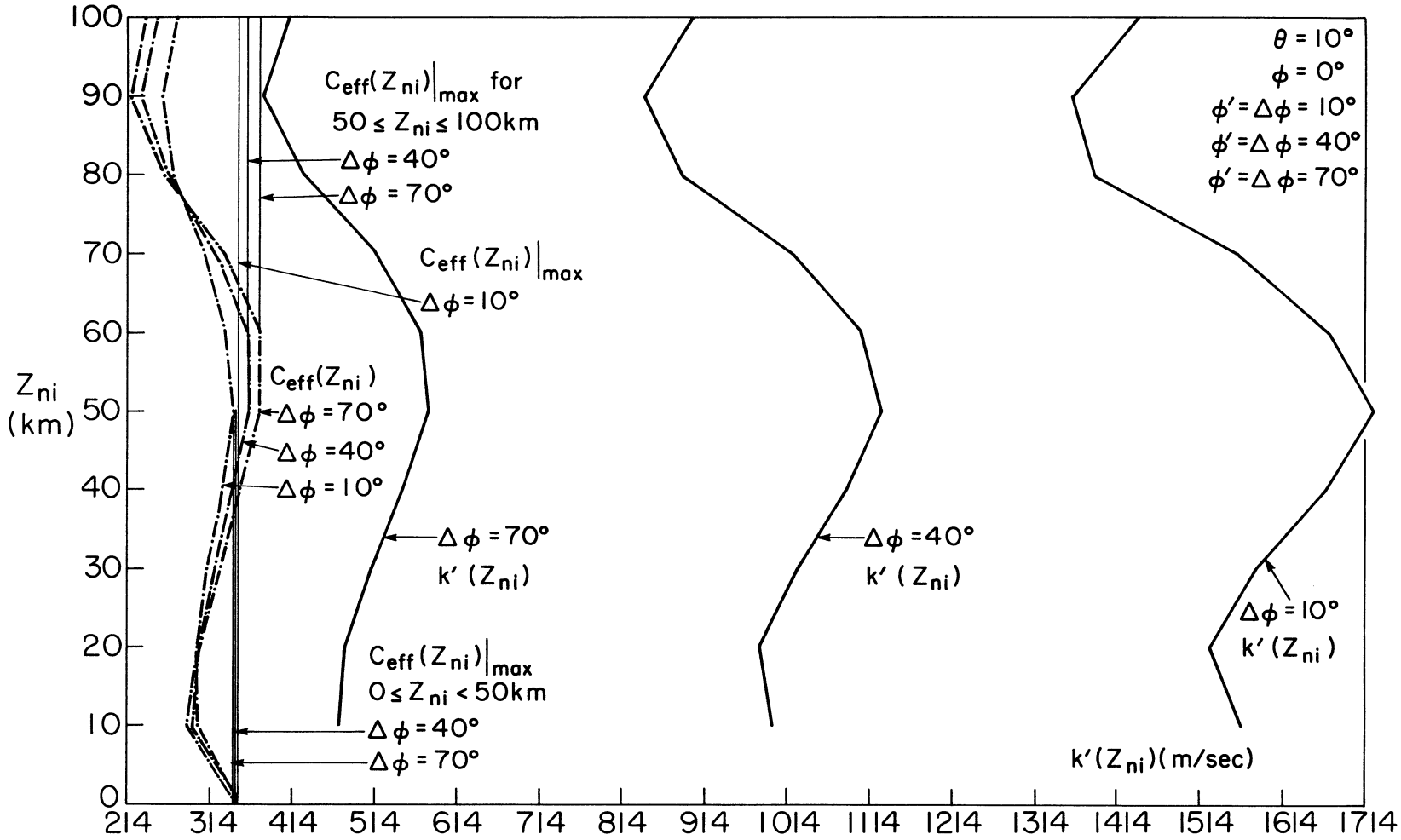


Figure 91. Effective sound velocity and characteristic velocity as a function of altitude out of the entry plane, $\phi=0^{o}$, $\Delta\phi=10^{o}$, $40^{o}$ and $70^{o}$; propagation in July for ray heading West of South, $\theta=10^{o}$. Dotted portions of curves represent situations for which ray paths to the ground are not allowed.

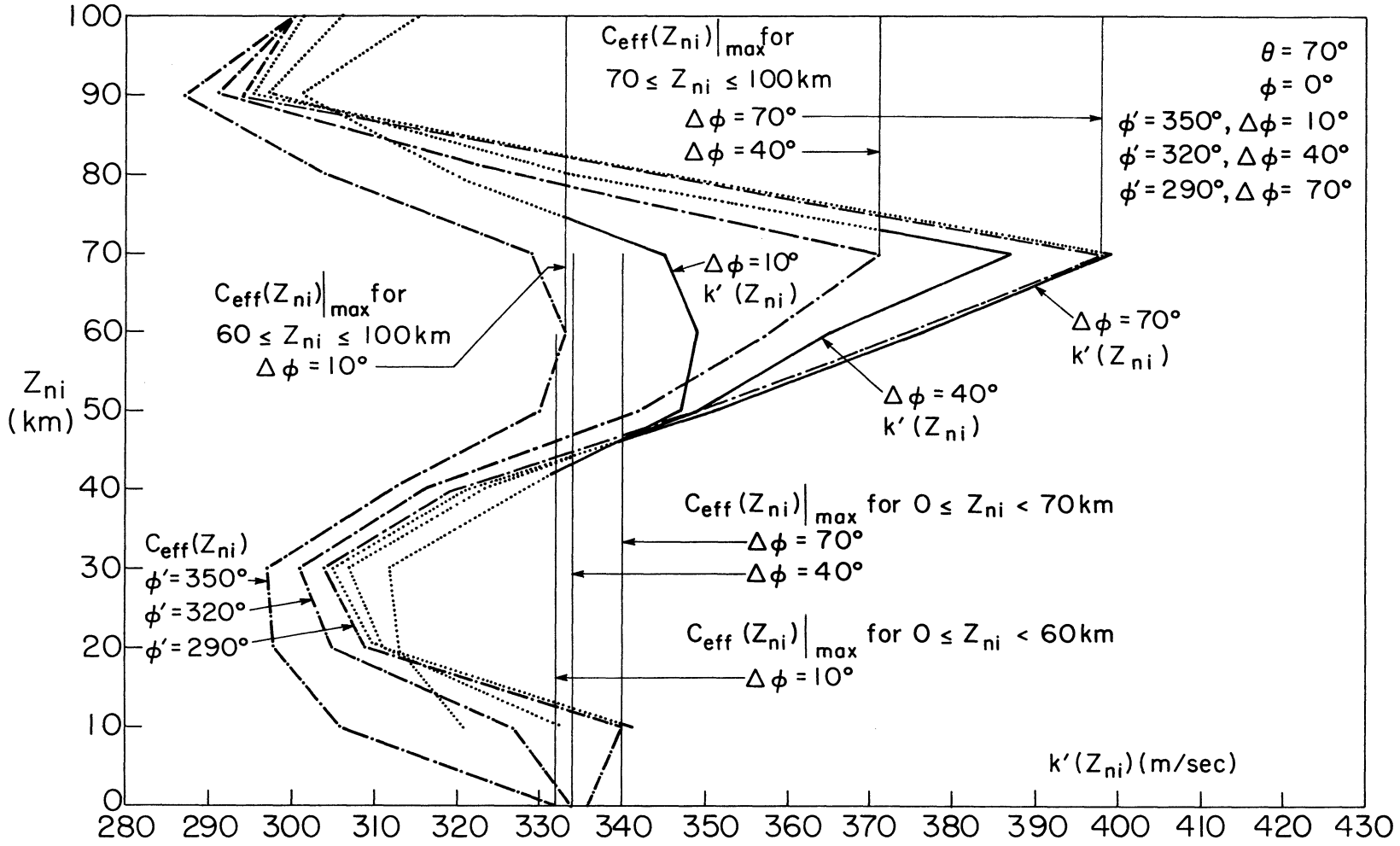


Figure 92. Effective sound velocity and characteristic velocity as a function of altitude out of the entry plane, $\emptyset = 0^{o}$, $\Delta\emptyset = 10^{o}$, $40^{o}$ and $70^{o}$; propagation in January for ray heading East of South, $\theta = 70^{o}$. Dotted portions of curves represent situations for which ray paths to the ground are not allowed.

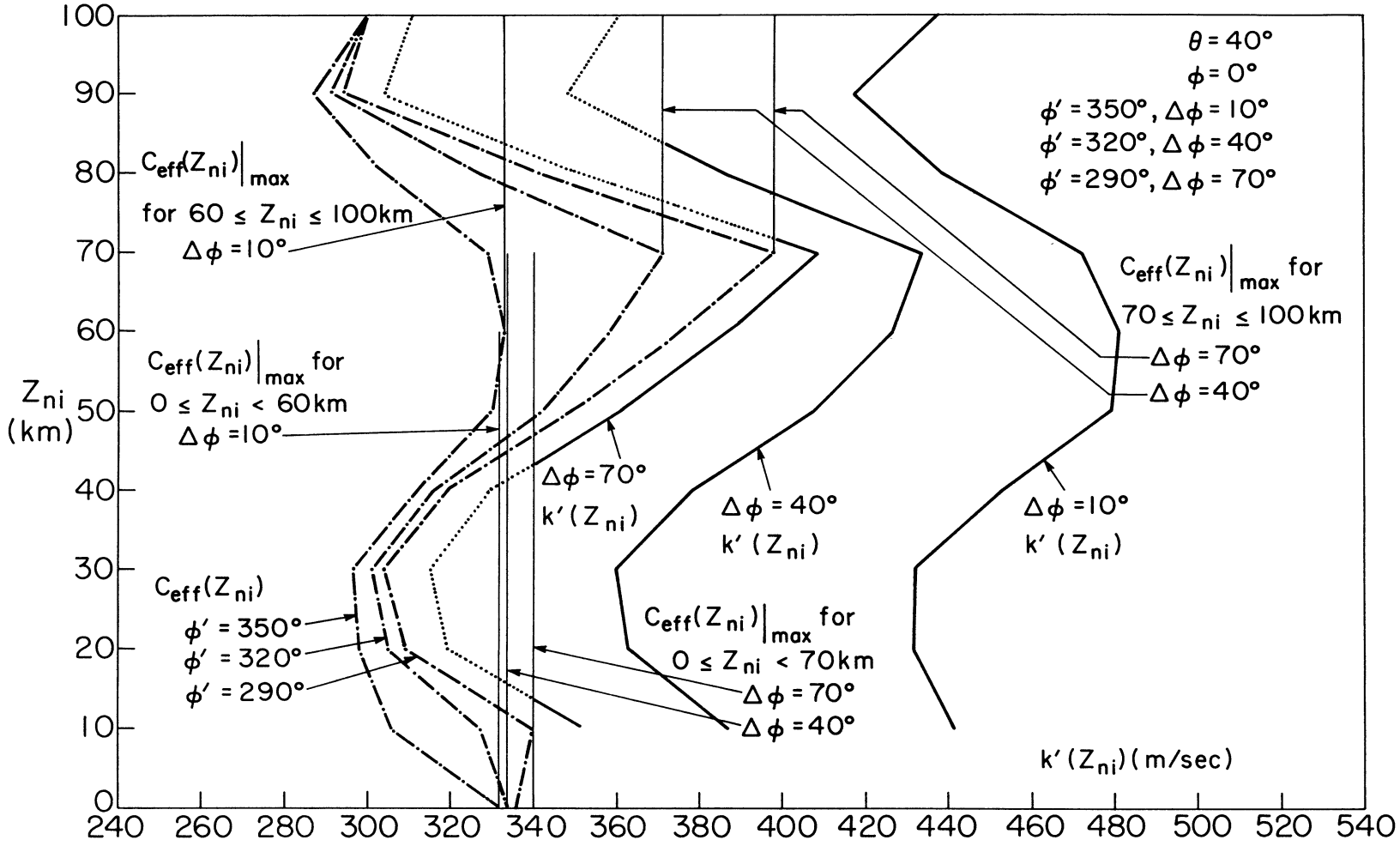


Figure 93. Effective sound velocity and characteristic velocity as a function of altitude out of the entry plane, $\phi=0^{o}$, $\Delta\phi= 10^{o}$, $40^{o}$ and $70^{o}$; propagation in January for ray heading East of South, $\theta=40^{o}$. Dotted portions of curves represent situations for which ray paths to the ground are not allowed.

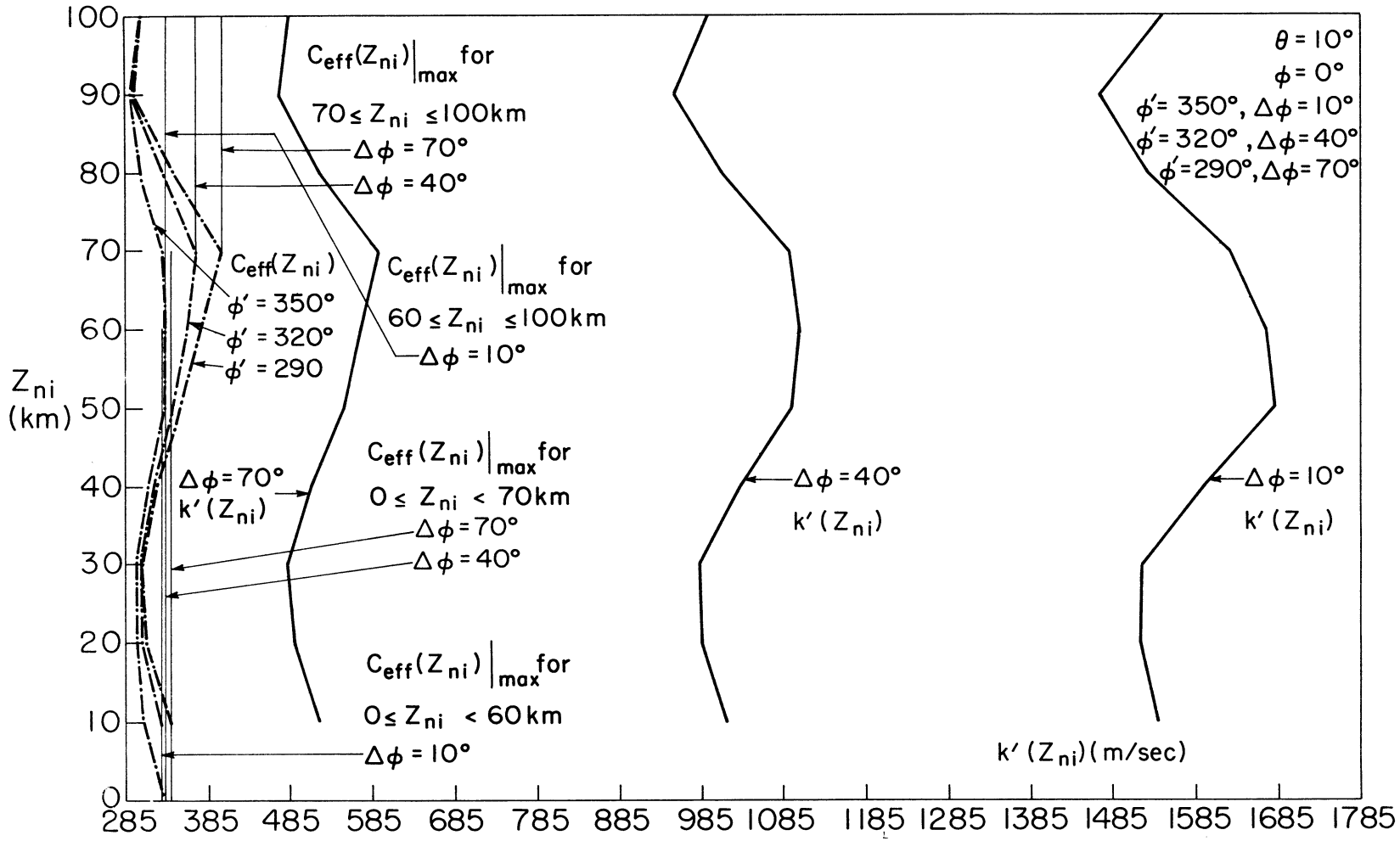


Figure 94. Effective sound velocity and characteristic velocity as a function of altitude out of the entry plane, $\phi=0^{o}$, $\Delta\phi=10^{o}$, $40^{o}$ and $70^{o}$; propagation in January for ray heading East of South, $\theta=10^{o}$. Dotted portions of curves represent situations for which ray paths to the ground are not allowed.

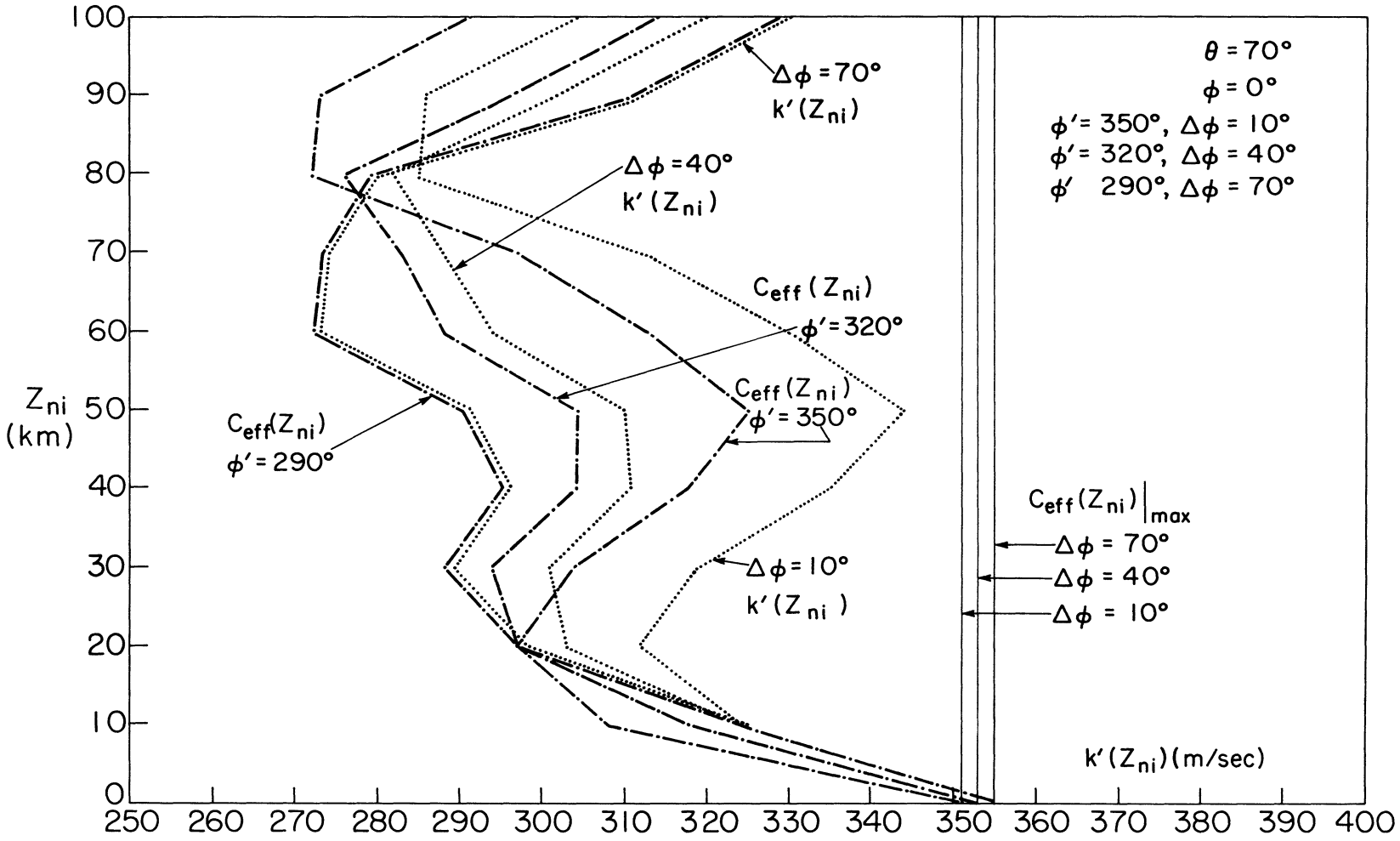


Figure 95. Effective sound velocity and characteristic velocity as a function of altitude out of the entry plane, $\phi=0^{o}$, $\Delta\phi=10^{o}$, $40^{o}$ and $70^{o}$; propagation in July for ray heading East of South, $\theta=70^{o}$. Dotted portions of curves represent situations for which ray paths to the ground are not allowed.

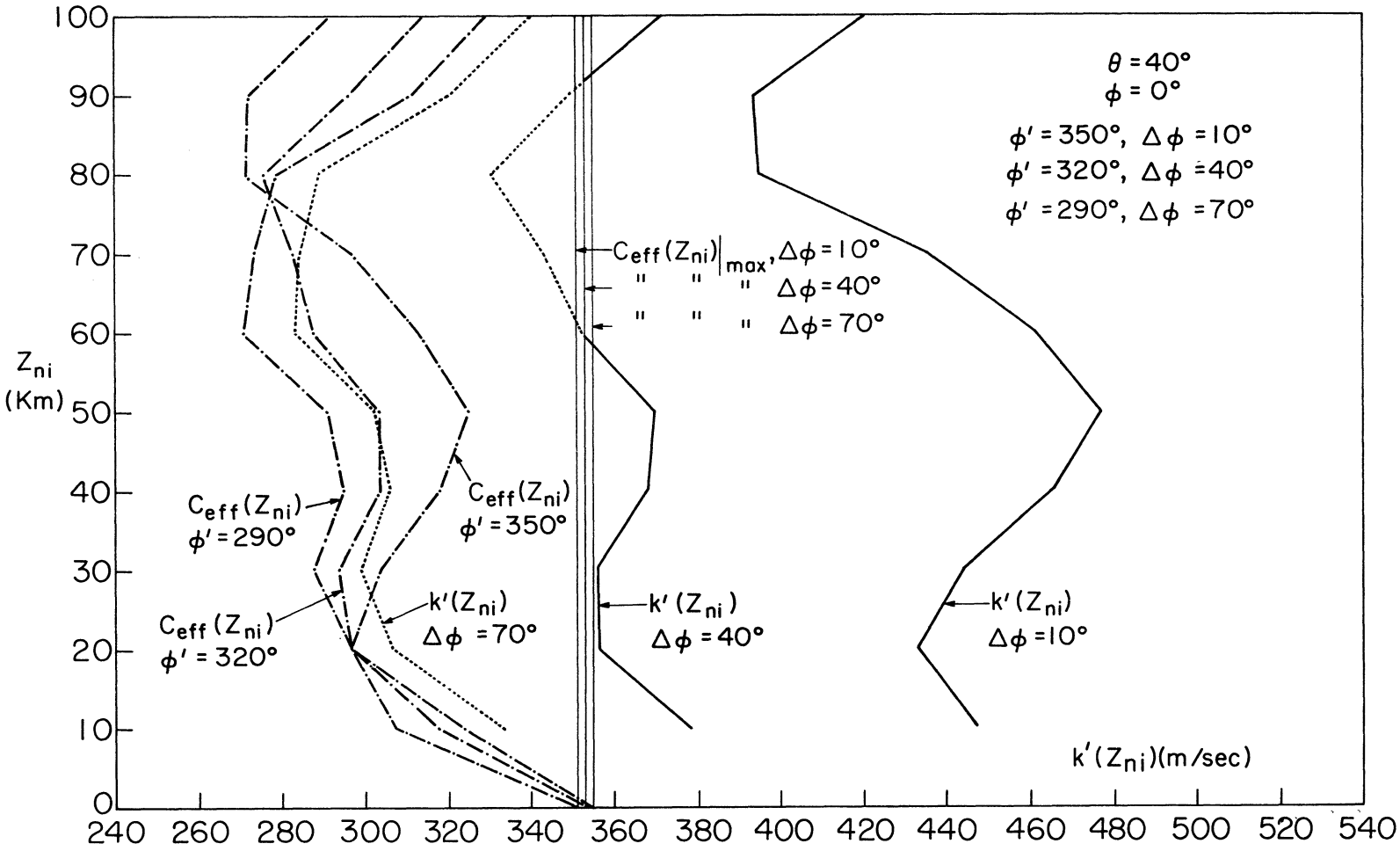


Figure 96. Effective sound velocity and characteristic velocity as a function of altitude out of the entry plane, $\emptyset=0^{o}$, $\Delta\emptyset= 10^{o}$, $40^{o}$ and $70^{o}$; propagation in July for ray heading East of South, $\theta=40^{o}$. Dotted portions of curves represent situations for which ray paths to the ground are not allowed.

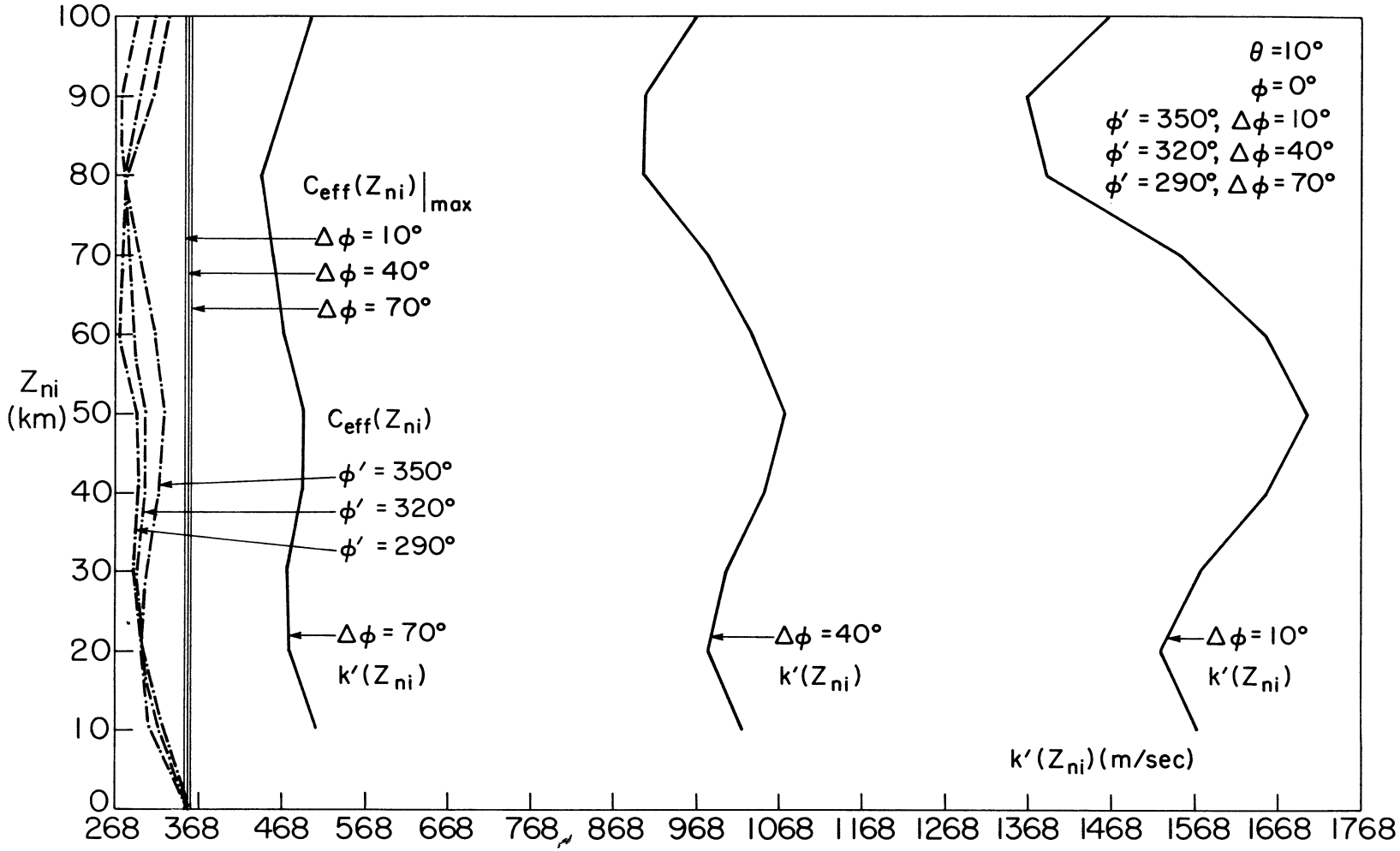


Figure 97. Effective sound velocity and [illegible] velocity as a function of altitude out of the entry plane, $\phi=0^{o}$, $\Delta\phi$= 10°, 40° and 70°, [illegible] in July for ray heading East of South, $\theta=10^{o}$. Dotted portions of curves represent situations for which ray paths to the ground are not allowed.

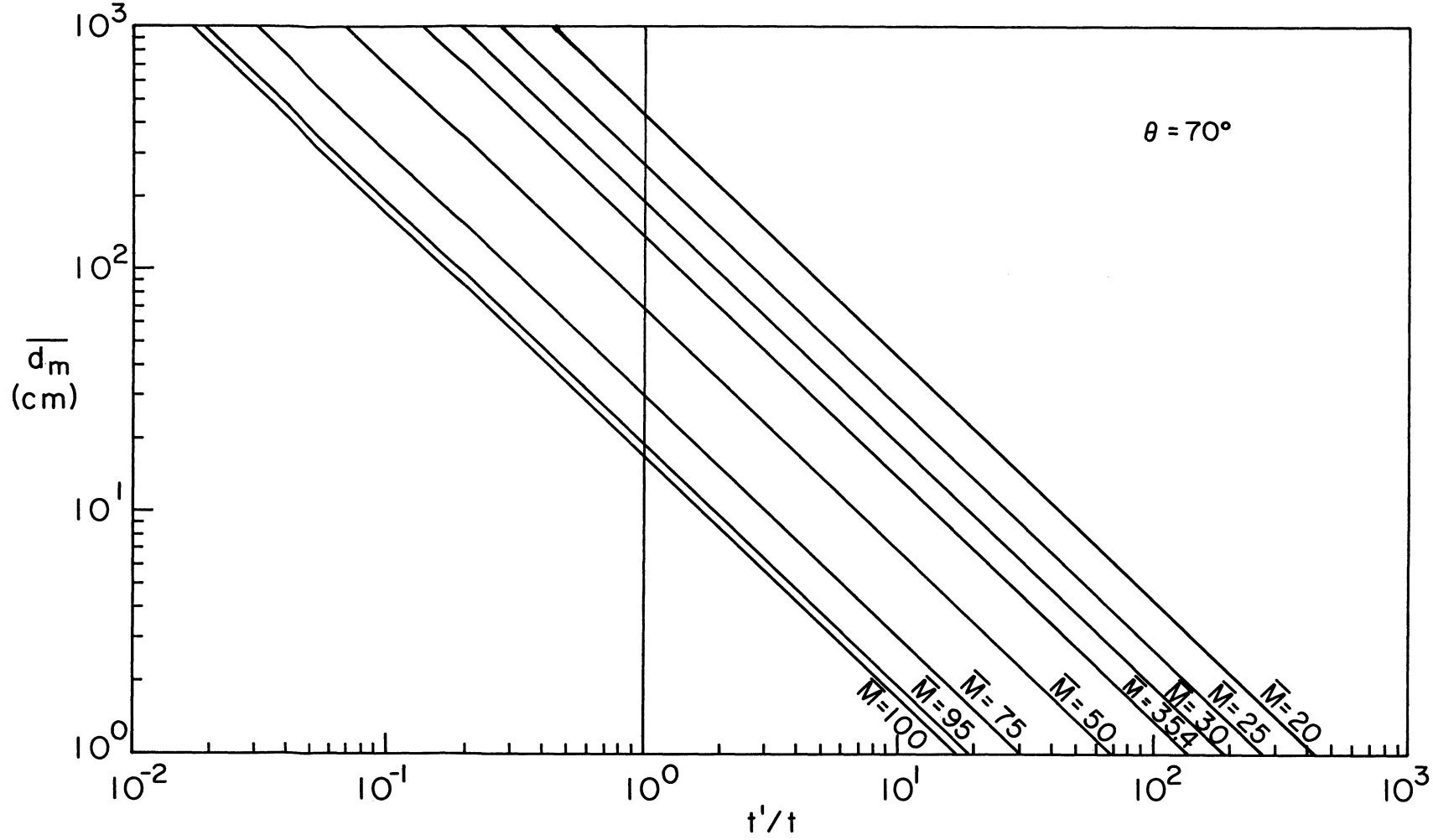


Figure 98a. Instantaneous energy release calculations as a function of meteor diameter, meteor mach number and horizontal entry angle evaluated for a 1 km path interval, $\theta = 70^{o}$.

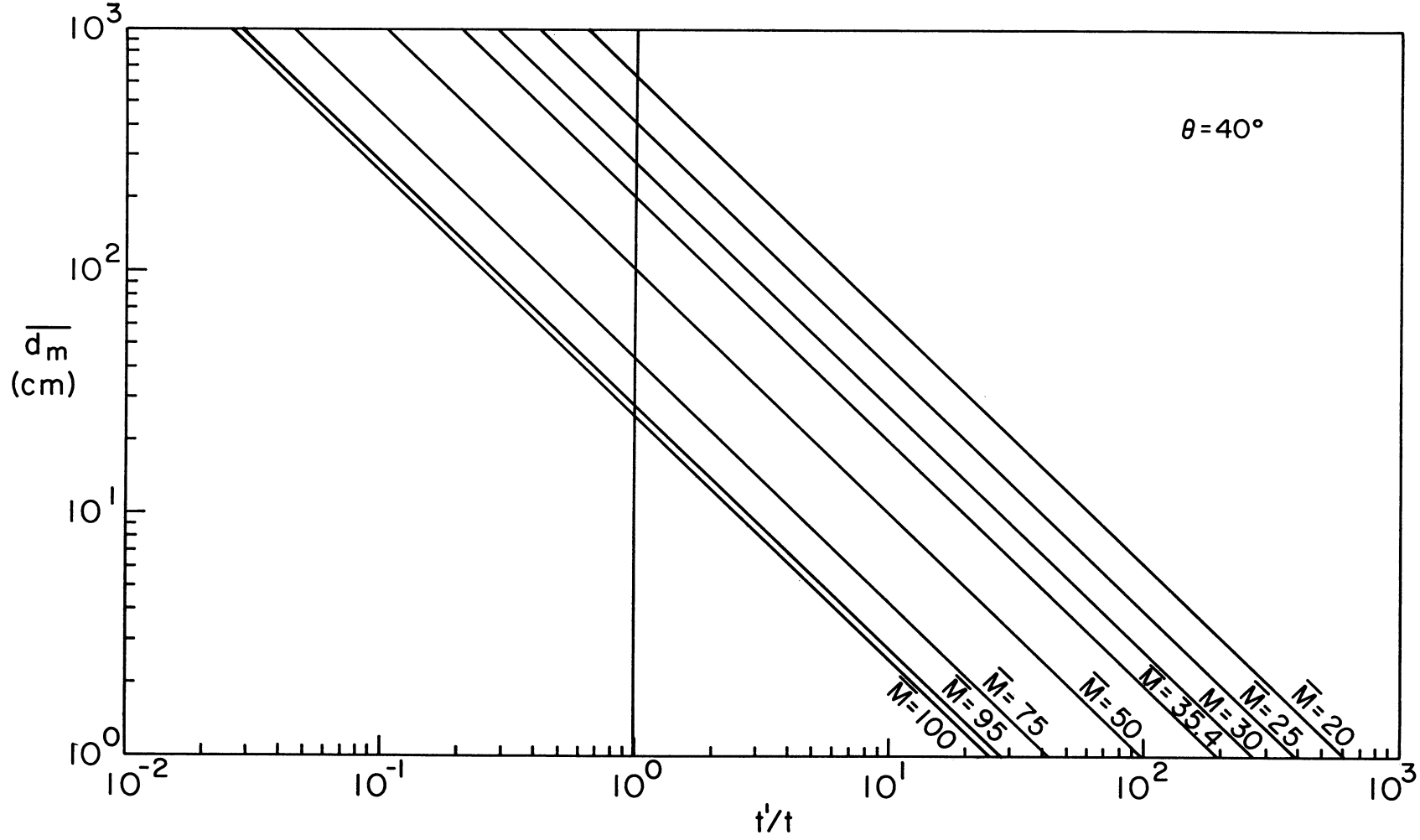


Figure 98b. Instantaneous energy release calculations as a function of meteor diameter, meteor mach number and horizontal entry angle evaluated for a 1 km path interval, $\theta=40^{o}$.

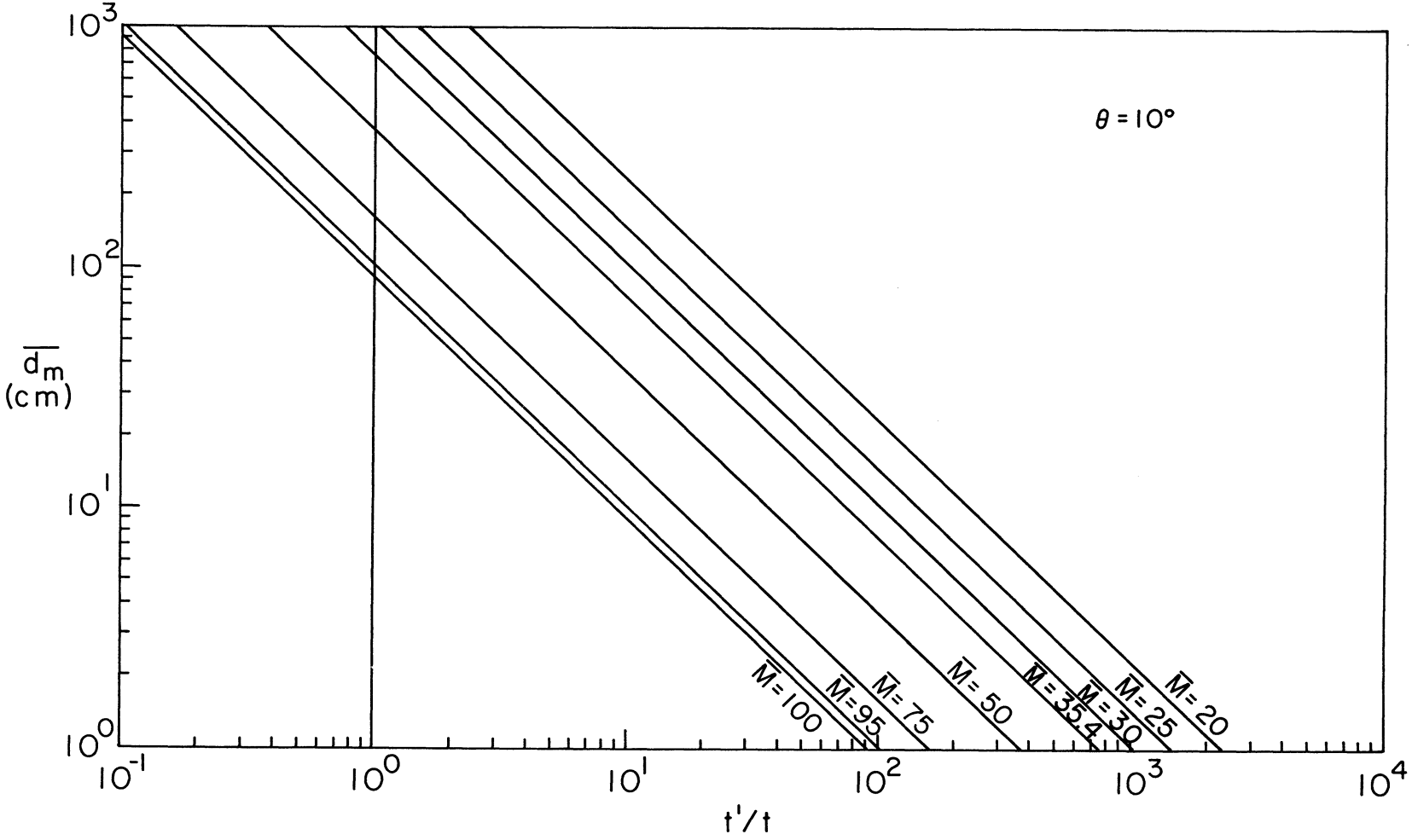


Figure 98c. Instantaneous energy release calculations as a function of meteor diameter, meteor mach number and horizontal entry angle evaluated for a 1 km path interval, $\theta=10^{o}$.

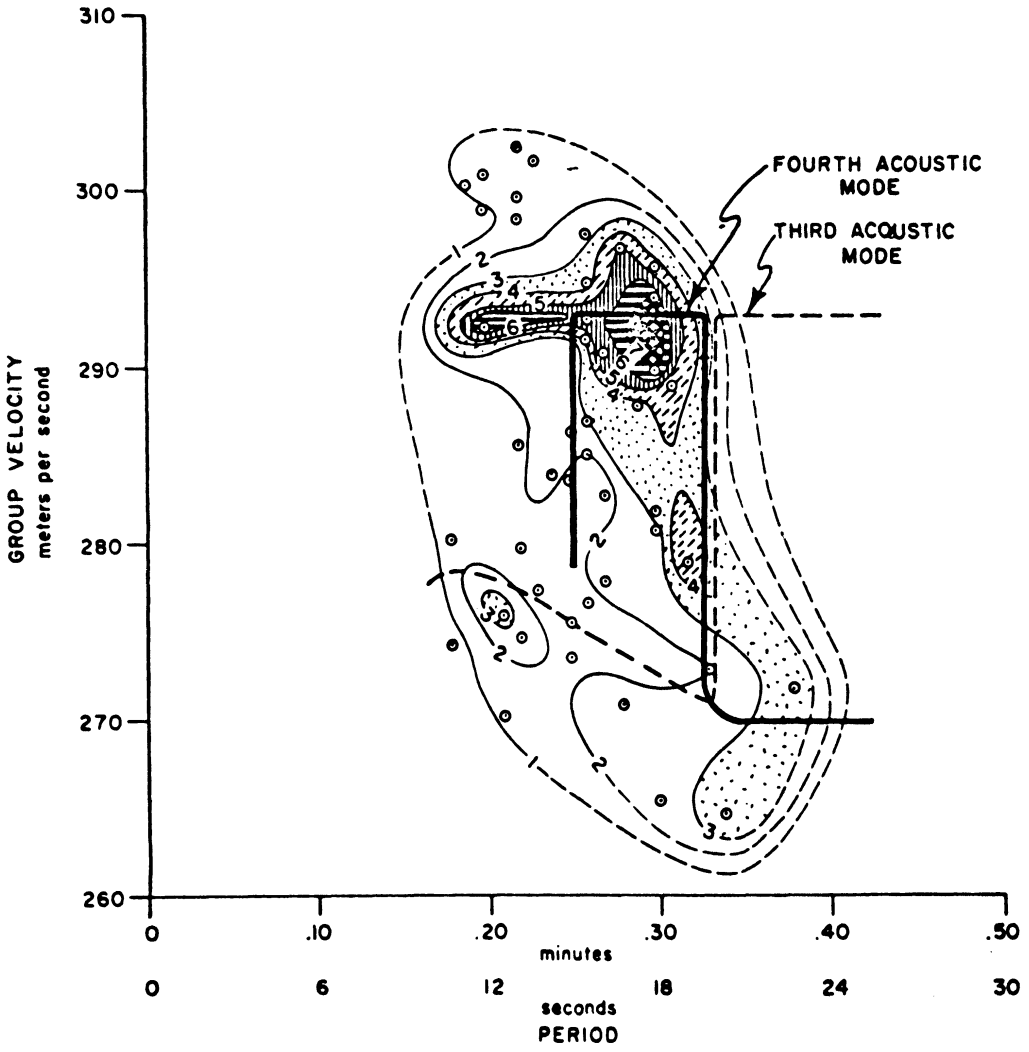


Figure 99. Airwave dispersion diagram from the Revelstoke Meteorite event in British Columbia; group velocity versus period, after Shoemaker, 1972.

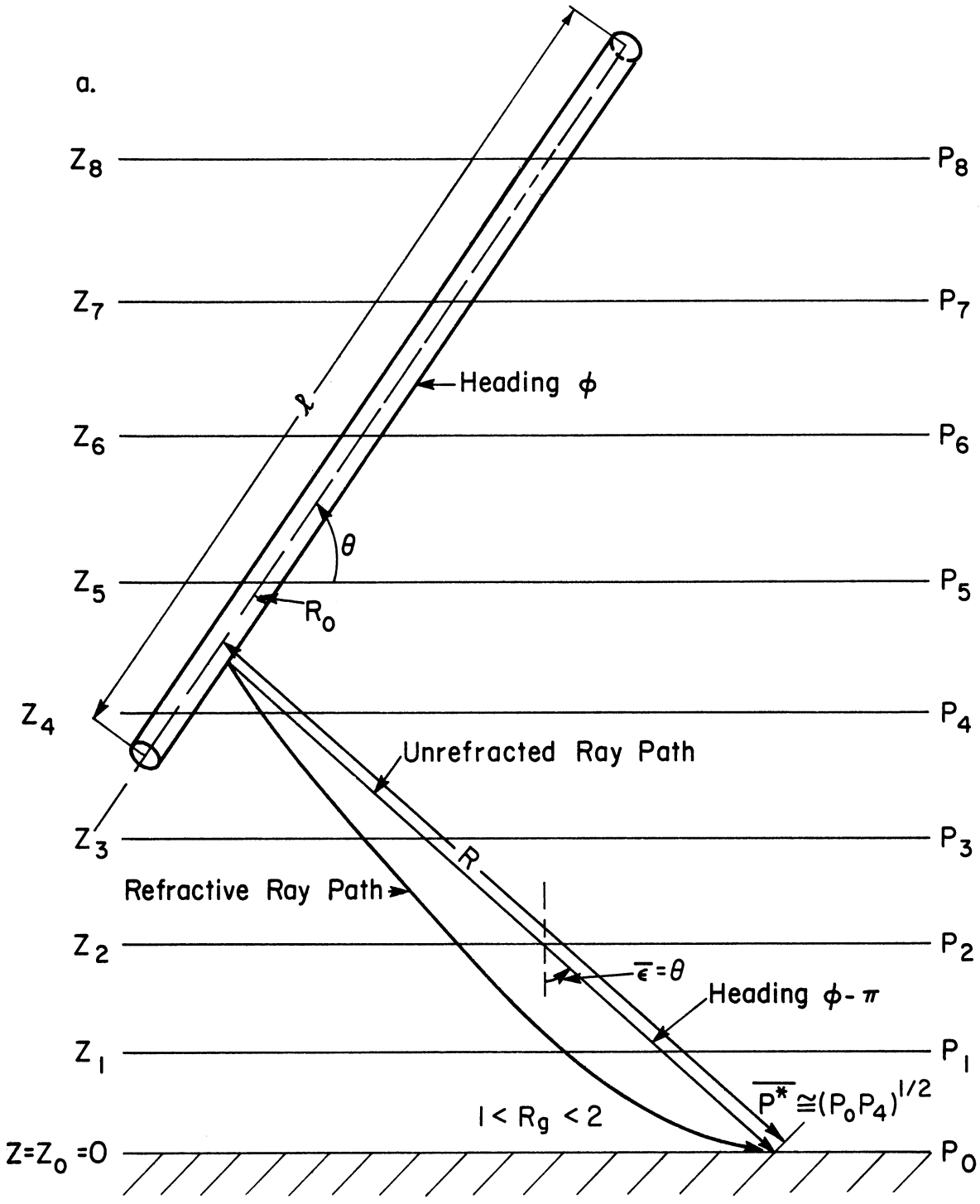


Figure 100a. Source, observer geometry for a horizontally stratified atmosphere in the entry plane.

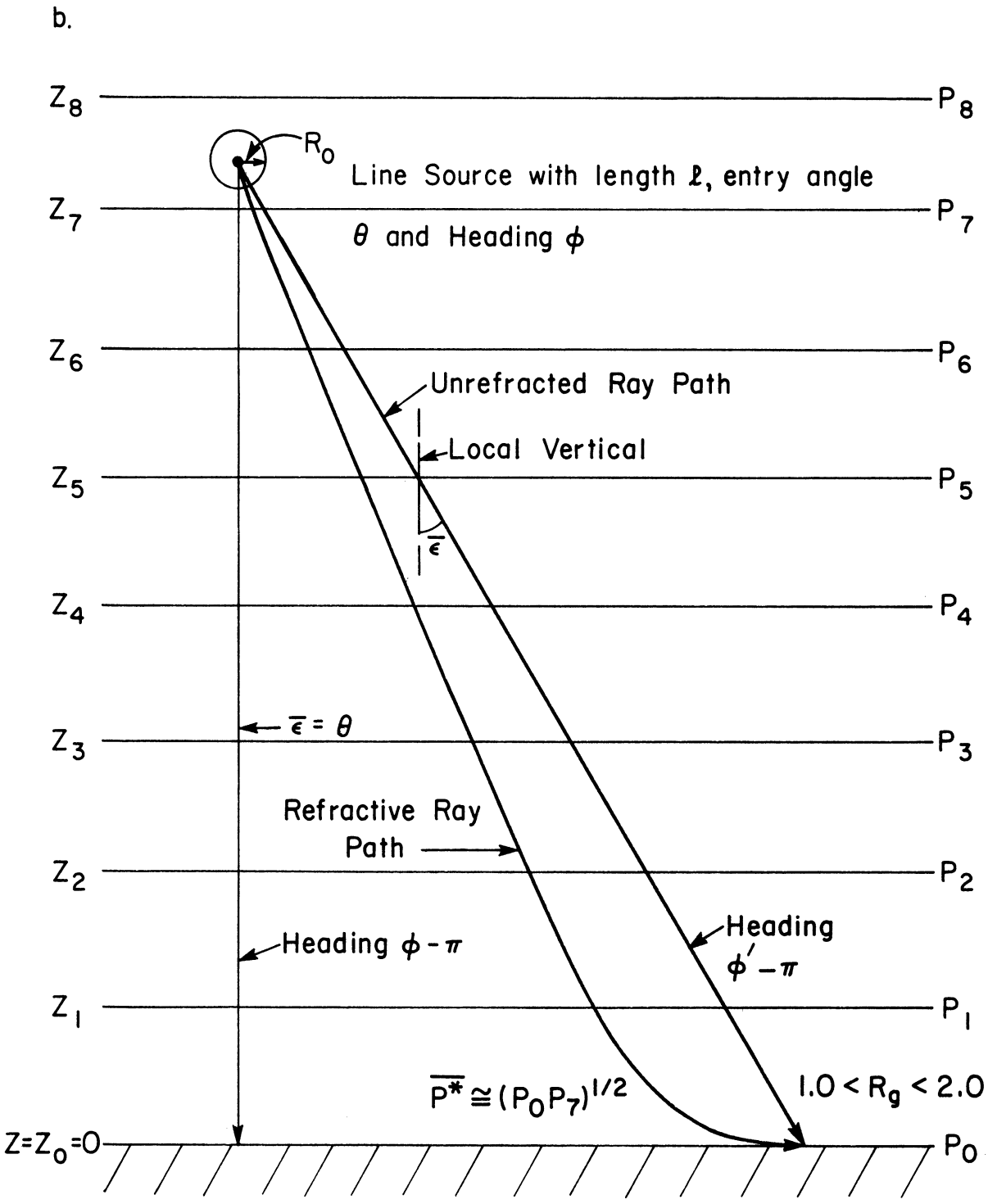


Figure 100b. Source, observer geometry for a horizontally stratified atmosphere out of the entry plane.

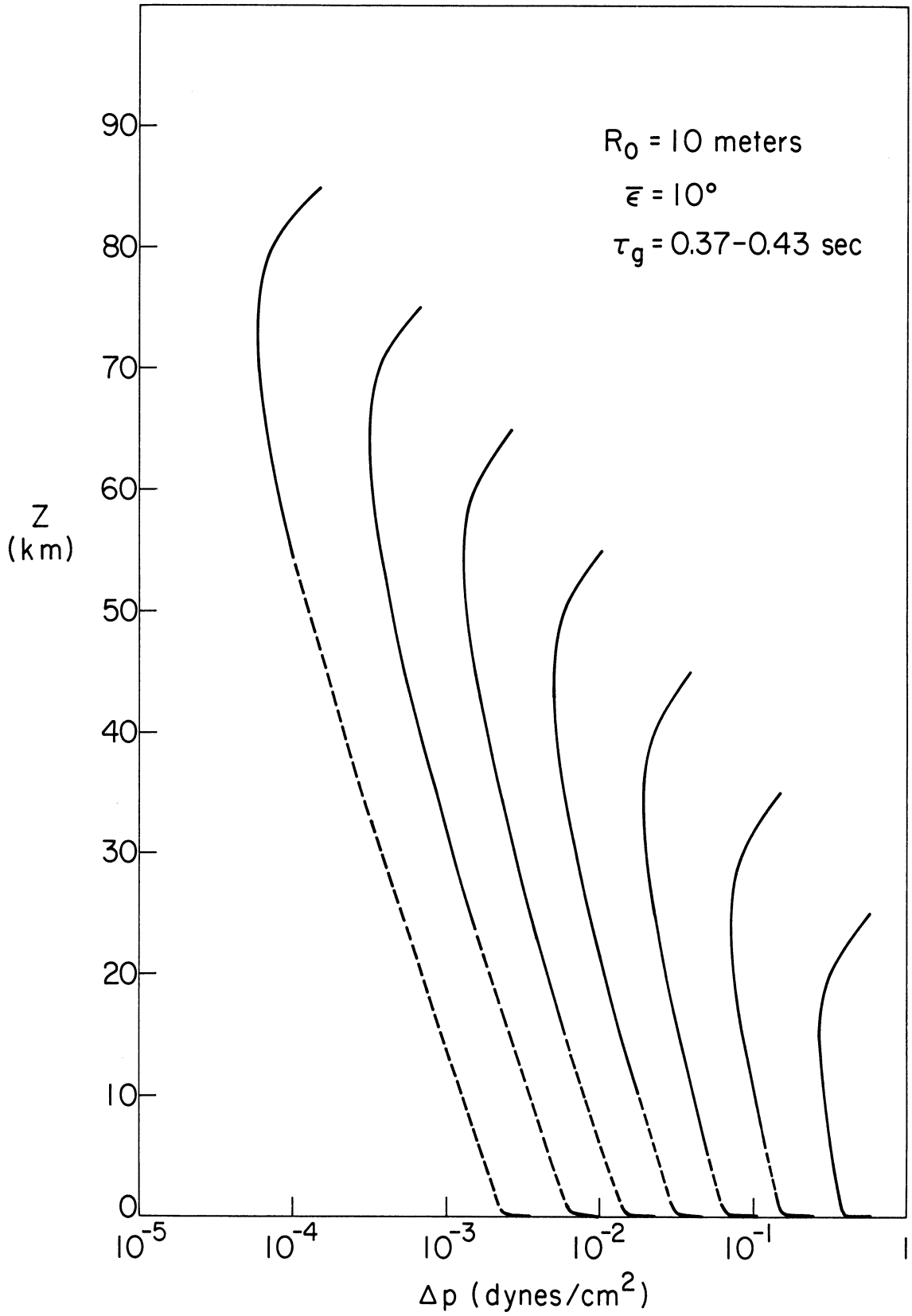


Figure 101. Predicted overpressure attenuation as a function of altitude for the family of source altitudes indicated. Solid portion represents propagation as a weak shock wave; dashed portion represents propagation as a linear acoustic wave; $R_o$= 10m, $\bar{\epsilon}$=10°.

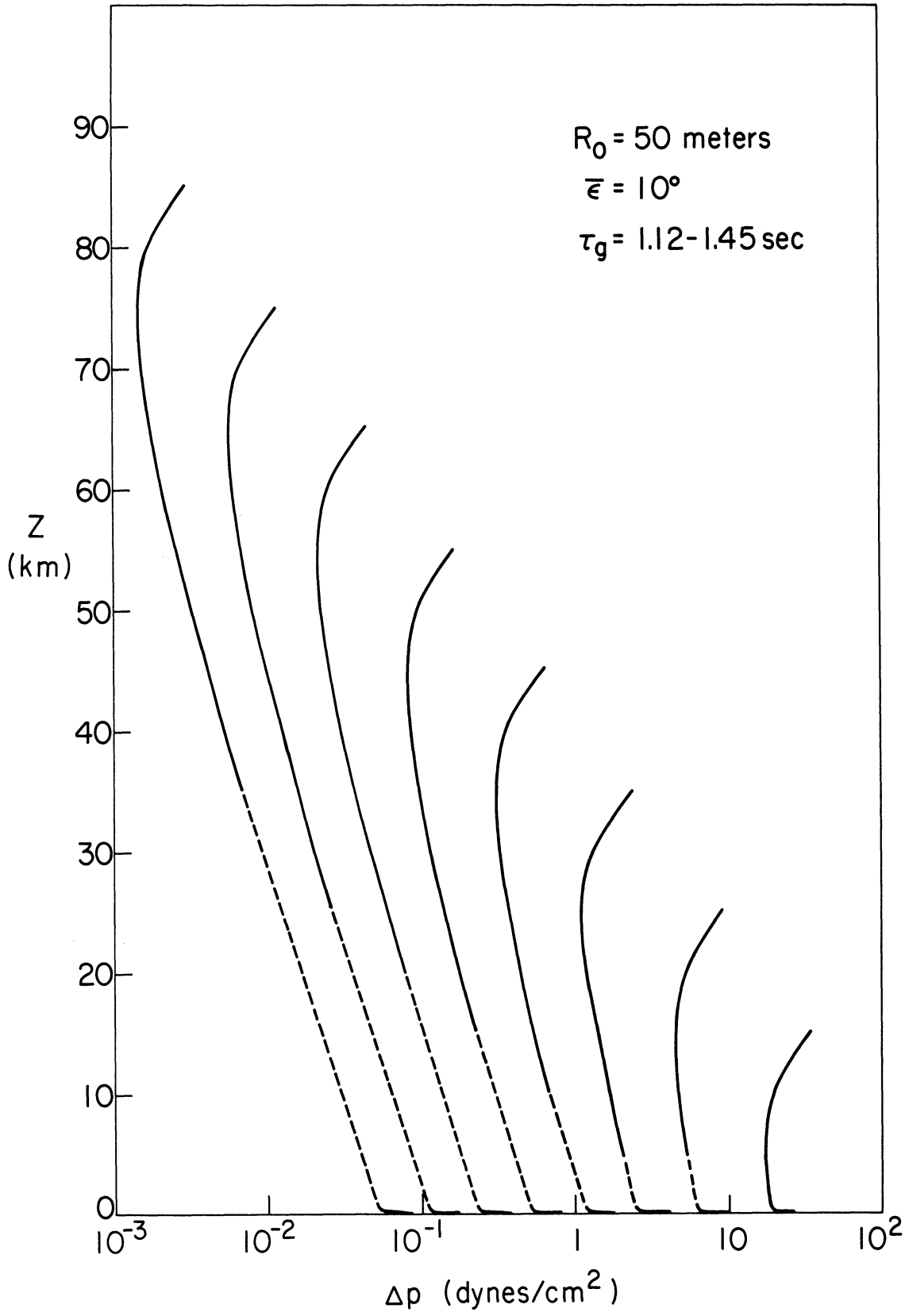


Figure 102. Predicted overpressure attenuation as a function of altitude for the family of source altitudes indicated. Solid portion represents propagation as a weak shock wave; dashed portion represents propagation as a linear acoustic wave; $R_o$= 50m, $\bar{\epsilon}$ = 10°.

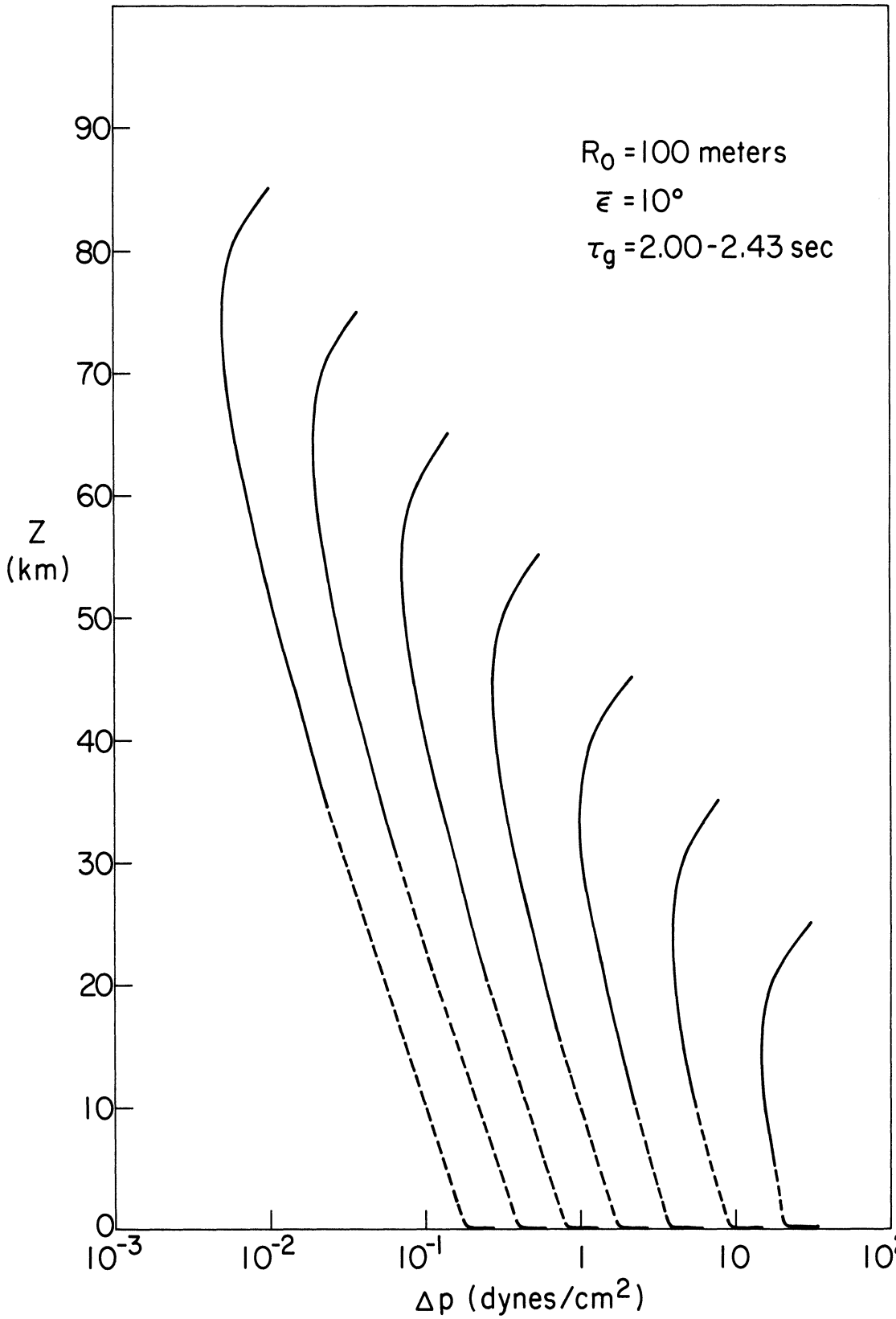


Figure 103. Predicted overpressure attenuation as a function of altitude for the family of source altitudes indicated. Solid portion represents propagation as a weak shock wave; dashed portion represents propagation as a linear acoustic wave; $R_o$= 100m, $\bar{\epsilon} = 10^o$.

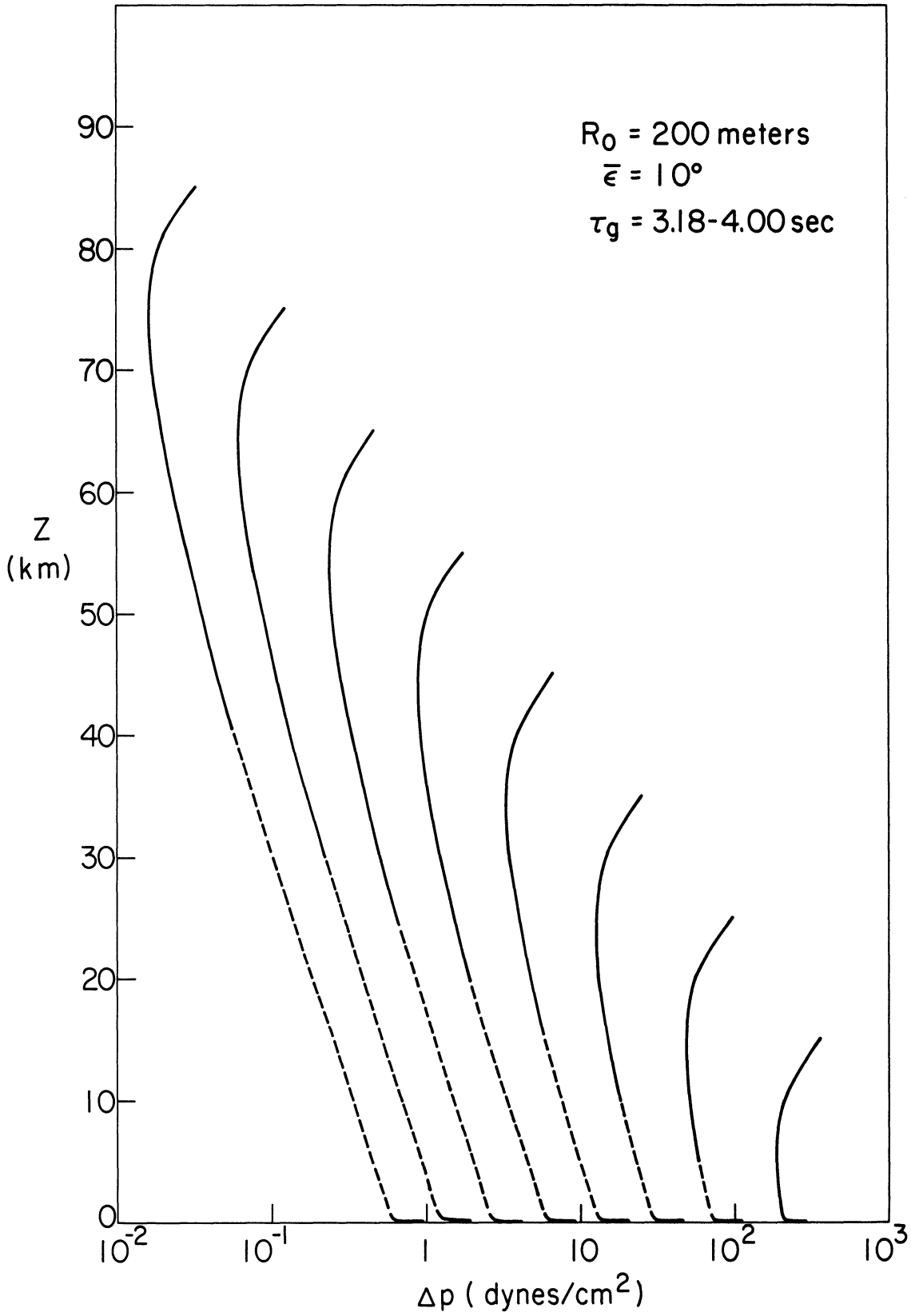


Figure 104. Predicted overpressure attenuation as a function of altitude for the family of source altitudes indicated. Solid portion represents propagation as a weak shock wave; dashed portion represents propagation as a linear acoustic wave; $R_o$= 200m, $\bar{\epsilon}$ = 10°.

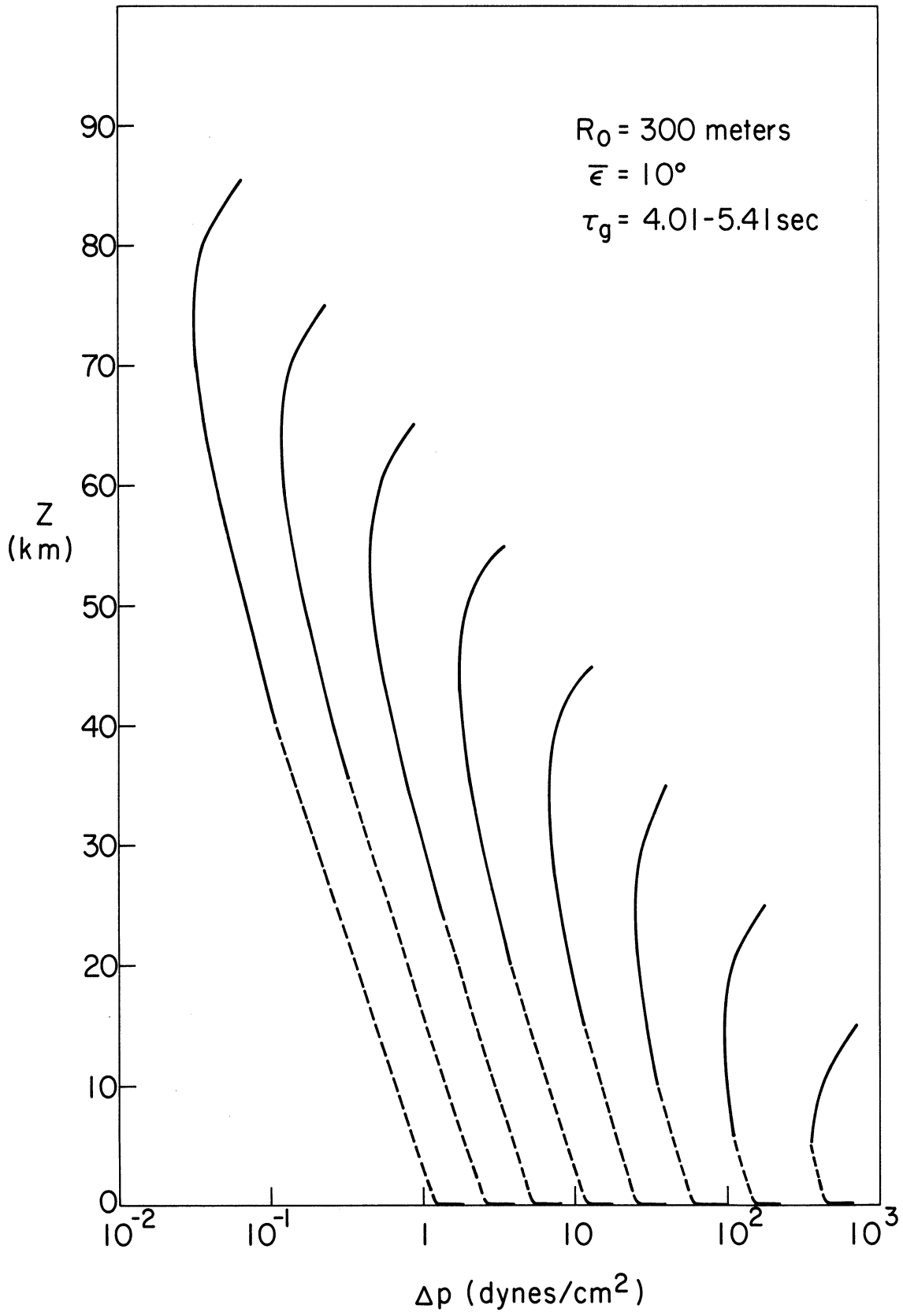


Figure 105. Predicted overpressure attenuation as a function of altitude for the family of source altitudes indicated. Solid portion represents propagation as a weak shock wave; dashed portion represents propagation as a linear acoustic wave; $R_o$= 300m, $\bar{\epsilon} = 10^o$.

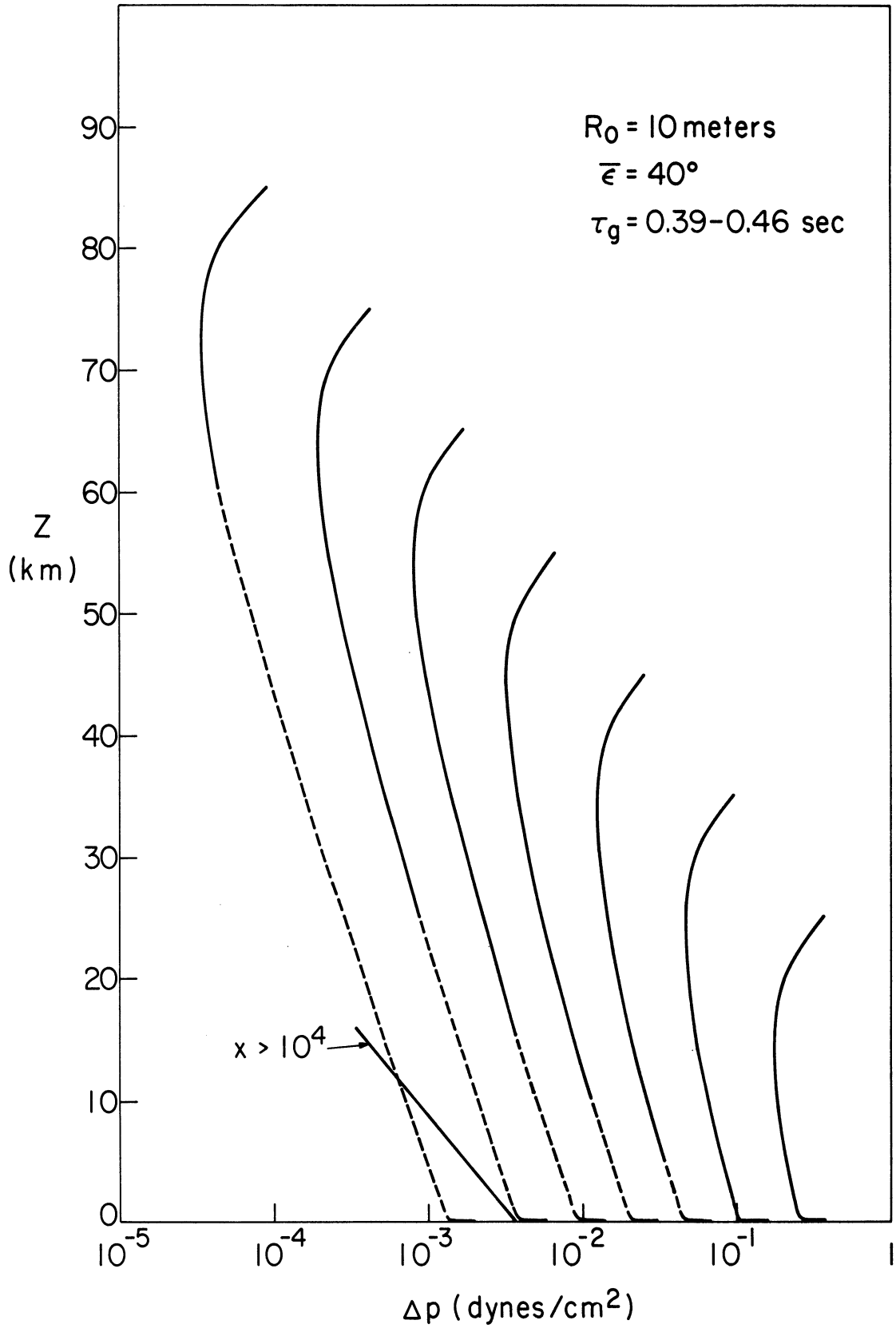


Figure 106. Predicted overpressure attenuation as a function of altitude for the family of source altitudes indicated. Solid portion represents propagation as a weak shock wave; dashed portion represents propagation as a linear acoustic wave; $R_0$= 10m, $\bar{\epsilon}$=40°.

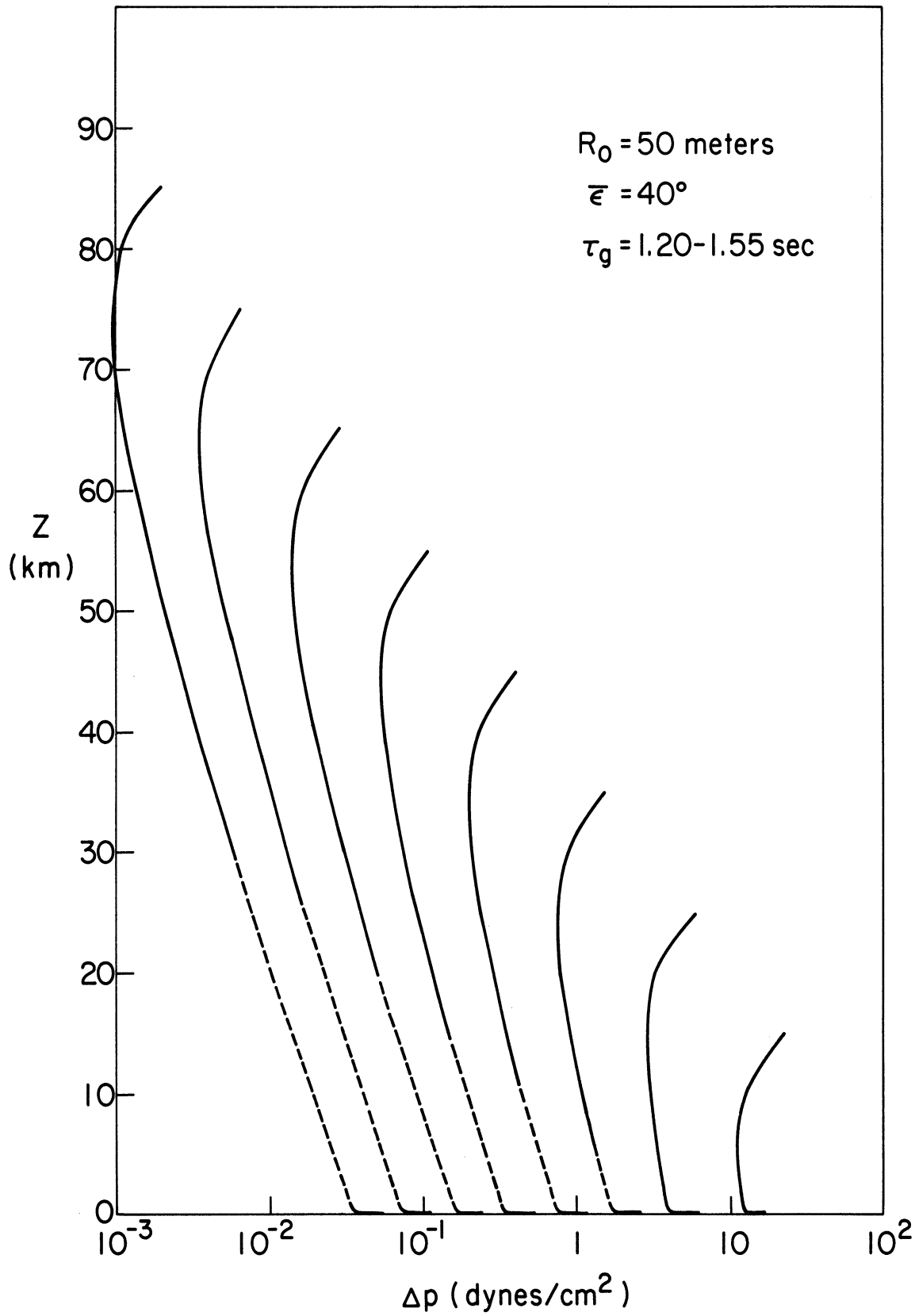


Figure 107. Predicted overpressure attenuation as a function of altitude for the family of source altitudes indicated. Solid portion represents propagation as a weak shock wave; dashed portion represents propagation as a linear acoustic wave; $R_0$= 50m, $\bar{\epsilon}$ = 40°.

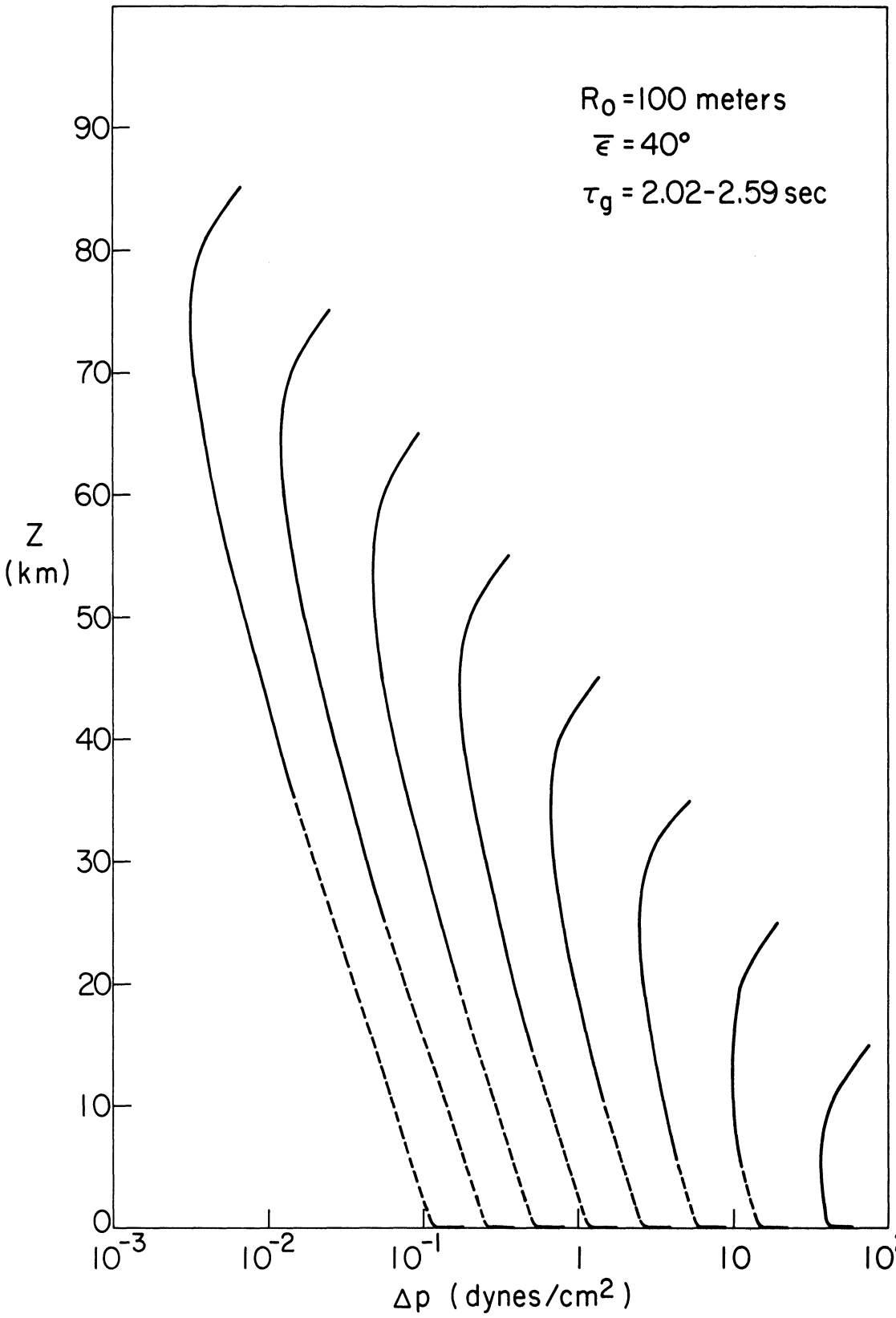


Figure 108. Predicted overpressure attenuation as a function of altitude for the family of source altitudes indicated. Solid portion represents propagation as a weak shock wave; dashed portion represents propagation as a linear acoustic wave; $R_O$= 100m, $\bar{\epsilon} = 40^o$.

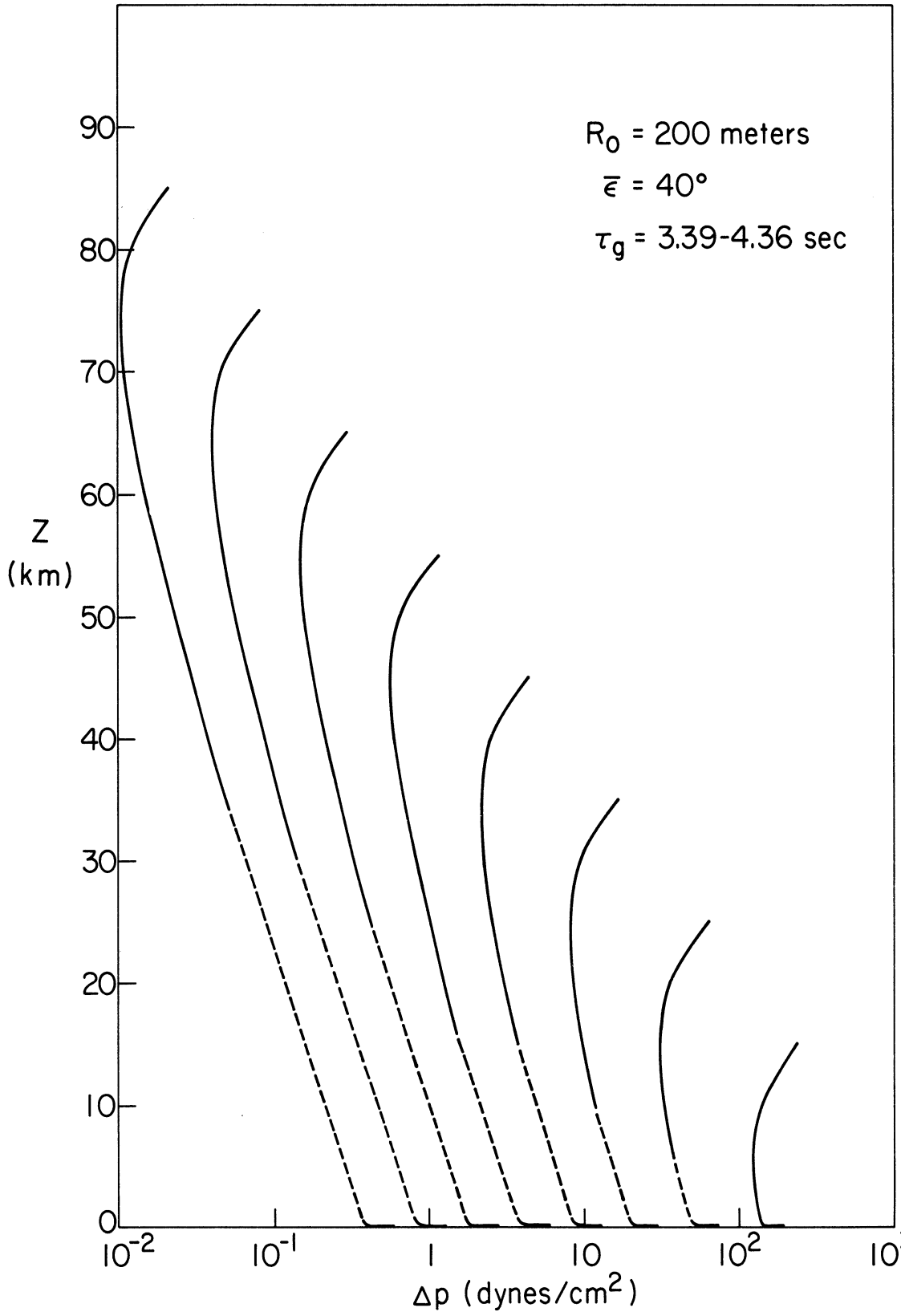


Figure 109. Predicted overpressure attenuation as a function of altitude for the family of source altitudes indicated. Solid portion represents propagation as a weak shock wave; dashed portion represents propagation as a linear acoustic wave; $R_o$= 200m, $\bar{\epsilon}$ =40°.

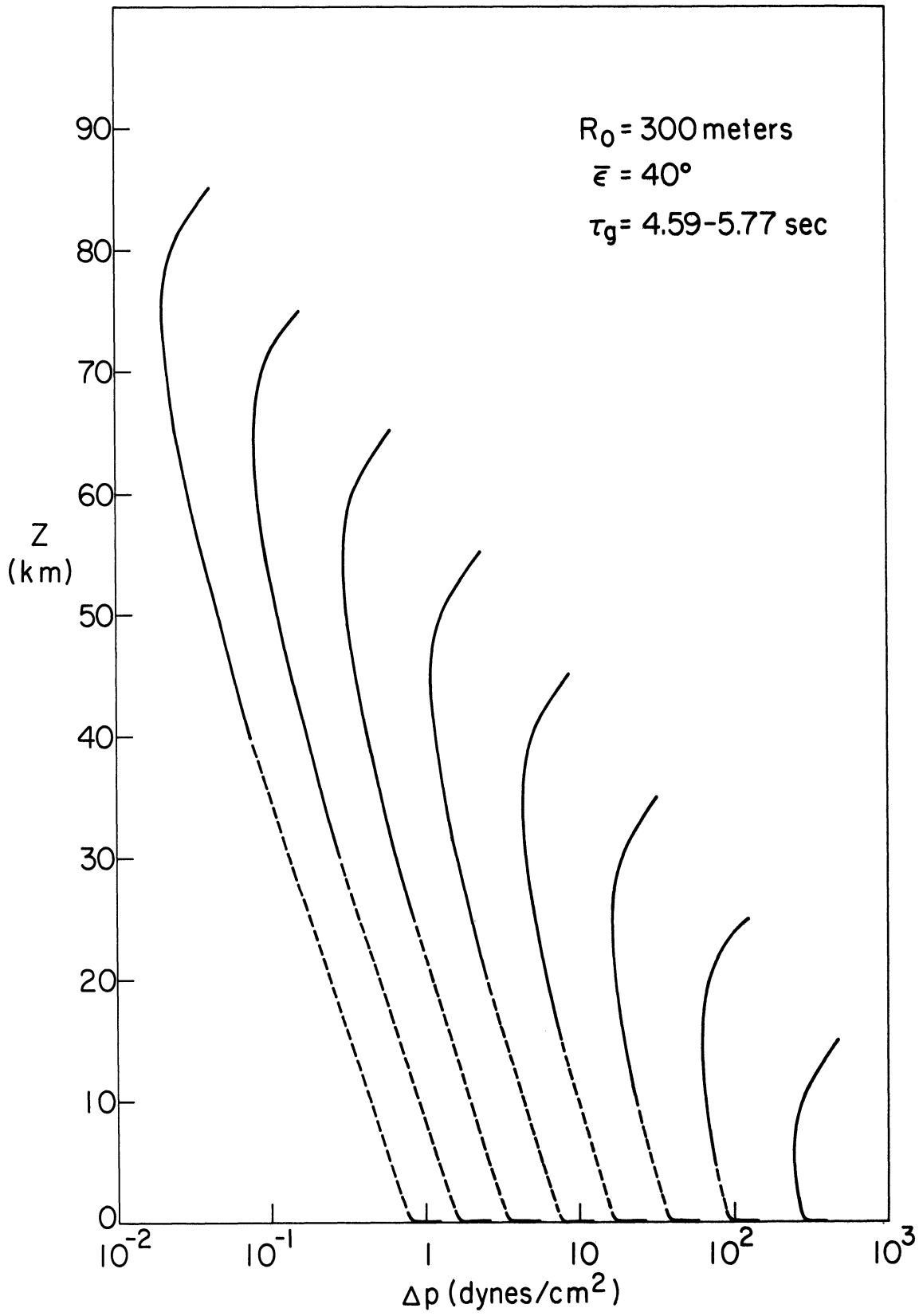


Figure 110. Predicted overpressure attenuation as a function of altitude for the family of source altitudes indicated. Solid portion represents propagation as a weak shock wave; dashed portion represents propagation as a linear acoustic wave; $R_0$ = 300m, $\bar{\epsilon} = 40^0$.

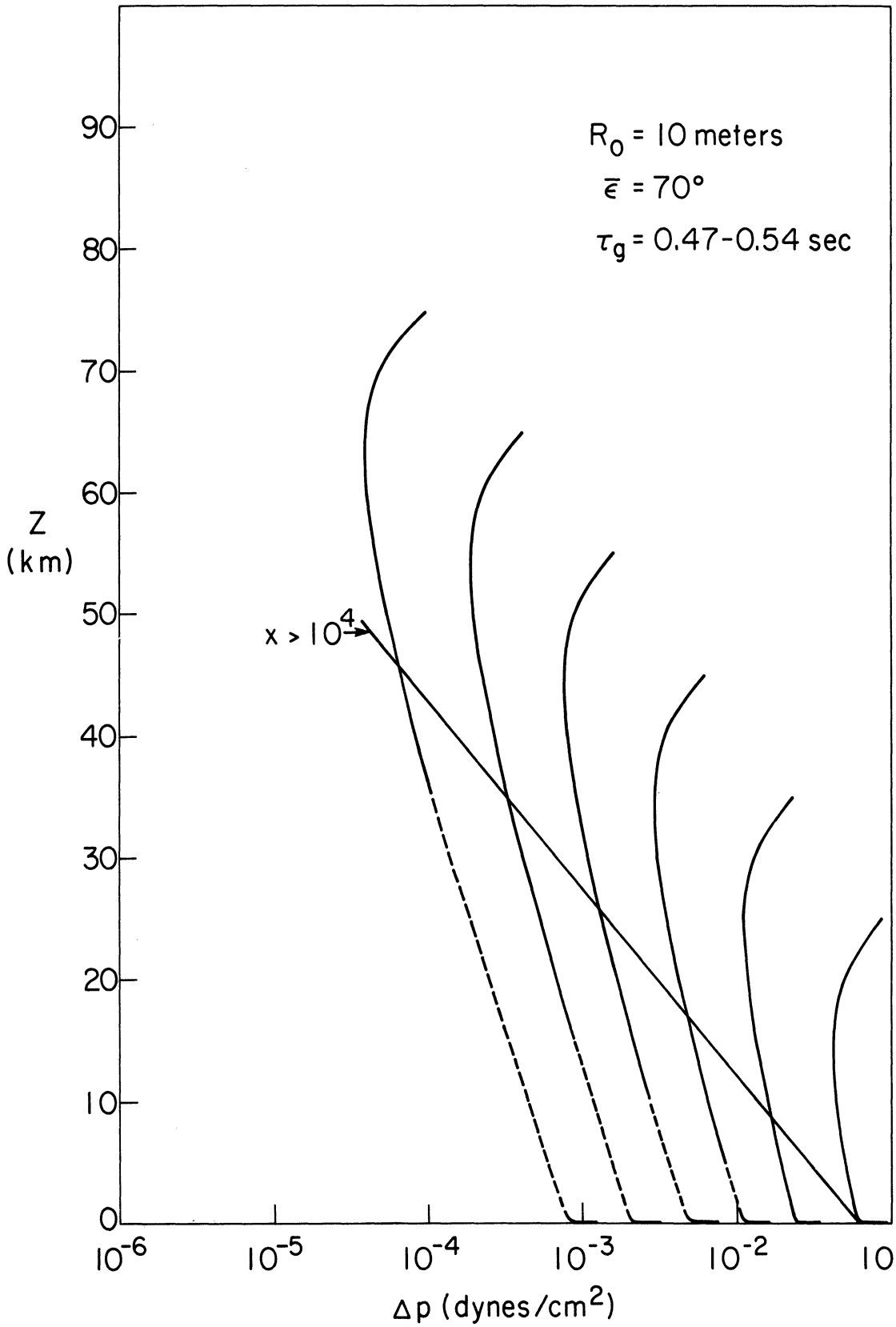


Figure 111. Predicted overpressure attenuation as a function of altitude for the family of source altitudes indicated. Solid portion represents propagation as a weak shock wave; dashed portion represents propagation as a linear acoustic wave; $R_0$= 10m, $\bar{\epsilon}$= 70°.

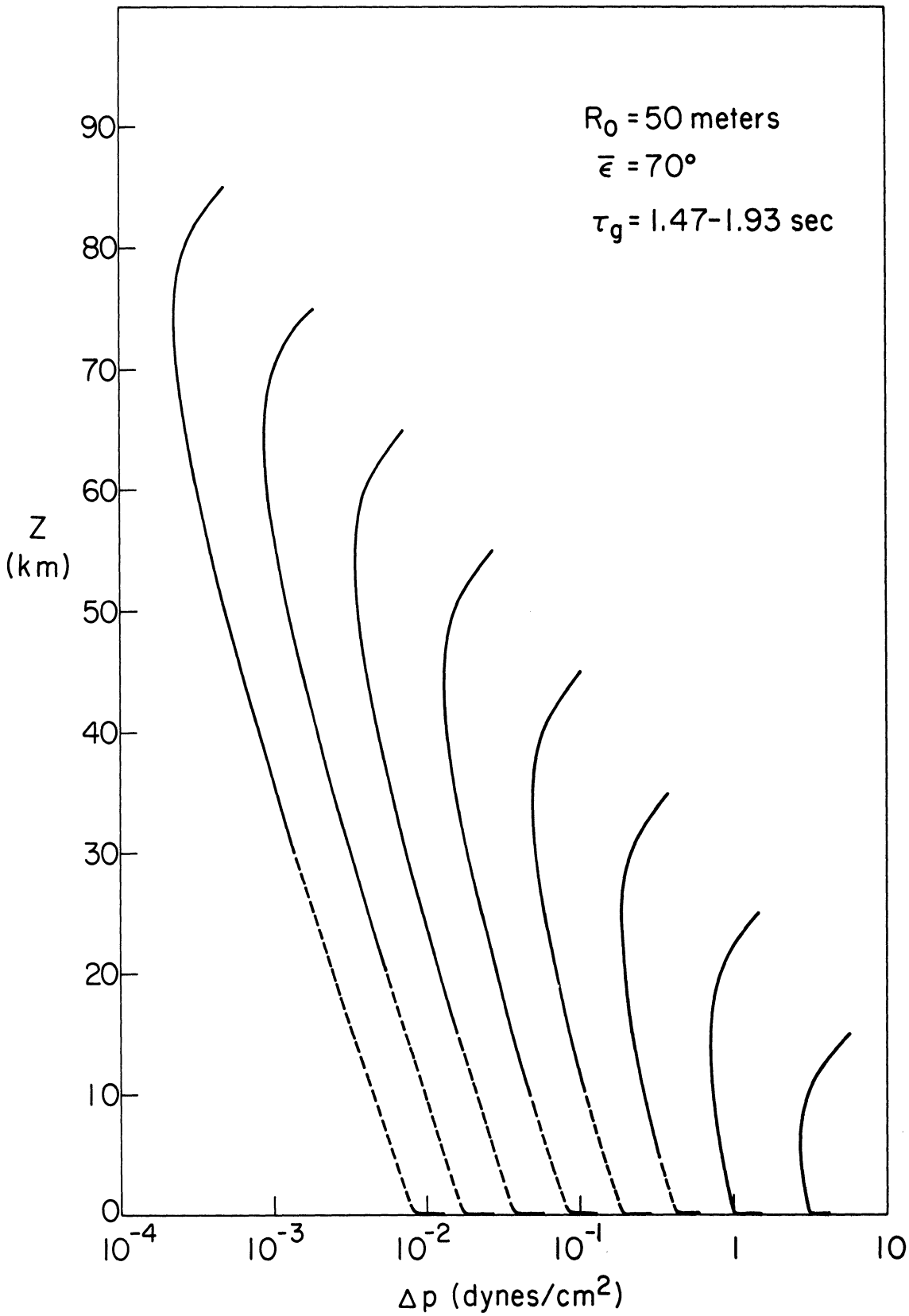


Figure 112. Predicted overpressure attenuation as a function of altitude for the family of source altitudes indicated. Solid portion represents propagation as a weak shock wave; dashed portion represents propagation as a linear acoustic wave; $R_o$= 50m, $\bar{\epsilon}$= 70°.

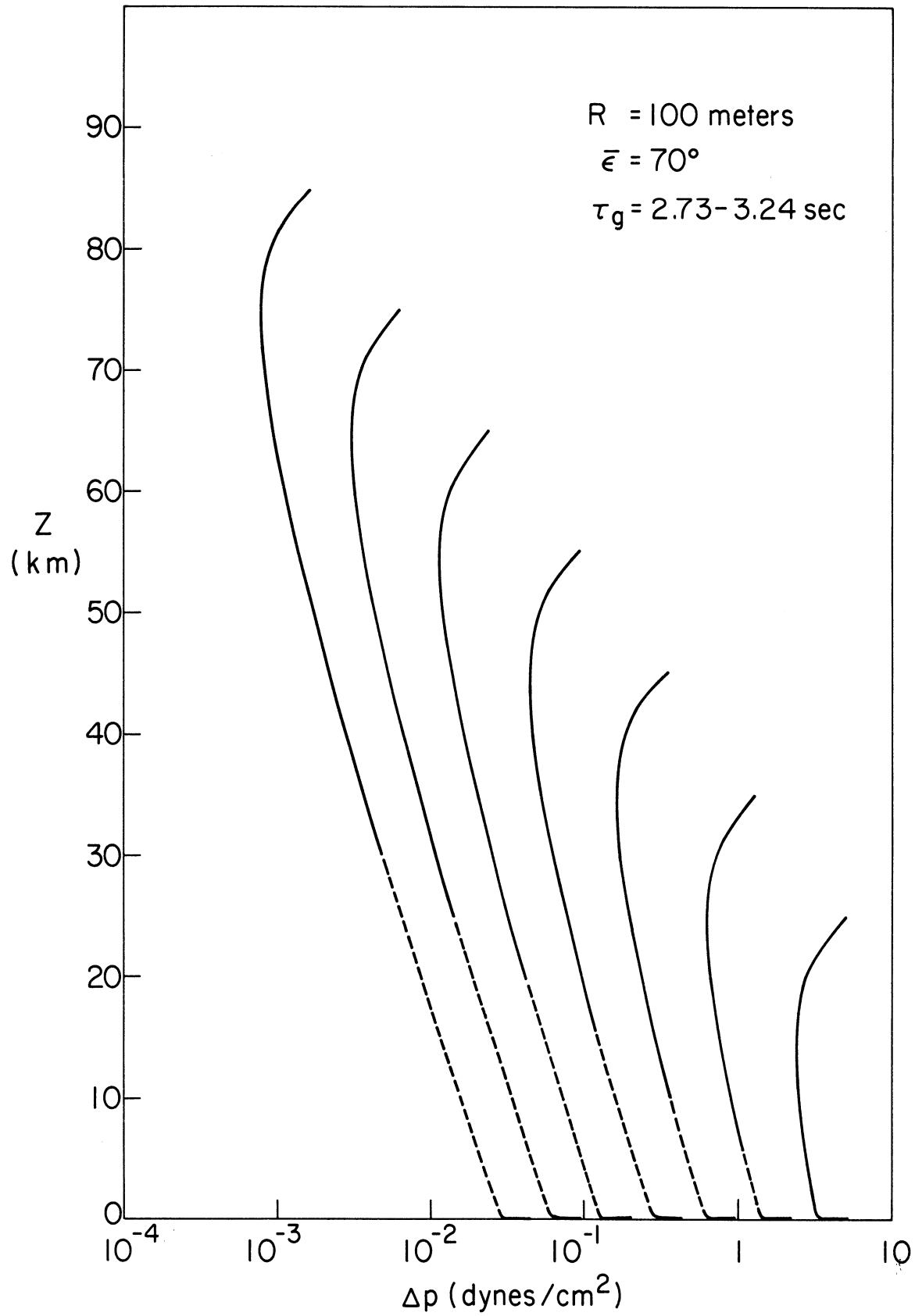


Figure 113. Predicted overpressure attenuation as a function of altitude for the family of source altitudes indicated. Solid portion represents propagation as a weak shock wave; dashed portion represents propagation as a linear acoustic wave; $R_o$= 100m, $\bar{\epsilon}$= 70°.

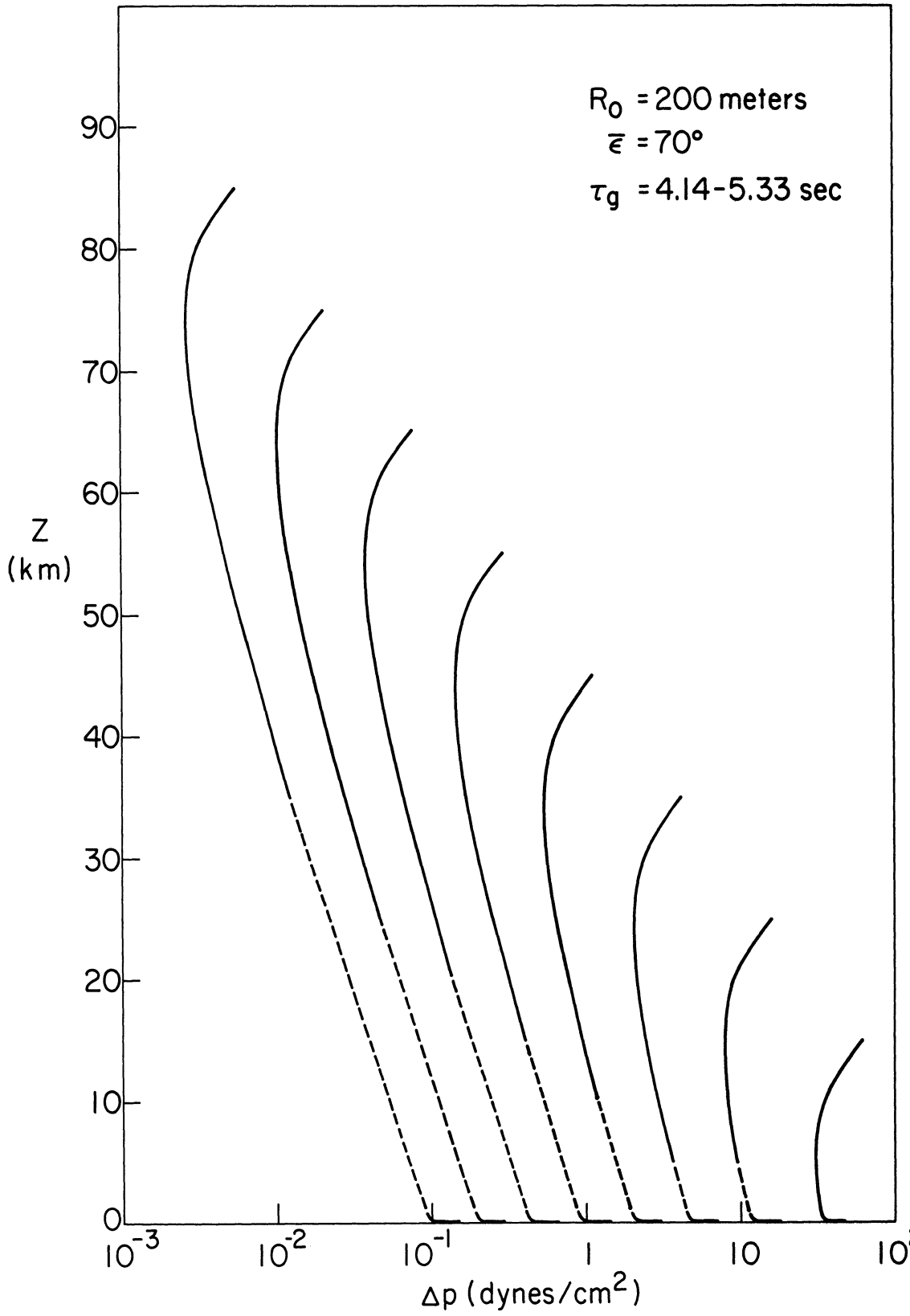


Figure 114. Predicted overpressure attenuation as a function of altitude for the family of source altitudes indicated. Solid portion represents propagation as a weak shock wave; dashed portion represents propagation as a linear acoustic wave; $R_o$= 200m, $\bar{\epsilon}$ = 70°.

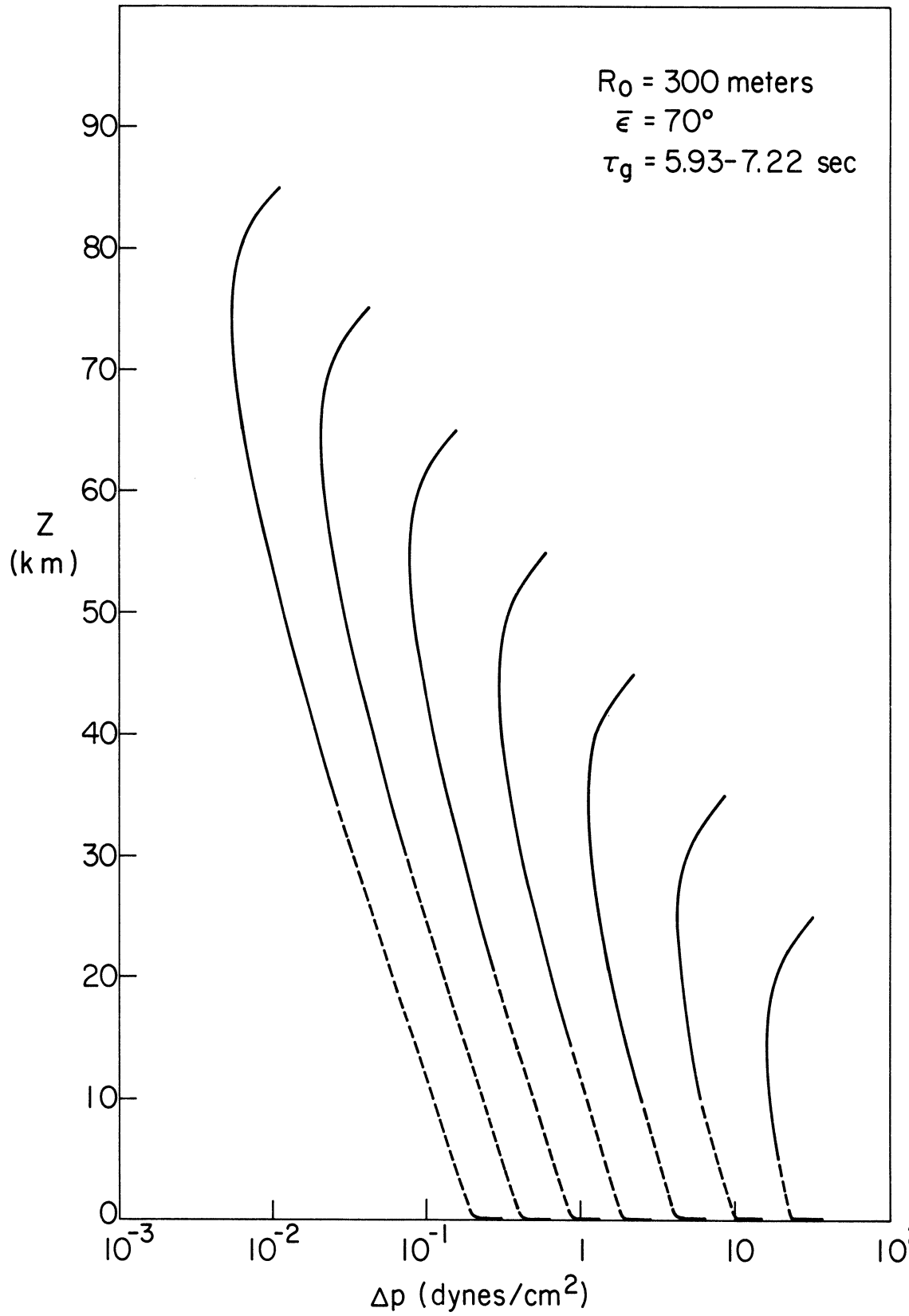


Figure 115. Predicted overpressure attenuation as a function of altitude for the family of source altitudes indicated. Solid portion represents propagation as a weak shock wave; dashed portion represents propagation as a linear acoustic wave; $R_o$= 300m, $\bar{\epsilon}$ = 70°.

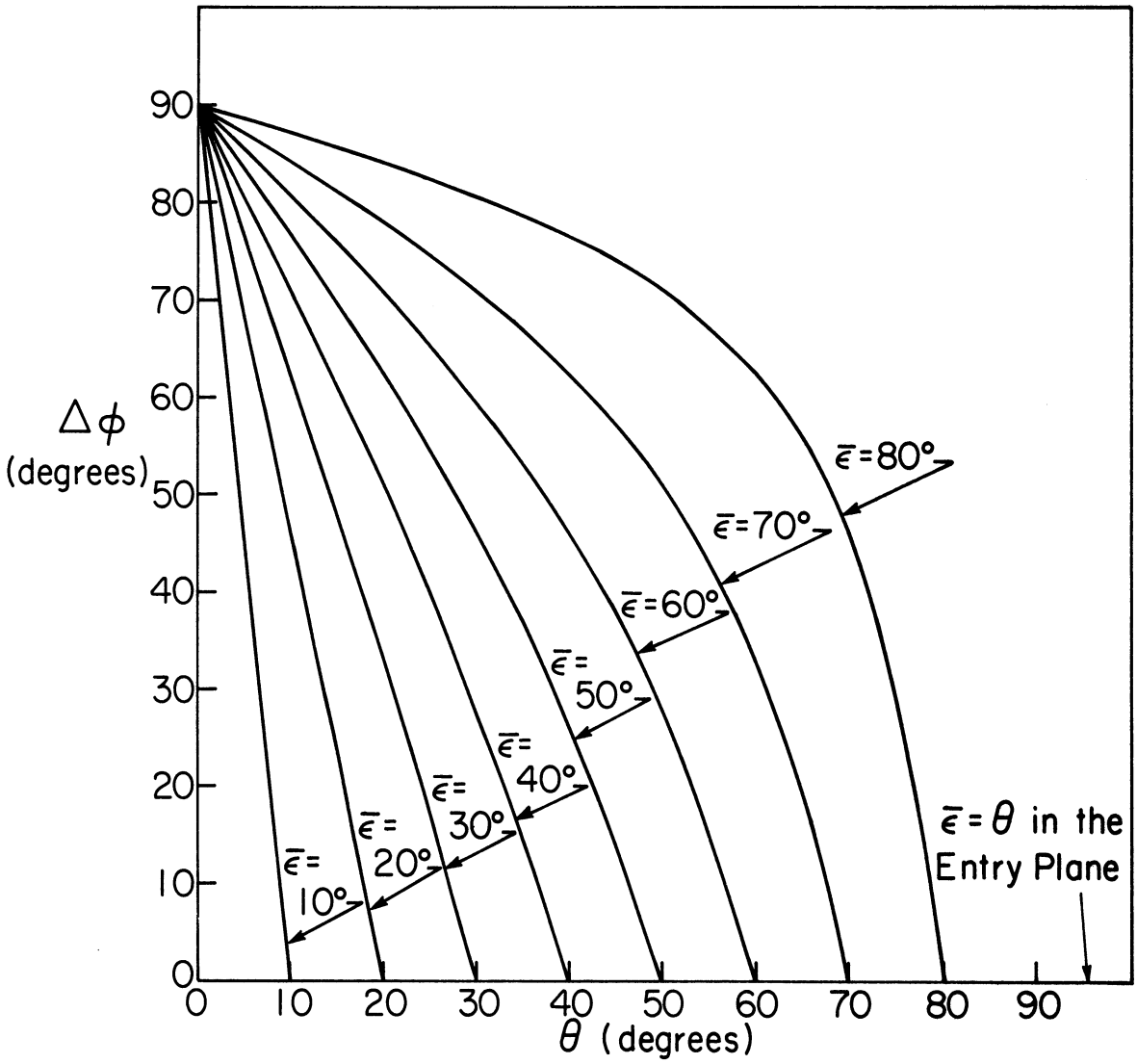


Figure 116. Zenith angle of the ray as a function of the azimuth interval outside of the entry plane and of the entry elevation angle of the meteor.

TABLE 4

Altitude Regions of Interest for the Effective Meteor Model

A. Dynamical Bow Shock Generation Possibilities (i.e., Ma $\geq$ 1 and Kn (or $\overline{Kn}$) $\lesssim$ 0.05)

| $r_{mE}$ (cm) | $\Theta$ (degrees) | $V_E$ (km/sec) | *z (km) | January $z_{ni}$ (km) | July $z_{ni}$ (km) |
|---|---|---|---|---|---|
| 5.0 | 70 | 11.2 | 83 / 15-8 \ 39-32 | 78 / 15-8 \ 35-29 | 80 / 16-9 \ 36-30 |
| 5.0 | 40 | 11.2 | 83 / 17-10 \ 42-35 | 78 / 17-10 \ 38-32 | 80 / 18-11 \ 39-33 |
| 5.0 | 10 | 11.2 | 83 / 28-21 \ 52-45 | 78 / 26-20 \ 47-40 | 80 / 26-21 \ 49-42 |
| 5.0 | 70 | 30.0 | 83 / 38-6 \ 62-30 | 78 / 34-7 \ 57-27 | 80 / 35-6 \ 60-28 |
| 5.0 | 40 | 30.0 | 83 / 40-8 \ 65-33 | 78 / 36-8 \ 61-30 | 80 / 37-9 \ 63-31 |
| 5.0 | 10 | 30.0 | 83 / 50-18 \ [27]-43 ** | 78 / 45-17 \ 25 -38 | 80 / 47-18 \ 26 -40 |
| 50.0 | 70 | 11.2 | 100 / 0 \ 21-14 | 92 / 0 \ 21-13 | 92 / 0 \ 21-15 |
| 50.0 | 40 | 11.2 | 100 / 0 \ 24-17 | 92 / 0 \ 22-17 | 92 / 0 \ 23-18 |
| 50.0 | 10 | 11.2 | 100 / 11-4 \ 35-38 | 92 / 11-5 \ 32-26 | 92 / 12-4 \ 33-26 |
| 50.0 | 70 | 30.0 | 100 / 19-0 \ 44-12 | 92 / 18-0 \ 39-12 | 92 / 19-0 \ 41-13 |
| 50.0 | 40 | 30.0 | 100 / 23-0 \ 47-16 | 92 / 21-0 \ 42-17 | 92 / 22-0 \ 44-17 |
| 50.0 | 10 | 30.0 | 100 / 32-1 \ 57-26 | 92 / 29-1 \ 52-25 | 92 / 30-1 \ 55-25 |

* Within each altitude grouping the following convention was used:

[Altitude for Kn $\lesssim$ 0.05 to Altitude for $\overline{Kn}$ $\lesssim$ 0.05] / [Altitude for Ma $\geq$ 1, $\sigma = 5 \cdot 10^{-12}$ sec$^2$/cm$^2$ to $\sigma = 0$, $\rho_{mE} = 7.7$ g/cm$^3$] \ [Altitude for Ma $\geq$ 1, $\sigma = 5 \cdot 10^{-12}$ sec$^2$/cm$^2$ to $\sigma = 0$, $\rho_{mE} = 0.30$ g/cm$^3$]

** Present Knudsen number calculations indicate that the upper limit ( $\rho_{mE} = 0.30$ g/cm$^3$, $\sigma = 5 \cdot 10^{-12}$ sec$^2$/cm$^2$) does not satisfy $\overline{Kn} \lesssim 0.05$ with Ma $\geq$ 1. This comment refers to the number in the brackets above. The altitude range shown; 83-43, represents the maximum penetration possible (for $\sigma = 0$, $\rho_{mE} = 0.30$ g/cm$^3$).

NOTE: All z and $z_{ni}$ values are given to the nearest kilometer.

TABLE 4 (continued)

B. Applicability of the Blast Wave Analogy to Hypersonic Flight (for meteors with $V >> C$, $V(z) \simeq$ constant, i.e., $V(z) = V_E - 0.05\ V_E$, and $Kn$(or $\overline{Kn}$) $\lesssim 0.05$)

| $r_{mE}$ (cm) | $\Theta$ (degrees) | $V_E$ (km/sec) | *z (km) | January $z_{ni}$ (km) | July $z_{ni}$ (km) |
|---|---|---|---|---|---|
| 5.0 | 70 | 11.2 | 83 / 40 / 64 | 78 / 36 / 60 | 80 / 37 / 62 |
| 5.0 | 40 | 11.2 | 83 / 43 / 67 | 78 / 38 / 63 | 80 / 40 / 65 |
| 5.0 | 10 | 11.2 | 83 / 53 / 77 | 78 / 48 / 73 | 80 / 51 / 76 |
| 5.0 | 70 | 30.0 | 83 / 43-40 / 67-64 | 78 / 38-36 / 63-60 | 80 / 40-37 / 65-62 |
| 5.0 | 40 | 30.0 | 83 / 46-43 / 70-67 | 78 / 41-38 / 66-63 | 80 / 43-40 / 69-65 |
| 5.0 | 10 | 30.0 | 83 / 56-53 / [27]-77 ** | 78 / 51-48 / 25 -73 | 80 / 54-51 / 26 -76 |
| 50.0 | 70 | 11.2 | 100 / 22 / 47 | 92 / 21 / 42 | 92 / 22 / 44 |
| 50.0 | 40 | 11.2 | 100 / 25 / 50 | 92 / 23 / 45 | 92 / 24 / 47 |
| 50.0 | 10 | 11.2 | 100 / 35 / 60 | 92 / 32 / 55 | 92 / 33 / 58 |
| 50.0 | 70 | 30.0 | 100 / 26-23 / 50-47 | 92 / 24-21 / 45-42 | 92 / 25-22 / 47-44 |
| 50.0 | 40 | 30.0 | 100 / 29-26 / 53-50 | 92 / 26-24 / 48-45 | 92 / 27-25 / 51-47 |
| 50.0 | 10 | 30.0 | 100 / 39-36 / 63-60 | 92 / 35-33 / 59-55 | 92 / 36-34 / 61-58 |

* See Table 4 A.

** See Table 4 A.

NOTE: All z and $z_{ni}$ values given are to the nearest kilometer.

TABLE 5

Isothermal Model Atmosphere Data

| Altitude (km) | Pressure (dynes/cm$^2$) | Density (g/cm$^3$) | Mean Free Path (cm) |
|---|---|---|---|
| 0.000E 00 | 0.101E 07 | 0.140E-02 | 0.781E-05 |
| 0.100E 01 | 0.887E 06 | 0.122E-02 | 0.892E-05 |
| 0.200E 01 | 0.776E 06 | 0.107E-02 | 0.102E-04 |
| 0.300E 01 | 0.679E 06 | 0.938E-03 | 0.117E-04 |
| 0.400E 01 | 0.594E 06 | 0.821E-03 | 0.133E-04 |
| 0.500E 01 | 0.520E 06 | 0.719E-03 | 0.152E-04 |
| 0.600E 01 | 0.455E 06 | 0.629E-03 | 0.174E-04 |
| 0.700E 01 | 0.398E 06 | 0.550E-03 | 0.199E-04 |
| 0.800E 01 | 0.349E 06 | 0.482E-03 | 0.227E-04 |
| 0.900E 01 | 0.305E 06 | 0.422E-03 | 0.259E-04 |
| 0.100E 02 | 0.267E 06 | 0.369E-03 | 0.296E-04 |
| 0.110E 02 | 0.234E 06 | 0.323E-03 | 0.339E-04 |
| 0.120E 02 | 0.205E 06 | 0.283E-03 | 0.387E-04 |
| 0.130E 02 | 0.179E 06 | 0.247E-03 | 0.442E-04 |
| 0.140E 02 | 0.157E 06 | 0.216E-03 | 0.505E-04 |
| 0.150E 02 | 0.137E 06 | 0.189E-03 | 0.577E-04 |
| 0.160E 02 | 0.120E 06 | 0.166E-03 | 0.659E-04 |
| 0.170E 02 | 0.105E 06 | 0.145E-03 | 0.753E-04 |
| 0.180E 02 | 0.919E 05 | 0.127E-03 | 0.861E-04 |
| 0.190E 02 | 0.804E 05 | 0.111E-03 | 0.984E-04 |
| 0.200E 02 | 0.704E 05 | 0.973E-04 | 0.112E-03 |
| 0.210E 02 | 0.616E 05 | 0.851E-04 | 0.128E-03 |
| 0.220E 02 | 0.539E 05 | 0.745E-04 | 0.147E-03 |
| 0.230E 02 | 0.472E 05 | 0.652E-04 | 0.168E-03 |
| 0.240E 02 | 0.413E 05 | 0.571E-04 | 0.192E-03 |
| 0.250E 02 | 0.361E 05 | 0.499E-04 | 0.219E-03 |
| 0.260E 02 | 0.316E 05 | 0.437E-04 | 0.250E-03 |
| 0.270E 02 | 0.277E 05 | 0.382E-04 | 0.286E-03 |
| 0.280E 02 | 0.242E 05 | 0.335E-04 | 0.327E-03 |
| 0.290E 02 | 0.212E 05 | 0.293E-04 | 0.373E-03 |
| 0.300E 02 | 0.186E 05 | 0.256E-04 | 0.426E-03 |
| 0.310E 02 | 0.162E 05 | 0.224E-04 | 0.487E-03 |
| 0.320E 02 | 0.142E 05 | 0.196E-04 | 0.557E-03 |
| 0.330E 02 | 0.124E 05 | 0.172E-04 | 0.636E-03 |
| 0.340E 02 | 0.109E 05 | 0.150E-04 | 0.727E-03 |
| 0.350E 02 | 0.953E 04 | 0.132E-04 | 0.831E-03 |
| 0.360E 02 | 0.834E 04 | 0.115E-04 | 0.949E-03 |
| 0.370E 02 | 0.730E 04 | 0.101E-04 | 0.108E-02 |
| 0.380E 02 | 0.639E 04 | 0.882E-05 | 0.124E-02 |
| 0.390E 02 | 0.559E 04 | 0.772E-05 | 0.142E-02 |
| 0.400E 02 | 0.489E 04 | 0.676E-05 | 0.162E-02 |
| 0.410E 02 | 0.428E 04 | 0.591E-05 | 0.185E-02 |
| 0.420E 02 | 0.375E 04 | 0.518E-05 | 0.211E-02 |
| 0.430E 02 | 0.328E 04 | 0.591E-05 | 0.241E-02 |
| 0.440E 02 | 0.287E 04 | 0.453E-05 | 0.276E-02 |
| 0.450E 02 | 0.251E 04 | 0.347E-05 | 0.315E-02 |

TABLE 5
(con't.)

| | | | |
|---|---|---|---|
| 0.460E 02 | 0.220E 04 | 0.304E-05 | 0.315E-02 |
| 0.470E 02 | 0.192E 04 | 0.266E-05 | 0.411E-02 |
| 0.480E 02 | 0.168E 04 | 0.233E-05 | 0.470E-02 |
| 0.490E 02 | 0.147E 04 | 0.204E-05 | 0.537E-02 |
| 0.500E 02 | 0.129E 04 | 0.178E-05 | 0.614E-02 |
| 0.510E 02 | 0.113E 04 | 0.156E-05 | 0.701E-02 |
| 0.520E 02 | 0.987E 03 | 0.136E-05 | 0.801E-02 |
| 0.530E 02 | 0.864E 03 | 0.119E-05 | 0.916E-02 |
| 0.540E 02 | 0.756E 03 | 0.104E-05 | 0.105E-01 |
| 0.550E 02 | 0.662E 03 | 0.915E-06 | 0.120E-01 |
| 0.560E 02 | 0.579E 03 | 0.800E-06 | 0.137E-01 |
| 0.570E 02 | 0.507E 03 | 0.700E-06 | 0.156E-01 |
| 0.580E 02 | 0.444E 03 | 0.613E-06 | 0.178E-01 |
| 0.590E 02 | 0.388E 03 | 0.537E-06 | 0.204E-01 |
| 0.600E 02 | 0.340E 03 | 0.470E-06 | 0.233E-01 |
| 0.610E 02 | 0.297E 03 | 0.411E-06 | 0.266E-01 |
| 0.620E 02 | 0.260E 03 | 0.360E-06 | 0.304E-01 |
| 0.630E 02 | 0.228E 03 | 0.315E-06 | 0.347E-01 |
| 0.640E 02 | 0.199E 03 | 0.275E-06 | 0.397E-01 |
| 0.650E 02 | 0.174E 03 | 0.241E-06 | 0.453E-01 |
| 0.660E 02 | 0.153E 03 | 0.211E-06 | 0.518E-01 |
| 0.670E 02 | 0.134E 03 | 0.185E-06 | 0.592E-01 |
| 0.680E 02 | 0.117E 03 | 0.162E-06 | 0.676E-01 |
| 0.690E 02 | 0.102E 03 | 0.141E-06 | 0.773E-01 |
| 0.700E 02 | 0.896E 02 | 0.124E-06 | 0.883E-01 |
| 0.710E 02 | 0.784E 02 | 0.108E-06 | 0.101E 00 |
| 0.720E 02 | 0.686E 02 | 0.948E-07 | 0.115E 00 |
| 0.730E 02 | 0.600E 02 | 0.830E-07 | 0.132E 00 |
| 0.740E 02 | 0.525E 02 | 0.726E-07 | 0.151E 00 |
| 0.750E 02 | 0.460E 02 | 0.635E-07 | 0.172E 00 |
| 0.760E 02 | 0.402E 02 | 0.556E-07 | 0.197E 00 |
| 0.770E 02 | 0.352E 02 | 0.487E-07 | 0.225E 00 |
| 0.780E 02 | 0.308E 02 | 0.426E-07 | 0.257E 00 |
| 0.790E 02 | 0.270E 02 | 0.373E-07 | 0.293E 00 |
| 0.800E 02 | 0.236E 02 | 0.326E-07 | 0.335E 00 |
| 0.810E 02 | 0.207E 02 | 0.286E-07 | 0.383E 00 |
| 0.820E 02 | 0.181E 02 | 0.250E-07 | 0.437E 00 |
| 0.830E 02 | 0.158E 02 | 0.219E-07 | 0.500E 00 |
| 0.840E 02 | 0.139E 02 | 0.191E-07 | 0.571E 00 |
| 0.850E 02 | 0.121E 02 | 0.168E-07 | 0.653E 00 |
| 0.860E 02 | 0.106E 02 | 0.147E-07 | 0.746E 00 |
| 0.870E 02 | 0.929E 01 | 0.128E-07 | 0.852E 00 |
| 0.880E 02 | 0.813E 01 | 0.112E-07 | 0.974E 00 |
| 0.890E 02 | 0.711E 01 | 0.983E-08 | 0.111E 00 |
| 0.900E 02 | 0.622E 01 | 0.860E-08 | 0.127E 01 |
| 0.910E 02 | 0.545E 01 | 0.753E-08 | 0.145E 01 |
| 0.920E 02 | 0.477E 01 | 0.659E-08 | 0.166E 01 |
| 0.930E 02 | 0.417E 01 | 0.576E-08 | 0.190E 01 |
| 0.940E 02 | 0.365E 01 | 0.505E-08 | 0.217E 01 |

TABLE 5
(con't.)

| | | | |
|---|---|---|---|
| 0.950E 02 | 0.320E 01 | 0.442E-08 | 0.248E 01 |
| 0.960E 02 | 0.280E 01 | 0.386E-08 | 0.283E 01 |
| 0.970E 02 | 0.245E 01 | 0.338E-08 | 0.323E 01 |
| 0.980E 02 | 0.214E 01 | 0.296E-08 | 0.369E 01 |
| 0.990E 02 | 0.187E 01 | 0.259E-08 | 0.422E 01 |
| 0.100E 03 | 0.164E 01 | 0.227E-08 | 0.482E 01 |
| 0.101E 03 | 0.144E 01 | 0.198E-08 | 0.551E 01 |
| 0.102E 03 | 0.126E 01 | 0.174E-08 | 0.630E 01 |
| 0.103E 03 | 0.110E 01 | 0.152E-08 | 0.719E 01 |
| 0.104E 03 | 0.962E 00 | 0.133E-08 | 0.822E 01 |
| 0.105E 03 | 0.842E 00 | 0.116E-08 | 0.939E 01 |
| 0.106E 03 | 0.737E 00 | 0.102E-08 | 0.107E 02 |
| 0.107E 03 | 0.645E 00 | 0.891E-09 | 0.123E 02 |
| 0.108E 03 | 0.565E 00 | 0.780E-09 | 0.140E 02 |
| 0.109E 03 | 0.494E 00 | 0.683E-09 | 0.160E 02 |
| 0.110E 03 | 0.432E 00 | 0.598E-09 | 0.183E 02 |
| 0.111E 03 | 0.378E 00 | 0.523E-09 | 0.209E 02 |
| 0.112E 03 | 0.331E 00 | 0.458E-09 | 0.239E 02 |
| 0.113E 03 | 0.290E 00 | 0.401E-09 | 0.273E 02 |
| 0.114E 03 | 0.254E 00 | 0.351E-09 | 0.312E 02 |
| 0.115E 03 | 0.222E 00 | 0.307E-09 | 0.356E 02 |
| 0.116E 03 | 0.194E 00 | 0.268E-09 | 0.407E 02 |
| 0.117E 03 | 0.170E 00 | 0.235E-09 | 0.465E 02 |
| 0.118E 03 | 0.149E 00 | 0.206E-09 | 0.532E 02 |
| 0.119E 03 | 0.130E 00 | 0.180E-09 | 0.607E 02 |
| 0.120E 03 | 0.114E 00 | 0.158E-09 | 0.694E 02 |

Note: For the above values, E, with its associated sign and two digits, refers to the positive or negative power of ten which each value is to be multiplied by.

TABLE 6

Altitude Regions for which Refractive Paths to the Ground are Allowed within the Entry Plane (using Table 4B. Information on $Z_{ni}$ , with $\sigma = 0$, $\rho_{mE} = 7.7$ g/cm$^3$ only)

| $r_{mE}$ (cm) | $\theta$ (degrees) | $V_E$ (km/sec) | $Z_{ni}$ to the West January (km) | $Z_{ni}$ to the East January (km) | $Z_{ni}$ to the West July (km) | $Z_{ni}$ to the East July (km) |
|---|---|---|---|---|---|---|
| 5.0 | 70 | 11.2 | * | 73-41 | 64-37 | * |
| 5.0 | 40 | 11.2 | 78-38 | 78-38 | 80-40 | 80-40 |
| 5.0 | 10 | 11.2 | 78-48 | 78-48 | 80-51 | 80-51 |
| 5.0 | 70 | 30.0 | * | 73-41 | 64-37 | * |
| 5.0 | 40 | 30.0 | 78-38 | 78-38 | 80-40 | 80-40 |
| 5.0 ** | 10 | 30.0 | 78-48 | 78-48 | 80-51 | 80-51 |
| 50.0 | 70 | 11.2 | * | 73-41 | 64-30 | * |
| 50.0 | 40 | 11.2 | 92-23 | 92-23 | 85-24 | 92-24 |
| 50.0 | 10 | 11.2 | 92-32 | 92-32 | 92-33 | 92-33 |
| 50.0 | 70 | 30.0 | * | 73-41 | 64-30 | * |
| 50.0 | 40 | 30.0 | 92-24 | 92-24 | 85-25 | 92-25 |
| 50.0 | 10 | 30.0 | 92-33 | 92-33 | 92-34 | 92-34 |

* Refractive paths to the ground are not allowed.

** See Table 4B.

TABLE 7

Altitude Regions for which Refractive Paths to the Ground are Allowed outside the Entry Plane
(using Table 4B. Information on $Z_{ni}$ , with $\sigma = 0$, $\rho_{mE} = 7.7\ g/cm^3$ only)

| $r_{mE}$ (cm) | $\theta$ (degrees) | $V_E$ (km/sec) | $Z_{ni}$(km) January $\Delta\phi=$ $10^\circ$ $\phi' = 10^\circ$ | $Z_{ni}$(km) January $\Delta\phi=$ $40^\circ$ $40^\circ$ | $Z_{ni}$(km) January $\Delta\phi=$ $70^\circ$ $70^\circ$ | $Z_{ni}$(km) January $\Delta\phi=$ $10^\circ$ $\phi' = 350^\circ$ | $Z_{ni}$(km) January $\Delta\phi=$ $40^\circ$ $320^\circ$ | $Z_{ni}$(km) January $\Delta\phi=$ $70^\circ$ $290^\circ$ | $Z_{ni}$(km) July $\Delta\phi=$ $10^\circ$ $\phi' = 10^\circ$ | $Z_{ni}$(km) July $\Delta\phi=$ $40^\circ$ $40^\circ$ | $Z_{ni}$(km) July $\Delta\phi=$ $70^\circ$ $70^\circ$ | $Z_{ni}$(km) July $\Delta\phi=$ $10^\circ$ $\phi' = 350^\circ$ | $Z_{ni}$(km) July $\Delta\phi=$ $40^\circ$ $320^\circ$ | $Z_{ni}$(km) July $\Delta\phi=$ $70^\circ$ $290^\circ$ |
|---|---|---|---|---|---|---|---|---|---|---|---|---|---|---|
| 5.0 | 70 | 11.2 | 60-44 | * | * | 75-42 | 73-44 | 70-46 | 63-44 | 61-39 | 60-37 | * | * | * |
| 5.0 | 40 | 11.2 | 78-38 | 67-38 | * | 78-38 | 78-38 | 72-42 | 80-40 | 73-40 | 62-40 | 80-40 | 60-40 | * |
| 5.0 | 10 | 11.2 | 78-48 | 78-48 | 78-48 | 78-48 | 78-48 | 78-48 | 80-51 | 80-51 | 80-51 | 80-51 | 80-51 | 80-51 |
| 5.0 | 70 | 30.0 | 60-44 | * | * | 75-42 | 73-44 | 70-46 | 63-44 | 61-39 | 60-37 | * | * | * |
| 5.0 | 40 | 30.0 | 78-38 | 67-38 | * | 78-38 | 78-38 | 72-42 | 80-40 | 73-40 | 62-40 | 80-40 | 60-40 | * |
| 5.0** | 10 | 30.0 | 78-48 | 78-48 | 78-48 | 78-48 | 78-48 | 78-48 | 80-51 | 80-51 | 80-51 | 80-51 | 80-51 | 80-51 |
| 50.0 | 70 | 11.2 | 60-44 | * | * | 75-42 | 73-44 | 70-46 | 63-44 | 61-39 | 60-37 | * | * | * |
| 50.0 | 40 | 11.2 | 92-23 | 92-84<br>67-23 | * | 92-23 | 84-23 | 72-42 | 92-24 | 73-24 | 62-33 | 92-24 | 92-91<br>60-24 | * |
| 50.0 | 10 | 11.2 | 92-32 | 92-32 | 92-32 | 92-32 | 92-32 | 92-32 | 92-33 | 92-33 | 92-33 | 92-33 | 92-33 | 92-33 |
| 50.0 | 70 | 30.0 | 60-44 | * | * | 75-42 | 73-44 | 70-46 | 63-44 | 61-39 | 60-37 | * | * | * |
| 50.0 | 40 | 30.0 | 92-24 | 92-84<br>67-24 | * | 92-24 | 84-24 | 72-42 | 92-25 | 73-25 | 62-33 | 92-25 | 92-91<br>60-25 | * |
| 50.0 | 10 | 30.0 | 92-33 | 92-33 | 92-33 | 92-33 | 92-33 | 92-33 | 92-34 | 92-34 | 92-34 | 92-34 | 92-34 | 92-34 |

* indicates that refractive paths to the ground are not allowed.

** see Table 4B.